Synthesis, Characterization and Application of Novel Ionic liquids

Submitted in fulfilment of the requirements for the degree of Doctor of Philosophy in Chemistry in the Faculty of Applied Sciences at the Durban University of Technology

Mr. Vasanthakumar Arumugam

MSc (B.U)

March 2018

Supervisor: Prof G. G. Redhi

Co-Supervisor: Prof R. M. Gengan

Declaration

This thesis is being submitted to the Durban University of Technology for the degree of Doctor of Philosophy in Chemistry. I declare that this work is my own and has not been submitted before for any degree or examination to this or any other university or institution for this or any other degree or award.

Student Number: 21452731

Student: [redacted] Date: 15.03.2018

Mr. Vasanthakumar Arumugam

Supervisor: [redacted] Date: 15.03.2018

Prof G. G. Redhi

Co- supervisor: [redacted] Date: 15.03.2018

Prof R. M. Gengan

Plagiarism

I declare that this thesis is my own work. I have appropriately referenced the work of other people that I have used. I have not and will not allow anyone to copy my work with the intentions of passing it as his or her own work.

Vasanthakumar Arumugam

Student Number: 21452731

Abstract:

Ionic liquids (ILs) or molten salts at room temperature presently experience significant attention in many areas of chemistry. The most attractive property is the "tenability" of the physical and chemical properties of ILs by varying structure. The use of ILs in solvents demands information about their behaviour in the presence of other compounds including organic solvents such as alcohols or carboxylic acids or water, commonly used for products extraction. In addition, the efficiency of chemical processes (synthesis, extractions and separations) is strongly influenced by the nature of ILs. In this study describes the synthesis and characterization of novel epoxy propyl substituted ionic liquids (ILs). The thermophysical properties of ILs and their binary mixtures with either water, alcohol or carboxylic acids were investigated and the results are discussed in terms of interactions through thermodynamic properties. Furthermore, 2-oxopyrrolidine (Pyr), 2-aminopicoline (Apic) and 1,4-diazabicyclo [2.2.2] octane (DABCO)-based dihydroxypropyl substituted ILs are synthesised and characterised successfully. These ILs were then used to synthesize and characterize a novel 4th-generation multi-ionic IL. A significant application of this IL is the synthesis of a unique nanomaterial using magnetic iron nanoparticles, h-boron nitride and titanium dioxide. The nanomaterial was strategically used to reduce selected dyes and series of nitroanilines (NAs).

The chapter 1 to 4 explains about the introduction, literature review, synthesis and thermophysical properties of ILs as well as thermodynamic properties of ILs.

The fifth chapter of this study describe the synthesis, characterization and thermophysical properties of a novel 2′, 3′-epoxypropyl-N-methyl-2-oxopyrrolidinium chloride IL and its binary mixtures, with either water or ethanol. The density (ρ), and speed of sound (u), were measured for the above IL and its corresponding binary systems with either water or ethanol at different temperatures ranging from (293.15 to 313.15) K. The derived thermodynamic properties for instance excess molar volumes (V_m^E), isentropic compressibility (k_s) deviation in isentropic compressibility (Δk_s) and intermolecular free length (L_f) were investigated from the ρ and u data, respectively. It is noted that V_m^E, k_s Δk_s and L_f values increase with increasing temperature. Derived properties such as V_m^E, and Δk_s data were fitted to the Redlich-Kister polynomial equation. The measured and calculated data were interpreted in terms of intermolecular interfaces and structural effects between similar and dissimilar molecules upon mixing **(Paper: I)**

The chapter six describes the synthesis and characterization of 2′, 3′-epoxypropyl-N-methyl-2-oxopyrrolidinium salicylate and 2′, 3′-epoxypropyl-N-methyl-2-oxopyrrolidinium acetate ILs. These ILs and their binary mixtures with either water or methanol were then studied to determine their thermophysical properties. The temperature dependent ρ and u for IL, methanol, water, and their corresponding binary mixtures of {IL (1) + methanol or water (2)} were measured over the entire range of mole fractions at temperatures from T = (293.15 to 313.15) K in intervals of 5 K, under atmospheric pressure. The calculated thermodynamic properties such as V_m^E , k_s Δk_s andL_f, were derived from the investigated ρ and u data. The resulting experimental data for V_m^E, L_f, and Δk_s, were well fitted to the Redlich-Kister polynomial equation. **(Paper: II & III)**

The chapter seven reports the thermophysical properties of binary mixtures for the combination of 2′, 3′- epoxypropyl-N-methyl-2-oxopyrrolidinium chloride with carboxylic acids either ethanoic or propionic acids. The novel IL $[EPMpyr]^+[Cl]^-$ was synthesized, and it has been mixed with ethanoic or propanoic acids. The influence of an epoxy group in this IL was more strongly affected with the acids, and their thermophysical properties at varied temperatures are discussed in term of density (ρ), viscosity (η), speed of sound (u), and refractive index (n) measurements. The ρ, u, η, and n of the IL, ethanoic acid, propanoic acid, and their corresponding binary mixtures {$[EPMpyr]^+[Cl]^-$ (1) + ethanoic or propanoic acid (2)} were measured at T = (293.15-313.15) K and at P = 0.1 MPa. The theoretical thermodynamic properties of V_m^E, k_s, Δk_s, and L_f are calculated using experimental ρ and u data. The V_m^E and Δk_s values for both binary mixtures were found to be negative over the entire mole fraction range of compositions at all the investigated temperatures. These results suggest the existence of specific interactions between components in the molecules. The experimental data could be helpful to understand the molecular interactions between the IL and carboxylic acid combinations. The experimental data were fitted to the Redlich-Kister polynomial equation. This study is very important for industries because most of the ILs are viscous and have high pH values, so making their applications in industries are difficult. Hence these main disadvantages could be addressed and rectified simultaneously without drastically altering the nature of the IL by using various carboxylic acid combinations. Moreover, the thermophysical data and information about acid and IL mixtures will provide insight into the use of these ILs in acidic conditions, thereby enabling the development of processes for future industries. Additionally, the measurements of thermophysical properties were used to calculate

thermodynamic properties, which lead to a better understanding of the interactions amongst unlike molecules and hydrogen bonds in binary mixtures. **(Paper: IV)**

In summary, the first four publications describes the synthesis, characterization and thermophysical properties of 2′,3′-epoxypropyl substituted 2-oxopyrrolidinium cation-based novel ILs with various anions such as chloride, acetate and salicylate. These ILs were characterized by FTIR, ^{1}H NMR, ^{13}C NMR and elemental analysis to confirm the chemical structure of the ILs. The binary mixtures of ILs with either water or methanol or ethanol were carefully prepared. Experimental measurements of the thermophysical properties of ρ, u, η and n, selected solvents, and their binary mixtures at various temperatures, across the entire mole fraction ranges of ILs, were determine. Thermodynamic properties of V_m^E, k_s, Δk_s and L_f were calculated from ρ, and u data. These thermodynamic properties were correlated using the Redlich-Kister polynomial equation. Molecular interactions, especially H-bonding and other interaction effects that occur between ILs and molecular solvents were discussed.

The chapter eight discusses the synthesis and characterization of novel 4th generation amino tris methyl phosphonate (ATMP) based IL such as [DABCO, PYR, APIC-PDO]$^{+}$[ATMP]$^{-}$ and their application to the synthesis and characterization of partially oxidized h-boron nitride modified nanomaterial with copper ferrite magnetic nanoparticles (NPs). This nanomaterial was characterized through various spectroscopic, microscopic and surface morphological techniques. Thereafter it was used as environmentally friendly heterogeneous catalyst for the reduction of a series of NAs and dyes such as 2-nitroaniline (2-NA), 3-nitroaniline (3-NA), 4-nitroaniline (4-NA), 4-nitro-1,2-phenylenediamine (4-NPD), methylene blue and allura red to their corresponding amino analogues. The rate constant, order of reaction, activation energy and constant ratio were calculated for each substrate. The order of reduction, was 4-NPD > 4-NA > 3-NA > 2-NA. Kinetic studies indicated either zero or pseudo-first order reactions. Furthermore, kinetic studies at various temperatures such as 25, 30, 40, 50 and 60 ^{o}C as well as the range of various quantities of catalyst such as 0.015, 0.030 and 0.045 ml (0.2mg/ml concentration) showed that either an increase in temperature or the amount of catalyst increased the rate of the reaction. It was found that the nanomaterial is an efficient catalyst in aqueous solution at ambient temperature, and the processes for recovery were simple. It was re-used more than seven times with negligible loss of its catalytic

activity. It is envisaged that new industrial applications of the ILs and their nanomaterials will emanate in the future. **(Paper: V)**

The chapter nine describes the synthesis, characterization and application to the reduction of NAs which were made using 2′,3′- epoxypropyl-N-methyl-2-oxopyrrolidinium salicylate IL, $NiFe_2O_4$ NPs and titanium dioxide (TiO_2). Here IL was used as a bonding or capping agent to synthesize $NiFe_2O_4$ NPs doped TiO_2 nanocomposite. This nanocomposite was characterized by various microscopic and surface morphological studies. The nanocomposite displayed a good catalytic activity for the reduction of 2-NA to 2-aminoaniline and can be recovered as well as recycled easily**. (Paper: VI)**

List of Publications

***Patent*:** **Arumugam Vasanthakumar**., Gengan, R.M., Redhi, G.G., Ionic liquids and preparation thereof. Patent file number A & A Ref: P73710ZA00 PJV/LG (In Press).

This dissertation is based on 6 research publications, which are referred to in the text by their Roman numerals. Reprints were made with permission from the publishers.

Articles Published:

Paper I: *Synthesis, characterization and thermophysical properties of ionic liquid N-methyl-N-(2', 3'-epoxypropyl)-2-oxopyrrolidinium chloride and its binary mixtures with water or ethanol at different temperatures*

A. Vasanthakumar, I. Bahadur, G.G. Redhi, R.M. Gengan, K. Anand

Journal of Molecular Liquids, 2016. **219**: p. 685-693. **(Impact Factor: 3.648)**

Paper II: *Synthesis, characterization of 2', 3'-epoxy propyl - N-methyl-2-oxopyrrolidinium salicylate ionic liquid and study of its interaction with water or methanol*

A. Vasanthakumar, I. Bahadur, G. Redhi and R. M. Gengan

RSC Advances, 2016. **6**: p. 61566-61575. **(Impact Factor: 3. 108)**

Paper III: *Synthesis, characterization and thermophysical properties of novel 2', 3'- N-epoxypropyl- N-methyl-2-oxopyrrolidinium acetate ionic liquid and their binary mixture with water or methanol*

Vasanthakumar Arumugam, G.G. Redhi, R.M. Gengan

Journal of Molecular Liquids, 2017. **242**: p. 1215-1227. **(Impact Factor: 3.648)**

Paper IV: *Influence of epoxy group in 2-pyrrolidonium ionic liquid interactions and thermo-physical properties with ethanoic or propanoic acid at various temperatures*

Arumugam Vasanthakumar, G. G. Redhi, and R. M. Gengan

ACS Sustainable & Chemistry Engineering, 2016. **4**: p. 4951-4964.

(Impact Factor: 5.951)

Publication V: *Nano-material as an excellent catalyst for reducing a series of nitroanilines and dyes: triphosphonated ionic liquid- $CuFe_2O_4$-modified boron nitride*

Vasanthakumar Arumugam, Pavithra. S, Ta-Jen. Y, Gengan. R. M, Redhi. G. G.

Applied Catalysis B: Environmental, 2018. **222**: p. 99-114.

(Impact Factor: 9.440)

Conference Proceeding

Publication VI: *Efficient catalytic activity of ionic liquid-supported $NiFe_2O_4$ magnetic nanoparticle doped titanium dioxide nano-composite*

Vasanthakumar Arumugam, Redhi, G.G, Gengan, R.M.

International Journal of Chemical Engineering and Applications, 2016. **7**(6): p. 422-427

Other research publications

Paper VII: *Ionic liquid based high-performance electrochemical sensor for ascorbic acid in various foods and pharmaceuticals*

Bhajanthri, N. K, **Arumugam Vasanthakumar**, Chokkareddy, R, and Redhi, G.G.

Journal of Molecular Liquids, 2016. **222**: p. 370-376. **(Impact Factor: 3.648)**

Article in Press

Vasanthakumar Arumugam., Redhi. G. G., and Gengan. R. M., Application of ionic liquids in Nanotechnology. Elsevier Book Chapter.

Articles communicated

Vasanthakumar Arumugam., Redhi. G. G., and Gengan. R. M., Synthesis, fabrication and application of metal and mixed metal oxide nanofibers. Book Title: Handbook of Nanofibers. Editors: Ahmed Barhoum, Mikhael Bechelany, Abdel Makhlouf. Publisher: Springer International Publishing. Reference ISBN: 978-3-319-53655-2, Print ISBN: 978-3-319-53654-5.

Contribution to the Papers

- In patent, outline of the study and performed all experimental work. Contributed to the interpretation of the results. Wrote the patent.
- Papers I to V, outline of the study and performed all experimental work. Contributed to the interpretation of the results. Wrote the manuscript.
- In conference proceeding paper, outline of the study and performed all experimental work. Contributed to the interpretation of the results. Wrote the manuscript.
- Paper VI, experimental work especially synthesis and characterization of nanomaterials.
- In two book chapters, outline of the study. Contributed to the interpretation of the results. Wrote the manuscript.

Dedication

To my family

Especially to My Mother

Mrs. Santhi Arumugam

Acknowledgements

First and foremost, I would like to thank God for giving me a wonderful opportunity to complete my Doctorate within the timeframe allocated for the degree.

My heartfelt thanks to my family, especially to my Mother A. Santhi and Brother A. Santhosh kumar for their full and enduring support in all my educational endeavours.

My sincere appreciation and gratitude to Prof G. G. Redhi for introducing me to the fascinating world of Ionic Liquids and his continuous support.

My genuine gratitude to my co-supervisor, Prof R. M. Gengan for his continuous support and guidance.

My indebtedness gratitude to Dr. K. Anand and Prof K. G. Moodley for all their efforts in making arrangements for my arrival to the Chemistry Department at Durban University of Technology, South Africa.

My thanks to Dr. Indrabhadur for useful discussions and technical assistance.

My thank to my lab mates and friends: Mr. M. Sureshkumar, Mr. T. Muthu, Mr. M. Arul, Mr. T. Makhanya and Ms. S. Raghunath for their much-appreciated contribution to this research.

My gratitude to: Mr. S. R. Chetty, Dr. T. Singh, Mrs. D. Naicker, Mr. R. Ramkrepal, and Mr. S. Mjola, for their constant advice and assistance.

My thanks to co-workers and research group members: Dr. N. K. Bhajanthri, Mr. R. Chokkareddy, Mrs. N. M. Xhakaza, Mrs. Pelumi and Mr. Kabane.

My sincere thanks to my mentors at Bharathiar University: Prof M. Illanchelian, Prof P. S. Mohan, Prof S. P. Rajendran and Prof K. J. Rajendra Prasad.

My special thanks to Mr. G. Sateesh Kumar, Govt. Arts College, Nandanam for his moral support.

My appreciation to Ms. Pavithra Sreeram and Prof Ta-Jen Yen, from National Tsing Hua University for their contributions to my research work.

My thanks to my friends from other institutions; Dr. B. Ravindran, Mr. K. Sivananthan, Mr. A. Nanthakumar, Mr. Raja Manikandan and Dr. Deepak Gusain for their assistance.

My sincere thanks to Prof G. Prinsloo for his expert assistance in the patent registering process.

My thanks to Prof S. Moyo and Dr. B. Dzwairo for their kind service in processing in my research finances.

My sincere thanks to Dr. D. H. Pienaar for his assistance in proof reading my dissertation.

My heartfelt thanks to Mr. R. Padmanabhan, Mr. P. Praveen and Mr. P. Prasana fromVidhya Enterprises, Chennai, Tamil Nadu, India, for supporting my research carrier.

My thanks to my best friends Mr. V. Vasanth kumar, Mr. M. Anbuselvan, Mr. S. Krishnamoorthy, Mrs. V. Lakshmi Devi, Mr. Vadivel, Mr. D. Prabakaran, Mr. Rajesh kumar, Mr. Visvanathan, Mr. Vekatachalam , Mr. Magavishnu, Mr. Sakthivel, and Mr. Muthukrishnan, for their moral support.

My gratitude to National Research Foundation (NRF) for the NRF Innovation Doctoral grant (Vasanthakumar Arumugam, Grant No: 101117 & 109839) and DUT Department of Research and Postgraduate Support, for their financial support.

Abbreviations

OAC	– Acetate
AFM	– Atomic force microscopy
ATMP	– Amino trimethyl phosphonic acid
APIC	- Amino Picoline
NR_3	– Amine
RX	– Alkyl halide
Br	– Bromide
HA	– Bronsted Acid
BNNSs	– Boron Nitride Nano Sheets
Tf_2N	– Bis (trifluoromethane Sulfonyl) imide
MS_2N	– Bis (methane Sulfonyl) amide
^{13}C NMR	– Carbon-13 Nuclear Magnetic Resonance
CNM	– Carbon Nanomaterial
Cl	– Chloride
COSMO-RS	– Conductor-like Screening Model for Real Solvents
ρ	– Density
Δk_s	– Deviation in Isentropic compressibility
DABCO	–1,4-diazabicyclo[2.2.2]octane
DCA [$N(CN)_2$]	– Dicyanamide
DMAP	– Dimethylaminopyridine
EDLCs	– Electric double-layer capacitors
ED	– Electron Diffraction
ESO_4	– Ethyl sulfate

Epmpyr	– 2’, 3’-Epoxypropyl-N- methyl-2- oxopyrrolidinium
EOS	– Equation of state
V_m^E	– Excess molar volume
FTIR	– Fourier Transform Infrared Spectroscopy
PF_6	– Hexafluoro phosphates
h-BN	– Hexagonal Boron Nitride
HRTEM	– High-Resolution Transmission Electron Microscope
HSO_4^-	– Hydrogen sulfate
HE	– Hybrid Electrolyte
L_f	– Intermolecular free length
IL	– Ionic Liquid
I^-	– Iodide anion
IC	– Ion Chromatography
Fe_3O_4	– Iron (II, III) oxide
k_s	– Isentropic compressibility
MXy	– Lewis Acid
$LiPF_6$	– Lithium hexafluoro phosphate
LLE	– Liquid-liquid extraction
Li-S battery	– Lithium-Sulfur battery
$LiNO_3$	– Lithium Nitrate
MA	– Metal Salt
NP	– Nanoparticle
C_4MPyrr (BMPyrr)	– N- butyl-N-methyl Pyrrolidinium
C_2MPyrr (EMPyrr)	–N-Ethyl-N-Methyl Pyrrolidinium

MPyr	– N-Methyl Pyrrolidinium
HNMP	– N-methyl pyrrolidone
NiO	– Nickel oxide
NADH	– Nicotinamide adenine dinucleotide (reduced form)
$C_7CO_2^-$	– Octanoate
PyrIL	– Pyrrolidinium ionic liquid
PC-SAFT	– Perturbed-Chain- Statistical Associating Fluid Theory
PMPyr	– 1-Propyl-1-methyl Pyrrolidinium
PDOL	– Propane-1, 2-diol
^{1}H NMR	– Proton Nuclear Magnetic Resonance
^{31}P NMR	– Phosphorous Nuclear Magnetic Resonance
PYR	– Pyrrolidinium
n	– Refractive index
RP-HPLC	– Reversed-Phase High-Performance Liquid Chromatography
RTIL	– Room Temperature ionic liquid
SAL	– Salicylate
SEM	– Scanning Electron Microscope
STEM	– Scanning Transmission Electron Microscope
SWOT	– Strengths, Weaknesses, Opportunities, Threats
SiNW	– Silicon Nanowire
Ag NPs	– Silver Nanoparticles
BF_4	– Tetrafluoro borate
TEM	– Transmission Electron Microscope
TFO (CF_3SO_3)	– Trifluoromethane sulfonate

SCN – Thiocyanate

η – Viscosity

XRD – X-Ray Powder Diffraction

XPS – X-ray photoelectron spectroscopy

$ZnFe_2O_4$ – Zinc Ferrite

$[EPMpyr]^+[Cl]^-$ – N-2′,3′-Epoxypropyl-N-methyl-2-oxopyrrolidinium chloride

$[EPMpyr]^+[SAL]^-$ – N-2′,3′-Epoxypropyl-N-methyl-2-oxopyrrolidinium salicylate

$[EPMpyr]^+[OAC]^-$ – N-2′,3′-Epoxypropyl-N-methyl-2-oxopyrrolidinium acetate

$[DABCO\text{-}PDO]^+[Cl]^-$ – N-2′,3′-Dihydroxypropyl-1,4-diazabicyclo[2.2.2]octylonium Chloride

$[PYR\text{-}PDO]^+[Cl]^-$ – N-2′,3′-Dihydroxypropyl-N-methyl-2-oxopyrrolidinium chloride

$[APIC\text{-}PDO]^+[Cl]^-$ – N-2′,3′-Dihydroxypropyl-2-aminopicolinium chloride

$[DABCO, PYR, APY\text{-}PDO]^+[ATMP]^-$ – N-2′,3′-Dihydroxypropyl-1,4-diazabicyclo [2.2.2]octylonium N-2′,3′-dihydroxypropyl-N-methyl-2-oxopyrrolidinium N-2′, 3′-dihydroxypropyl-2-amino picolinium aminotris(methylene phosphonate)

1 Table of Contents

Motivation

Room temperature ionic liquids (RTILs) are important materials for modern industries due to the wide variety of applications because of their excellent thermophysical properties. They are used as green solvents, electrolytes, sensors and catalysts for organic synthesis. For example, pyrrolidinium-based ILs are used in the battery industries due to their outstanding electrolyte properties. This class of IL-based electrolytes is popular in lithium-ion battery research, and it is envisaged that the current study will contribute immensely to the future development of better industries.

The current study aim to develop oxopyrrolidinium ILs and rectify the general drawbacks of ILs, such as high viscosity (see Table. 1). Chemical industries desperately require new ILs to avoid difficulties encountered with highly viscosity of ILs. Highly viscous ILs are unpopular in research and development processes in chemical industries due to their difficulties in mixing with solvents. Also, the overall recovery, purification and re-usability of ILs are poor. Hence these disadvantages of ILs, prompted this study to synthesize better ILs and determine their thermophysical and thermodynamic properties.

The viscosity of some of the ILs are reported in Table.1. As a result of strong interionic interactions, ILs usually show higher viscosities than commonly used organic fluids. The high viscosities of ILs narrow their applications in synthesis and extraction techniques which involve mixing and/or mass transfer operations. This study helps to rectify these drawback for example, high viscous ILs have been modified to lower viscosity via the addition of relatively cheap molecular solvents to make binary mixtures of ILs with negligible loss of their properties. Nowadays, reputed chemical companies such as SIGMA ALDRICH and FLUKA are selling dilute ILs for example 1-Methyl-3-propylimidazolium methyl carbonate solution ~50 % in methanol in Sigma.

Mixing of the ILs with molecular solvents is one of the alternative steps to minimize the usage of expensive ILs. Ionic liquid mixtures with molecular solvents shows reduced viscosity without affecting their advantages as green solvents. Mixtures of ILs and molecular organic solvents are gaining IL interest of researchers, as resultant liquid mixtures have the advantages over both IL and molecular organic solvents.

The measurement and interpretation of physical properties of ILs and their binary mixtures are necessary to develop applications and to explain the physical and chemical behaviour of ILs. In spite of importance of properties of ILs in aqueous or non-aqueous solutions, there is limited information available on the thermodynamic properties of IL mixtures with other fluids and these properties still lacking. However, due to the enormous number of possible binary systems, a lot of work still remains to be done. Many efforts in this field have been devoted to the study of (RTIL + water), (RTIL + carboxylic acid) and (RTIL + alcohol) binary systems, mainly motivated by solubility of ILs in these molecular solvents as well as low environmental impact of these mixtures.

Many researchers have focused on the synthesis of ILs from pyrrolidine whilst few have attempted the synthesis of ILs from oxopyrrolidine. In comparison with pyrrolidine, oxopyrrolidine based ILs are considerably less viscous (see Table. 1) whilst the choice of anion could also be account for decreased. Hence this study interrogates oxopyrrolidinium ILs. Furthermore, since salicylate based organic molecules are already used in drug formulations because of their good biological activity, this study utilized a salicylate anion to combine with oxopyrrolidinium cation. Their thermophysical and thermodynamic properties are elaborated. It is hoped that the results emanating from this study will encourage investigation of these new systems in drug discovery programs.

In this study fourth-generation IL, like tricationic phosphonated multi ionic-ionic liquid i.e., multi-ions with the same or different cations and anions were also presented. The synthesis of a fourth-generation multi-ionic phosphonate IL will become useful because, this is a starting point for synthesizing new ILs: it will also give a basic insight into the synthesis of other innovative multi-ionic ILs. The studied ILs contains various cations, for instance five, six and seven membered heterocyclic cations with multi-membered anionic groups, making them multi-ionic entities. Since, this is a good route to synthesize new types of ILs, it is hoped that this will lead to the synthesis of other novel ILs with new combinations of cations and anions. These IL have good physical and chemical properties because they contain many large cations and anions.

ILs in nanotechnology is developing into a significant research area, especially for the synthesis of nanocomposites. There excellent thermophysical properties of ILs enabled extraordinary applications in various research areas such as pharmaceuticals, catalysis, censors, adhesives and electrolyte devices. ILs, h-boron nitride modified material, titanium dioxide and magnetic nanoparticles are industrially viable materials, for new development. Hence this study uses these

three materials to synthesize novel nanomaterials which possess excellent catalytic activities for the reduction of a series of NAs and dyes. The synthesis of the novel type of catalyst can lead to further catalyst development in the near future.

The pyrrolidinium-based ILs were used in the preparation of a novel class of polymer electrolytes based on polymer-ionic liquid gels, which can be applied in electrochemical devices, especially in chemical capacitors. Specifically in this case epoxy substituted ILs were synthesized, for possible use in the capacitors industries. Furthermore, in this study salicylate anion based IL was synthesized, for possible the pharmaceutical industries, because of its biological activity of salicylate.

2 Aim and outline of the thesis

2.1 Aim

The aims of this study were to:

Synthesize and characterize the epoxypropyl and dihydroxypropyl substituted ILs were investigated. Furthermore, the thermophysical and thermodynamic properties of epoxypropyl substituted ILs and its corresponding binary mixtures with either molecular solvents or carboxylic acids in fixed mole fractions at various temperatures, under atmospheric pressure were determined.

Synthesize and characterize phosphonated anion based novel ionic liquid-modified magnetic nanoparticles decorated with either partially oxidized boron nitride or titanium dioxide nanomaterials and assess their excellent catalytic effect for reduction of a series of NAs and dyes.

2.2 Outline of the thesis

This study completely describes the synthesis and characterization of ILs and IL based nanomaterials, as well as the catalytic application of synthesized nanomaterials in terms of reduction of series of nitroanilines and dyes. Six new ILs were synthesized and characterized successfully. All ILs has been analysed by FTIR, ^{1}H NMR, ^{13}C NMR and elemental analysis in order to identify and ascertain their chemical structure. The first three ILs were based on N-2′,3′-epoxypropyl substituted N-methyl-2-oxopyrrolidinium cations with various anions such as chloride, acetate and salicylate, through the ILs like N-2′,3′-epoxypropyl-N-methyl-2-oxopyrrolidinium chloride, N-2′,3′-epoxypropyl-N-methyl-2-oxopyrrolidinium salicylate and N-2′,3′-epoxypropyl-N-methyl-2-oxopyrrolidinium acetate. The next three ILs N-2′,3′-dihydroxypropyl-N-methyl-2-oxopyrrolidinium chloride, N-2′,3′-dihydroxypropyl-1,4-diazabicyclo [2.2.2] octanium chloride and N-2′,3′-dihydroxypropyl-2-amino-4-methylpyridinium chloride ILs were synthesized by the substitution of propanediol with chloride anion. The above three ILs as mentioned like {$[DABCO]^{+}[PDOL]^{-}$, $[APIC]^{+}[PDOL]^{-}$ and $[PYR]^{+}[PDOL]^{-}$ }. These were used to synthesize a unique 4th generation multi-ionic tri-cationic phosphonate ionic liquid (TCPIL) through the exchange of chloride anions by metathesis reaction with amino trimethyl phosphonate (ATMP) anion. A multi-ionic IL was one that contains more than one cation linked to the same type of anions. A 4th generation ionic liquid (4-ILs) is a new concept and is described as one that contains more than one cation linked to a single substrate that contains multiple anionic

sites. This is the first synthesized 4-ILs which was not documented in any scientific journals world-wide, so a patent has been filed for this work. Particularly, this 4-ILs have fascinating physical and chemical properties, therefore it will be certainly providing for unique applications in future.

These novel ($[Epmpyr]^+[Cl]^-$, $[Epmpyr]^+[SAL]^-$, $[Epmpyr]^+[OAC]^-$ $[APIC\text{-}PDOL]^+[Cl]^-$ and $[PYR\text{-}PDOL]^+[Cl]^-$) ILs have not been reported in literature. Moreover, the thermophysical and thermodynamic properties of ILs and their corresponding binary mixtures with the molecular solvents including either water, alcohols or carboxylic acids were investigated for fixed mole fractions at various temperatures under atmospheric pressure. The thermophysical properties of ρ,u, η and n were determined experimentally. In addition, the derived thermodynamic properties were calculated from these experimental data. The interaction in between IL and solvent molecules were explained in terms of studies like H-bonds, dipole interactions and chemical structure related properties. The comparison studies of FTIR spectra of the IL and their corresponding mixtures also provided information about the interaction between the molecules and H-bonding. Furthermore, these thermodynamic properties were fitted to correlate for smoothing using the Redlich-Kister polynomial equation.

The application of ILs in nanotechnology is becoming a trend in recent years. The extraordinary thermophysical properties of ILs contribute incredibly to the development of nanotechnology. In this study, bimetallic magnetic nanoparticles were used namely $CuFe_2O_4$ and $NiFe_2O_4$, this being due to particularly the d-block elements having considerably more catalytic activity because of their ability to change their oxidation state or in the case of the metals, to adsorb other substances on to their surface and activate them in the process. The reason for choosing magnetic nanoparticles were that they could be recovered easily with external magnets and recycled. The purification and re-using abilities were simple and it works well even after using the above products up to seven times. Graphene-like layered h-boron nitride was modified to synthesize partially oxidized h-boron nitride nanosheets (BNONS). In this study two efficient nanomaterials i.e., TCPIL/$CuFe_2O_4$/BNONS and $NiFe_2O_4$/IL/TiO_2 were synthesized and characterized successfully. Advanced microscopic and surface analysing techniques such as FTIR, XRD, SEM, EDS, TEM, HRTEM, STEM, ED, XPS, and AFM were used to investigate the functional groups and physical nature of the nanomaterials. The first nanomaterial was composed by $CuFe_2O_4$ nanoparticles, tri-cationic phosphonate ionic liquid (TCPIL), and BNONS in the mass ratio of chemicals 2:1:1. Moreover, these nanomaterials were used as effective catalyst for the reduction

of series of NAs such as 2-NA, 3-NA, 4-NA and 4-nitro-2-phenylene diamine to corresponding 1,2-diaminobenzene; 1,3-diaminobenzene; 1,4-diaminobenzene; 4-triaminobenzene as well as dyes like methylene blue and allura red. The kinetic studies of these reduction reactions were investigated to determine the rate constant, order and activation energy of the reactions. Also, kinetic studies were undertaken at several temperatures and various concentration of catalyst. This reduction reaction was monitored by the time dependent UV-visible spectroscopy in an aqueous solution and this catalyst was eco-friendly, easily recoverable and re-usable after 7 times with negligible loss of its activity. The second catalyst was synthesized by the blending of $NiFe_2O_4$ nanoparticles, $[EPmpyr]^+[SAL]^-$ and TiO_2 with the same mass ratio of chemicals 2:1:1. However, this mass ratio could be changed, depending on the reaction conditions and type of reactions. This reaction shows that the reduction of 2-NA to 1,2-diamino benzene in aqueous solution at room temperature under atmospheric pressure and it was monitored by time-dependent UV-visible spectroscopy. Advantage of this synthesized nanomaterial was that they were environmentally friendly, easily recoverable, re-usable after 5 times with negligible loss of activity, economically viable and chemically effective.

3 Objective

3.1 Chapter: I

- Introduction

3.2 Chapter: 2

- Literature Review

3.3 Chapter: 3

- Synthesis of ionic liquids
- Thermophysical properties

3.4 Chapter: 4

- Thermodynamic properties

3.5 Chapter: 5

The objectives of this study were to:

- Synthesize a novel $[Epmpyr]^+[Cl]^-$ IL and confirm the chemical structure by characterization with FTIR, ^1H NMR and ^{13}C NMR as well as elemental analyses techniques.
- Determine the percentage of moisture content in the synthesized IL by Karl Fisher titration.
- Measured the thermophysical properties of ρ and u for $[Epmpyr]^+[Cl]^-$ IL as well as its corresponding binary mixtures with either water or ethanol at various mole fractions (0.1 to1.0) at temperatures (293.15 to 313.15) K, in intervals of 5 K under atmospheric pressure.
- Calculate the theoretical thermodynamic properties such as V_m^E, k_s $\Delta k_s$and L_f experimental data.
- Investigate the molecular interactions, such as Van-der-Waals interactions, dipole interaction, ionic interaction and hydrogen bonds among the molecules present in the liquid mixtures.
- Explain the interfaces of intermolecular interactions and effects of chemical structure among the similar and dissimilar molecules upon mixing, in terms of the experimental data obtained.

- Fit the Redlich-Kister polynomial equation for smoothing the thermodynamic data of V_M^E, and Δk_s.

3.6 Chapter: 6

The objectives of this study were to:

- Synthesize novel N-2′,3′-epoxypropyl-N-methyl-2-oxopyrrolidinium salicylate and $[Epmpyr]^+[SAL]^-$, N-2′,3′-epoxypropyl-N-methyl-2-oxopyrrolidinium acetate $[Epmpyr]^+[OAC]^-$ ILs successfully.
- Characterize these ILs using FTIR, ^{1}H NMR and ^{13}C NMR as well as elemental analysis techniques.
- Inspect the physicochemical properties of ρ and u, for $[Epmpyr]^+[SAL]^-$ IL and its related binary mixtures with either water or methanol in fixed mole fractions (0.1 to 1.0) from temperatures (293.15 to 313.15) K, at 5 K interval, under atmospheric pressure.
- Determine the thermophysical properties of ρ, u, η and n for $[Epmpyr]^+[OAC]^-$ IL and its equivalent binary mixture system with either ethanoic or propanoic acid in standard mole fraction ranges of the IL (0.1 to 1.0) at temperatures (288.15 to 313.15) K, intervals of 5 K under atmospheric pressure.
- Compute and analyse the important thermodynamic data which were derived from experimental properties such as V_m^E, k_s, $\Delta k_s$and L_f.
- Investigate the nature of the interactions that provide valuable information, for example Van-der-Waals interactions, dipole interactions, ionic interactions, and formation of hydrogen bonds among the molecules present in the liquid mixtures.
- Analyse the experimental and derived data for information about the influence of the functional group's interaction and possible hydrogen bond formation between IL and solvents were studied.
- Correlate the thermodynamic data such as V_m^E, k_s $\Delta k_s$and L_f with the Redlich-Kister polynomial equations.

3.7 Chapter: 7

Objectives of this study were to:

- Investigate the thermophysical properties and influence of the epoxypropyl group on $[EPMpyr]^+[Cl]^-$ IL as a result of the mixing with carboxylic acids.
- Determine the experimental thermophysical properties of ρ, u, η and n for this IL ($[Epmpyr]^+[Cl]^-$) and its related binary mixtures with either ethanoic acid or propanoic acid across the whole mole fraction range from 0.1 to 1.0 at temperatures (288.15 to 313.15) K in steps of 5 K at atmospheric pressure.
- Calculate and analyse the derived thermodynamic data of V_m^E, k_s, $\Delta k_s$and L_f..
- Correlate the measured similar quantities viz., thermophysical data of V_m^E, k_s $\Delta k_s$and L_f with the Redlich-Kister polynomial smoothing equations.

3.8 Chapter: 8

Objectives of this study were to:

- Synthesize and characterize the three different unique ILs namely, $[DABCO\text{-}PDOL]^+[Cl]^-$, $[APIC\text{-}PDOL]^+[Cl]^-$ and $[PYR\text{-}PDOL]^+[Cl]^-$ effectively and evaluate the chemical structure of the IL by FTIR, ^{1}H NMR, ^{13}C NMR and elemental analysis.
- Synthesize the novel 4-IL, $\{[(DABCO, PYR, APY)\text{-}PDO]^+[ATMP]^-\}$ and characterize and elucidate the chemical structure of the IL with the aid of FTIR, ^{1}H NMR, ^{13}C NMR and ^{31}P NMR.
- Synthesize a partially oxidised h-boron nitride nanosheets (BNONS) material for increasing the surface area, active sites on surface and binding efficiency of the h-BN for improving the ability to interact strongly with nanoparticles and ILs to get highly stable more efficient nanocomposite.
- Synthesize copper ferrite ($CuFe_2O_4$) bi-magnetic nanoparticles.
- Synthesize novel multi-ionic, IL-bonded $CuFe_2O_4$ nanoparticles (NPs) and dope with BNONS nanocomposite (TCPIL/$CuFe_2O_4$/BNONS).
- Characterize the nanocomposite using an advanced microscopic, morphological, and surface analysing techniques such as FTIR, XRD, SEM, EDS, TEM, HRTEM, STM, ED,

XPS and AFM to evaluate the surface information, functional group identifier, electronic concentration, elements and its bonds.

- Investigate the catalytic activity by reducing a series of NAs such as 2-NA, 3-NA, 4-NA and 4-nitro-2-phenylene diamine and dyes like allura red and methylene blue in aqueous solution at ambient temperature.
- Undertaken kinetics studies for find the rate constant, order of the reaction and activation energy for reduction reactions at various temperatures as well as different concentration of catalyst.
- Recover and re-use the nano catalyst TCPIL/$CuFe_2O_4$/BNONS as a function of activity.

3.9 Chapter: 9

Objectives of this study were to:

- Apply the synthesized $[EPMpyr]^+[SAL]^-$ IL for the creation of novel nanocomposites for improving their effectiveness in terms of catalytic activity.
- Synthesize the $NiFe_2O_4$ magnetic ferrite nanoparticles through co-precipitation method.
- Synthesize the novel IL-bonded $NiFe_2O_4$ magnetic nanoparticle doped TiO_2 as an efficient nanocomposite.
- Characterize the above nanocomposite by advanced microscopic and surface analysing technologies such as FTIR, SEM, EDS, TEM and HRTEM.
- Determine catalytic efficiency using the reduction reaction of 2-NA to 1,2-diamino benzene with the help of sodium borohydride in an aqueous solution at room temperature.
- Recover and re-use the synthesized nanocomposite catalysts around more than five times, with negligible loss of catalytically activity.

4 Chapter 1

4.1 Introduction

4.1.1 Ionic Liquids

4.1.1.1 General aspects

Ionic liquids (ILs) are organic salts which are mainly composed of organic cations and inorganic or organic anions with melting points less than 100 ^{o}C [1, 2]. Generally, many ILs are thermally stable up to 250 ^{o}C, but may decompose at higher temperatures. One of the most important property of an ILs is their strong solubilizing nature and is been used to dissolve a wide range of inorganic and organic compounds [3], and many polymers such as cellulose [4], chitin [5, 6], chitosan [7], polyvinylchloride [8] and polystyrene [9]. All these polymers are insoluble in conventional solvents. The classical molten salts are distinguished from modern ILs, by their high-melting point, high viscosity and very corrosive nature. Usually, bulky asymmetric organic cations are present in ILs, examples of which are imidazolium, pyridinium, pyrrolidinium, quaternary ammonium, tetra-alkyl phosphonium and sulfonium which all have weak intermolecular interactions, low symmetry, and low charge densities [10-14]. Therefore, the crystal lattice in ILs are not closely-packed due to these large cations [15]. The use of an anion with delocalized charge enhances this effect [16]. A selection of distinctive cations and anions is shown in Fig. 1.

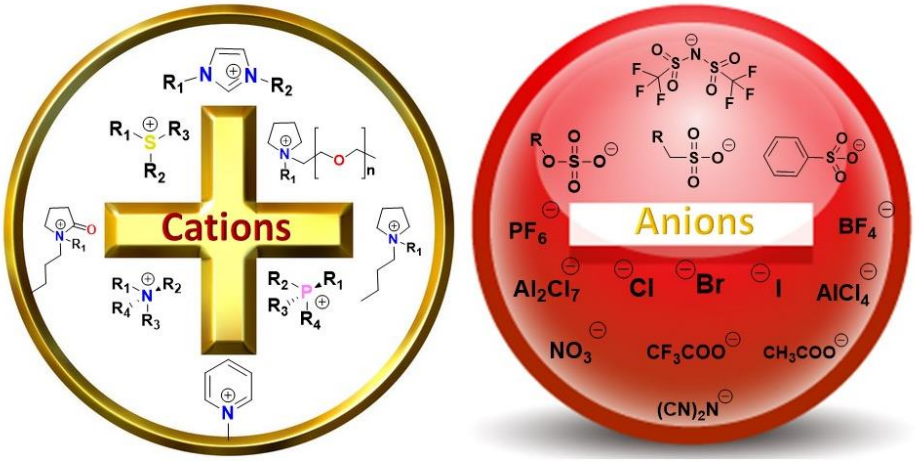

Figure 1: Schematic representation of selected structures depicting common cations and anions in ionic liquids

The characteristics of ILs are their interesting physical properties especially their negligible vapour pressure and non-flammability. The various ions such as organic compounds and other materials significantly influence the actual properties of ILs, therefore, the composition of functional ions contributes more to thermophysical properties of ILs. The properties of ionic salts can be completely and solely attributed to their ionic nature since strong ionic bonds hold their particles together. Ionic salts are mostly made of small monoatomic ions in the close vicinity of one and other in their lattice crystal network. The lattice energy of crystalline compounds is proportional to the inverse of the distance between their lattice points. The ionic bonds in salts are very strong due to the relatively short distance between the small ions contributing to high values of melting point. On the contrary, ILs are made up of larger multi-atomic cations and anions resulting in weaker ionic bonds. This explains the considerably low melting point and viscosity of ILs compared to those of ionic salts (see Table.1 show viscosity of various cations based ILs).

The multi atomic nature of cations and anions in ILs is a great opportunity for researchers to fine tune their properties with customizing them for different applications. In ILs, cations, and occasionally anions, are composed of alkyl side chain groups (CH_2, CH_3, etc.) which can be accompanied with a number of functional groups (OH, NH_2, COOH, etc.) to functionalize ILs for different applications. A vast number of ILs (estimated to be about 1014) can be potentially synthesized through distinct combinations of different cation-cores, alkyl groups, functional groups, and anions. Careful evaluation of experimental data from literature on the physical and thermodynamic properties of ILs shows that substituting functional groups can drastically alter a property of interest in ILs.

Furthermore, ILs can be recovered and recycled easily due to their hydrophilic or hydrophobic, low vapour pressure, and solubility nature in a wide range of different solvents [13, 17-20]. ILs are used for many applications such as solvents for catalyst synthesis [21, 22], chemical reactions [23, 24], extractions [25] and electrochemical purposes due to their fascinating properties. ILs are classified as green solvents or designer solvents [17, 18, 26-29] due to their non-volatile nature. The important thermophysical properties of ILs such as viscosity, polarity, melting point, solubility, thermal and electrochemical stability can be determined by choosing a suitable combination of cations and anions. Therefore, ILs are always labelled as designer solvents or task-specific ionic liquids (TSIL) [1]. The selected combination of cations and anions are able to change their chemical properties and not only change their physical properties. Furthermore, the influence

of the substituting or functional group plays an important role, and it may depend on the attached alkyl group chain length as well as functionality. Substitution of the functional groups which are incorporated on the cations, include, imidazolium, pyrrolidinium and pyridinium, while functionalized anions are also developing rapidly [30-33].

The green chemistry aspect of ILs are simple for recovery and recyclability, chemical waste reduction and an increased lifetime of the liquid. The other special characteristics of ILs are their hydrophilic and hydrophobic properties. This means that the IL which is hydrophilic can be reacted with other hydrophilic compounds to form hydrophobic products.

Table 1: The viscosity for various types of cationic ionic liquids

IL	viscosity/mPa s	Refs
[PYR][TFSAM]	0.19	34
[PYR][DCA]	0.28	34
$[1m(C_1py)_2C_4]^{2+}$	473	35
$[1m4m(C_1py)_2C4]^{2+}$	506	35
$[3m(C1py)_2C_5]^{2+}$	1026	35
$[3m_2(C1py)_2C_5]_{2+}$	1138	35
$[1m(C_1C_1im)_2C_3]^{2+}$	266	35
[BMPYR][FSI]	53.24	36
$[P_{2225}][FSI]$	69.38	36
[BMPYR][TFSI]	77.76	36
$[P_{222201}][TFSI]$	48.14	37
$[P_{2225}][TFSI]$	85.3	37
[BMP[TFSI]	188.9	36
$[Et_3S][TFSI]$	33.36	38
$[Et_2MeS][TFSI]$	40.71	38
$[C_1(C_2O(CO)OC_3)Py][NTf_2]$	571	39
$[BMPy][BF_4]$	202.8	40
[BMPy][DCA]	35.2	40
[BMpyr] [Br]	5	41

4.2 The History of ionic liquids

Although red oil [42] was discovered as a by-product of the $AlCl_3$ catalysed Friedel-Crafts reaction, only recently it was identified as a carbocation containing a tetrachloro aluminate anion and categorized as an IL [43]. The first true IL was ethyl ammonium nitrate (Fig. 2a) and widely credited to Paul and Walden in 1914: its melting point was found to be 12 ^oC [10, 42, 44-46]. The synthesis of ILs resulted in their use over a wide range of applications such as separation processes [47-49], as a solvent for organic synthesis [50-52] and use as a catalyst [53-55]. In the 1940's high-temperature electroplating processes were developed with aluminium chloride based molten salts. At the same time low-temperature electroplating was also established for aluminium which was performed by using an IL, based on warmed mixtures of 1-ethylpyridinium chloride and aluminium chloride (Fig. 2b), as reported by *Hurley et al*. in 1951 [56, 57]. *Robinson et al.* [58, 59] and *Hussey et.at* [60-62] investigated ambient temperature ILs, which were based on organic chloride and aluminium chloride mixtures. In the 1970's, researchers faced problems related to the use of molten salt electrolytes at low temperatures. During that time molten salts were used at high temperatures, but at low temperatures, the solids crystallized out. As a direct consequence, *Wilkes et al.* [63] created lower melting point electrolytes to solve these problems. The first review based on RTILs was written by Hussey in 1983 [64]. However organic synthesise were achieved using lower melting point ILs in the 1980s [65, 66]. Generally, ILs are more sensitive in nature, because they are highly hygroscopic, easily affected by air, and hence it is difficult to synthesize their free of H_2O. However, in 1992, air and water free stable ILs based on 1-ethyl-3-methylimidazolium cation with various anions such as tetrafluoro borate (Fig. 2c) and hexafluoro phosphate were synthesized successfully (Fig. 2d) [67].

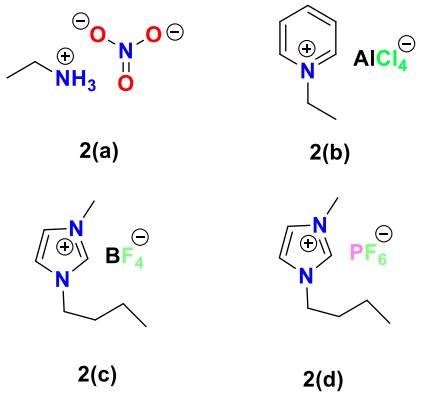

Figure 2: a) Ethyl ammonium nitrate, b) 1-Ethylpyridinium tetrachloro aluminate, c) 1-Ethyl-3-methylimidazolium tetrafluoro borate, d) 1-Ethyl-3-methylimidazolium hexafluoro phosphate

This was a good starting point for encouraging interest in ILs, and many researchers began to focus on synthesizing ILs with good stability, whilst industries were developing rapidly. Industries wanted to use ILs in their processes even though the cost of ILs is high (see Table. 2) [68]. Ionic liquids are generally expensive but due to their outstanding properties and applications, are being used in chemical, pharmaceutical and battery industries. However, due to many companies now producing ILs, the cost of ILs is expected to be lower. In 1998, *Davis et al.* [69] prepared a new type of IL known as functionalized ILs in which the cation was derived from the antifungal drug miconazole. These types of ILs have covalently embedded functional groups attached either to the cation or anion or even for both. The fine tuning of this structure allows for the creation of new applications for ILs, which are significant to introducing functional groups into the ILs. Currently, researchers in academia and industries are focusing on ILs, due to their outstanding physical and chemical properties and obviously the fascinating applications of ILs as well. More than 18000 research papers and 4000 patents were published in the field of ILs [70]. The simple combination of various cations and anions has resulted in more than one million ILs being synthesized [71]. However, currently only about 300 commercialized ILs (see Table. 3 show some commercially available ILs and its processes) are used and therefore the synthesis of new ILs provides good challenging opportunities.

Table 2: Price and quantity of commercially available pyrrolidinium based ILs (In SIGMA ALDRICH)

Name of ILs	ILs	Price in USD	Quantity in grams
1-Butyl-1-methylpyrrolidinium bis(trifluoro methyl sulfonyl)imide	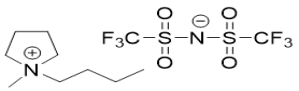	505.00	50
1-Butyl-1-methylpyrrolidinium bromide ≥99.0%	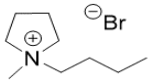	167.00	50
1-Butyl-1-methylpyrrolidinium bromide	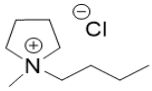	313.00	50
1-Butyl-1-methylpyrrolidinium dicyanamide	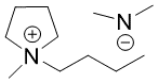	1195.00	50
1-Butyl-1-methylpyrrolidinium hexafluoro phosphate	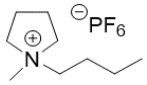	283.00	50
1-Butyl-1-methylpyrrolidinium iodide	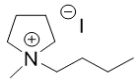	321.50	50
1-Butyl-1-methylpyrrolidinium methyl carbonate solution	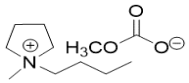	124.00	10
1-Butyl-1-methylpyrrolidinium trifluoro methane sulfonate	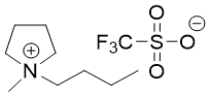	526.00	50
1-Ethyl-1-methylpyrrolidinium bis(trifluoro methyl sulfonyl)imide	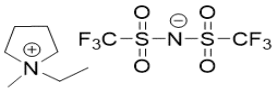	328.50	50
1-Ethyl-1-methylpyrrolidinium bromide	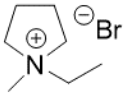	116.50	50
1-Ethyl-1-methylpyrrolidinium hexafluoro phosphate	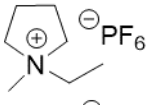	281.00	50
1-Ethyl-1-methylpyrrolidinium tetrafluoro borate	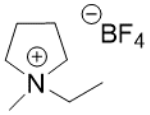	377.50	50

5 Chapter 2

5.1 Literature Review

Apart from imidazolium ILs, pyrrolidinium analogue ILs were also important because of their fascinating thermophysical properties and applications [72]. Low viscosity, more stable and good electrolytic nature were reasons for the development of pyrrolidinium based ILs [73, 74]. The viscosity of some oxopyrrolidinium, pyrrolidinium, imidazolinium, phosphonium and sulfonium based ILs are shown in Table. 1. New technologies are planned and developed using ILs, therefore ILs have a chance to revolutionize chemical processes in industries. The measurements of phase equilibria and activity coefficients at infinite dilution provides important advantage of pyrrolidinium based ILs [75-81].

The fascinating thermophysical properties are a significant reason for the tremendous growth and development of ILs. These fundamental thermophysical properties of ILs were established, using chromatographic and spectroscopic methods, resulting in more than 200 ILs including pyrrolidinium based ILs being characterized and described by those methods [82]. The attractive thermophysical properties of pyrrolidinium based ILs include low viscosity, low melting points, low volatility, ease of recycling, high conductivity, large electrochemical windows, negligible vapour pressure, thermal stability, use for the separation of aromatic hydrocarbons from aliphatic hydrocarbon mixtures and lower toxicity in nature [83-91]. Reverse phase high-performance liquid chromatography (RP-HPLC) and ion chromatography (IC) were used to analyse pyrrolidinium cations in ILs [92-94]. The substitution of functional groups in cations plays important role in their physical properties. For example, the chain length of the alkyl group in the pyrrolidinium cation influences solubility, i.e., long chains substitution can increase the solubility or vice versa [95]. Moreover, the solubility of the ILs in water is very important for industrial applications, and the hydrophobic natured pyrrolidinium cation based ILs exhibit enhanced solubility in water and when this is compared with other ILs, it is much more soluble than piperidinium based ILs, whilst less soluble than imidazolium and pyridinium based ILs.

The investigation of toxicity and bio-degradability for ILs are very important. In recent years they are being used in various industries especially, pharmaceutical and greener solvents industries. It was found that most of the quaternary pyrrolidinium cations are degradable. Pure *Corynebacterium* sp. and *Sphingomonas paucimobilis* or isolated enzymes readily degrades pyridinium based ILs

(80-100 % degradation) including long chain alkyl substitutions. In about 3 cases out of 10, unwanted accumulation of metabolites occurs during biodegradation processes [96]. On the contrary, pyrrolidinium based ILs are also readily biodegradable from longer alkyl chain to lower alkyl chain substitution, for example, an ethyl substituent is not readily biodegradable but a butyl and octyl substituted quaternary pyrrolidinium compounds are readily biodegradable [97]. The toxicity of the ILs can be reduced significantly using oxygenated alkyl chains instead of alkyl substitutions in the pyrrolidinium cation. Algae are not affected by this class of ILs due to their less toxic in nature. Furthermore, these ILs were tested with crustaceans and the results confirm that pyrrolidinium ILs with alkoxy substitutions were less toxic than the alkyl analogues [98].

Additionally, some of the mixtures of pyrrolidinium based ILs with the common cations butyl-1-methylpyrrolidinium ($[C_4MPyrr]^+$) or 1-ethyl-1-methylpyrrolidinium ($[C_2MPyrr]^+$) were investigated: $[C_4MPyrr]Cl$ + $[C_4MPyrr]Br$; $[C_4MPyrr]Br$ + $[C_4MPyrr][BF_4]$; $[C_4MPyrr]Cl$ + $[C_4MPyrr][BF_4]$; and $[C_2MPyrr][NTf_2]$ + $[C_2MPyrr][BF_4]$ (where $[NTf_2]$ = bis(trifluoromethyl sulfonyl) amide) [99]. Moreover, some other important pyrrolidinium based ILs have been established such as $[pyr][C_7CO_2]$ [100], $[EMpyr][ESO_4]$ [101], $[BMpyr][CF_3SO_3]$ [102-104], $[BMpyr][N(CN)_2]$ [100, 104] and [BMpyr][SCN] [105].

The main interest of Pyrrolidinium ionic liquids (PyrILs) are their outstanding electrochemical properties. The N-butyl-N-methyl pyrrolidinium bis(trifluoromethyl sulfonyl) imide ($BMPyNTf_2$) (Fig. 3c) IL is one of an important pyrrolidinium based IL that was reported [106]. The oxide, Eu_2O_3, and perhaps other oxides of lanthanides and actinides can be conveniently dissolved by treating with $HNTf_2$ followed by dilution in $BMPyNTf_2$, which could act as the electrolytic medium for non-aqueous reprocessing application. The determination of toxic chemical species in the environment is not easy, so there is increasing demand for simple, selective and inexpensive methods. RTILs could avoid these problems by replacing the conventional electrochemical solvents. Novel N,N-dimethyl pyrrolidinium dicyanamide ($[C_1mpyr][N(CN)_2]$) (Fig. 3b), N-methyl-N-ethyl pyrrolidinium bis(trifluoro methane sulfonyl)imide (Fig. 3a), and N-methyl-N-ethyl pyrrolidinium iodide (Fig. 3d) ILs were synthesized and used for development of dye-sensitized solar cells due to the stability and electrolytic nature of PyrILs. [107-110]. DCA anion based PyrILs such as N-methyl-N-propyl pyrrolidinium dicyanamide (Fig. 4a), N-butyl-N-methyl pyrrolidinium dicyanamide (Fig. 4b) and N-methoxy ethyl-N-methyl pyrrolidinium dicyanamide

(Fig. 4c), have been used in placed of organic solvents as electrolytes in electric double layer capacitors (EDLCs) because of their strong electrochemical properties [111].

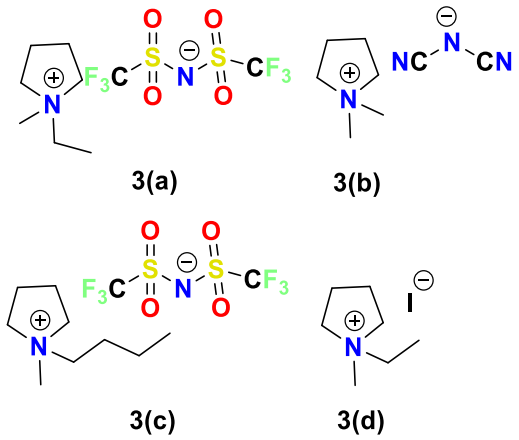

Figure 3: a) 1-Methyl-1-ethylpyrrolidinium bis(trifluoro methane sulfonyl)imide, b) N, N -Dimethyl pyrrolidinium dicyanamide ([C_1mpyr][$N(CN)_2$]), c) N- Butyl-N- methyl pyrrolidinium bis (trifluoro methyl sulfonyl) imide (BMPyNTf_2) and d) 1-Methyl-1-ethyl pyrrolidinium iodide

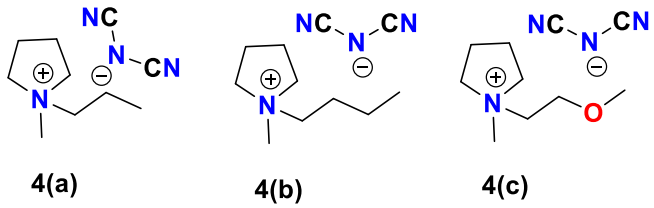

Figure 4: a) N-Methyl-N-propyl pyrrolidinium dicyanamide, b) N-Butyl-N-methyl pyrrolidinium dicyanamide and c) N-Methoxy ethyl-N-methyl pyrrolidinium dicyanamide

The anionic effect plays an important role in Li-S battery electrolyte solutions with N-methyl-N-butyl-pyrrolidinium ILs [112, 113]. The combination of organic electrolytes with PyrILs like C_4mpyr-TFSI leads to capacity retention during cycling and the polysulfide stabilization occurs due to the performance of ILs [114]. $LiNO_3$ additives in the PyrILs leads to higher efficiency with the solid electrolyte interphase in the lithium-sulphur battery [115]. In a largely parallel stream of research, $LiNO_3$ has come to be known as an additive for improving Li-S battery performance through its influence on protecting the lithium anode and beneficial interaction with the polysulfide shuttle. It was found that the PyrILs develop synergistic effects in a hybrid electrolyte (HE), for instance, 38 % of N-methyl-N-propyl-pyrrolidinium bis(trifluoromethane sulfonyl) imide ([C_3mpyr][TFSI]) with the conventional electrolyte mixtures such as $LiPF_6$ and alkyl carbonate solvents act as a better electrolyte compared traditional electrolytes [116]. PyrILs were used in

rechargeable IL based lithium ion batteries, other electrochemical devices and electrochemical development industries [85, 117-120].

The conductor like screening model for real solvents (COSMO-RS) was used to predict the liquid-liquid equilibria (LLE) for [PMpyr][NTf_2] and [BMpyr][NTf_2] with water [93, 122]. Toxic aromatic compounds such as benzene, toluene, ethylbenzene and xylene were separated from a reformate fraction using novel 2-oxopyrrolidinium based ILs such as $[BMpyr]^+[Br]^-$ ILs [123, 124]. PyrILs have excellent extracting properties, therefore it can be used for extraction of olefins from paraffin, separation of sulphur or nitrogen compounds from aliphatic hydrocarbons with great selectivity, extraction of Cu(II) ions and finally extraction of cycloalkanes from cycloalkenes at infinite dilutions. The partial molar excess Gibbs free energy, $\Delta G_1^{E,\infty}$, enthalpy, $\Delta H_1^{E,\infty}$ and entropy term T_{ref} $\Delta S_1^{E,\infty}$ at infinite dilution over the range of temperatures (308.15 to 378.15) K were computed from experimental data [125, 126]. Compared with imidazolium ILs, PyrILs are more eco-friendlier.

The current advanced development of sensor manufacturing, the thermophysical properties of ILs or ionic liquid carbon nanomaterial (IL-CNM) hybrids, incorporating the biologically-derived component to measure and detect the analyte, are called biosensors. [127, 128]. Due to the strong attractive and specific properties of ILs, they have been using in pharmaceutical and biomedical applications [129-131], as electrolytes in batteries [132-134], fuel cells [135, 136], nanotechnology [137, 138], polymerization [139-141] as well as industrial and technical applications [142-149]. PyrILs are chemically more stable, biologically active and environmentally readily biodegradable, therefore researchers synthesized herbicidal active unique pyrILs with phenoxy carboxylate anions, which is cheap, reactive and act as an environmentally friendly herbicide [150].

Conventional organic solvents are one of the important causes of environmental pollution, therefore RTILs are used as an alternative green solvent for the metathesis of oleo chemical feedstocks [151]. Pyrrolidinium based ILs are used as a green solvent for the extraction of aromatic compounds such as benzene from aliphatic hydrocarbon mixtures [124].

The capture and separation of CO_2 is a one of the important process to reduce global warming impact on the environment. The polymerization of ILs to synthesize polyionic liquids are very useful for the manufacturing of active membranes. These membranes are used in fuel cells and CO_2 capture. For example, a composite membrane containing N-ethyl-N-methyl-pyrrolidinium

fluoro hydrogenate as IL and poly (vinylidene fluoride hexafluoro propylene) as copolymer were used for non-humidified fuel cells [152]. High-performance membranes were developed using cyano counter anions based new polymeric pyrrolidinium ILs for the separation of CO_2 via post-combustion method [153]. The low volatility and significant chemically tunable nature of task specific ionic liquids (TSILs), led to the design and development of ILs for their specific and remarkable affinity for CO_2 over other fuel gases. These reasons have stimulated attention on ILs as an alternative media for CO_2 capture and separation [154-158].

Generally, ILs have outstanding catalytic activities due to their excellent thermophysical properties and ionic nature in a liquid state, which facilitates electron transfer movements. The recovery and recycling of IL, is easy because they are soluble in water and have low vapour pressures. The IL of $[HNMP]^+[HSO_4]^-$ was used for the conversion of styrene oxides to 2-phenylnaphthalenes. In this reaction, the ILs act as recyclable Brønsted acids catalyst [159]. PyrILs also have a highly effective catalytic nature, good recovery and recycling properties with acceptable costs compared with other ILs. For instance, N-butyl-N-methyl pyrrolidinium triflate is a simple and an effective catalyst for the direct asymmetric aldol reaction of cyclic ketones with aromatic aldehydes [160]. ILs are not only used as catalysts in organic reactions but they also act as solvents as well. [161-163].

The thermophysical and thermodynamic properties of binary mixtures of pyrILs with molecular solvents were determined. N-butyl-N-methyl-2-oxopyrrolidinium bromide IL was synthesized and characterized by FTIR and NMR spectroscopic techniques. Furthermore, the thermophysical properties of this IL and its binary mixtures with either water or methanol was investigated at various temperatures [164]. It was found that effect of transfer and storage of heat may change with concentration of mixtures, temperature and pressure [165]. The thermodynamic properties of binary mixtures of N-butyl-N-methyl pyrrolidinium dicyanamide IL with molecular solvents were examined and the experimental data were modelled with the PC-SAFT equation [166]. The phase diagrams and thermodynamic properties of binary mixture systems of {N-propyl-N-methyl pyrrolidinium trifluoro methane sulfonate (triflate) $[PMpyr][CF_3SO_3]$ + water or alcohol (1-butanol, 1-hexanol, 1-octanol and 1-decanol)} were investigated and they got good results in terms of interactions and the data were plotted [167].

This investigation has been carried the compatibility, miscibility and interactions of IL with either water, alcohol or carboxylic acids. Many industries such as the batteries, pharmaceutical, and chemical industries use ILs in their processes. The compatibility of ILs with other solvents be determined from the experimental data obtained. Furthermore the ILs are generally highly viscous, so the use of either water, alcohol or carboxylic acid to reduce that properties without affecting the nature of the ILs would be ascertained for possible for commercial applications. Since ILs are expensive, therefore using relatively cheap solvents like water or other organic solvents will help to reduce cost. In addition there are negligible side effects and eco-friendly as well. Water is the ‘‘greenest’’ solvent; its adventitious presence influences the performance of ILs, sometimes dramatically with consequences for reactions that are carried out therein [168-170]. Therefore it is important to understand the properties of these mixtures, in particular solvation, at the molecular level [171-173].

The epoxy group is widely used because of its high reactivity and good specific properties (ionic conductivity, aqueous solubility, thermodynamic stability and electrochemical/chemical durability): therefore, epoxy functionalized compounds have merited much attention. For instance, *Jayalak-shmi et al.* [174] synthesized high performance cellulose acetate membranes using epoxy functionalized poly(ether-sulfone), which improved the membrane morphology, pure water flux, water content porosity, hydrophobicity as well as a remarkable effectiveness in removing chromium ions. *Sydlik et al.* [175] synthesized epoxy-functionalized multi-walled carbon nanotubes (EpCNTs) by multiple covalent functionalization method, which improved adhesive properties and notably increased lap shear strength compared to commercial epoxy. *Dou et al.* [176] prepared epoxy-functionalized magnetic polymer core-shell microspheres with high magnetic responsiveness and a single hydrophilic monomer. The combination of the epoxy group and magnetic properties introduces the microspheres to a wide range of applications in stabilizers, targeted drug delivery and biological detection [177]. In our previous studies, epoxy propyl dodecyl dimethyl ammonium chloride [178], diethyl-2,3-epoxypropyl-[3-methyldimethoxyl] isopropyl ammonium chloride and mono epoxy-terminated polydimethylsiloxane [179] were synthesized and applied to modify gelatin, a renewable and biodegradable material. Therefore, the synthesis and property investigation of epoxy functionalized ILs will be more useful in future.

Due to relatively few reports available in the literature regarding epoxy substituted ionic liquids, this provided the motivation for this research work. Current epoxy functionalised compound while significantly improved over earlier materials have lower flammability issues, especially in confined environments.

Researchers developed IL-bonded graphene based carbon nanotube gel on graphene paper: Pt(Au) alloy nanoparticles were loaded to make high-performance flexible electrodes for electrochemical bio-sensing of blood glucose [180]. The investigations of tramadol (TRA) in pharmaceutical and biological samples were done using a new glassy carbon electrode modified with ILs and nanofibers [181]. The 1,3-dipropylimidazolium bromide IL was used as a conductive binder for synthesizing a new $CuFe_2O_4$-modified highly sensitive paste electrode, which was utilized for the selective determination of adrenaline in real samples [182]. A highly selective sensor which is an IL modified nanostructure material, was developed for the detection of vitamin C and nicotinamide adenine dinucleotide (NADH). This sensor was used to determine vitamin C selectively in the presence of NADH [183]. A selective sensor for the determination of 4-chlorophenol, in the presence of nitrite, was made using a carbon paste electrode by a combination of graphene oxide and NiO NPs modified with the IL [184]. Recently, an IL-altered $ZnFe_2O_4$ carbon paste electrode was revealed for the sensing of the 5-fluorouracil anticancer drug [185]. Additionally, high performance micro-supercapacitors were created using protic IL-adapted diamond-coated SiNW nanostructured electrode [186].

The high-performance anode material, a combination of Fe_3O_4/void/N-doped carbon, was established for a Li-ion battery which showed outstanding reversible capacity [187]. The IL was used as a dispersing phase for superparamagnetic Fe_3O_4 NPs to prepare a magnetically responsive pickering emulsion [188]. Ethylene glycol was oxidized and reduced using a unique synthesized gold-platinum alloy nano dendrites as an effective electrocatalyst [189]. Fe_3O_4 NPs were bonded with ILs to synthesize an effective recyclable catalyst for the Mannich reaction under ultrasonic irradiation and also for the synthesis of polyhydroquinolines [190, 191]. A heterogeneous catalyst which was an iron (III)-doped IL matrix-immobilized mesoporous silica NP, was synthesized. It was a successful recyclable catalyst for pyrimidine synthesis in water [192]. An innovative carbon IL electrode modified with electrodeposited palladium NPs was used as an efficient electrocatalyst to investigate and quantify isoniazid [193]. A metal NPs-decorated ILs were act as effective electrocatalysts. For example, the IL/metal sputtering method and tunable electrocatalytic material

were developed using Pt-supported Au NPs monolayer on IL [194]. Chemo selective effective reduction of nitroarenes to aniline based compounds were performed using an iron metal-immobilized IL heterogeneous catalyst [195]. Dispersed graphene-supported Au and Fe_3O_4 NPs were developed as an efficient catalyst for the catalytic conversion of 4-nitrophenol to 4-aminophenol [196]. Ultra-small CuNi NPs were spread over graphene layers to synthesize a stable nanocomposite for the reduction of aromatic nitro compounds [197].

The IL, 1-octyl-3-methylimidazolium hexafluoro phosphate was used for the liquid-liquid micro extraction of silver NPs in water [198]. Furthermore, applications have emerged using the combination of ILs and NPs hybrid systems [199]. The nanomaterial (BNNSs/AgNPs) which was reported by *Wang, F. et al.* shows high thermal conductivity due to the composition of the material such as silver NPs deposited on h-boron nitride nanosheets [200]. Additionally, a silver NPs-decorated h-boron nitride nanosheet based polymer nanocomposite with high thermal conductivity was developed [201]. The thermostability of the nanomaterials which were composited by the ILs and nanoparticles have excellent thermostability. Generally nanoparticles are less thermostable, but when using IL to make nanomaterial it will be thermally stable due to IL being strongly bonded with NPs, as well as IL develops a layer over the NPs

6 Chapter 3

6.1 Synthesis of Ionic Liquids

Most ILs can easily be synthesized by common methods, which are outlined in Fig. 5.

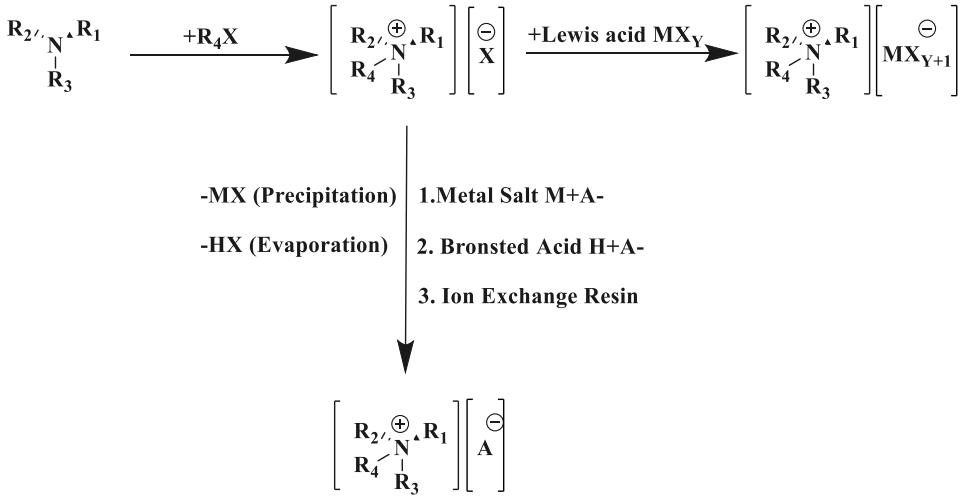

Figure 5: *Synthetic paths for preparing quaternary ammonium ionic liquids*

Where, R_1, R_2, R_3, R_4 are organic substituting groups such as alkane, alkene, alkyne and aromatic compounds, M = metal ion, X = anion, A = sulfate, phosphates.

Generally, ILs are synthesizing from amines, phosphates or sulphonates depending on what class of ILs are required (Fig. 5). The quarterisation reaction of amines (NR_3) such as alkylation and functional group substitution with an organic molecule, attached by appropriate reagents (RX) to obtain the corresponding ILs, is the first step. This is the first generation ILs. The drawback of this method is that it is not possible to synthesize ILs with preferred anions since halides might be the anions used for these types of ILs. Therefore, anion exchange reactions or metathesis reactions are necessary to obtain the desired anions. The metathesis reaction or Lewis acid (MXy) is used to replace the existing anion while reacting with previously synthesized ILs. Metal salt (MA), Brønsted acid (HA) or ion exchange resin is used for metathesis reactions. Currently, many companies such as Sigma-Aldrich, Fluka, Acros Organics, Merck, Solvent Innovation, Covalent Associates and Waco are involved in the production and sale of commercial ILs as shown in Table. 3.

Imidazole plays a vital role in the field of ILs, and a number of imidazolium ILs with good stability were reported. The reasons are ease to synthesis, increased yields, excellent stability, and their wide range of applications. 1- Methyl imidazole reacts with dimethyl carbonate to give the 1,3-dimethylimidazolium-2-carboxylate zwitterion with high yield as reported by *Holbrey, J. D et al.* in 2003 [164]. The imidazolium based ILs were synthesized from their zwitterions using microwave or ultrasonic techniques. These techniques especially help to avoid solvent and excess reagent for the substitution reaction in synthesis, reduces the reaction time and improves the quality in terms of purity and yield [1, 10, 202-205]. The presence of trace quantities of water, halides, residual solvents, acids, unreacted starting materials or metal salts could be the impurities that were encountered in the synthesis of ILs. These contaminants which were strongly affect the physical and chemical properties of the ILs were reported by Seddon and co-workers [202-206]. Halide contaminations normally increase the viscosity, while water or co-solvents impurities decrease the viscosity of the IL [206].

Generally, the method of purification for ILs is difficult due to their thermophysical properties. In particular, only a few methods are available to purify ILs, viz., decolourisation with activated charcoal, column chromatography with alumina or silica gel, crystallization, solvent washing or distillation as in the current study [207-210]. SWOT (Strengths, Weaknesses, Opportunities and Threats) analyses provide a critical assessment of the sustainability of IL and this was the first reported purification method by Seddon and Co-worker. Researchers used this method to find the drawbacks in existing method of preparation and purifications and determined the preferred routes to optimize the production parameters for ILs [211].

6.2 Commercial ionic liquids manufacturing industries

Table 3: Overview of chemical processes and relevant applications of ionic liquids and their manufacturing industries.

Company	Reaction Process	Application of IL as	Scale
Iolitch (Ionic liquids technologies)	Electrolytes, Analytics, Heat transfer, Process Technology, Functional fluids.	Batteries, Supercaps, solvent, Photonics, Performance additive and fuel cells	Commercial
BASF	BASILTM (Biphasic Acid Scavenging utilizing ILs), Chlorination, Extractive distillation (Breaking water-ethanol and water-tetrahydrofuran azeotropes),	Auxiliary, solvent, Extractant,	Commercial
Eastman Chemical	Production of 2,5-dihydrofuran	Catalyst	Commercial
TCI Europe N. V.	Bioscience, Enzymes and Antibodies and Glycoscience.	Pharmaceuticals	Commercial
Scionix	Electrolytes, Analytics.	Metal Plating, Electro polishing, Metal Reprocessing, and Phase transfer media.	Commercial
Sigma-Aldrich	Analytics, synthesis,	Catalyst, solvent	Commercial
Eli Lilly	Cleavage of ethers	Catalyst/ reagent	Pilot
Degussa	Hydrosilylation, Compatibilizer	Solvent, Performance additive	Commercial
Arkema	Fluorination	Solvent	Commercial
IFP (Axens)	Olefin dimerization (Dimersol process)	Solvent	Commercial
Chevron Phillips	Olefin oligomerization	Catalyst	Commercial
University of Twente	Extraction	Extractant	Pilot
Air Products	Storage of gasses (Phosphine (PH_3), arsinarsine (AsH_3) and boron trifluoride (BF_3)	Liquid support for PH_3 and	Pilot
Linde	Gas compression	Liquid piston	Pilot
Central Glass Company	Sonogashira coupling reaction (to produce pharmaceutical intermediates	Catalyst	Commercial
SASOL	Metathesis and Olefin trimerisation	Solvent	Commercial
PetroChina	Alkylation	Catalyst	Commercial
BP	Aromatic alkylation	Catalyst	Commercial

6.3 Thermophysical Properties

Generally, the properties of ILs are dependent on the ions, which are present in the IL and it may be a either cation, anion or the composition of both. These ions influence the physical and chemical properties of ILs. It might also vary with the type of ILs or functional groups. For instance, some of them are related to cations whilst others may be influenced by anions. The most important thermophysical properties are ρ, u, η and n, these properties can be tuned by specific cations, anions and substituting groups [212-214]. The thermodynamic, acoustic and transport properties of ILs and liquid mixtures are used to study the molecular interactions between the various components of the mixtures and also to understand engineering applications concerning heat transfer, mass transfer and fluid flow. In chemical process industries, materials are normally handled in fluid form and as a consequence, the physical, chemical and transport properties of fluids, assume importance. Thus, data on some of the properties associated with the liquids and liquid mixtures like density, viscosity, refractive index and ultrasonic velocity find extensive application in solution theory and molecular dynamics.

Furthermore, binary or ternary systems of ILs are made via the mixing of various other components of ILs to obtain different physical and chemical properties. The unsymmetrical ions play an important role in lowering the melting point because of the charge distribution over a large volume, ILs have zero vapour pressure and therefore it will not easily evaporate but after a certain temperature it will be decomposes. The influence of the anion plays a vital role in thermal stability. Ionic liquids are popular and their applications also vast due to their unexpected thermophysical properties. These occur especially after the invention of the third generation ILs or TSILs. Eventually, the properties of these ILs are tunable, therefore, researchers are interested in the development of this class of ILs. Furthermore, they help to improve the biological properties of drugs [215, 216].

Normally, ILs are miscible with polar solvents, but not with non-polar solvents. The reason is that the anions influence the solubilizing effect significantly more than cations. However, the substituted alkyl group chain length also helps to fine tune the solubility. The non-polar solvents are miscible with ILs which contain longer alkyl chain substituents. More importantly, ILs generally possess multiple solvation interactions [217], enhanced H-bond basicity [218] and H-bonding interaction [219, 220]. Previously researchers, synthesized three new long-chain

carboxylate ILs with asymmetric phosphonium cations that had relatively low viscosity and good thermal stability, and exhibited very high solubility and excellent selectivity for hydrocarbons with different carbon number at ambient condition [221]. The solubility of ILs in water is a desirable and significant property, especially in industrial applications and these are strongly influenced by the anions. Usually, ILs having common anions such as halides, tetrafluoro borate and triflate are miscible with water, whilst ILs containing hexafluoro phosphate and bis(trifluoromethyl sulfonyl) imide anions are immiscible with water. Most of the ILs are non-flammable and recyclable. The unique properties of ILs are their negligible vapour pressure, non-flammability, wide chemical/electrochemical/thermal stability, high ionic conductivity, good tunable solubilizing nature, liquid crystal structure, high electro-elasticity, high heat capacity and hydrophobicity [24, 222]. These are the prime reasons for using ILs in a wide range of applications. The structure of ILs have a significant impact on their physical properties. The standard uncertainties related to the measurements of ρ, u, η, temperature and pressure are estimated to be $\pm 2.0 \times 10^{-4}$ g·cm^{-3}, ±1.0 m·s^{-1}, and ±1.0 mPa.s, ± 0.01 K and 0.09 kPa respectively. The estimation of uncertainty excludes the effects of minor impurities due to ILs sometimes containing a bit of water, and it may affect the uncertainty.

6.3.1 Density

The mass of the substance per unit volume is called density. Density is one of the most important properties for academic as well as industrial research, due to the fact that this is the basic property used to calculate other theoretical thermodynamic properties, and if it is intended to use ILs for industrial research and development, that process will require these properties. Normally ILs are denser than water. When the alkyl chain length of the substituting group in cation is increased, the associated density of the corresponding ILs could be decreased [223-225]. The equation (6.1) is defined as the calculation of the density (ρ) as follows:

$$\rho = \frac{M}{V} \qquad (6.1)$$

Where *M* stands for the molecular weight of the compound. For a mixture, a weighted average of the molecular weights of the compounds and here the molar volume (V) is used in the numerator of equation (6.1).

ILs containing anions and their molar masses have a substantial effect on the density. For example, the pyrrolidinium ILs with the bis(trifluoro methane sulfonyl) amide [Tf_2N] anion is denser than the bis(methane sulfonyl) amide [Ms_2N] anion [144]. These anions have similar molecular weight, but fluorine atom has a larger mass compared to others and is a possible reason for this relatively large difference in densities. The density of the ILs decreases when increasing the water content for both hydrophobic and hydrophilic ILs as reported by Rogers and co-workers [216], while the presence of halide impurities influences the density of ILs by increasing their density as described in *Seddon et al.* [216].

6.3.2 Viscosity

Viscosity is the quantity that describes a fluid's resistance to flow. Generally, the viscosity of ILs and their mixtures is an important property, since in chemical industries as well as research laboratories developing chemical processes, mixing, stirring and pumping operations are strongly influenced by viscosity parameters. Viscosity plays a significant role in the application of ILs. Moreover, transport properties such as diffusion are also affected by viscosity. Viscosity varies widely from 20 cP to 30000 cP, therefore viscosity of the molecular solvents such as water and other common organic solvents are necessary to know [223, 226]. The two major types of viscosities are dynamic viscosity (η) and kinetic viscosity (ν). The resistance of a fluid to flow is a way to measure is known as dynamic viscosity. Viscosity relates to the force per unit area it is essential to maintain a unit velocity gradient among two equivalent planes a unit distance separately (*Riddick et al.* 1986). It is defined via Newton's law of viscosity as shown in equation (6.2)

$$\tau_{yx} = -\eta . \frac{\partial V_X}{\partial y} \qquad (6.2)$$

Where τ_{yx} is the force in the *x*-direction on a unit area perpendicular to the *y*-direction, $\frac{\partial V_X}{\partial y}$ is the component in the *x* direction of the velocity vector of the fluid, and η acts as the proportionality constant. Those fluids whose resistance to flow is well described by equation (6.2) are referred to as Newtonian fluids.

The method of calculating the dynamic viscosity (η) is derived from kinematic viscosity (ν) and density (ρ), using equation (6.3).

$$\eta = \nu\rho \qquad (6.3)$$

The viscosity of the ILs is strongly affected by the ions which are present in the ILs. Therefore, the choice of cations and anions are very important in the synthesis of the desired ILs. *Toduka et al*. explained the influence of alkyl chain groups and anions in imidazolium ILs [12, 227]. The hydrogen bonds are formed due to the symmetric nature of the anion and its ability of H-bond formation. These will be the stimulus for the viscosity of the ILs. Besides, the viscosities of the ILs are fundamentally influenced by the formation of hydrogen bonds but it also helps to strengthen their Van der Waals interactions [228]. The presence of the ions obviously affects the hydrogen bonds in their corresponded ILs. Ionic liquids containing fluorinated anions such as $[BF_4]^-$ and $[PF_6]^-$ are mostly viscous in nature, due to the capability for formation of complex between anions of ILs and solvent, high molecular weight and electro negativity of fluorine. The substituted longer alkyl chain of the ILs could be the reason for the increased Van der Waals forces between the cations, and this effect increases the viscosity, and therefore it satisfies the requirement of high energy in molecular motions. One of the significant disadvantage of the ILs is high viscosity, and this is a problem for some industrial applications. To addition of organic solvents overcomes this drawback and reduces the viscosity of the ILs drastically [216]. Moreover, the temperature also has strongly inverse effect on the viscosity of the ILs.

6.3.3 Speed of sound

The Anton Paar DSA-5000 M vibrating tube densitometer was used to measure the speed of sound for the ILs and their corresponding binary liquid mixtures. This instrument is more sensitive and its precision in sound velocity is ±1.00 m s^{-1}. Generally, speed of sound is independent of the sound amplitude, frequency or wavelength but it may only change with temperature. The interaction of (solvent + solvent), (solute + solvent) and (solute + solute) has been revealed through the u, so it can be used to understand the molecular interaction in liquid mixtures [229].

6.3.4 Refractive index

The Anton Paar refractometer was used to measure the refractive index of ILs and their binary mixtures with $\pm 2.10^{-4}$ precision at various temperatures. The temperature fluctuation of the refractometer is ±0.02 K, which gave a resolution better than ±0.1 K of measured values, with 0.02 K uncertainty in temperature. Degassed water and toluene were used to calibrate the instrument. The refractive index was investigated for the entire mole fraction ranges of IL mixtures at the different required temperatures. The behaviour of solutions and the force among the molecules are derived from electronic polarizability of molecules. It is measured using the n. The molar

refraction or molar polarizability was expressed by the electronic polarizability with n could being related to the equation of Lorenz-Lorentz [230].

7 Chapter 4

7.1 Thermodynamic properties

Thermodynamic properties are very useful for ILs, because it is a powerful tool to investigate the interactions amongst unlike molecules, H-bonding, interaction forces and ionic interactions in liquid mixtures. This study focusses on V_m^E, k_s, Δk_s and L_f for binary mixtures of ILs. These theoretical properties were computed from experimental ρ and u values. The strong interactions among molecules in a binary liquid mixture indicates that the competing effect plays a vital role to decrease the free spaces in the liquid mixtures; the negative Δk_s. Another reason for the negative thermodynamic computing value is due to how the structural effects influence in the geometrical fitting of one component into the another, because of the size differences and shape of the component molecules in the liquid mixtures. The positive values of thermodynamic data occur due to the chemical effects such as breaking of molecular association in the liquid mixtures as well as dispersion forces or weak interactions

7.1.1 Excess molar volume

The excess molar volume (V_m^E) is calculated from the experimental ρ data using the following equation (7.1).

$$V_m^E = \sum_{i=1}^{2} x_i M_i (\rho^{-1} - \rho_i^{-1}) \qquad (7.1)$$

Where x, M and ρ are the mole fractions, molecular weights, and densities of pure components, respectively.

The intermolecular interaction of a binary mixture is identified via V_m^E. The small magnitude in the change of the components in binary mixtures is recognized with the help of V_m^E. The composition, molecular size, shape of the component and temperature have a relatively strong influence on the behaviour or properties of the binary mixture in the solution. The differences in V_m^E reveal the interactions among the species, which are present in the binary solutions. The effects which impact on the excess molar functions arise as a result of the physical, chemical, and structural contributions. Ionic interactions, dispersive forces, dipolar interactions and hydrogen bonds occurred in the binary mixture of IL and solvents, due to the organic components molecules which are present in the ILs for example imidazolium, pyrrolidinium, pyridinium etc. which have the properties enhancing these interactions [231, 232]. The appropriate cubic equation of state (EOS)

model was used to predict the (vapour + liquid) equilibria from excess volume data and it was shown that the proposed models predict vapour pressure with greater accuracy and consistency. Water is a universal green solvent and it could completely solubilize the many ILs, albeit some of them only partially. ILs were separated after completion of their chemical processes using water as extracting agent and distillation processes [231, 232]. It was found that the addition of water in IL had a major effect on the physicochemical properties and applications of ILs [233]. The strong chemical effects of the specific interactions such as the formation of H-bonds, ion-dipole interactions, donor-acceptor complexes and strong dipole-dipole interactions among solvent and solute molecules resulted in negative values for the excess molar functions. Normally the positive V_m^E represent the weak interactions and breaking up of the molecular associates or dissociation.

7.1.2 Isentropic compressibility

The Newton-Laplace equation is used to calculate the isentropic compressibility (k_s) from experimental ρ and u. The k_s is a value which is characterized by the sound waves passing through a fluid, each microscopic volume fluctuating with the temperature and pressure, but the entropy of the whole system remaining constant. If the u is measured using a generator which is low frequency (DSA 5000M transducer produces approximately 3 MHz frequency) [234] it obeys the conditions, but at high frequency, there is absorption of sound waves as well as velocity dispersion, due to the coupling with molecular processes within the fluid [235, 236]. The sequence of compressions and rarefactions are produced by sound waves travelling via liquid mixture fluid.

The existing molecular interaction of the solution depends upon the composition of the liquid mixtures, and it is described by the variation of k_s [237, 238]. The molecules from solvents surrounded by IL, creates an electrostatic field and give a low value of k_s. At the same time, nonlinear k_s increases due to attraction and the nature of solute present in the liquid mixture. In particular, the influence of the chemical structure of the solute plays a vital role in k_s. The significant contribution to the formation of ion-dipole interactions and charge transfer complexes are established by the negative Δk_s.

Isentropic compressibility (k_s) defined as equation (7.2) as follows

$$k_s = \rho^{-1} u^{-2} \qquad (7.2)$$

The error is estimated for k_s and Δk_s, and it is found to be less than ±0.40 x 10^8 Pa^{-1} and ±1.00 x 10^8 Pa^{-1}, respectively.

As predictable, generally k_s increases with increasing temperature and decreases with increase concentration of the IL in the liquid mixtures. Similarly Δk_s also follows the same pattern/relationship in the same manner.

7.1.3 Deviation in Isentropic Compressibility

The deviation in isentropic compressibility (Δk_s) is defined from the k_s as illustrated in equation. (7.3)

$$\Delta k_s = k_s - \sum_{i}^{2} x_i k_{s,i} \qquad (7.3)$$

The u increases with increasing x_i of the liquid mixture and decreases with increasing temperature. The k_s is inversely proportional to the mole fraction and directly proportional to the temperature.

7.1.4 Intermolecular free length

The intermolecular forces, which in one way or another determine the said properties of liquids, consist of attractive forces and repulsive forces. These forces have opposite directions but are numerically equal under given external conditions. The attractive forces are dependent on the distance between what are called the centres of attraction of the molecules, whereas the repulsive forces are dependent on the distance between the surfaces of the molecules. The distance between centres of attraction is a property extremely difficult of definition, one reason being that this centre does not coincide with the geometrical centre of the molecules of the liquid (Hildebrand [239], Hudleston [240]). The distances between the surfaces of the molecules, on the other hand, have a clear physical significance, and thus lend themselves more easily to clear definition. For these reason, we may anticipate the simplest relations if the intermolecular free length is used.

The intermolecular free length L_f is given by the following equation (7.4) below.

$$L_f = k_j (k_s)^{1/2} \qquad (7.4)$$

Where k_j is the Jacobson's constant and is a temperature dependent constant. Its value is (93.875 + 0.375T) 10^{-8}.

L_f is calculated from equation 7.4. The L_f describes the distance between the adjacent molecules in the liquids mixtures. This distance depends upon the attractive and repulsive forces between the

solute and solvent molecules in the solutions. This is one of the methods which may be used to investigate the nature of the molecular interactions among the components in the liquid mixtures.

8 References

1. Wasserscheid, P., and Welton, T., Ionic Liquids in Synthesis. 2nd Edition, Wiley-VCH Verlag GmbH & Co. KGaA, Weinheim, 2007.
2. Rogers, R. D., and Voth, G. A., Ionic Liquids. Accounts of Chemical Research, 2007. **40**: p. 1077-1078.
3. Stark, A., and Seddon, K. R., Ionic liquids. Kirk-Othmer Encycl. Chemical Technology, John Wiley & Sons, Inc. New York. 2007.
4. Kadokawa, J. I., Ionic liquid as useful media for dissolution, derivatization, and nanomaterial processing of chitin. Green sustainable chemistry, 2013. **03**(02): p. 19-25.
5. Wang, W. T., Zhu, J., Wang, X. L., Huang, Y., Wang, and Y. Z., Dissolution behavior of chitin in ionic liquids. Journal of Macromolecule Sciences Part B, 2010. **49**(3): p. 528-541.
6. Xiao, W., Chen, Q., Wu, Y., Wu, T., and Dai, L., Dissolution and blending of chitosan using 1, 3- dimethylimidazolium chloride and 1-H-3-methylimidazolium chloride binary ionic liquid solvent. Carbohyhydrate Polymerization, 2011. **83**(1): p. 233-238.
7. Glas, D., Hulsbosch, J., Dubois, P., Binnemans, K., and De Vos, D. E., End of life treatment of poly(vinyl chloride) and chlorinated polyethylene by dehydrochlorination in ionic liquids. ChemSusChem, 2014. **7**(2): p. 610-617.
8. Winterton, N., Solubilisation of polymers by ionic liquids. Journal of Material Chemistry, 2006. **16**(44): p. 4281-4293.
9. Carmichael, A. J., Deetlefs. M., Earle, M. J., Fröhlich, U., and Seddon, K. R., Ionic Liquids as Green Solvents: Progress and Prospects. ACS Symposium Series, American Chemical Society, Washington DC, 2003. **856**: p. 14-31.
10. Welton, T., Room-temperature ionic liquids solvents for synthesis and catalysis. Chemical Reviews, 1999. **99**: p. 2071-2083.
11. Plechkova, N. V., and Seddon, K. R., Applications of ionic liquids in the chemical industry. Chemical Society Reviews, 2008. **37**: p. 123-150.
12. Tokuda, H., Hayamizu, K., Ishii, K., Susan, Md. A. B. H., and Watanabe, M., Physicochemical properties and structures of room temperature ionic liquids. 1. Variation of anionic species. Journal of Physical Chemistry. B, 2004. **108**(42): p. 16593–16600

13. Wasserscheid, P., Ionische Flüssigkeiten: Innovative lösungsmittel für die zweiphasenkatalyse. Chemie in unserer Zeit, 2003. **37**: p. 52-63.
14. Wilkes, S., Wasserscheid, P., and Welton, T., Ionic Liquids in Synthesis, 1st edition Wiley-VCH: Weinheim, Germany, 2003. p. 1.
15. Krossing, I., Slattery, J. M., Daguenet, C., Dyson, P. J., Oleinikova, A., and Weingärtner, H., Why are ionic liquids liquid? a simple explanation based on lattice and solvation energies. Journal of the American Chemical Society, 2006. **128**: p. 13427-13434.
16. Xue, H., Verma, R., and Shreeve, J. M., Review of ionic liquids with fluorine-containing anions. Journal of Fluorine Chemistry, 2006. **127**: p. 159-176.
17. Turner, E. A., Pye, C. C., and Singer, R. D., Use of ab initio calculations toward the rational design of room temperature ionic liquids. Journal of Physical Chemistry A, 2003. **107**(13): p. 2277-2288.
18. Varma, R. S., and Namboodiri, V. V., An expeditious solvent-free route to ionic liquids using microwaves. Chemical Communication, 2001. **7**: p. 643-644.
19. Huddleston, J. G., Visser, A. E., Reichert, W. M., Willauer, H. D., Broker, G. A., and Rogers, R. D., Characterization and comparison of hydrophilic and hydrophobic room temperature ionic liquids incorporating the imidazolium cation. Green Chemistry, 2001. **3**: p. 156-164.
20. Park, S., and Kazlauskas, R. J., Improved preparation and use of room-temperature ionic liquids in lipase-catalysed enantio and regioselective acylation's. Journal Organic Chemistry, 2001. **66**(25): p. 8395-8401.
21. Van Rantwiijk, F., and Sheldon, R. A., Bio-catalysis in ionic liquids. Chemical Reviews, 2007. **107**(6): p. 2757-2785.
22. Pârvulescu, V. I., and Hardacre, C., Catalysis in ionic liquids. Chemical Reviews, 2007. **107**(6): p. 2615-2665.
23. Haumann, M., and Riisager, A., Hydroformylation in room temperature ionic liquids (RTILs): Catalyst and Process Developments. Chemical Reviews, 2008, **108**(4): p. 1474-1497.
24. Martins, M. A. P., Frizzo, C. P., Moreira, D. N., Zanatta, N., and Bonacorso, H. G., Ionic liquids in heterocyclic synthesis. Chemical Reviews, 2008. **108**: p. 2015-2050.

25. Blanchard, L. A., Hancu, D., Beckman, E. J., and Brenecke, J. F., Green processing using ionic liquids and CO_2. Nature, 1999. **399**: p. 28-29.
26. Ohno, H., Electrochemical Aspects of Ionic Liquids. John Wiley & Sons Inc., Hoboken, New Jersey, 2005.
27. Earle, M. J., and Seddon, K. R., Ionic liquids. Green solvents for the future. Pure and Applied Chemistry, 2000. **72**(7): p. 1391-1398.
28. Freemantle, M., Designer Solvents: Ionic liquids may boost clean technology development. Chemical Engineering News, 1998. **76**: p. 32-37.
29. Swatloski, R. P., Spear, S. K., Holbrey, J. D., and Rogers, R. D., Dissolution of cellulose with ionic liquids. Journal of the American Chemical Society, 2002. **124**(18): p. 4974-4975.
30. Brown, R. J. C., Dyson, P. J., Ellis, D. J., and Welton, T., 1-Butyl-3-methylimidazolium cobalt tetracarbonyl [bmim][$Co(CO)_4$]: a catalytically active organometallic ionic liquid. Chemical Communication, 2001. **18**: p. 1862-1863.
31. Dyson, P. J., McIndoe, J. S., and Zhao, D., Direct analysis of catalysts immobilized in ionic liquids using electrospray ionization ion trap mass spectrometry. Chemical Communication, 2003. **4:** p. 508-509.
32. Larsen, A. S., Holbrey, J. D., Tham, F. S., and Reed, C. A., Designing ionic liquids: imidazolium melts with inert carborane anions. Journal of the American Chemical Society, 2000. **122**(30): p. 7264-7272.
33. Zhou, Z. B., Matsumoto, H., and Tatsumi, K., Low-melting, low-viscous, hydrophobic ionic liquids: 1-alkyl (alkyl ether)-3-methylimidazolium perfluoro alkyl trifluoro borate. Chemistry a European Journal, 2004. **10**(24): p. 6581-6591.
34. Hoffknecht, J.P., Drews, M., He, X. and Paillard, E., Investigation of the N-butyl-N-methyl pyrrolidinium trifluoromethanesulfonyl-N-cyanoamide (PYR_{14}TFSAM) ionic liquid as electrolyte for Li-ion battery. Electrochimica Acta, 2017. **250:** p. 25-34.
35. Talebi, M., Patil, R. A., Armstron, D. W., Physicochemical properties of branched-chain dicationic ionic liquids. Journal of Molecular Liquids, 2018. **256**: p. 247-255.

36. Sánchez-Ramírez, N., Assresahegn, B. D., Bélanger, D., and Torresi, R.M., A Comparison among Viscosity, Density, Conductivity, and Electrochemical Windows of N-Butyl-N-methyl pyrrolidinium and Triethyl-n-pentyl phosphonium Bis(fluorosulfonyl imide) Ionic Liquids and Their Analogues Containing Bis(trifluoromethylsulfonyl) Imide Anion. Journal of Chemical & Engineering Data, 2017. ***62***(10): p. 3437-3444.
37. Martins, V.L., Sanchez-Ramirez, N., Ribeiro, M.C., and Torresi, R.M., Two phosphonium ionic liquids with high Li+ transport number. Physical Chemistry Chemical Physics, 2015. ***17***(35): p. 23041-23051.
38. Nazet, A., Sokolov, S., Sonnleitner, T., Friesen, S., and Buchner, R., Densities, Refractive Indices, Viscosities, and Conductivities of Non-Imidazolium Ionic Liquids $[Et_3S][TFSI]$,$[Et_2MeS][TFSI]$,[BuPy][TFSI],$[N_{8881}][TFA]$, and $[P_{14}][DCA]$. Journal of Chemical & Engineering Data, 2017. ***62***(9): p. 2549-2561.
39. Srour, H., Darwich, W., Lindl, F., Husson, P., Rouault, H., and Santini, C., New route to carbonate-functionalized imidazolium and pyrrolidinium-based ionic liquids. New Journal of Chemistry, 2017. ***41***(20): p. 11915-11920.
40. Sanchez, L. G., Espel, J. R., Onink, F., Meindersma, G. W., and Haan, A. B. D., Density, viscosity, and surface tension of synthesis grade imidazolium, pyridinium, and pyrrolidinium based room temperature ionic liquids. Journal of Chemical & Engineering Data, ***54***(10): p. 2803-2812.
41. Bahadur, I., Sapei, E., Singh, S., Ebenso, E. E., and Redhi, G.G., Physicochemical properties of N-butyl-N-methyl-2-oxopyrrolidonium bromide and its binary mixtures with water or methanol. ACS Sustainable Chemistry & Engineering, 2015. **4**(2):p. 601-608.
42. Forsyth, S. A., Pringle, J. M., and MacFarlane, D. R., Ionic liquids-an overview. Australian Journal of Chemistry, 2004. **57**: p. 113-119.
43. Calloway, N. O., The friedel-crafts syntheses. Chemical Reviews, 1935. **17**: p. 327-392.
44. Walden, P., Ueber die Molekulargrosse., and elektrische Leitfahigkeit einiger geschmolzenen Salze., Bulletin de Academie Imperiale des Sciences de St.-Petersbourg. VI serie, 1914. **8**(6): p. 405-422.

45. Sugden, S., and Wilkins, H., CLXVII.-The parachor and chemical constitution. Part XII. Fused metals and salts. Journal of the Chemical Society (Resumed), 1929. **0**: p. 1291-1298.
46. Poole, C. F., and Poole, S. K., Extraction of organic compounds with room temperature ionic liquids. Journal of Chromatography A, 2010. **1217**: p. 2268-2286.
47. Marciniak, A. I., and Marciniak, A. I., Influence of cation and anion structure of the ionic liquid on extraction processes based on activity coefficients at infinite dilution. A review. Fluid Phase Equilibria, 2010. **294**: p. 213-233.
48. Han, D., and Row, K. H., Recent Applications of ionic liquids in separation Technology. Molecules, 2010. **15**: p. 2405-2426.
49. Hakkou, H., Carrie, D., Paquin, L., and Bazureau, J. P., Ionic liquid-phase organic synthesis (IOLIPOS) methodology applied to cross aldol reaction. Russian Journal of Organic Chemistry, 2011. **47**: p. 371-373.
50. Sawant, A. D., Raut, D. G., Darvatkar, N. B., and Salunkhe, M. M., Recent developments of task-specific ionic liquids in organic synthesis. Green Chemistry Letter Reviews, 2011. **4**: p. 41-54.
51. Ni, B., and Headley, A. D., Ionic-liquid-supported (ILs) catalysts for asymmetric organic synthesis. Chemistry of European Journal, 2010. **16**: p. 4426-4436.
52. Olivier-Bourbigou, H., Magna, L., and Morvan, D., Ionic liquids and catalysis: Recent progress from knowledge to applications. Applied Catalysis A: General, 2010. **373**(1-2): p. 1-56.
53. Lee, J. W., Shin, J. Y., Chun, Y. S., Jang, H. B., Song, C. E., and Lee, S. G., Toward understanding the origin of positive effects of ionic liquids on catalysis: formation of more reactive catalysts and stabilization of reactive intermediates and transition states in ionic liquids. Accounts of Chemical Research, 2010. **43**(7): p. 985-994.
54. Zhang, L. F., Fu, X. L., and Gao, G. H., Anion-cation cooperative catalysis by ionic liquids. ChemCatChem, 2011. **3**(8): p. 1359-1364.
55. Gordon, C. M., New developments in catalysis using ionic liquids. Applied Catalysis A: General, 2001. **222**(1-2): p. 101-117.
56. Hurley, F. H., and Wier, T. P., electrodeposition of metals from fused quaternary ammonium salts. Journal of the Electrochemical Society, 1951. **98**: p. 203-206.

57. Endres, F., and Zein El Abedin, S., Air and water stable ionic liquids in physical chemistry. Physical Chemistry Chemical Physical, 2006. **8**: p. 2101-2116.
58. Chum, H. L., Koch, V. R., Miller, L. L., and Osteryoung, R. A., Electrochemical scrutiny of organometallic iron complexes and hexamethyl benzene in a room temperature molten salt. Journal of the American Chemical Society, 1975. **97**(11): p. 3264-3265.
59. Robinson, J., and Osteryoung, R. A., An electrochemical and spectroscopic study of some aromatic hydrocarbons in the room temperature molten salt system aluminium chloride-n-butylpyridinium chloride. Journal of the American Chemical Society, 1979. **101**(2), p. 323-327.
60. Wilkes, J. S., Levisky, J. A., Wilson, R. A., and Hussey, C. L., Dialkyl imidazolium chloroaluminate melts: a new class of room-temperature ionic liquids for electrochemistry spectroscopy and synthesis. Inorganic Chemistry, 1982. **21**(3): p. 1263-1264.
61. Appleby, D., Hussey, C. L., Seddon, K. R., and Turp, J. E., Room-temperature ionic liquids as solvents for electronic absorption spectroscopy of halide complexes. Nature, 1986. **323**: p. 614-616.
62. Scheffler, T. B., Hussey, C. L., Seddon, K. R., Kear, C. M., and Armitage, P. D., Molybdenum chloro complexes in room-temperature chloroaluminate ionic liquids: stabilization of hexachloromolybdate(2-) and hexachloromolybdate(3-). Inorganic Chemistry, 1983. **22**(15): p. 2099-2100.
63. Wilkes, J. S., A short history of ionic liquids-from molten salts to neoteric solvents. Green Chemistry, 2002. **4**: p. 73-80.
64. Hussey, C. L., Room temperature molten salt systems. Advances in molten salt chemistry, 1983. **5**: p. 185-230.
65. Fry, S. E., and Pienta, N. J., Effects of molten salts on reactions. Nucleophilic aromatic substitution by halide ions in molten dodecyl tributyl phosphonium salts. Journal of the American Chemical Society, 1985. **107**(22): p. 6399-6400.
66. Boon, J. A., Levisky, J. A., Pflug, J. L., and Wilkes, J. S., Friedel-Crafts reactions in ambient-temperature molten salts. The Journal of Organic Chemistry, 1986. **51**(4): p 480-483.

67. Wilkes, J. S., and Zaworotko, M. J., Air and water stable 1-ethyl-3-methylimidazolium based ionic liquids. Journal of the Chemical Society, Chemical Communications, 1992. **13**: P. 965-967.
68. Wadekar, V.V., Ionic liquids as heat transfer fluids-An assessment using industrial exchanger geometries. Applied Thermal Engineering, 2017. 111: p.1581-1587.
69. Davis, J. H., Jr, Forrester, K. J., and Merrigan, T., Novel organic ionic liquids (OILs) incorporating cations derived from the antifungal drug miconazole. Tetrahedron Letters, 1998. **39**(49): p. 8955-8958.
70. Deetlefs, M., Fanselow, M., and Kenneth, R., Seddon ionic liquids: the view from mount improbable. RSC Advances, 2016. **6**: p. 4280-4288
71. Rogers, R. D., and Seddon, K. R., Ionic liquids-solvents of the future? Science, 2003. **302**(5646): p. 792-793.
72. Trulove, P.C., Mantz, R.A., Wasserscheid, P., and Welton, T., Electrochemical properties of ionic liquids, in: (Eds.), Ionic liquids in synthesis, second edition, Wiley, Wenheim, 2008. p. 141-174.
73. Handa, N., Sugimoto, T., Yamagata, M., Kikuta, M., Kono, M., and Ishikawa, M., A neat ionic liquid electrolyte based on FSI anion for electric double layer capacitor. Journal of Power Sources, 2008. **185**(2): p. 1585-1588.
74. Hagiwara, R., and Lee, V, Ionic Liquids for electrochemical devices. Electrochemistry, 2007. **75**: p. 23-34.
75. Kato, R., and Gmehling, J., Systems with ionic liquids: Measurements of VLE and $\gamma\infty$ data and prediction of their thermodynamic behavior using original UNIFAC, mod. UNIFAC (Do) and COSMO-RS (01). Journal of Chemical Thermodynamics, 2005. **37**(6): p. 603-619.
76. Nebig, S., Liebert, V., and Gmehling, J., Measurements and prediction of activity coefficients at infinite dilution ($\gamma\infty$), vapor-liquid equilibria (VLE) and excess enthalpies (HE) of binary systems with 1,1-dialkyl-pyrrolidinium bis(trifluoromethylsulfonyl)imide using mod. UNIFAC (Dortmund). Fluid Phase Equilibria, 2009. **277**(1): p. 61-67.
77. Brennecke, J.F., and Maginn, E. J., Ionic liquids: Innovative fluids for chemical processing. AIChE Journal, 2001. **47**(11): p. 2384-2389.

78. Holbrey, J. D., López-Martin, I., Rothenberg, G., Seddon, K. R., Sivero, G., and Zheng, X., Desulfurisation of oils using ionic liquids: Selection of cationic and anionic components to enhance extraction efficiency. Green Chemistry, 2008. **10**: p. 87-92.
79. Pereiro, A. B., and Rodríguez, A., An ionic liquid proposed as solvent in aromatic hydrocarbon separation by liquid extraction. AIChE Journal, 2010. **56**(2): p. 381-386.
80. Westerholt, A., Liebert, V., and Gmehling, J., Influence of ionic liquids on the separation factor of three standard separation problems. Fluid Phase Equilibria, 2009. **280**: p. 56-60.
81. Domańska, U., Redhi, G. G., and Marciniak, A., Activity coefficients at infinite dilution measurements for organic solutes and water in the ionic liquid 1-butyl-1-methylpyrrolidinium trifluoromethanesulfonate using GLC. Fluid Phase Equilibria, 2009. **278**: p. 97-102.
82. Poole C.F., Chromatographic and spectroscopic methods for the determination of solvent properties of room temperature ionic liquids. Journal of Chromatography, 2004. **1037**: p. 49-82.
83. Yang, G. M., Zhao, F. Q., and Zeng, B. Z., Facile fabrication of a novel anisotropic gold nanoparticle-chitosan-ionic liquid/graphene modified electrode for the determination of theophylline and caffeine. Talanta, 2014. **127**: p. 116-122.
84. Domańska, U., and Królikowska, M., Phase behaviour of 1-butyl-1- methylpyrrolidinium thiocyanate ionic liquid. Fluid Phase Equilibria, 2011. **308**: p. 55-63.
85. Marciniak, A., and Karczemna, E., Influence of cation structure on binary liquid-liquid equilibria for systems containing ionic liquids based on trifluoromethane sulfonate anion with hydrocarbons. Journal of Physical Chemistry. B, 2010. **114**: p. 5470-5474.
86. Salminen, J., Papaiconomou, N., Kumar, R. A., Lee, J. M., Kerr, J., Newman, J.; and Prausnitz, J. M., Physicochemical properties and toxicities of hydrophobic piperidinium and pyrrolidinium ionic liquids. Fluid Phase Equilibria, 2007. **261**: p. 421-426.
87. Corderí, S., Calvar, N., Gómez, E., and Domínguez, A., Capacity of ionic liquids [EMim][NTf_2] and [EMpy][NTf_2] for extraction of toluene from mixtures with alkanes: Comparative study of the effect of the cation. Fluid Phase Equilibria, 2012. **315**: p. 46-52.

88. Requejo, P. F., Gonzalez, E. J., Macedo, E. A., and Dominguez, A., Effect of the temperature on the physical properties of the pure ionic liquid 1-ethyl-3-methylimidazolium methyl sulfate and characterization of its binary mixtures with alcohols. Journal of Chemical Thermodynamics, 2014. **74**: p. 193-200.
89. Holbrey, J. D., and Seddon, K. R., The phase behaviour of 1-alkyl-3-methylimidazolium tetrafluoro borates; ionic liquids and ionic liquid crystals. Journal of Chemical Society Dalton Transition, 1999. **13**: p. 2133-2140.
90. Zhong, Y., Wang, H., and Diao, K., Cover image densities and excess volumes of binary mixtures of the ionic liquid 1-butyl-3-methylimidazolium hexafluoro phosphate with aromatic compound at T = (298.15 to 313.15) K. Journal of Chemical Thermodynamics, 2007. **39**: p. 291-296.
91. An, Y., Yu, H., and Zou, C. M., Rapid determination of pyrrolidinium ionic liquid cations by monolithic column-ion-pair chromatography with indirect ultraviolet detection, Chinese Journal of Analytical Chemistry, 2013. **41**: p. 1057-1062.
92. Zhang, R. Q., Yu, H., and Sun, X.J., Separation and determination of pyrrolidinium ionic liquid cations by ion chromatography with direct conductivity detection. Chinese Chemical Letters, 2013. **24**: p. 503-505.
93. Chao Guan, H. Y., Hydrophilic interaction liquid chromatography with indirect ultraviolet detection for the separation and quantification of pyrrolidinium ionic liquid cations. Chinese Chemical Letters, 2015. **26**: p. 1371-1375.
94. Freire, M. G., Ventura, S. P. M., Santos, L. M. N. B. F., Marrucho, I. M., and Coutinho, J.A.P., Evaluation of COSMO-RS for the prediction of LLE and VLE of water and ionic liquids binary systems. Fluid Phase Equilibria, 2008. **268**: p. 74-84.
95. Deng, Y., Beadham, I., Ghavre, M., Costa Gomes, M. F., Gathergood, N., Husson, P., Légeret, B. Quilty, B., Sancelmea, M., and Besse-Hoggan, P., When can ionic liquids be considered readily biodegradable? Biodegradation pathways of pyridinium, pyrrolidinium and ammonium-based ionic liquids. Green Chemistry, 2015. **17**: p. 1479
96. Neumann, J., Steudte, S., Cho, C. W., Thoming, J., and Stolte, S., Biodegradability of pyrrolidinium, morpholinium, piperidinium, imidazolium and pyridinium ionic liquid cations under aerobic conditions. Green Chemistry, 2014. **16**: p. 2174-2184.

97. Samori, C., Campisi, T., Fagnoni, M., Galletti, P., Pasteris, A., Pezzolesi, V., Protti, V., Ravelli, D., and Tagliavini, E., Pyrrolidinium-based ionic liquids: Aquatic eco-toxicity, biodegradability, and algal sub-inhibitory stimulation. ACS Sustainable and Chemical Engineering, 2015. **3**: p. 1860-1865.
98. Olga. S., and Héctor Rodríguez, M. S., Eutectic mixtures of pyrrolidinium-based ionic liquids. Fluid Phase Equilibria, 2016. **408**: p. 1-9.
99. Anouti, M., Vigeant, A., Jacquemin, J., Brigouleix, C., and Lemordant, D., Volumetric properties, viscosity and refractive index of the protic ionic liquid, pyrrolidinium octanoate, in molecular solvents. The Journal of Chemical Thermodynamics, 2010. **42**: p. 834-845.
100. Królikowska, M., Lipinski, P., and Maik, D., Density, viscosity and phase equilibria study of {ethylsulfate-based ionic liquid + water} binary systems as a function of temperature and composition. Thermochimica Acta, 2014. **582**: p. 1-9.
101. González, B., Calvar, N., Gómez, E., and Domínguez, A., Physical properties of the ternary system (ethanol + water + 1-butyl-3-methylimidazolium methyl sulfate) and its binary mixtures at several temperatures. The Journal of Chemical Thermodynamics, 2008. **40**: p. 1274-1281.
102. Vercher, E., Miguel, P. J., Llopis, F. J., Orchillés, A.V., and Martínez-Andreu, A., Volumetric and acoustic properties of aqueous solutions of trifluoro methyl sulfonate-based ionic liquids at several temperatures. Journal of Chemical Engineering Data, 2012. **57**: p. 1953-1963.
103. González, E. J., Domínguez, A., and Macedo, E. A., Physical and excess properties of eight binary mixtures containing water and ionic liquids. Journal of Chemical Engineering Data, 2012. **57**: p. 2165-2176.
104. Krolikowska, M., Zawadzki, M., and Krolikowski, M., Physicochemical and thermodynamic study on aqueous solutions of dicyanamide - based ionic liquids. Journal of Chemical Thermodynamics, 2014. **70**: p. 127-137.
105. Domanska, U., and Królikowska, M., Density and viscosity of binary mixtures of thiocyanate ionic liquids + water as a function of temperature. Journal of Solution Chemistry, 2012. **41**: p. 1422-1445.

106. Rao, C. J., Venkatesan, K. A., Nagarajan, K., Srinvasan, T. G., and Rao, P.R.V., Electrochemical behavior of europium (III) in N-butyl-N-methyl pyrrolidinium bis(trifluoro methyl sulfonyl)imide. Electrochimica Acta, 2009. **54**: p. 4718.
107. He, T., Feng Wang, Y., and Zeng, J. H., Stable, High-efficiency pyrrolidinium based electrolyte for solid-state dye-sensitized solar cells. ACS Applied Materials & Interfaces, 2015. **7**(38): p. 21381-21390.
108. Armel, V., Forsyth, M., MacFarlane, D. R., and Pringle, J. M., organic ionic plastic crystal electrolytes; A New class of electrolyte for high efficiency solid state dye-sensitized solar cells. Energy Environmental Science, 2011. **4**: p. 2234-2239.
109. Li, Q., Chen, X., Zhao, J., Qiu, L., Zhang, Y., Sun, B., and Yaan, F., organic ionic plastic crystal-based electrolytes for solid-state dye-sensitized solar cells. Journal of Material Chemistry, 2012. **22**: p. 6674-6679.
110. Li, Q., Zhao, J., Sun, B., Lin, B., Qiu, L., Zhang, Y., Chen, X., Lu, J., and Yan, F., High-temperature solid-state dye-sensitized solar cells based on organic ionic plastic crystal electrolytes. Advanced Materials, 2012. **24**: p. 945-950.
111. Wolff, C., Jeong, S., Paillard, E., Balducci, A., and Passerini, S., High power, solvent-free electrochemical double layer capacitors based on pyrrolidinium dicyanamide ionic liquids. Journal of Power Sources, 2015. **293**: p. 65-70.
112. Marzieh Barghamadi, Adam S., Best, Anand I., Bhatt, Anthony F., Hollenkamp, Peter J., Mahonc, Mustafa M., and Thomas, R., Effect of anion on behaviour of li-s battery electrolyte solutions based on N-methyl-N-butyl-pyrrolidinium ionic liquids. Electrochimica Acta, 2015. **180**: p. 636-644.
113. Morenoa, J. S., Deguchib, Y., Paneroa, S., Scrosatia, B., Ohnob, H., Simonetti, E., and Appetecchie. G. B., N-Alkyl-N-ethylpyrrolidinium cation-based ionic liquid electrolytes for safer lithium battery systems. Electrochimica Acta, 2016. **191**: p. 624-630
114. Zhang, S. S., New insight into liquid electrolyte of rechargeable lithium/sulfur battery, Electrochimica Acta, 2013. **97**: p. 226.
115. Marzieh Barghamadi, Adam S., Best, Anand I., Bhatt, Anthony F., Hollenkamp, Peter J., Mustafa Musameh, M., and Thomas. R., Effect of $LiNO_3$ additive and pyrrolidinium ionic liquid on the solid electrolyte interphase in the lithium sulfur battery. Journal of Power Sources, 2015. **295**: p. 212-220.

116. Sowmiya Theivaprakasama, D. R., and MacFarlaneb, S. M., Electrochemical studies of N-Methyl N-Propyl Pyrrolidinium bis(trifluoro methane sulfonyl) imide ionic liquid mixtures with conventional electrolytes in $LiFePO_4$/Li cells. Electrochimica Acta, 2015. **180**: p. 737-745.
117. Belhocine, T., Forsyth, S.A., Gunaratne, H.N., Nieuwenhuyzen, M., Nockemann, P., Puga, A.V., Seddon, K.R., Srinivasan, G., and Whiston, K., 2015. 3-Methylpiperidinium ionic liquids. Physical Chemistry Chemical Physics, **17**(16): p.10398-10416.
118. Sun, J., MacFarlane, R. D., and Forsyth, M., A new family of ionic liquids based on the 1-alkyl-2-methyl pyrrolinium cation. Electrochimica Acta, 2003. **48**: p. 1707-1711.
119. Baek, B., Lee, S., and Jung, C., pyrrolidinium cation-based ionic liquids with different functional groups: butyl, butyronitrile, pentenyl, and methyl butyrate. International Journal of Electrochemical Science, 2011. **6**: p. 6220-6234.
120. Golding, J., Forsyth, S., MacFarlane, R. D., Forsyth, M., and Deacon, G. B., Methane sulfonate and p-toluene sulfonate salts of the N-methyl-N-alkyl pyrrolidinium and quaternary ammonium cations: novel low cost ionic liquids. Green Chemistry, 2002. **4**: p. 223-229.
121. Forsyth, S. A., Fraser, K. J., Howlett, P. C., MacFarlane, R. D., and Forsyth, M., N-methyl-N-alkyl pyrrolidinium nonafluoro-1-butanesulfonate salts: ionic liquid properties and plastic crystal behavior. Green Chemistry, 2006. **8**: p. 256-261.
122. Freire, M. G., Neves, C. M. S. S., Carvalho, P. J., Gardas, R. L., Fernandes, A. M., Marrucho, I. M., Santos, L. M. N. B. F., and Coutinho, J. A. P., Mutual solubility's of water and hydrophobic ionic liquids. Journal of Physical Chemistry. B, 2007. **111**: p. 1382-1389.
123. Bahadur, I., Singh, P., Kumar, S., Moodley, K., Mabaso, M., and Redhi, G. G., Separation of aromatic solvents from oil refinery reformates by a newly designed ionic liquid using gas chromatography with flame ionization detection. Separation Science and Technology, 2014. **49**: p. 1883-1888.
124. Patricia, F., Requejo, E., Noelia Calvar, G., and Domínguez. Á., Application of pyrrolidinium-based ionic liquid as solvent for the liquid extraction of benzene from its mixtures with aliphatic hydrocarbons. Industrial & Engineering Chemical Research, 2015. **54**: p. 1342-1349.

125. Hsu, S. C. N., Su, C. J., Yu, F. L., Chen, W. J., Zhuang, D. X., Deng, M. J., Sun, I. W., and chen, P. Y., Extracting Cu(II) from aqueous solutions with hydrophobic room-temperature ionic liquid in the presence of a pyridine-based ionophore to attempt Cu recovery: A laboratory study. Electrochimica Acta, 2009. **54**: p. 1744-1751.
126. Domanska, U., Karpinska, M., and Zawadzki, M., Activity coefficients at infinite dilution for organic solutes and water in 1-ethyl-1-methylpyrrolidinium lactate. The Journal of Chemical Thermodynamics, 2015. **89**: p. 127-133.
127. Turner, A.P., Biosensors-sense and sensitivity, Science, 2000. **290**: p. 1315-1317.
128. Turner, A.P., Biosensors: sense and sensibility. Chemical Society Reviews, 2013. **42**: p. 3184-3196.
129. Sekhon, B. S., Ionic liquids based active pharmaceutical ingredients. ARS Pharmaceutical, 2013. **54**: p. 37−44.
130. Kumar, V., Parmar, V. S., and Malhotra, S. V., Structural modifications of nucleosides in ionic liquids. Biochimie, 2010. **92**: p. 1260-1265.
131. Hough, W. L., Smiglak, M., Rodríguez, H., Swatloski, R. P., Spear, S. K., Daly, D. T., Pernak, J., Grisel, J. E., Carliss, R. D., Soutullo, M. D., Davis, J. H. Jr., and Rogers, R. D., The third evolution of ionic liquids: active pharmaceutical ingredients. New Journal of Chemistry, 2007. **31**: p. 1429-1436.
132. Nguyen, N. L., and Rochefort, D., Electrochemistry of ruthenium dioxide composite electrodes in diethyl methyl ammonium-triflate protic ionic liquid and its mixtures with acetonitrile. Electrochimica Acta, 2014. **147**: p. 96-103.
133. Terasawa, N., and Asaka, K., High performance polymer actuators based on single-walled carbon nanotube gel using ionic liquid with quaternary ammonium or phosphonium cations and with electrochemical window of 6V. Sensors and Actuators, B, 2014. **193**: p. 851-856.
134. Sun, X., Do-Thanh, C. L., Luo, H., and Dai, S., The optimization of an ionic liquid-based TALSPEAK-like process for rare earth ions separation. Chemical Engineering Journal, 2014. **239**: p. 392-398.
135. Domańska, U., and Wlazło, M., Effect of the cation and anion of the ionic liquid on desulfurization of model fuels. Fuel, 2014. **134**: p. 114-125

136. Qiu, B., Lin, B., Qiu, L., and Yan, F., Alkaline imidazolium- and quaternary ammonium-functionalized anion exchange membranes for alkaline fuel cell applications. Journal of Material Chemistry, 2012. **22**: p. 1040-1045.
137. Minamimoto, H., Irie, H., Uematsu, T., Tsuda, T., Imanishi, A., Seki, S., and Kuwabata, S., Polymerization of room-temperature ionic liquid monomers by electron beam irradiation with the aim of fabricating three dimensional micropolymer/nanopolymer structures. Langmuir, 2015. **31**: p. 4281-4289.
138. Smith, A. M., Parkes, M. A., and Perkin, S., Molecular friction mechanisms across nanofilms of a bilayer-forming ionic liquid. Journal of Physical Chemistry Letter, 2014. **5**: p. 4032-4037.
139. He, H., Zhong, M., Adzima, B., Luebke, D., Nulwala, H., and Matyjaszewski, K., A simple and universal gel permeation chromatography technique for precise molecular weight characterization of well-defined poly (ionic liquids). Journal of the American Chemical Society, 2013. **135**: p. 4227-4230.
140. Jangu, C., and Long, T. E., Phosphonium cation-containing polymers: From ionic liquids to polyelectrolytes. Polymer, 2014. **55**: p. 3298-3304.
141. Zhang, H., Li, L., Feng, W., Zhou, Z., and Nie, J., Polymeric ionic liquids based on ether functionalized ammoniums and perfluorinated sulfonimides. Polymer, 2014. **55**: p. 3339-3348.
142. Li, J., Wang, P., Huang, J., and Sun, J., Design and application of a novel ionic liquid with the property of strengthening coenzyme regeneration for whole-cell bio-reduction in an ionic liquid-distilled water medium. Bio-resource Technology, 2015. **175**: p. 42-50.
143. Pisarova, L., Gabler, C., Dorr, N., Pittenauer, E., and Allmaier, G., Thermo-oxidative stability and corrosion properties of ammonium based ionic liquids. Tribology International, 2012. **46**: p. 73-83.
144. Li, Y., Wu, X., Wu, Q., Ding, H., and Yan, W., Ammonium-and phosphonium-based temperature control-type polyoxometalate ionic liquids. Dalton Transition, 2014. **43**: p. 13591-13595.
145. Bell, T. J., and Ikeda, Y., The application of novel hydrophobic ionic liquids to the extraction of uranium (VI) from nitric acid medium and a determination of the uranyl complexes formed. Dalton Transition, 2011. **40**: p. 10125-10130.

146. Aono, M., Abe, H., Takekiyo, T., and Yoshimura, Y., Protonated/deprotonated properties of a room temperature ionic liquid-water system: N, N-Diethyl-N-methyl-N-2-methoxyethyl ammonium tetrafluoroborate. Chemical Physics Letter, 2014. **598**: p. 65-68.
147. Hayyan, M., Mjalli, F. S., Hashim, M. A., and AlNashef, I. M., Generation of superoxide ion in pyridinium, morpholinium, ammonium, and sulfonium-based ionic liquids and the application in the destruction of toxic chlorinated phenols. Industrial & Engineering Chemical Research, 2012. **51**: p. 10546-10556.
148. Eguizábal, A., Lemus, J., Urbiztondo, M., Moschovi, A. M., Ntais, S., Soler, J., and Pina, M. P., Ammonium based ionic liquids immobilized in large pore zeolites: Encapsulation procedures and proton conduction performance. Journal of Power Sources, 2011. **196**: p. 4314-4323.
149. Sasi, R., Rao, T. P., and Devaki, S. J., Bio-based ionic liquid crystalline quaternary ammonium salts: properties and applications. ACS Applied Material & Interfaces, 2014. **6**: p. 4126-4133.
150. Syguda, A., Marcinkowska, K., and Materna. K., Pyrrolidinium herbicidal ionic liquids. RSC Advances. 2016. **6**: p. 63136-63142.
151. Priya. A. T., and Bassy. B. M., Room temperature ionic liquids as green solvent alternatives in the metathesis of oleochemical feedstocks. Molecules, 2016. **21**: p. 184.
152. Wilkes, J. S., Properties of ionic liquid solvents for catalysis. Journal of Molecular Catalysis A: Chemical. 2004, **214**(1): p. 11-17.
153. Liliana. C. T., MehmetIsik, C., David Mecerreyes, S. R. F., and Marrucho, I. M., Novel pyrrolidinium-based polymeric ionic liquids with cyano counter- anions: High performance membrane materials for post-combustion CO_2 separation. Journal of Membrane Science, 2015. **483**: p. 155-165.
154. Zhang, X., Zhang, X., Dong, H., Zhao, Z., Zhang, S., and Huang, Y., Carbon capture with ionic liquids: over view and progress, Energy Environmental Science, 2012. **5**: p. 6668-6681.
155. Ramdin, M., Deloos, T. W., and Vlugt, T. J. H., State of the art of CO_2 capture with ionic liquids, Industrial and Engineering Chemical Research, 2012. **51**: p. 8149-8177.

156. Wang, C., Luo, X., Luo, H., Jiang, D. E., Li, H., and Dai, S., Tuning the basicity of ionic liquids for equimolar CO_2 capture, Angewandty & Chemical International Edition, 2011. **50**: p. 4918-4922.
157. Wang, C., Luo, X., Zhu, X., Cui, G., Jiang, D. E., Deng, D., Li, H., and Dai, S., The strategies for improving carbon dioxide chemisorption by functionalized ionic liquids. RSC Advances, 2013. **3**: p. 15518-15527.
158. Wu, C., Senftle, T. P., and Schneider, W. F., First-principles-guided design of ionic liquids for CO_2 capture. Physical Chemistry Chemical Physics, 2012. **14**: p. 13163-13170.
159. Kishor, V. W., and Bhalchandra, M. B., Synthesis of 2-phenylnaphthalenes from styrene oxides using a recyclable Brønsted acidic $[HNMP]^+[HSO_4]^-$ ionic liquid. Green Chemistry, 2015. **17**: p. 4446.
160. Lombardo, M., Easwar, S., Pasi, F., Trombini, C., and Dhavale, D. D., Protonated arginine and lysine as catalysts for the direct asymmetric aldol reaction in ionic liquids. Tetrahedron, 2008. **64**: p. 9203-9207.
161. Qureshi, Z. S., Deshmukh, K. M., Bhor, M. D., and Bhanage, B. M., Bronsted acidic ionic liquid as an efficient and reusable catalyst for transesterification of β-ketoesters. Catalysis Communications, 2009. **10**: p. 833-837.
162. Deshmukh, K. M., Qureshi, Z. S., Nandurkar, N. S., and Bhanage, B. M., One-pot synthesis of β-amido ketones using Brønsted acidic ionic liquid as an efficient and reusable catalyst. Canadian Journal of Chemistry, 2009. **87**: p. 401-405.
163. Qureshi, Z. S., Deshmukh, K. M., and Bhanage, B. M., Applications of ionic liquids in organic synthesis and catalysis. Clean Technologies and Environmental Policy, 2014. **8**: p. 1487-1513.
164. Bahadur, I., Sapei, E., Singh, S., Ebenso, E. E., and Redhi, G. G., Physicochemical Properties of N-Butyl-N-methyl-2-oxopyrrolidonium Bromide and Its Binary Mixtures with Water or Methanol. ACS Sustainable Chemical & Engineering, 2016. **4**(2): p. 601-608.
165. Bahadur, I., and Deenadayalu, N., Densities and excess molar volume for the ternary systems (1-butyl-3-methylimidazolium methyl sulfate + nitromethane + methanol or ethanol or 1-propanol) at T = (303.15 and 313.15) K. S. South African Journal of Chemistry, 2013. **66**: p. 200-206.

166. Paduszyński, K., Vadimovna Lukoshko, E., Królikowski, M., Domańska, U., and Szydłowski. J., Thermodynamic study of binary mixtures of 1-butyl-1-methylpyrrolidinium dicyanamide ionic liquid with molecular solvents: New experimental data and modeling with PC-SAFT equation of state. Journal of Physical Chemistry. B, 2015. **119**: p. 543-551.
167. Domańska. U., Physico-chemical properties and phase behaviour of pyrrolidinium-based ionic liquids. International Journal of Molecular Sciences, 2010. **11**: p. 1825-1841.
168. Seddon, K. R., Stark, A., and Torres, M.J., Templated electrodeposition of Silver nanowires in a nanoporous polycarbonate membrane from a non-Aqueous ionic Liquid electrolyte. J. Pure Appl. Chem, 2000. **72**: p. 2275-2278.
169. Stark, A., Behrend, P., Braun, O., Müller, A., Ranke, J., Ondruschka, B., and Jastorff, B., Purity specification methods for ionic liquids. Green chemistry, 2008. **10**(11): p. 1152-1161.
170. Aparicio, S., Atilhan, M., and Karadas, F., Thermophysical properties of pure ionic liquids: review of present situation. Industrial & Engineering Chemistry Research, 2010. **49**(20): p. 9580-9595.
171. Martins, C. T., Sato, B. M., and Seoud, O. A. E., First study on the thermo-solvatochromism in aqueous 1-(1-butyl)-3-methylimidazolium tetrafluoroborate: a comparison between the solvation by an ionic liquid and by aqueous alcohols. The Journal of Physical Chemistry B, 2008. **112**(28): p. 8330-8339.
172. Sato, B. M., de Oliveira, C. G., Martins, C. T. and El Seoud, O. A., Thermo-solvatochromism in binary mixtures of water and ionic liquids: on the relative importance of solvophobic interactions. Physical Chemistry Chemical Physics, 2010. **12**(8): p. 1764-1771.
173. Freire, M. G., Carvalho, P. J., Gardas, R. L., Marrucho, I. M., Santos, L. M., and Coutinho, J. A., Mutual solubilities of water and the [Cnmim][Tf2N] hydrophobic ionic liquids. The Journal of Physical Chemistry B, 2008. **112**(6): p. 1604-1610.
174. Jayalakshmi, A., Rajesh, S., Senthilkumar, S., and Mohan, D., Epoxy functionalized poly (ether-sulfone) incorporated cellulose acetate ultrafiltration membrane for the removal of chromium ions. Separation and purification technology, 2012. **90**: p. 120-132.

175. Sydlik, S. A., Lee, J. H., Walish, J. J., Thomas, E. L., and Swager, T. M., Epoxy functionalized multi-walled carbon nanotubes for improved adhesives. Carbon, 2013. **59**, p. 109-120.
176. Dou, J., Zhang, Q., Ma, M., and Gu, J., Fast fabrication of epoxy-functionalized magnetic polymer core-shell microspheres using glycidyl methacrylate as monomer via photo-initiated miniemulsion polymerization. Journal of Magnetism and Magnetic Materials, 2012. **324**(19): p. 3078-3082.
177. Zhang, X., Hao, L., Sun, H., Chen, X., Jiang, W., Wu, J., Xu, M., and Pan, Q., Preparation of epoxy-functionalized magnetic polymer nanospheres for magnetically targeted radiotherapy. Journal of Macromolecular Science, Part A, 2015. **52**(3): p. 168-174.
178. Liu, Y. M., Cui, X., Hao, C. M., Tao, F. R., and Li, J. Y., Modified gelatin with quaternary ammonium salts containing epoxide groups. Chinese Chemical Letters, 2014. **25**(8): p. 1193-1197.
179. Xu, J., Li, T. D., Jiang, Q. W., Qiao, C. D. and Cheng, J. Y., Microstructure transformation of PDMS-E grafted gelatin polymers induced by SDS and SDBS. Colloids and Surfaces B: Biointerfaces, 2013. **103**: p. 375-380.
180. He, W., Sun, Y., Xi, J., Abdurhman, A. A. M., Ren, J., and Duan. H., printing graphene-carbon nanotube-ionic liquid gel on graphene paper: Towards flexible electrodes with efficient loading of PtAu alloy nanoparticles for electrochemical sensing of blood glucose. Analytica Chimica Acta, 2016, **903**: P. 61-68.
181. Fathirad, F., Mostafavi, A., and Afzali, D., Electro spun Pd nanoparticles loaded on vulcan carbon/conductive polymeric ionic liquid nanofibers for selective and sensitive determination of tramadol. Analytica Chimica Acta, 2016. **940**: p. 65-72.
182. Bavandpour, R., Karimi-Maleh, H., Asif, M., Gupta, V. K., Atar, N., and Abbasghorbani, M., Liquid phase determination of adrenaline uses a voltammetry sensor employing $CuFe_2O_4$ nanoparticles and room temperature ionic liquids. Journal of Molecular Liquids, 2016. **213**: p. 369-373.
183. Arabali, V., Ebrahimi, M., Abbasghorbani, M., Gupta, V. K., Farsi, M., Ganjali, M. R., and Karimi, F., Electrochemical determination of vitamin C in the presence of NADH using a CdO nanoparticle/ionic liquid modified carbon paste electrode as a sensor. Journal of Molecular Liquids, 2016. **213**: p. 312-316.

184. Shabani-Nooshabadi, M., Roostaee, M., and Tahernejad-Javazmi, F., Graphene oxide/NiO nanoparticle composite-ionic liquid modified carbon paste electrode for selective sensing of 4-chlorophenol in the presence of nitrite. Journal of Molecular Liquids, 2016. **219**: p. 142-148
185. Shojaei, A. F., Tabatabaeian, K., Shakeri, S., and Karimi. F., A novel 5-fluorouracile anticancer drug sensor based on $ZnFe_2O_4$ magnetic nanoparticles ionic liquids carbon paste electrode. Sensors and Actuators B, 2016. **230**: p. 607-614.
186. Aradilla, D., Gaod, F., Lewes-Malandrakis, G., Müller-Sebert, W., Gaboriau, D., Gentile, P., Iliev, B., Schubert, T., Sadki, S., Bidan, G., and Nebel. C. E., A step forward into hierarchically nanostructured materials for high performance micro-supercapacitors: Diamond-coated SiNW electrodes in protic ionic liquid electrolyte. Electrochemistry Communications, 2016. **63**: p. 34-38.
187. Yang, L., Guo, G., Sun, H., Shen, X., Hu, J., Dong, A., and Yang, D., Ionic liquid as the C and N sources to prepare yolk-shell Fe_3O_4@N doped Carbon Nanoparticles and its high performance in lithium-ion battery. Electrochimica Acta, 2016. **190**: p. 797-803.
188. Yang, H., Zhang, H., Peng, J., Zhang, Y., Du, G., and Fang, Y., Smart magnetic ionic liquid-based pickering emulsions stabilized by amphiphilic Fe_3O_4 nanoparticles: Highly efficient extraction systems for water purification. Journal of Colloid and Interface Science, 2016. **485**: p. 213-222.
189. Song, P., Liu, L., Feng, J. J., Yuan, J., Wang, A. J., and Xu. Q. Q., Poly (ionic liquid) assisted synthesis of hierarchical gold-platinum alloy nanodendrites with high electro catalytic properties for ethylene glycol oxidation and oxygen reduction reactions. International journal of hydrogen energy, 2016. **41**: p. 14058-14067
190. Ghomi, J. S., and Zahedi. S., Novel ionic liquid supported on Fe_3O_4 nanoparticles and its application as a catalyst in Mannich reaction under ultrasonic irradiation. Ultrasonics Sonochemistry, 2017. **34**: p. 916-923.
191. Yarie, M., Zolfigol, M. A., Bayat, Y., Asgari, A., Alonso, D. A., and Khoshnood. A., A novel magnetic nanoparticles with ionic liquids tags as a reusable catalyst in the synthesis of polyhydroquinolines. RSC Advances, 2016. **6**: p. 82842-82853.

192. Naeimi, H., Nejadshafiee, V., and Islami, M. R. Iron (III)-doped, ionic liquid matrix-immobilized, mesoporous silica nanoparticles: Application as recyclable catalyst for synthesis of pyrimidines in water. Microporous and Mesoporous Materials, 2016. **227**: p. 23-30.
193. Absalan, G., Akhond, M., Soleimani, M., and Ershadifar, H., Efficient electrocatalytic oxidation and determination of isoniazid on carbon ionic liquid electrode modified with electrodeposited palladium nanoparticles. Journal of Electroanalytical Chemistry. 2016. **761**: p. 1-7.
194. Sugioka, D., Kameyama, T., Kuwabata, S., Yamamoto, T., and Torimoto, T., Formation of a Pt-decorated au nanoparticle monolayer floating on an ionic liquid by the ionic liquid/metal sputtering method and tunable electro catalytic activities of the resulting monolayer. ACS Applied sciences & interfaces, 2016. **8**(17): p. 10874–10883.
195. Patil, N. M., Sasaki, T., and Bhanage. B. M., Immobilized iron metal-containing ionic liquid-catalyzed chemoselective transfer hydrogenation of nitroarenes into anilines. ACS Sustainable Chemical & Engineering. 2016. **4**(2): p. 429–436.
196. Wang, Y., Li, H., Zhang, J., Yan, X., and Chen, Z., Fe_3O_4 and Au nanoparticles dispersed on the graphene support as a highly active catalyst toward the reduction of 4-nitrophenol. Physical Chemistry Chemical Physics, 2016. **18**: p. 615-623.
197. Fang, H., Wen, M., Chen, H., Wu, Q., and Li, W., Graphene stabilized ultra-small CuNi nanocomposite with high activity and recyclability toward catalyzing the reduction of aromatic nitro-compounds. Nanoscale, 2016. **8**: p. 536.
198. Chen, S., Sun, Y., Chao, J., Cheng, L., Chen, Y., and Liu, J., Dispersive liquid-liquid microextraction of silver nanoparticles in water using ionic liquid1-octyl-3-methylimidazolium hexafluoro phosphate. Journal of Environment Al Sciences, 2016. **41**: p. 211-217.
199. He, Z., and Alexandridis, P., Ionic liquid and nanoparticle hybrid systems: Emerging applications. Advances in Colloid and Interface Science, 2016. **244**: p. 54-70.
200. Wang, F., Zeng, X., Yao, Y., Sun, R., Xu, J., and Wong, C.-P., silver nanoparticle-deposited boron nitride nanosheets as fillers for polymeric composites with high thermal conductivity. Scientific Reports, 2016. **6**: p. 19394.

201. Wang, F., Zeng, Y. Y. X., Huang, T., Sun, R., Xu, J., and Wong, C.-P., Highly thermally conductive polymer nanocomposites based on boron nitride nanosheets decorated with silver nanoparticles. RSC Advances, 2016. **6**: p. 41630-41636.
202. Freemantle, M., An introduction to ionic liquids. The Royal Society of Chemistry, Cambridge. 2009.
203. Leitner, W., Jessop, P. G., Li, C. J., Wasserscheid, P., and Stark, A., Handbook of Green Chemistry - Green Solvents: 2. Wiley-VCH Verlag GmbH & Co. KGaA, Weinheim. 2010.
204. Hallett, J. P., and Welton, T., Room-temperature ionic liquids: Solvents for synthesis and catalysis. 2. Chemical. Reviews, 2011. **111**(5): p. 3508-3576.
205. Seddon, K. R., Stark, A., and Torres, M. J., Influence of chloride, water, and organic solvents on the physical properties of ionic liquids. Pure Applied Chemistry, 2000. **72**: p. 2275-2287.
206. Earle, M. J., Esperanca, J. M. S. S., Gilea, M. A., Canongia Lopes, J. N., Rebelo, L. P. N., Magee, J. W., Seddon, K. R., and Widegren, J. A., The distillation and volatility of ionic liquids. Nature, 2006. **439**: p. 831-834.
207. Earle, M. J., Gordon, C. M., Plechkova, N. V., Seddon, K. R., and Welton, T., Decolorization of ionic liquids for spectroscopy. Analytical Chemistry, 2006. **79**(2): p. 758-764.
208. Stark, A., Behrend, P., Braun, O., Muller, A., Ranke, J., Ondruschka, B., and Jastorff, B., Purity specification methods for ionic liquids. Green Chemistry, 2008. **10:** p. 1152-1161.
209. Taylor, A. W., Lovelock, R. J., Deyko, A., Licence, P., and Jones, R. G., High vacuum distillation of ionic liquids and separation of ionic liquid mixtures. Physical Chemistry Chemical Physical, 2010. **12**: p. 1772-1783.
210. Deetlefs, M., and Seddon, K. R., Assessing the greenness of some typical laboratory ionic liquid preparations. Green Chemistry, 2010. **12**: p. 17-30.
211. Regueira, T., Lugo, L., and Fernandez, J., High-pressure volumetric properties of 1- ethyl-3-methylimidazolium ethyl sulfate and 1-(2-methoxyethyl)-1-methylpyrrolidinium bis(trifluoromethyl sulfonyl)imide. Journal of Chemical Thermodynamics, 2012. **48**: p. 213-220.

212. Domanska, U., Thermophysical properties and thermodynamic phase behavior of ionic liquids. Thermochim Acta, 2006. **448**(1): p. 19-30.
213. Govinda, V., Madhusudhana Reddy, P., Bahadur, I., Attri, P., Venkatesu, P., and Venkateswarlu, P., Effect of anion variation on the thermophysical properties of triethyl ammonium based protic ionic liquids with polar solvent. Thermochim Acta, 2013. **556**: p. 75-88.
214. Hough, W. L., Smiglak, M., Rodriguez, H., Swatloski, R. P., Spear, S. K., Daly, D. T., Pernak, J., Grisel, J. E., Carliss, R. D., Soutullo, D. M., Davis, J. H., and Rogers, R. D., The third evolution of ionic liquids: active pharmaceutical ingredients. New Journal of Chemistry, 2007. **31**: p. 1429-1436.
215. Hough, W. L., and Rogers, R. D., Ionic liquids then and now: From solvents to materials to active pharmaceutical ingredients. Bull. Chemical Society, Japan, 2007. **80**: p. 2262-2269.
216. Rogers, J.R.D., and Seddon, K.R., Ionic Liquids: industrial application to green chemistry (ACS symposium series). American Chemical Society, Washington, 2002. p. 818.
217. Anderson, J.L., Ding, J., Welton, T., and Armstrong, D.W., Characterizing ionic liquids on the basis of multiple solvation interactions. Journal of the American Chemical Society, 2002. **124**(47): p. 14247-14254.
218. Xu, D., Yang, Q., Su, B., Bao, Z., Ren, Q., and Xing, H., Enhancing the Basicity of Ionic Liquids by Tuning the Cation–Anion Interaction Strength and via the Anion-Tethered Strategy. The Journal of Physical Chemistry B, 2014. **118**(4): p. 1071-1079.
219. Hunt, P.A., Ashworth, C.R., and Matthews, R.P., Hydrogen bonding in ionic liquids. Chemical Society Reviews, 2015. **44**(5): p. 1257-1288.
220. Dong, K., and Zhang, S., Hydrogen bonds: a structural insight into ionic liquids. Chemistry-A European Journal, 2012. **18**(10): p. 2748-2761.
221. Zhang, Y., Zhao, X., Yang, Q., Zhang, Z., Ren, Q. and Xing, H., Long-Chain Carboxylate Ionic Liquids Combining High Solubility and Low Viscosity for Light Hydrocarbon Separations. Industrial & Engineering Chemistry Research, 2017. **56**(25): p. 7336-7344.
222. Marsh, K. N., Boxall, J. A., and Lichtenthaler, R., Room temperature ionic liquids and their mixtures-a review. Fluid Phase Equilibria, 2004. **219**(1): p. 93-98.

223. Mantz, R. A., and Trulove, P. C., Ionic Liquids in Synthesis. Wiley-VCH, weihem, 2003.
224. Seddon, K. R., Stark, A., and Torres, M., Viscosity and Density of 1-Alkyl-3-methylimidazolium ionic liquids. Journal of ACS Symposium Series, 2002. **819**: p. 34-49.
225. Pringle, J. M., Golding, J., Baranyai, K., Forsyth, C. M., Deacon, G. B., Scott, J. L., and MacFarlane, D. R., The effect of anion fluorination in ionic liquids-physical properties of a range of bis(methanesulfonyl)amide salts. New Journal of Chemistry, 2003. **27**: p. 1504-1510.
226. Tokuda, H., Hayamizu, K., Ishii, K., Susan, Md. A. B. H., and Watanabe, M., Physicochemical properties and structures of room temperature ionic liquids. 2. Variation of alkyl chain length in imidazolium cation. Journal of Physical Chemistry B, 2005. **109**: p. 6103-6110.
227. Bonhôte, P., Dias, A. P., Papageorgiou, N., Kalyanasundaram, K., and Grätzel, M., Hydrophobic, highly conductive ambient-temperature molten salts. Inorganic Chemistry, 1996. **35***(5)*: p. 1168-1178.
228. Roy, M. N., Ekka, D., and Dewan, R., Physico-chemical studies of some bio-active solutes in pure methanoic acid. Acta Chim. Slov, 2011. **58**: p. 792-796.
229. Moldover, M. R., In: IUPAC Experimental thermodynamics, measurement of the thermodynamic properties of single phases. Elsevier, 2008. **IV**: p. 435-451.
230. Singh, S., Bahadur, I., Redhi, G. G., Ebenso, E. E., and Ramjugernath, D., Density and speed of sound of 1-ethyl-3-methylimidazolium ethyl sulfate with acetic or propionic acid at different temperatures. Journal of Molecular Liquids, 2014. **199**: p. 518-523.
231. Deenadayalu, N., and Bhujrajh, P., Excess molar volumes and partial molar volumes for (propionitrile + an alkanol) at T = 298.15 K and p = 0.1 MPa. The Journal of Chemical Thermodynamics, 2006. **38**(3): p. 278-282.
232. Liu, W., Zhao, T., Zhang, Y., Wang, H., and Yu, M., The physical properties of aqueous solutions of the ionic liquid [BMIM][BF_4]. Journal of Solution Chemistry, 2006. **35**(10): p. 1337-1346.
233. Fortin, T. J., Laesecke, A., Freund, M., and Outcalt, S., Advanced calibration, adjustment, and operation of a density and sound speed analyzer. The Journal of Chemical Thermodynamics, 2013. **57**: p. 276-285.

234. Hayward, A. T. J., Experimental verification at high pressure of the relationship between compression, density and sonic velocity. Nature, 1969. **221**: p. 1047-1047.
235. Blandamer, M. J., Introduction to chemical ultrasonics. Academic Press, New York. 1973.
236. Fort, R. J., and Moore, W. H., Adiabatic compressibility's of binary liquid mixtures. Transactions of the Faraday Society, 1965. **61**: p. 2102-2111.
237. Oswal, S. L., and Patel, I. N., Excess molar volumes of binary mixtures of alkyl acetates with hexane, tetrachloromethane, and trichloromethane. Fluid Phase Equilibria, 1998. **149**: p. 249-259.
238. Wasserscheid, P., Keim, W., Ionic liquids-new "solutions" for transition metal catalysis. Angewandty Chemie International Edition. 2000, **39**: p. 3772.
239. Hildebrand, J. H., The solubility of nonelectrolytes, Ed. 3, Reinhold Publishing Co. New York. 1950. p. 48.
240. Hudleston, L.J., Intermolecular forces of normal liquids. Transactions of the Faraday Society, 1937. **33**: p. 97-103.

9 Chapter 5

9.1 1st Publication

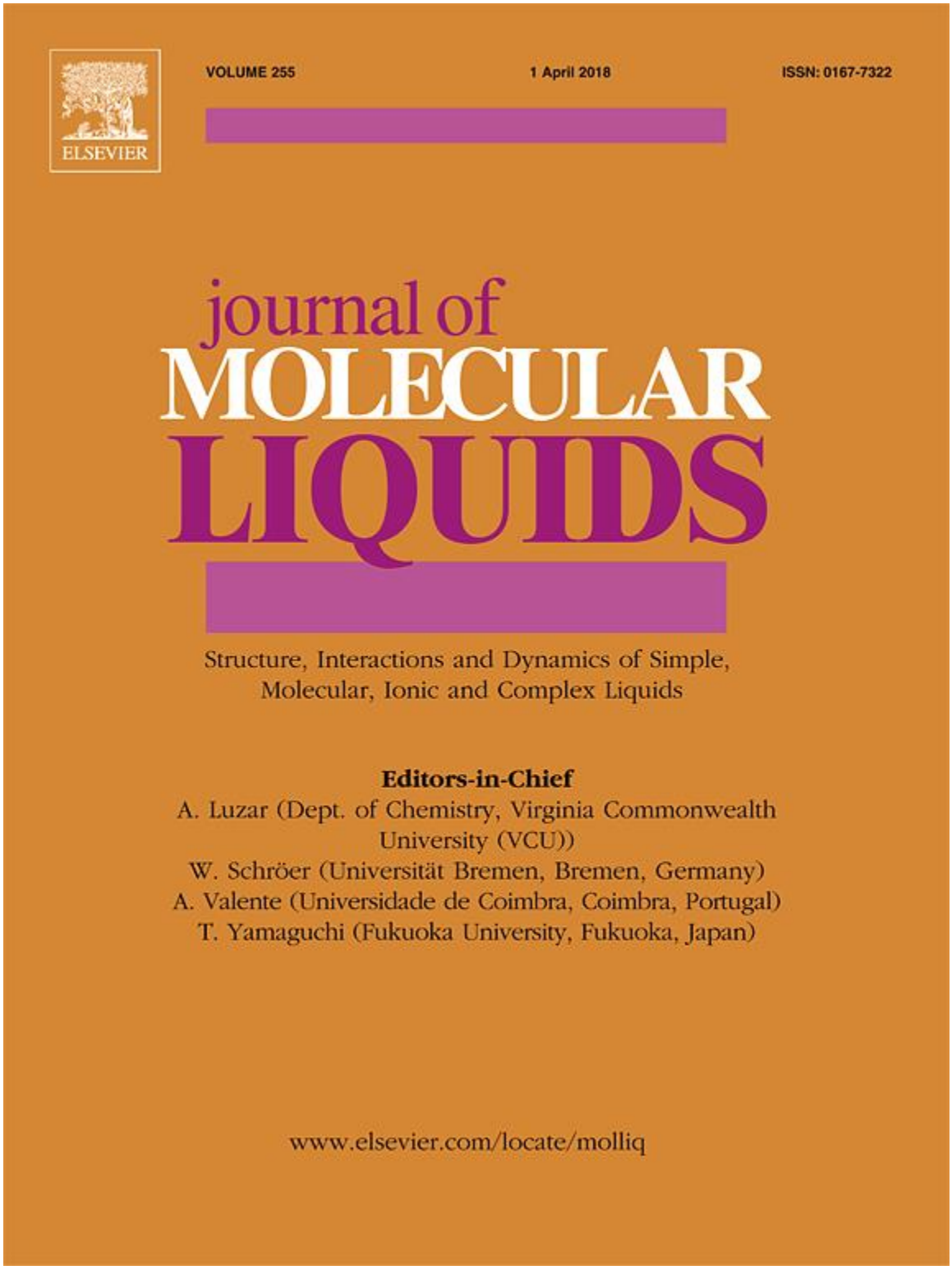

Graphical abstract

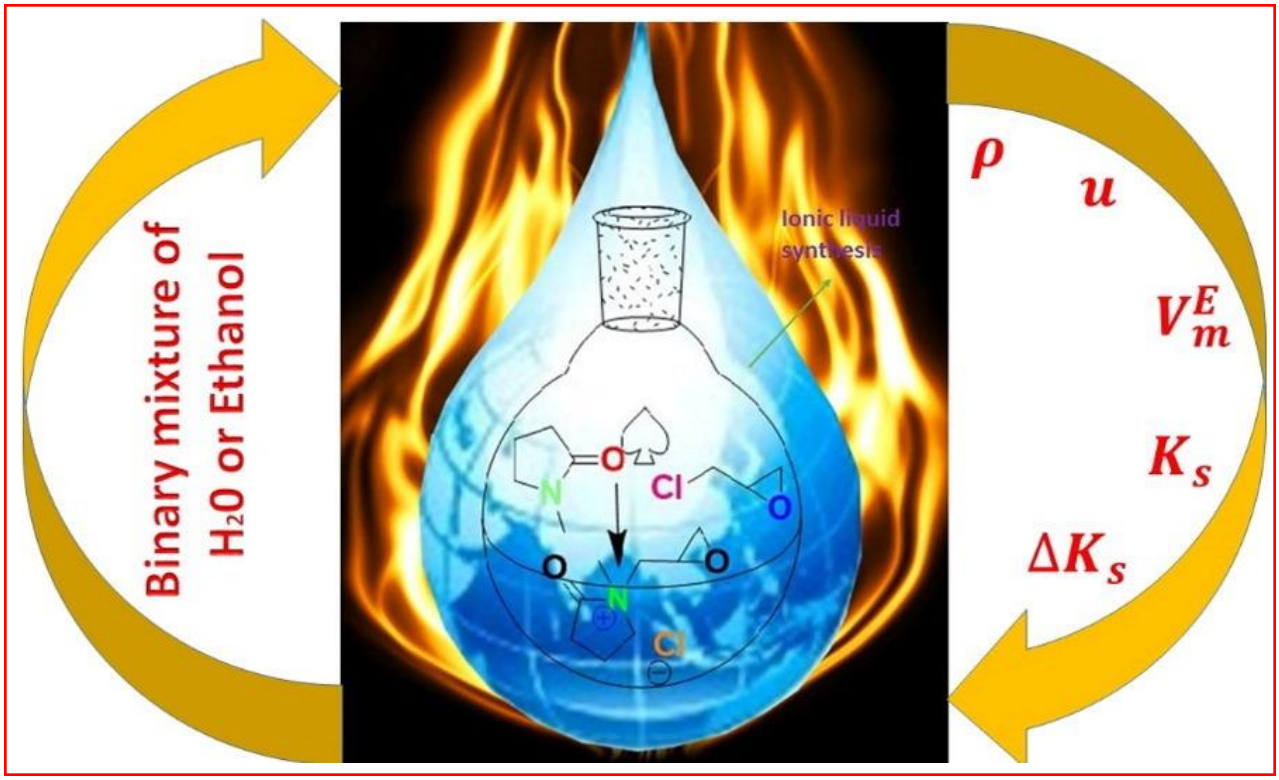

Journal of Molecular Liquids 219 (2016) 685–693

Contents lists available at ScienceDirect

Journal of Molecular Liquids

journal homepage: www.elsevier.com/locate/molliq

Synthesis, characterization and thermophysical properties of ionic liquid *N*-methyl-*N*-(2′,3′-epoxypropyl)-2-oxopyrrolidinium chloride and its binary mixtures with water or ethanol at different temperatures

A. Vasanthakumar [a], I. Bahadur [b,*], G.G. Redhi [a,*], R.M. Gengan [a], K. Anand [a]

[a] Department of Chemistry, Durban University of Technology, P O Box 1334, Durban 4000, South Africa
[b] Department of Chemistry, Material Science Innovation and Modelling (MaSIM) Research Focus Area, School of Mathematical and Physical Sciences, Faculty of Agriculture, Science and Technology, North-West University, (Mafikeng Campus), Private Bag X2046, Mmabatho 2735, South Africa

ARTICLE INFO

Article history:
Received 24 February 2016
Received in revised form 30 March 2016
Accepted 31 March 2016
Available online xxxx

Keywords:
Density
Speed of sound
Ionic liquid
Water
Ethanol
Redlich–Kister equation

ABSTRACT

A novel ionic liquid, namely, *N*-methyl-*N*-(2′,3′-epoxypropyl)-2-oxopyrrolidinium chloride $[Epmpyr]^+[Cl]^-$ was synthesized and characterized by different techniques such as NMR (^1H and ^{13}C), FTIR, and elemental analysis. The water content of the ionic liquid was checked by Karl Fisher titration. Further, the density, ρ, and speed of sound, u, were measured for the above ionic liquid and the corresponding binary systems with water or ethanol at different temperatures ranging from (293.15 to 313.15) K. The derived thermodynamic properties for instance excess molar volumes, V_m^E isentropic compressibility, κ_s, and deviation in isentropic compressibility, $\Delta\kappa s$, were investigated from the density and speed of sound data, respectively. It is noted that density and speed of sound of the ionic liquid and its binary mixtures were decreased with increase in temperature, whereas excess molar volume, isentropic compressibility, and deviation in isentropic compressibility values increased. Derived properties such as excess molar volumes, and deviation in isentropic compressibility data were fitted to the Redlich-Kister polynomial equation. The measured and calculated data were interpreted in terms of intermolecular interfaces and structural effects between similar and dissimilar molecules upon mixing.

1. Introduction

Ionic liquids (ILs) which have acquired labels such as “green” and environment-friendly solvents are the combination of cations and anions, which exist as salts with low melting points [1,2]. In the past decade, ILs, have been increasingly used for applications; *inter alia* organic synthesis, catalysis, manufacture of electrochemical devices and solvent extraction for a variety of compounds [2–6]. In addition, ILs are used as designer solvents [7–9]. Examples of the latter include those used in dissolution of CO_2, O_2 and N_2 gases [10–14]. ILs have received considerable attention for their use as possible replacements for the conventional volatile organic solvents in liquid–liquid extraction because of their notable unique properties [15–20]. For separation processes, ILs have been considered as “green solvents” with countless applications in an extensive range of disciplines due to their interesting and unique physicochemical properties [21–23].

$[Bmpyr]^+[Cl]^-$ is an ionic liquid which was used as an extracting agent in the separation of benzene, toluene, ethyl benzene, and xylene (BTEX) from the reformate fraction of an oil refinery process [23]. Compared to the conventional extractants such as sulpholane and tetra ethylene glycol, $[BMIM]^+[BF_4]^-$ ionic liquid showed higher extraction efficiency [24,25]. To optimize the use of $[Epmpyr]^+[Cl]^-$ in separation processes designed by industry, the knowledge of thermo-physical properties of $[Epmpyr]^+[Cl]^-$ is essential. The properties of ILs can be finely tuned by changing the cation or the anion. The information regarding the thermo-physical properties of pure ILs as well as their mixtures with other compounds is required for the design and development of new equipment for commercial applications [26]. The physical properties of an IL are changed when mixing with water, and play a major role in industrial applications [24,25,27]. *N*-vinyl-2-pyrrolidinone is used as co-solvent in the petroleum industry to increase the selectivity and solvent influence for extracting aromatic hydrocarbons. Further, it has excellent thermal and chemical stability and was used as an absorbent of sour gases from crude natural gas [28].

In the light of the foregoing, $[Epmpyr]^+[Cl]^-$ IL was selected for investigation of the thermophysical properties of its binary mixtures with water or ethanol since the pyrrolidinone based ionic liquids have attracted huge interests because they possess low viscosity, low melting points and high conductivity and also the separation ability of which already been demonstrated for separation of aromatic hydrocarbons from aliphatic hydrocarbon mixtures, an additional feature of these ILs is their lower toxicity than ILs containing other cations [29–31]. The above properties of IL make the selection of this IL for the present work. In addition, the aqueous and alcohol miscibility of ILs is applicable

* Corresponding authors.
E-mail addresses: bahadur.indra@gmail.com (I. Bahadur), redhigg@dut.ac.za (G.G. Redhi).

http://dx.doi.org/10.1016/j.molliq.2016.03.080
0167-7322/

regarding their environmental impacts. Although it is well known that ILs reduce air pollution risks because of their negligible vapor pressures, their release into aquatic environments could result in contamination because of their potential toxicity and limited biodegradability. The present work is aimed at studying the thermophysical properties and intermolecular interactions of binary mixtures of the $[Epmpyr]^+[Cl]^-$ with water or ethanol, and is a continuation of our systematic studies in the same area [32–42].

2. Experimental

2.1. Materials

N-methyl pyrrolidone, epichlorohydrin, acetonitrile, methanol, acetone and hexane were purchased from Fluka with purity of ≥99%. The densities and speed of sound of the pure compounds in comparison with literature [43,44] values at 298.15 K are presented in Table 1. Ultra-pure deionized water was used in the experiments. The water content was found to be 0.06% in $[Epmpyr]^+[Cl]^-$ using a Metrohm 702 SM Titrino Metter before the experiments.

2.2. Synthesis of N-methyl-N-(2′,3′-epoxypropyl)-2-oxopyrrolidinium

The reaction system was set up as follows: The heating oil bath with internal thermometer was fixed over the mechanical magnetic stirrer. A 500 mL three-necked round bottomed flask with a thermometer inlet over cold water flowing condenser was suspended. The round bottom flask was flushed with nitrogen gas and thereafter 1 mol of newly distilled *N*-methyl-pyrrolidone in 100 mL of acetonitrile and 1.1 mol of epichlorohydrin was added and then brought to a moderate reflux (90–100) °C internal temperature. The resulting solution was then heated under reflux for 48 h and thereafter cooled to room temperature. The volatile materials were removed under reduced pressure from the resulting solution, to yield the yellow coloured ionic liquid, *N*-(2′,3′-epoxypropyl)-*N*-methyl-2-oxopyrrolidinium chloride. This product was purified by solvent washing with acetone and hexane, to remove the unwanted starting materials, and then further distilled again at 80 °C for 48 h to obtain pure moisture free Ionic liquid. The afforded yield was established with FTIR, NMR (proton and carbon) and elemental analysis. The purity of the synthesized ionic liquid was checked using HPLC. Scheme 1 shows the schematic diagram for the synthetic route of $[Epmpyr]^+[Cl]^-$.

2.3. Characterization of N-(2′,3′-epoxypropyl)-N-methyl-2-oxopyrrolidinium chloride

The $[Epmpyr]^+[Cl]^-$ was characterized by the following methods: NMR (^1H & ^{13}C), elemental analysis, FTIR and HPLC. Analytical data for the synthesized ionic liquid, $[Epmpyr]^+[Cl]^-$ was checked by HPLC and found to have a purity of 98.1%. The structure of $[Epmpyr]^+[Cl]^-$ is shown in Fig. 1.

FTIR: ($\upsilon = cm^{-1}$) 3442, 2995, 1621, 1501, 1403, 1332, 1256, 1113, 967, 856, 756, 679, 561, 479. ^1H NMR (400 MHz, DMSO): δ 3.48–3.51 (m, 1H), 3.30–3.32 (t, 2H), 2.76–3.29 (s, 1H), 2.61–2.62 (s, 3H). 2.26–2.30 (d, 2H) 1.96–1.98 (t, 2H) 1.90–1.94 (m, 2H) ^{13}C NMR (100 MHz, DMSO): δ 175.03, 51.22, 49.38, 45.72, 45.00, 30.62, 29.50, and 17.59.

Table 1
Comparison of experimental densities, ρ, and speeds of sound, *u*, of pure liquids with literature values at 298.15 K.

Component	% purity	$u/(m\cdot s^{-1})$		$\rho/(g\cdot cm^{-3})$	
		Exp.	Lit.	Exp.	Lit.
Water	99.0	1497.4	1497.0[43]	0.9971	0.99704[43]
Ethanol	99.0	1145.4	1145.0[44]	0.7858	0.78640[44]
$[Epmpyr]^+[Cl]^-$	98.0	1483.6	–	1.0637	–

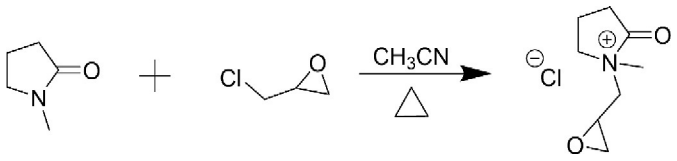

Scheme 1. Schematic diagram for the synthetic route of the $[Epmpyr]^+[Cl]^-$.

Elemental Analysis: theoretical calculation for (in %): $C_8H_{14}NO_2$: C, 50.14; H, 7.36; N, 7.31; the values found (in %): C, 50.45; H, 7.10; N, 7.17.

2.4. Density and speed of sound measurement

The density and speed of sound measurements were done according to literature [40–41,43,45]. The measurements of densities and speed of sound were done using an Anton Paar DMA 5000 vibrating U-tube with a temperature uncertainty of ±0.01 K. An OHAUS analytical balance with a precision of ±0.0001 g was used to prepare the binary mixtures. The instrument was calibrated with dry air and freshly distilled degassed water once a day. The speed of sound was measured using a propagation time technique with frequency around 3 MHz [39]. The details about the speed of sound measurements can be found elsewhere [39]. The estimated uncertainty in density and speed of sound was less than $\pm 2 \times 10^{-4}\ g\cdot cm^{-3}$ and $\pm 1.0\ m\cdot s^{-1}$, respectively. The estimated uncertainty in excess molar volume, isentropic compressibility, and deviation in isentropic compressibility was $\pm 0.005\ cm^3\cdot mol^{-1}$, $\pm 0.2 \times 10^{-8}\ Pa^{-1}$ and $\pm 0.7 \times 10^{-8}\ Pa^{-1}$, respectively.

3. Result and discussion

3.1. Density measurement

Thermo-physical properties of ILs and their binary mixtures with solvents are of fascinating and great practical impact in understanding the structural features of the pure ILs and its interactions when mixed with solvents. The comparison between literature and experimental

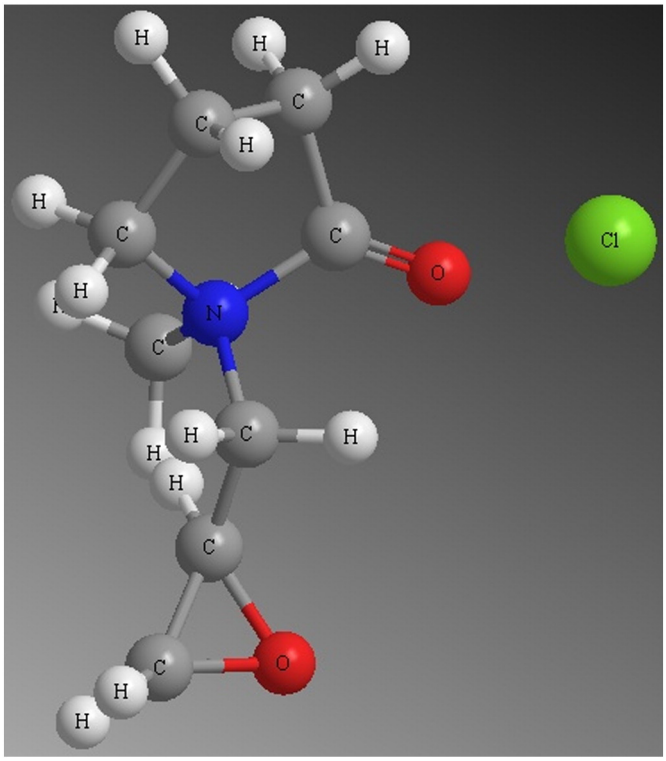

Fig. 1. Structure of the ionic liquid $[Epmpyr]^+[Cl]^-$.

Table 2
Density, ρ, excess molar volume, V_m^E, speed of sound, u, isentropic compressibility, κ_s, and deviation in isentropic compressibility, $\Delta\kappa_s$, for the binary system {[Epmpyr]$^+$[Cl]$^-$ (x_1) + water (x_2)} at (293.15 to 313.15) K.

x_1	ρ/(g·cm^{-3})	V_m^E/(cm^3·mol^{-1})	u/(m·s^{-1})	κ_s/(10^8 Pa^{-1})	$\Delta\kappa_s$/(10^8 Pa^{-1})
T = 293.15 K					
0.0000	0.9982	0.000	1483.5	45.5	0.0
0.0067	1.0044	−0.038	1522.2	42.9	−2.6
0.0143	1.0113	−0.096	1558.3	40.7	−4.7
0.0229	1.0185	−0.164	1589.8	38.8	−6.6
0.0327	1.0258	−0.243	1615.2	37.3	−8.1
0.0441	1.0329	−0.327	1628.6	36.5	−8.8
0.0574	1.0397	−0.415	1639.4	35.7	−9.6
0.0731	1.0461	−0.506	1646.3	35.2	−10.0
0.0921	1.0522	−0.604	1650.2	34.9	−10.2
0.1153	1.0578	−0.706	1650.7	34.7	−10.3
0.1446	1.0630	−0.817	1647.1	34.7	−10.2
0.1822	1.0674	−0.926	1639.0	34.8	−9.9
0.2333	1.0708	−1.021	1625.0	35.3	−9.2
0.3054	1.0728	−1.075	1604.6	36.2	−8.1
0.4149	1.0734	−1.055	1577.7	37.4	−6.4
0.6034	1.0717	−0.790	1543.5	39.1	−3.9
1.0000	1.0685	0.000	1502.4	41.4	0.0
T = 298.15 K					
0.0000	0.9971	0.000	1497.4	44.7	0.0
0.0067	1.0030	−0.038	1532.2	42.4	−2.3
0.0143	1.0096	−0.092	1564.3	40.4	−4.3
0.0229	1.0164	−0.157	1591.9	38.8	−5.8
0.0327	1.0233	−0.232	1613.8	37.5	−7.1
0.0441	1.0301	−0.313	1624.5	36.7	−7.9
0.0574	1.0365	−0.396	1633.0	36.1	−8.5
0.0731	1.0426	−0.484	1637.8	35.7	−8.8
0.0921	1.0483	−0.575	1639.6	35.4	−9.1
0.1153	1.0537	−0.676	1638.0	35.3	−9.2
0.1446	1.0587	−0.785	1632.7	35.4	−9.0
0.1822	1.0628	−0.888	1623.1	35.7	−8.6
0.2333	1.0661	−0.984	1607.9	36.2	−8.0
0.3054	1.0680	−1.038	1586.7	37.1	−7.0
0.4149	1.0685	−1.018	1559.5	38.4	−5.5
0.6034	1.0669	−0.771	1525.0	40.3	−3.2
1.0000	1.0637	0.000	1483.6	42.7	0.0
T = 303.15 K					
0.0000	0.9957	0.000	1509.7	44.1	0.0
0.0067	1.0014	−0.038	1540.8	42.1	−2.0
0.0143	1.0077	−0.090	1569.1	40.3	−3.8
0.0229	1.0142	−0.153	1593.2	38.8	−5.3
0.0327	1.0207	−0.223	1611.7	37.7	−6.4
0.0441	1.0271	−0.300	1619.7	37.1	−7.0
0.0574	1.0331	−0.377	1626.0	36.6	−7.5
0.0731	1.0390	−0.464	1628.6	36.3	−7.8
0.0921	1.0444	−0.551	1628.3	36.1	−8.0
0.1153	1.0496	−0.651	1624.8	36.1	−8.0
0.1446	1.0543	−0.754	1617.7	36.2	−7.8
0.1822	1.0582	−0.854	1606.8	36.6	−7.4
0.2333	1.0613	−0.946	1590.6	37.2	−6.8
0.3054	1.0631	−0.999	1568.5	38.2	−5.8
0.4149	1.0636	−0.984	1540.8	39.6	−4.4
0.6034	1.0620	−0.744	1506.1	41.5	−2.5
1.0000	1.0589	0.000	1464.6	44.0	0.0
T = 308.15 K					
0.0000	0.9941	0.000	1520.6	43.5	0.0
0.0067	0.9996	−0.037	1548.0	41.7	−1.8
0.0143	1.0055	−0.086	1572.8	40.2	−3.3
0.0229	1.0117	−0.146	1593.5	38.9	−4.6
0.0327	1.0179	−0.213	1608.9	37.9	−5.6
0.0441	1.0240	−0.287	1614.3	37.5	−6.1
0.0574	1.0297	−0.360	1618.4	37.1	−6.5
0.0731	1.0352	−0.441	1618.9	36.8	−6.8
0.0921	1.0405	−0.529	1616.6	36.8	−6.9
0.1153	1.0454	−0.623	1611.3	36.8	−6.9
0.1446	1.0498	−0.720	1602.6	37.1	−6.7
0.1822	1.0536	−0.820	1590.3	37.5	−6.3
0.2333	1.0565	−0.906	1573.1	38.2	−5.7
0.3054	1.0582	−0.957	1550.3	39.3	−4.7
0.4149	1.0587	−0.944	1522.2	40.8	−3.5
0.6034	1.0572	−0.718	1487.2	42.8	−1.9

(continued on next page)

Table 2 (*continued*)

x_1	$\rho/(g\cdot cm^{-3})$	$V_m^E/(cm^3\cdot mol^{-1})$	$u/(m\cdot s^{-1})$	$\kappa_s/(10^8\ Pa^{-1})$	$\Delta\kappa_s/(10^8\ Pa^{-1})$
1.0000	1.0542	0.000	1445.8	45.4	0.0
T = 313.15 K					
0.0000	0.9922	0.000	1530.4	43.0	0.0
0.0067	0.9975	−0.037	1554.2	41.5	−1.6
0.0143	1.0033	−0.087	1575.5	40.1	−2.9
0.0229	1.0091	−0.142	1592.9	39.0	−4.1
0.0327	1.0150	−0.207	1605.4	38.2	−4.9
0.0441	1.0208	−0.277	1608.3	37.9	−5.3
0.0574	1.0262	−0.347	1610.2	37.6	−5.7
0.0731	1.0315	−0.426	1608.7	37.5	−5.8
0.0921	1.0364	−0.507	1604.5	37.5	−5.9
0.1153	1.0411	−0.599	1597.4	37.6	−5.8
0.1446	1.0453	−0.693	1587.2	38.0	−5.6
0.1822	1.0489	−0.788	1573.5	38.5	−5.2
0.2333	1.0517	−0.874	1555.4	39.3	−4.6
0.3054	1.0533	−0.923	1531.9	40.4	−3.7
0.4149	1.0537	−0.907	1503.4	42.0	−2.6
0.6034	1.0523	−0.693	1468.3	44.1	−1.2
1.0000	1.0494	0.000	1427.2	46.8	0.0

values of density and speed of sound corresponding to pure components was performed. In the present study, the IL $[Epmpyr]^+[Cl]^-$ is completely miscible with ethanol and water over the entire mole fraction range and at all studied temperatures. Studies on structural features of combinations of ILs with water or ethanol as a function of temperature are very interesting and useful to the chemical industry. The experimental ρ values for pure $[Epmpyr]^+[Cl]^-$, ethanol, water and binary mixtures are presented in Tables 2 and 3 as well as plotted in Figs. 2 and 3, respectively, as a function of IL concentration for the entire composition range at temperatures from (293.15 to 313.15) K in steps of 5 K under atmospheric pressure. The ρ values for pure IL as well as both systems decreases as temperature increases are shown in Figs. 2 and 3. In general, it can be observed that the ρ values increase as composition increases for both systems. Virtually, The IL is completely miscible with medium-to-high dielectric liquids and immiscible with low dielectric liquids [12–14].

3.2. Speed of sound measurements

The speed of sound data for pure $[Epmpyr]^+[Cl]^-$, ethanol, water and their binary mixtures are presented in Tables 2 and 3 as well as plotted in Figs. 4 and 5, respectively, for the entire composition range at temperatures from (293.15 to 313.15) K in steps of 5 K under atmospheric pressure. The results show that the value of u decreases as temperature increases.

3.3. Excess molar volume

Excess molar volumes of binary mixtures were calculated from the density data by using the following equation:

$$V_m^E = \frac{x_1M_1 + x_2M_2}{\rho} - \frac{x_1M_1}{\rho_1} - \frac{x_2M_2}{\rho_2} \quad (1)$$

where x_1 and x_2 are mole fractions; M_1 and M_2 denote molar masses; ρ_1 and ρ_2 are the densities; where 1 refers to $[Epmpyr]^+[Cl]^-$ and 2 refers to water or ethanol, while ρ is the density of their binary mixtures. In endeavoring to elucidate the communications among ILs and water or an alcohol, it is significant to bear in mind the self-associations among the IL moieties which can be (ion + ion) association and also van der Waals associations between the alkyl epoxide and other organic parts of the ILs; and the robust H-bonding among H_2O molecules. The excess molar volume results for both systems are tabulated in Tables 2 and 3 as well as plotted in Fig. 6. It is evident from the results reported in Tables 2 and 3, that the V_m^E values are negative for both systems. ILs are complex solvents, and have a capability to interact with water or ethanol molecules simultaneously through, dispersive, ionic, hydrogen bonding, and dipolar interaction [46]. The negative V_m^E values for the both binary system suggest that a more efficient packing and/or attractive interaction occurred when the $[Epmpyr]^+[Cl]^-$ and water or ethanol were mixed [46]. The water or ethanol molecules tends to fill the interstices of $[Epmpyr]^+[Cl]^-$, and the ion–dipole interactions between the water and ethanol molecules, all contribute to the negative values of excess molar volumes [46].

The negative V_m^E values of {$[Epmpyr]^+[Cl]^-$ + water (x_2)} > {$[Epmpyr]^+[Cl]^-$ (x_1) + ethanol (x_2)} are an indication that the interaction of $[Epmpyr]^+[Cl]^-$ with water is stronger than $[Epmpyr]^+[Cl]^-$ with ethanol. The $V_{m,min}^E$ values were $-1.075\ cm^3\cdot mol^{-1}$ and $-0.694\ cm^3\cdot mol^{-1}$ and occurs at x_1 = 0.3054 and 0.4375, respectively for the systems {$[Epmpyr]^+[Cl]^-$ + water or ethanol (x_2)} at all temperatures. The V_m^E minimum values increase with an increase in temperature for both the systems. An association among the $[Epmpyr]^+[Cl]^-$ and H_2O must compete with the two comparatively strong self-associations of ion-ion and H-bonded water. The results display a robust association between H_2O and $[Epmpyr]^+[Cl]^-$, perhaps through H-bonding with the chloride anion and the proton of H_2O.

3.4. Isentropic compressibility and deviation in isentropic compressibility

Tables 2 and 3, illustrates a significant thermodynamic properties of the $[Epmpyr]^+[Cl]^-$, namely, the isentropic compressibility. The isentropic compressibility κ_s is designed from the Newton–Laplace equation

$$\kappa_s = \rho^{-1}u^{-2}. \quad (2)$$

The isentropic compressibility has been defined as the inverse of the product of the density and the square of the speed of sound. The isentropic means that as the sound waves pass through a fluid, the pressure and temperature oscillate within respectively microscopic volume, but the entropy of the system should be constant. This situation holds true when we measure the speed of sound using a low-frequency generator (DSA 5000 M transducer produces around 3 MHz frequency) [47], but at high frequency (>100 MHz) there is velocity dispersion as well as absorption of sound waves due to the coupling with molecular processes within the fluid [48,49].

Table 3
Density, ρ, excess molar volume, V_m^E, speed of sound, u, isentropic compressibility, κ_s, and deviation in isentropic compressibility, $\Delta\kappa_s$, for the binary system {[Epmpyr]$^+$[Cl]$^-$ (x_1) + ethanol (x_2)} at (293.15 to 313.15) K.

x_1	ρ/(g·cm^{-3})	V_m^E/(cm^3·mol^{-1})	u/(m·s^{-1})	κ_s/(10^8 Pa^{-1})	$\Delta\kappa_s$/(10^8 Pa^{-1})
T = 293.15 K					
0.0000	0.7901	0.000	1162.0	93.7	0.0
0.0170	0.8044	−0.093	1180.2	89.2	−3.6
0.0356	0.8189	−0.172	1198.3	85.0	−6.8
0.0565	0.8336	−0.225	1215.8	81.2	−9.6
0.0797	0.8489	−0.290	1234.7	77.3	−12.3
0.1053	0.8647	−0.373	1254.2	73.5	−14.7
0.1346	0.8813	−0.467	1274.6	69.8	−16.8
0.1679	0.8980	−0.529	1295.1	66.4	−18.5
0.2059	0.9150	−0.577	1316.0	63.1	−19.8
0.2500	0.9325	−0.616	1337.2	60.0	−20.6
0.3019	0.9505	−0.637	1358.8	57.0	−20.8
0.3635	0.9691	−0.657	1387.2	53.6	−21.0
0.4375	0.9885	−0.694	1405.2	51.2	−19.4
0.5290	1.0076	−0.611	1436.6	48.1	−17.8
0.6450	1.0285	−0.626	1453.4	46.0	−13.7
0.7957	1.0479	−0.329	1485.9	43.2	−8.6
1.0000	1.0685	0.000	1510.6	41.0	0.0
T = 298.15 K					
0.0000	0.7858	0.000	1145.4	97.0	0.0
0.0170	0.8000	−0.089	1163.3	92.4	−3.7
0.0356	0.8145	−0.171	1181.4	88.0	−7.1
0.0565	0.8292	−0.227	1198.7	83.9	−10.0
0.0797	0.8444	−0.287	1217.6	79.9	−12.8
0.1053	0.8602	−0.374	1236.7	76.0	−15.2
0.1346	0.8767	−0.462	1257.0	72.2	−17.4
0.1679	0.8934	−0.528	1277.3	68.6	−19.2
0.2059	0.9104	−0.578	1298.1	65.2	−20.5
0.2500	0.9279	−0.619	1319.2	61.9	−21.4
0.3019	0.9458	−0.633	1340.6	58.8	−21.6
0.3635	0.9644	−0.655	1369.2	55.3	−21.8
0.4375	0.9837	−0.684	1386.7	52.9	−20.2
0.5290	1.0029	−0.611	1418.4	49.6	−18.5
0.6450	1.0237	−0.616	1434.9	47.4	−14.2
0.7957	1.0431	−0.317	1467.4	44.5	−8.9
1.0000	1.0638	0.000	1492.0	42.2	0.0
T = 303.15 K					
0.0000	0.7815	0.000	1128.5	100.5	0.0
0.0170	0.7957	−0.093	1146.3	95.6	−3.9
0.0356	0.8101	−0.170	1164.2	91.1	−7.4
0.0565	0.8247	−0.222	1181.4	86.9	−10.4
0.0797	0.8399	−0.286	1200.2	82.6	−13.3
0.1053	0.8556	−0.368	1219.4	78.6	−15.9
0.1346	0.8721	−0.459	1239.3	74.7	−18.2
0.1679	0.8887	−0.520	1259.8	70.9	−20.0
0.2059	0.9057	−0.573	1280.2	67.4	−21.4
0.2500	0.9232	−0.617	1301.4	63.9	−22.3
0.3019	0.9411	−0.634	1322.9	60.7	−22.6
0.3635	0.9597	−0.658	1351.0	57.1	−22.7
0.4375	0.9790	−0.691	1368.6	54.5	−21.0
0.5290	0.9982	−0.621	1399.8	51.1	−19.2
0.6450	1.0189	−0.616	1416.3	48.9	−14.8
0.7957	1.0384	−0.331	1448.6	45.9	−9.3
1.0000	1.0590	0.000	1472.8	43.5	0.0
T = 308.15 K					
0.0000	0.7771	0.000	1111.6	104.1	0.0
0.0170	0.7912	−0.088	1129.3	99.1	−4.0
0.0356	0.8057	−0.177	1147.1	94.3	−7.7
0.0565	0.8202	−0.223	1164.2	89.9	−10.8
0.0797	0.8353	−0.282	1182.8	85.6	−13.8
0.1053	0.8510	−0.366	1202.0	81.3	−16.6
0.1346	0.8675	−0.461	1221.8	77.2	−18.9
0.1679	0.8841	−0.524	1242.2	73.3	−20.9
0.2059	0.9010	−0.571	1262.5	69.6	−22.3
0.2500	0.9184	−0.607	1283.5	66.1	−23.2
0.3019	0.9364	−0.635	1305.1	62.7	−23.5
0.3635	0.9549	−0.651	1332.9	58.9	−23.7
0.4375	0.9742	−0.684	1350.4	56.3	−21.9
0.5290	0.9934	−0.614	1381.4	52.7	−20.0
0.6450	1.0141	−0.609	1397.7	50.5	−15.4
0.7957	1.0337	−0.334	1429.8	47.3	−9.7

(continued on next page)

Table 3 (*continued*)

x_1	$\rho/(g\cdot cm^{-3})$	$V_m^E/(cm^3\cdot mol^{-1})$	$u/(m\cdot s^{-1})$	$\kappa_s/(10^8\ Pa^{-1})$	$\Delta\kappa_s/(10^8\ Pa^{-1})$
1.0000	1.0543	0.000	1453.7	44.9	0.0
T = 313.15 K					
0.0000	0.7727	0.000	1094.9	107.9	0.0
0.0170	0.7868	−0.092	1112.4	102.7	−4.2
0.0356	0.8012	−0.176	1130.1	97.7	−8.0
0.0565	0.8157	−0.225	1147.1	93.2	−11.3
0.0797	0.8308	−0.287	1165.6	88.6	−14.5
0.1053	0.8464	−0.367	1184.6	84.2	−17.3
0.1346	0.8628	−0.456	1204.6	79.9	−19.8
0.1679	0.8794	−0.522	1224.7	75.8	−21.8
0.2059	0.8963	−0.572	1245.2	71.9	−23.3
0.2500	0.9137	−0.611	1265.9	68.3	−24.2
0.3019	0.9316	−0.631	1287.5	64.7	−24.6
0.3635	0.9502	−0.659	1315.0	60.8	−24.7
0.4375	0.9694	−0.684	1332.4	58.1	−22.9
0.5290	0.9886	−0.615	1363.1	54.4	−20.9
0.6450	1.0093	−0.612	1379.3	52.1	−16.1
0.7957	1.0289	−0.336	1411.2	48.8	−10.1
1.0000	1.0495	0.000	1434.9	46.3	0.0

The deviations in isentropic compressibility, $\Delta\kappa_s$, were calculated using Eq. (3)

$$\Delta\kappa_s = \kappa_s - \sum_i^2 x_i\kappa_{s,i} \tag{3}$$

where, $\kappa_{s,i}$ and x_i are the isentropic compressibility and mole fractions of the pure component *i*, respectively.

The results of isentropic compressibility, κ_s, and deviation in isentropic compressibility, $\Delta\kappa s$, for {[Epmpyr]$^+$[Cl]$^-$ (x_1) + water or ethanol (x_2)} systems at (293.15 to 313.15) K are also given in Tables 2 and 3. It is evident from the results reported in Tables 2 and 3 that in general, the isentropic compressibility, κ_s, values increases with an increase in temperature at a fixed composition for both systems due to an increase in thermal agitation, making the solution more compressible [50].

Fig. 7, shows the negative values of deviation in isentropic compressibility, $\Delta\kappa_s$, over the entire composition range of [Epmpyr]$^+$[Cl]$^-$ for both systems indicating that these mixtures are less compressible than the ideal mixture and in addition the closer approach of unlike molecules as well as a stronger interaction between water or ethanol and [Epmpyr]$^+$[Cl]$^-$ mixtures, leads to a decrease in the compressibility of mixtures. These results are in good agreement with those obtained from the volumetric studies for both systems. In general, the $\Delta\kappa_s$ values decrease with an increase in temperature for the system {[Epmpyr]$^+$[Cl]$^-$ (x_1) + ethanol (x_2)} and increase for the system {[Epmpyr]$^+$[Cl]$^-$ (x_1) + water (x_2)} at a fixed composition of [Epmpyr]$^+$[Cl]$^-$ as shown in Fig. 7. The $\Delta\kappa_s$ values for {[Epmpyr]$^+$[Cl]$^-$ (x_1) + water (x_2)} > {[BMIM]$^+$[SCN]$^-$ (x_1) + ethanol (x_2)} indicate that there is a decrease in compressibility from the ideal mixture in the order: water > ethanol. The decrease in compressibility is due to stronger interaction between components of mixtures due to the proximity of unlike molecules [51]. The $\Delta\kappa_{s,min}$ values are $-10.3 \times 10^8 \times Pa^{-1}$

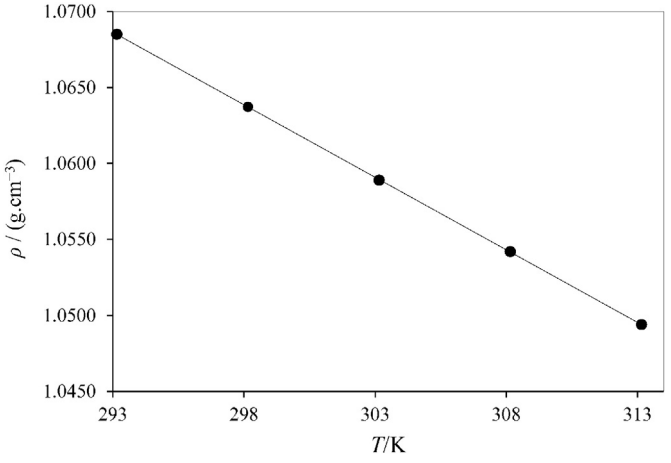

Fig. 2. Density, ρ, of [Epmpyr]$^+$[Cl]$^-$ at temperatures from (293.15 to 313.15) K.

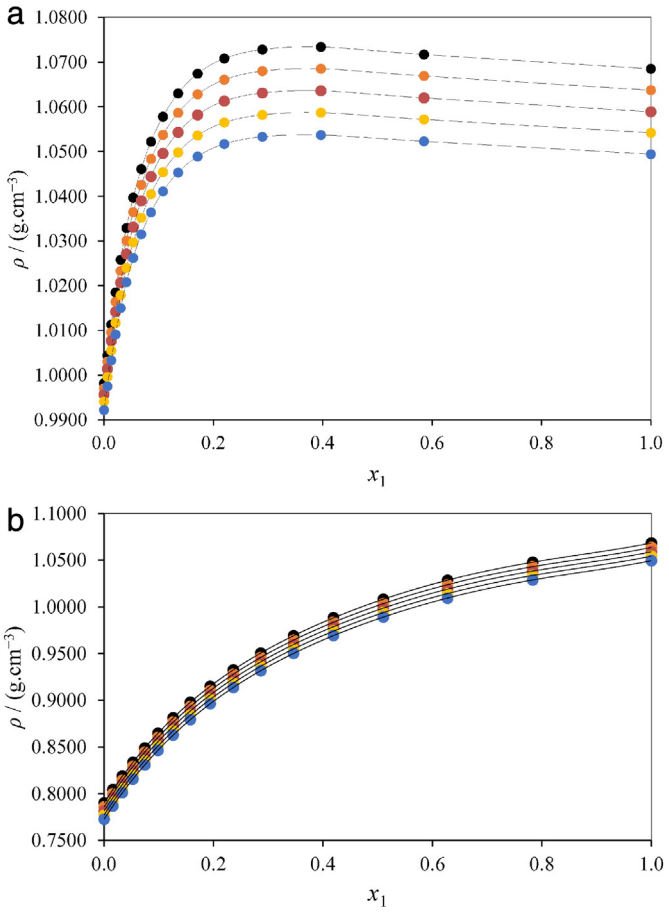

Fig. 3. Density, ρ, for the mixture of (a) {[Epmpyr]$^+$[Cl]$^-$ (x_1) + water (x_2)} and (b) {[Epmpyr]$^+$[Cl]$^-$ (x_1) + ethanol (x_2)} as function of the composition expressed in the mole fraction of [Epmpyr]$^+$[Cl]$^-$ at 293.15 K (●), 298.15 K (●), 303.15 K (●), 308.15 K (●) and 313.15 K (●).

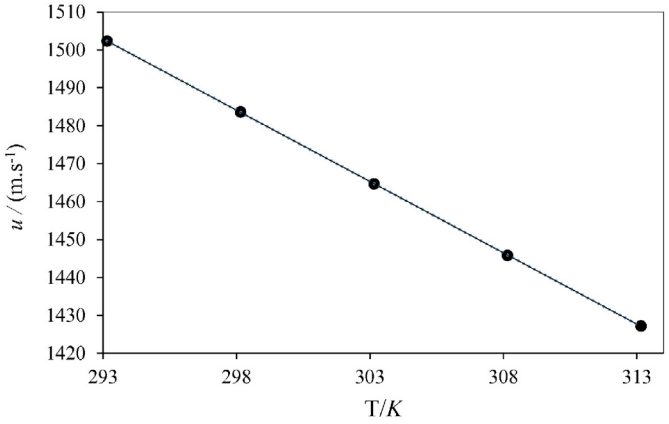

Fig. 4. Speed of sound velocity of {[Epmpyr]$^+$[Cl]$^-$ at temperatures from (293.15 to 313.15) K.

and $-24.7 \times 10^8 \times \mathrm{Pa}^{-1}$ and occurs at $x_1 = 0.1153$ and 0.3635, respectively, for each system at all temperatures.

3.5. Correlation of derived properties

The excess/deviation properties calculated from the density and speed of sound data for {[Epmpyr]$^+$[Cl]$^-$ (x_1) + water or ethanol (x_2)} systems were fitted to the Redlich–Kister equation [52] given below:

$$X = x_1 x_2 \sum_{i=1}^{k} A_i \, (1\text{-}2x_1)^{\,i-1} \tag{4}$$

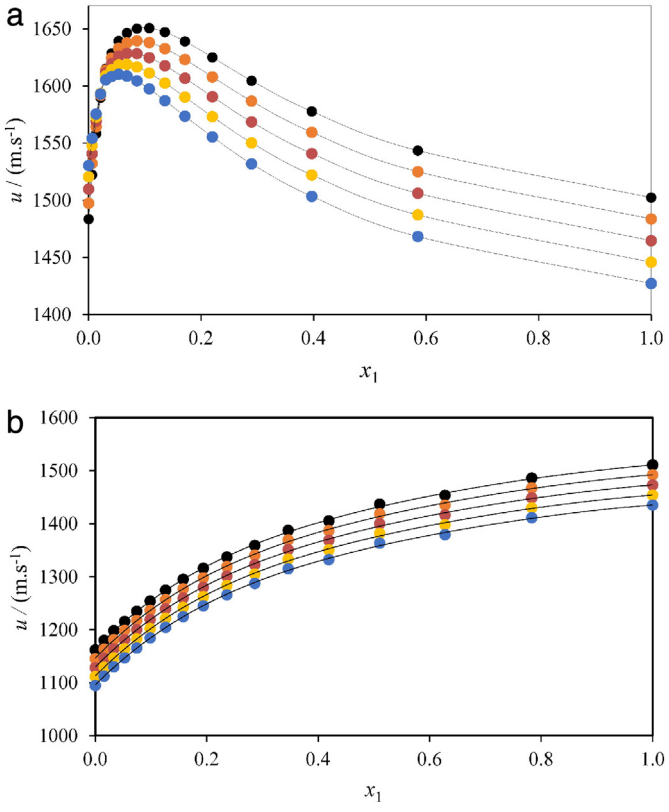

Fig. 5. Speed of sound, u, for the mixture of (a) {[Epmpyr]$^+$[Cl]$^-$ (x_1) + water (x_2)} and (b) {[Epmpyr]$^+$[Cl]$^-$ (x_1) + ethanol (x_2)} as function of the composition expressed in the mole fraction of [Epmpyr]$^+$[Cl]$^-$ at 293.15 K (●), 298.15 K (●), 303.15 K (●), 308.15 K (●) and 313.15 K (●).

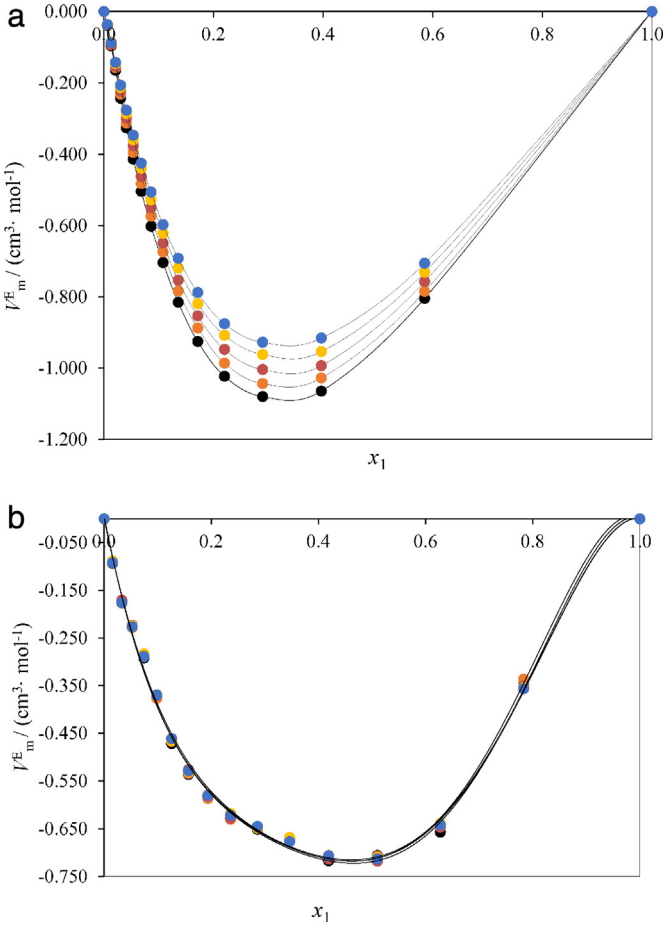

Fig. 6. Excess molar volumes, V_m^E, for the mixture of (a) {[Epmpyr]$^+$[Cl]$^-$ (x_1) + water (x_2)} and (b) {[Epmpyr]$^+$[Cl]$^-$ (x_1) + ethanol (x_2)} as function of the composition expressed in the mole fraction of [Epmpyr]$^+$[Cl]$^-$ at 293.15 K (●), 298.15 K (●), 303.15 K (●), 308.15 K (●) and 313.15 K (●).

where X is the excess molar volumes, V_m^E, and deviation in isentropic compressibility, $\Delta\kappa_s$. The values of the fitting parameters A_i have been determined using a least-square method. These results are summarized in Table 4, together with the corresponding standard deviations, σ, for the correlation as determined using the equation given below:

$$\sigma(X) = \sum_{i=1}^{N} \left[\frac{(X_{\mathrm{expt}} - X_{\mathrm{calc}})^2}{(N-k)} \right]^{1/2} \tag{5}$$

where N is the number of experimental points and k is the number of coefficients used in the Redlich–Kister equation. The plots of the Redlich–Kister model together with the experimental V_m^E, and $\Delta\kappa_s$ are displayed in Figs. 6(a), (b) and 7(a) and (b), respectively. The standard deviations show very low values for both V_m^E and $\Delta\kappa_s$ at the investigated temperatures for both systems indicate that these data have a very good correlation with Redlich-Kister equation.

4. Conclusions

In this study *N*-(2′,3′-epoxypropyl)-*N*-methyl-2-oxopyrrolidinium chloride [Epmpyr]$^+$[Cl]$^-$ was synthesized and characterized by different techniques such as NMR (^{1}H and ^{13}C), FTIR, and elemental analysis. Thermo-physical properties of [Epmpyr]$^+$[Cl]$^-$ and its binary mixture with water and ethanol were measured at temperatures from (293.15 to 313.15) K under atmospheric pressure, from which various acoustical and thermodynamic parameters such as excess molar volume, isentropic compressibility and deviation in isentropic compressibility were

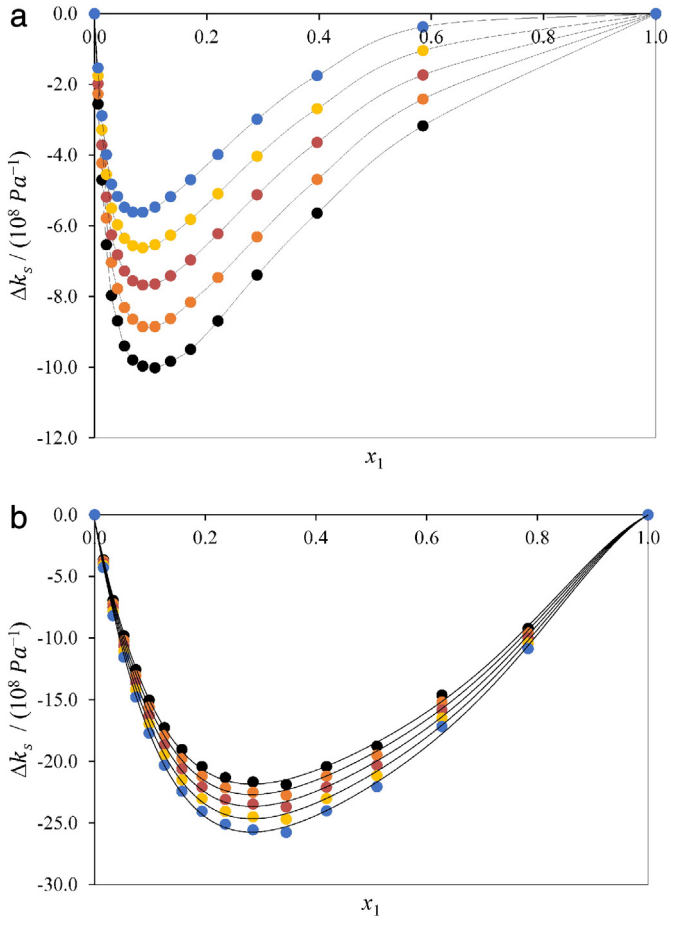

Fig. 7. Deviation of isentropic compressibility, $\Delta\kappa_s$, for the mixture of (a) {[Epmpyr]$^+$[Cl]$^-$ (x_1) + water (x_2)} and (b) {[Epmpyr]$^+$[Cl]$^-$ (x_1) + ethanol (x_2)} as function of the composition expressed in the mole fraction of [Epmpyr]$^+$[Cl]$^-$ at 293.15 K (●), 298.15 K (●), 303.15 K (●), 308.15 K (●) and 313.15 K (●).

calculated. The intermolecular interactions between the binary mixture of [Epmpyr]$^+$[Cl]$^-$ with water or ethanol were analyzed by studying the variations in the parameters determined. Structural readjustments, and efficient packing upon mixing of the liquids. The negative values of V_m^E suggest that water or ethanol molecules give a relatively more packed arrangement in [Epmpyr]$^+$[Cl]$^-$ as compared to the pure state, due to smaller molar volume of water or ethanol compared to [Epmpyr]$^+$[Cl]$^-$. The negative values are attributed to the strong attractive interactions due to the solvation of the ions in the mixture, specific interactions between unlike molecules in the liquid mixture and structural readjustments in the liquid mixture. Satisfactory correlations for the excess thermodynamic parameters were obtained by fitting with the Redlich–Kister polynomial equation.

Acknowledgement

Mr. Vasantha Kumar Arumugam and also other authors are grateful to Durban University of Technology, the National Research Foundation (NRF) South Africa for the Innovation Doctoral Grant (Grant UID: 101117).

References

[1] J. Flieger, E.B. Grushka, A. Czajkowska-Żelazko, J. Austin, Anal. Pharm. Chem. 1 (2014) 1–8.
[2] T. Fan, C. Chen, T. Fan, F. Liu, Q. Peng, J. Hazard. Mater. 297 (2015) 340–346.
[3] P. Wasserchеid, T. Welton, Ionic Liquids in Synthesis, Wiley-VCH Verlag, Germany, 2002.
[4] H. Weingartner, Angew. Chem. Int. Ed. 47 (2008) 654–670.
[5] R.G. Azevedo, J.S.S. Esperanca, V.N. Visak, Z.P. Visak, H.J.R. Guedes, M.N. Ponte, L.P.N. Rebelo, J. Chem. Eng. Data 50 (2005) 997–1008.
[6] C. Chiappe, D. Pieraccini, J. Phys. Org. Chem. 18 (2005) 275–297.
[7] P. Wasserscheid, T. Welton, Ionic Liquids in Synthesis, second ed. Wiley-VCH, Weinheim, 2008.
[8] S. Aparicio, M. Atilhan, F. Karadas, Ind. Eng. Chem. Res. 49 (2010) 9580–9595.
[9] J.P. Hallett, T. Welton, Chem. Rev. 111 (2011) 3508–3576.
[10] L.C. Tome, C. Florindo, C.S.R. Freire, L.P.N. Rebelo, I.M. Marrucho, Phys. Chem. Chem. Phys. 16 (2014) 17172–17182.
[11] Y.S. Sistla, A. Khanna, J. Ind. Eng. Chem. 20 (2014) 2497–2509.
[12] D.A. Glasscock, J.A. Critchfield, G.T. Rochelle, Chem. Eng. Sci. 46 (1991) 2829–2845.
[13] V. Linek, J. Sinkule, P. Havelka, Ind. Eng. Chem. Res. 33 (1994) 2731–2737.
[14] J.G. Huddleston, A.E. Visser, W.M. Reichert, H.D. Willauer, G.A. Broker, R.D. Rogers, Green Chem. 3 (2001) 156–164.
[15] L.P.N. Rebelo, J.N.C. Lopes, J.M.S.S. Esperanca, H.J.R. Guedes, J. Lachwa, V. Najdanovic-Visak, Z.P. Visak, Acc. Chem. Res. 40 (2007) 1114–1121.
[16] X. Han, D.W. Armstrong, Acc. Chem. Res. 40 (2007) 1079–1086.
[17] P. Attri, P. Venkatesu, A. Kumar, J. Phys. Chem. B 114 (2010) 13415–13425.
[18] T. Kavitha, P. Attri, P. Venkatesu, R.S. Rama Devi, T. Hofman, Thermochim. Acta 545 (2012) 131–140.
[19] I. Bahadur, T.M. Letcher, S. Singh, G.G. Redhi, P. Venkatesu, D. Ramjugernath, J. Chem. Thermodyn. 82 (2015) 34–46.

Table 4
Coefficients A_i and standard deviations, σ, obtained for the binary systems {[Epmpyr]$^+$[Cl]$^-$ (x_1) + water or ethanol (x_2)} at different temperatures for the Redlich-Kister equation.

	T/K	A_0	A_1	A_2	A_3	A_4	σ
{[Epmpyr]$^+$[Cl]$^-$ (x_1) + water (x_2)}							
V_m^E/(cm^3·mol^{-1})	293.15	−3.941	−2.392	1.283	−8.750	5.875	0.007
	298.15	−3.796	−2.288	0.700	−7.062	4.874	0.006
	303.15	−3.678	−2.194	0.993	−7.416	5.040	0.005
	308.15	−3.540	−2.048	1.008	−7.447	5.125	0.005
	313.15	−3.373	−2.042	0.165	−4.791	3.282	0.004
$\Delta\kappa_s$/(10^8 × Pa^{-1})	293.15	−8.1	−78.7	−296.9	1134.0	−1075.0	0.6
	298.15	−6.2	−71.0	−260.7	1000.9	−960.4	0.5
	303.15	−3.9	−62.2	−235.7	905.6	−860.6	0.5
	308.15	−1.8	−54.8	−208.5	804.8	−766.4	0.4
	313.15	−0.5	−48.6	−187.9	728.2	−692.0	0.4
{[Epmpyr]$^+$[Cl]$^-$ (x_1) + ethanol (x_2)}							
V_m^E/(cm^3·mol^{-1})	293.15	−2.636	−0.109	−1.609	−3.292	3.250	0.021
	298.15	−2.614	−0.128	−1.622	−3.422	3.450	0.018
	303.15	−2.643	−0.186	−1.387	−2.970	2.817	0.018
	308.15	−2.611	−0.210	−1.442	−2.833	2.691	0.019
	313.15	−2.652	−0.225	−1.352	−2.752	2.488	0.018
$\Delta\kappa_s$/(10^8 × Pa^{-1})	293.15	−73.4	−51.5	−19.0	−18.3	−55.4	0.1
	298.15	−76.3	−53.5	−19.6	−19.0	−57.7	0.1
	303.15	−79.5	−55.8	−20.4	−19.6	−60.3	0.1
	308.15	−82.8	−58.4	−21.3	−19.9	−63.1	0.2
	313.15	−86.7	−61.1	−22.5	−20.6	−65.7	0.2

[20] I. Bahadur, N. Deenadayalu, S. Afr. J. Chem. 66 (2013) 200–206.
[21] V. Govinda, P. Attri, P. Venkatesu, P. Venkateswarlu, J. Phys. Chem. B 117 (2013) 12535–12548.
[22] A.B. Pereiro, J.M.M. Araújo, J.M.S.S. Esperança, I.M. Marrucho, L.P.N. Rebelo, J. Chem. Thermodyn. 46 (2012) 2–28.
[23] I. Bahadur, P. Singh, S. Kumar, K. Moodley, M. Mabaso, G.G. Redhi, Sep. Sci. Technol. 49 (2014) 1883–1888.
[24] A. Marciniak, Fluid Phase Equilib. 249 (2010) 213–218.
[25] A. Marciniak, E. Karczemna, J. Phys. Chem. B 114 (2010) 5470–5474.
[26] W. Liu, T. Zhao, Y. Zhang, H. Wang, M. Yu, J. Solut. Chem. 35 (2006) 1337–1346.
[27] M.G. Freire, L.M.N.B.F. Santos, A.M. Fernandes, J.A.P. Coutinho, I.M. Marrucho, Fluid Phase Equilib. 261 (2007) 449–454.
[28] J. George, N.V. Sastry, J. Chem. Eng. Data 49 (2004) 235–242.
[29] U. Domańska, M. Krolikowska, Fluid Phase Equilib. 308 (2011) 55–63.
[30] J. Salminen, N. Papaiconomou, R.A. Kumar, J.-M. Lee, J. Kerr, J. Newman, J.M. Prausnitz, Fluid Phase Equilib. 261 (2007) 421–426.
[31] S. Corderí, N. Calvar, E. Gomez, A. Domínguez, Fluid Phase Equilib. 315 (2012) 46–52.
[32] N. Deenadayalu, I. Bahadur, T. Hofman, J. Chem. Thermodyn. 42 (2010) 726–733.
[33] N. Deenadayalu, I. Bahadur, T. Hofman, J. Chem. Eng. Data 55 (2010) 2636–2642.
[34] N. Deenadayalu, I. Bahadur, T. Hofman, J. Chem. Eng. Data 56 (2011) 1682–1686.
[35] I. Bahadur, N. Deenadayalu, J. Solut. Chem. 40 (2011) 1528–1543.
[36] I. Bahadur, N. Deenadayalu, Z. Tywabi, S. Sen, T. Hofman, J. Chem. Thermodyn. 49 (2012) 24–38.
[37] I. Bahadur, N. Deenadayalu, Thermochim. Acta 566 (2013) 77–83.
[38] V. Govinda, P.M. Reddy, I. Bahadur, P. Attri, P. Venkatesu, P. Venkateswarlu, Thermochim. Acta 556 (2013) 75–88.
[39] S. Singh, I. Bahadur, G.G. Redhi, E.E. Ebenso, D. Ramjugernath, J. Mol. Liq. 199 (2014) 518–523.
[40] S. Singh, I. Bahadur, G.G. Redhi, D. Ramjugernath, E.E. Ebenso, J. Mol. Liq. 200 (2014) 160–167.
[41] S. Singh, I. Bahadur, G.G. Redhi, E.E. Ebenso, D. Ramjugernath, J. Chem. Thermodyn. 89 (2015) 104–111.
[42] I. Bahadur, M.I.K. Momin, N.A. Koorbanally, M. Sattari, E.E. Ebenso, L.M. Katata-Seru, S. Singh, D. Ramjugernath, J. Mol. Liq. 213 (2016) 13–16.
[43] S. Singh, M. Aznar, N. Deenadayalu, J. Chem. Thermodyn. 57 (2013) 238–247.
[44] M. Hasan, A.P. Hiray, U.B. Kadam, D.F. Shirude, K.J. Kurhe, A.B. Sawant, J. Solut. Chem. 40 (2011) 415–429.
[45] I. Bahadur, N. Deenadayalu, P. Naidoo, D. Ramjugernath, J. Solut. Chem. 43 (2014) 487–803.
[46] N. Deenadayalu, P. Bhujrajh, J. Chem. Thermodyn. 38 (2006) 278–282.
[47] T.J. Fortin, A. Laesecke, M. Freund, S. Outcalt, J. Chem. Thermodyn. 57 (2013) 276–285.
[48] A.T.J. Hayward, Nature 221 (1969) 1047.
[49] M.J. Blandamer, Introduction to Chemical Ultrasonics, Academic Press, New York, 1973.
[50] M.T. Zafarani-Moattar, H. Shekaari, J. Chem. Thermodyn. 37 (2005) 1029–1035.
[51] M.T. Zafarani-Moattar, H. Shekaari, J. Chem. Eng. Data 50 (2005) 1694–1699.
[52] O. Redlich, A.T. Kister, Ind. Eng. Chem. 40 (1948) 345–348.

9.2 Critical review for 1st Publication

Synthesis, characterization and thermophysical properties of ionic liquid N-methyl-N-(2',3'-epoxypropyl)-2-oxopyrrolidinium chloride and its binary mixtures with water or ethanol at different temperatures.

In this research publication, a novel N-2′,3′-epoxypropyl-N-methyl-2-oxopyrrolidinium chloride IL was successfully synthesized and characterized by FTIR, ^{1}H NMR, ^{13}C NMR and elemental analysis in order to confirm the chemical structure of the IL. The significant thermophysical properties such as ρ and u were measured experimentally for this IL and its related binary mixtures with either water or ethanol at temperatures from (293.15 to 313.15) K at 5 K intervals under atmospheric pressure. Furthermore, the derived thermodynamic properties of V_m^E, k_s, $\Delta k_s$and L_f were computed from investigated density and velocity of sound data. These experimentally derived thermodynamic data were correlated using the Redlich-Kister polynomial equation.

The physicochemical properties of ρ and u of the IL and its corresponding binary mixtures increased with increasing temperature. In this case, the IL (N-2′,3′-epoxypropyl-N-methyl-2-oxopyrrolidinium chloride) was completely miscible with water or ethanol to form homogeneous binary liquid mixtures. The u measurement helps to get information about solute-solute, solute-solvent and solvent-solvent interactions. These physicochemical properties are very important for research and development processes in chemical industries. Generally, many chemical industries are trying to use ILs in their "Research and Development" processes but the main disadvantages of ILs are their high viscosity. The designed IL, with its low viscosity and comparatively low costs to synthesize, satisfies many of the challenges faced with current ILs and holds great promise for future use in industry. The experimental ρ and u data obtained in this study as a function of temperature may also be used to "solvent designers" in the future for commercialization. The methods of synthesis and recovery are simple, and reusability was easily accomplished.

The derived thermodynamic properties such as V_m^E, k_s, $\Delta k_s$and L_f (shown in Fig. 6 and 7 as well as Table 4 and 5) decreased with increasing temperature. Theoretical principles help to explain the interactions between the various types of molecules, such as hydrogen bonding, ionic interactions and dipole moment effect. The substitution of epoxy group to effectively interacted with water or ethanol and reduces self-association of ILs and enhances the ionic interaction, Van der Waals associations and significant H-bonding among water and IL molecules. The negative values of

the V_m^E for both the binary systems indicated the packing or filling effects. Water or ethanol molecules perfectly fitted in the free space of the interstices in $[Epmpyr]^+[Cl]^-$ and ion-dipole strong interaction contributed to creating the negative effect or packing effects. The synthesized IL has a higher dielectric constant, resulting in strong interaction occurring for the binary system with water {$[Epmpyr]^+[Cl]^-$ (x_1) + water (x_2)} when compared with the other binary system with ethanol{$[Epmpyr]^+[Cl]^-$ (x_1) + ethanol (x_2)}. The minima values of (V_m^E) corresponding binary mixtures are $V_{m,min}^E$= -1.075 $cm^3 \cdot mol^{-1}$ at the mole fraction of x_1 = 0.3054 and $V_{m,min}^E$= -0.694 $cm^3\ mol^{-1}$ at the mole fraction of x_1 = 0.4375 respectively for the related binary mixtures of $[Epmpyr]^+[Cl]^-$ (x_1) + water and $[Epmpyr]^+[Cl]^-$ + ethanol (x_2) at various investigated temperatures. These values for both binary system increased with increasing temperatures. The decreasing order in term of competing effect of the binary systems is as follows $[Epmpyr]^+[Cl]^-$ + water (x_2)} > {$[Epmpyr]^+[Cl]^-$ (x_1) + ethanol (x_2)} from computed thermodynamic properties data.

The product of the inverse of the ρ and square of the u is defined as the k_s.

$$k_s = \rho^{-1}u^{-2} \qquad (9.1)$$

The resulting data for k_s shows that the k_s increases with increasing temperature across the entire mole fraction ranges for both binary systems. This possibly increased due to the thermal agitation enhancing the compressibility efforts. The Δk_s gave negative values for the entire mole fraction ranges, confirming the presence of filling or packing effects operating in both binary systems. The strong interactions of $[Epmpyr]^+[Cl]^-$ with water or ethanol is due to increased dielectric constant values, more H-bonds, and the closer attractions together of uneven molecules (such as IL and solvent molecules). The solvent molecules exactly fitted into the free space of the $[Epmpyr]^+[Cl]^-$ moiety. There was a decrease in k_s values with increasing temperature for both the binary systems. In particular, the graphical images of these derived thermodynamic properties data show that, these values initially decrease with increasing mole fraction of IL then after reaching their saturation point, increases in both systems due to the concentration of IL in binary mixture is more, compare molecular solvents. This phenomenon could be due to the fact that the initial concentration was low, so the IL molecules are not able to interact properly but after addition of more ILs, the interaction becomes stronger and effective. The minima values of $\Delta k_{s,min}$ = -10.3 × 10^8 Pa and -24.7 × 10^8 Pa and occurs at x_1 = 0.1153 and x_1 = 0.3635, mole fraction of IL respectively, for both binary system at all investigated temperatures. Good correlation was obtained using the Redlich-

Kister polynomial equation for all derived thermodynamic properties in both binary mixtures at fixed temperatures.

Table 4: Intermolecular free length ($L_f/10^7$ m) for binary mixture of [EPMpyr]$^+$[Cl]$^-$ with ethanol at temperatures from 293.15 to 313.15 K

x_1	293.15K	298.15K	303.15K	308.15K	313.15K
0.0000	1.9731	2.0257	2.0805	2.1371	2.2473
0.0157	1.9253	1.9767	2.0297	2.0849	2.1920
0.0331	1.8794	1.9291	1.9807	2.0340	2.1382
0.0526	1.8360	1.8843	1.9345	1.9863	2.0877
0.0743	1.7914	1.8383	1.8869	1.9372	2.0357
0.0984	1.7475	1.7932	1.8401	1.8887	1.9845
0.1260	1.7030	1.7476	1.7932	1.8402	1.9331
0.1576	1.6606	1.7035	1.7476	1.7930	1.8833
0.1938	1.6189	1.6605	1.7036	1.7476	1.8347
0.2361	1.5782	1.6185	1.6598	1.7026	1.7875
0.2862	1.5384	1.5774	1.6173	1.6582	1.7405
0.3461	1.4922	1.5295	1.5681	1.6078	1.6873
0.4190	1.4587	1.4954	1.5326	1.5713	1.6487
0.5101	1.4131	1.4480	1.4839	1.5211	1.5958
0.6275	1.3827	1.4167	1.4517	1.4878	1.5610
0.7831	1.3398	1.3724	1.4060	1.4407	1.5110
1.0000	1.3051	1.3364	1.3694	1.4030	1.4713

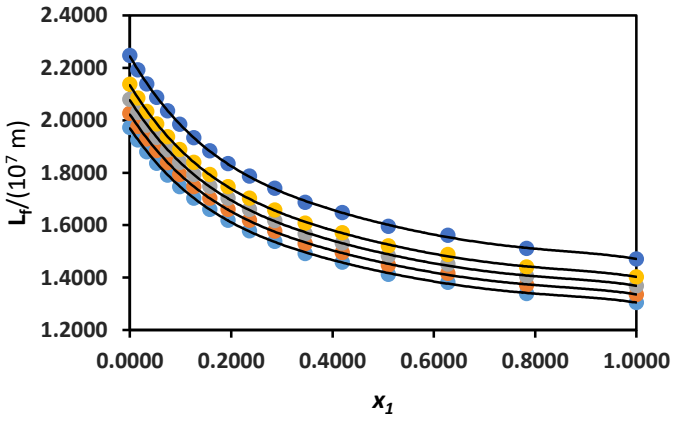

Figure 6: Intermolecular free length for binary mixture of $[EPMpyr]^+[Cl]^-$ with ethanol at temperatures 293.15 to 313.15K

Table 5: Intermolecular free length ($L_f/10^7\ m$) for binary mixture of $[EPMpyr]^+[Cl]^-$ with water at temperatures from 293.15 to 313.15 K

x_1	293.15K	298.15K	303.15K	308.15K	313.15K
0.0000	1.3747	1.3751	1.3777	1.3813	1.4189
0.0067	1.3349	1.3393	1.3460	1.3531	1.3934
0.0143	1.3002	1.3073	1.3176	1.3279	1.3706
0.0229	1.2695	1.2812	1.2928	1.3065	1.3517
0.0327	1.2447	1.2595	1.2744	1.2902	1.3372
0.0441	1.2313	1.2460	1.2642	1.2820	1.3313
0.0574	1.2177	1.2358	1.2556	1.2751	1.3260
0.0731	1.2091	1.2289	1.2501	1.2713	1.3239
0.0921	1.2040	1.2238	1.2472	1.2699	1.3240
0.1153	1.2005	1.2220	1.2467	1.2712	1.3270
0.1446	1.2005	1.2238	1.2494	1.2755	1.3328
0.1822	1.2022	1.2289	1.2556	1.2828	1.3421
0.2333	1.2109	1.2375	1.2666	1.2951	1.3560
0.3054	1.2262	1.2528	1.2833	1.3132	1.3757
0.4149	1.2463	1.2746	1.3061	1.3371	1.4015
0.6034	1.2744	1.3057	1.3370	1.3695	1.4359
1.0000	1.3113	1.3440	1.3770	1.4107	1.4794

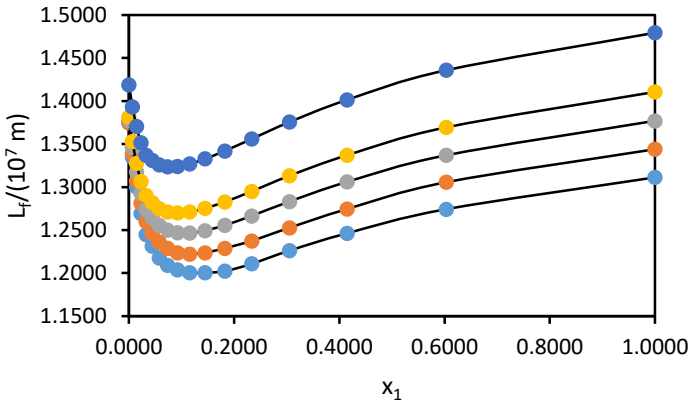

Figure 7: Intermolecular free length for binary mixture of $[EPMpyr]^+[Cl]^-$ with water at temperatures 293.15 to 313.15 K

10 Chapter 6

10.1 2nd Publication

Graphical abstract

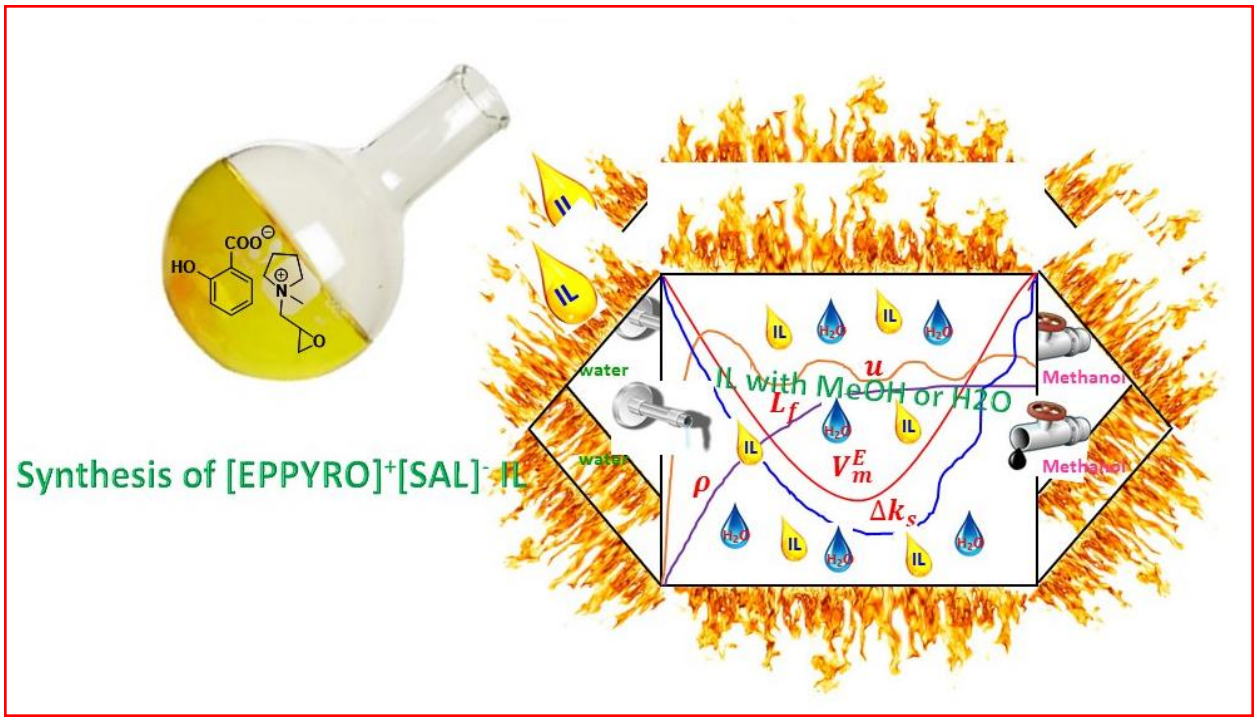

RSC Advances

PAPER

View Article Online
View Journal | View Issue

Cite this: *RSC Adv.*, 2016, **6**, 61566

Synthesis and characterization of 2′,3′-epoxy propyl-*N*-methyl-2-oxopyrrolidinium salicylate ionic liquid and study of its interaction with water or methanol

A. Vasanthakumar,[a] I. Bahadur,*[bc] G. Redhi*[a] and R. M. Gengan[a]

Received 2nd May 2016
Accepted 16th June 2016

DOI: 10.1039/c6ra11327c

www.rsc.org/advances

Important physico-chemical properties of ionic liquids (ILs) can be manipulated by adjusting the nature of the cation or anion. These properties are exploited in applications such as organic synthesis, catalysis and electrochemical processes to mention a few. In this work, the novel pyrrolidone ionic liquid *N*-(2′,3′-epoxypropyl)-*N*-methyl-2-oxopyrrolidinium salicylate $[EPMpyr]^+[SAL]^-$ was synthesized using two steps and characterized. The temperature dependent density and speed of sound for ionic liquid, methanol, water, and their corresponding binary mixtures of {IL (1) + methanol or water (2)} were measured over the entire range of mole fractions at temperatures from T = (293.15 to 313.15) K in steps of 5 K, under atmospheric pressure. The calculated thermodynamic properties such as excess molar volume V_m^E, isentropic compressibility k_s, intermolecular free length L_f, and deviation in isentropic compressibility Δk_s, were derived from the investigated density and speed of sound data. The resulting experimental data for excess molar volumes V_m^E, intermolecular free length L_f, and deviation in isentropic compressibility Δk_s, were well fitted to the Redlich–Kister polynomial equation. The effect of temperature and concentration on thermophysical properties was also provided.

1. Introduction

Ionic liquids (ILs) are low melting salts which are a combination of cations and anions; cations are usually found in the organic part of the molecule whilst the anion may be inorganic or organic in nature. These ILs have been developed in the last two decades. Nowadays ILs are an important research area of study, with many researchers focusing on fundamental physical and chemical properties, such as density, ρ, viscosity, η sound velocity, u, low vacuum pressure, Pa, low melting point, high conductivity, S, and solubility.[1] The density, viscosity, and sound velocities are essential for developing industrial processes and design.[1–4]

Industrial chemicals are being manufactured by using environment-friendly green solvents ILs, instead of toxic organic volatile solvents.[5–7] In the last decade, concerted attention by the scientific community has significantly improved the nature and potential applications of ILs, in particular, because of their exclusive physico-chemical properties.[8–11] Most of the industrial technological applications of ILs are occurring in mixtures, whilst the number of research groups has increased worldwide.[12–16] Properties such as vapor–liquid equilibrium, liquid–liquid equilibrium and importantly the physico-chemical properties of mixtures are studied. ILs have interesting properties such as negligible vapor pressure,[17] high ionic conductivity.[18] high thermal stability,[19] chemical and electrochemical stability, non-flammability[20] and low or negligible toxicity; these are the potential variables to completely substitute or replace the conventional organic solvents as electrolyte solutions or as co-solvents or additives to improve productivity and performance in industrial applications. The more important physico-chemical properties of ILs such as density, ρ, speed of sound, u, refractive index, n, conductivity, s, polarity and dielectric permittivity's can be adjusted by exchanging cations or anions. These significant properties have been exploited in a several successful applications such as organic synthesis, catalysis, separation technology, extraction and electrochemical processes.[1–4] In the modern world ILs are used as environment-friendly green and clean solvents for an excessive diversity of materials: pharmaceuticals,[21] biomass feedstocks[22–24] and greenhouse gases.[25]

Ionic liquids have materialized as a successful alternative to substitute for traditional toxic volatile organic solvents for separation of aromatic hydrocarbons from liquid mixtures,[26] due to their exclusive properties such as non-flammability, reusable

[a]*Department of Chemistry, Durban University of Technology, P O Box 1334, Durban, 4000, South Africa. E-mail: redhigg@dut.ac.za*

[b]*Department of Chemistry, School of Mathematical and Physical Sciences, Faculty of Agriculture, Science and Technology, North-West University (Mafikeng Campus), Private Bag X2046, Mmabatho 2735, South Africa. E-mail: bahadur.indra@nwu.ac.za; bahadur.indra@gmail.com; Fax: +27 0866741159; Tel: +27 31 373 2936*

[c]*Material Science Innovation and Modelling (MaSIM) Research Focus Area, Faculty of Agriculture, Science and Technology, North-West University (Mafikeng Campus), Private Bag X2046, Mmabatho 2735, South Africa*

capability, negligible volatilities, high thermal stabilities, non-corrosiveness, to be co-ordinate to a specific application by the combination of altered cation and anion with aliphatic hydrocarbons,[27,28] Currently ILs have been applicable more in pharmaceutical industries, solvent and anti-solvent for active pharmaceutical ingredient (API),[29,30] thereby improving water solubility of API[31] used to extract biological components from active materials,[32] and as a medium to synthesize pharmaceutically active materials.[33] Ionic liquids are often used for those applications to reduce cost as well as the viscosity of the materials.

Pyrrolidinium based ILs are potentially applicable as an electrolyte in batteries due to its attractive properties, some of the research done using pyrrolidinium based ILs in lithium batteries such as 1-(2-methoxyethyl)-1-methylpyrrolidinium-bis-(trifluoro methylsulfonyl)imide are used as a potential alternate for electrolyte components to substitute volatile toxic organic solvents in supercapacitors and lithium batteries.[34,35] Pyrrolidinium dicyanamide ILs are successful candidates for application as electrolytes in electrochemical double layer capacitors (EDLCs).[4–7]

In recent years, the usage of ILs have been increased as potential solvents to extract aromatic hydrocarbons from aliphatic hydrocarbons.[26,36–40] The thermo-physical properties of *N*-butyl-*N*-methyl-2-oxopyrrolidinium bromide was measured and reported at several temperatures from (293.15–343.15) K.[41] The present work discloses, the synthesis, characterization and determination of thermo-physical properties of novel *N*-2′,3′-epoxy propyl-*N*-methyl-2-oxo pyrrolidinium salicylate and its binary mixtures of water or methanol to understand the molecular interactions which occurs in this solutions. The present work is a part of our investigations on physicochemical properties of ILs with solvents at different temperatures.[41–53]

Table 1 Comparison of experimental densities, ρ, of pure liquids with literature values at different temperatures

Component	Supplier	% Mass purity	T/K	ρ/g cm^{-3} Exp.		Lit.
Water			293.15	0.9982	0.9998	54
					0.9996	
			298.15	0.9971		
			303.15	0.9957	0.9974	54
			308.15	0.9941	0.9940	54
			313.15	0.9922		
Methanol	Fluka	≥99.0	293.15	0.7914	0.7915	55
					0.7912	56
					0.7910	58
					0.7912	57
			298.15	0.7867	0.7868	55
					0.7866	56
					0.7865	57
					0.7866	59
			303.15	0.7820	0.7821	55
					0.7818	56
					0.7819	58
					0.7817	57
					0.7819	59
			308.15	0.7772	0.7770	57
					0.7772	59
			313.15	0.7724	0.7726	55
					0.7726	56
					0.7720	58
					0.7722	57
					0.7727	61
$[EPMPYR]^+[SAL]^-$			293.15	1.0685	—	
			298.15	1.0637	—	
			303.15	1.0590	—	
			308.15	1.0542	—	
			313.15	1.0495	—	

2. Experimental section

2.1. Materials

N-methyl-2-pyrrolidone, epichlorohydrin, sodium salicylate, acetonitrile, methanol, acetone, and hexane were purchased from Fluka Chemicals with purity of ≥99%. The purity and density of the pure compounds in comparison with literature[54–59] values are presented in Table 1. Ultra-pure deionized water was used in all experiments. The water content using a Metrohm Karl Fishcher coulometer (model KF Titrando) was found to be 0.05% in *N*-2′,3′-epoxy propyl-*N*-methyl-2-oxo pyrrolidinium salicylate $[EPMpyr]^+[SAL]^-$.

2.2. Step 1: synthesis of *N*-(2′,3′-epoxypropyl)-*N*-methyl-2-oxo pyrrolidinium chloride

The reaction system was set up as follows: a 500 mL three-necked round bottomed flask with a thermometer inlet over cold water flowing condenser was used. Nitrogen gas was flushed into the round bottomed flask 1.0 mol of freshly distilled *N*-methyl-2-pyrrolidone was mixed with 100 mL of acetonitrile, followed by 1.10 mol of epichlorohydrin. The mixture was now brought to a moderate reflux (90–100) °C, then heated under reflux for 48 hours with constant stirring and finally cooled to room temperature. The volatile materials were removed under reduced pressure to give a yellow coloured ionic liquid, *N*-(2′,3′-epoxypropyl)-*N*-methyl-2-oxopyrrolidinium chloride. The structure was confirmed by FTIR, ^{1}H NMR, ^{13}C NMR and elemental analysis.

2.3. Characterization of *N*-(2′,3′-epoxypropyl)-*N*-methyl-pyrrolidonium chloride

The $[EPMpyr]^+[Cl]^-$ was characterized by the following technique: NMR (^{1}H and ^{13}C), elemental analysis and FTIR. FTIR (ν = cm^{-1}): 3442, 2995, 1621, 1501, 1403, 1332, 1256, 1113, 967, 856, 756, 679, 561, 479. $[EPMpyr]^+[Cl]^-$ ^{1}H NMR (400 MHz, DMSO): δ 3.48–3.51 (m, 1H), 3.30–3.32 (t, 2H), 2.76–3.29 (s, 1H), 2.61–2.62 (s, 3H). 2.26–2.30 (d, 1H) 1.96–1.98 (t, 2H) 1.90–1.94 (m, 2H) ^{13}C NMR (100 MHz, DMSO): δ 175.03, 51.22, 49.38, 45.72, 45.00, 30.62, 29.50, and 17.59. Elemental analysis (in %): theoretical calculation for: $C_8H_{14}NO_2$: C, 50.14; H, 7.36; N, 7.31; the values found (in %) are C, 50.45; H, 7.10; N, 7.17.

2.4. Step 2: synthesis of *N*-(2′,3′-epoxypropyl)-*N*-methyl-2-oxo pyrrolidinium salicylate

The *N*-(2′,3′, epoxypropyl)-*N*-methyl-2-oxopyrrolidinium salicylate was synthesized by dissolving the desire quantity 1.12 mole

of sodium salicylate separately in methanol to make a clear solution in round bottomed flask. Then, the above synthesized intermediate IL *N*-(2′,3′-epoxypropyl)-*N*-methyl-2-oxopyrrolidium chloride was added to exchange the salicylate anion. The product was purified by a solvent wash with acetone, petroleum ether and hexane to remove unwanted starting materials and sodium chloride, then distilled again at 80 °C for 48 h to get pure moisture free ILs. The product identity was established with FTIR, NMR (proton and carbon) and elemental analysis. Scheme for synthesis of 2′,3′-epoxy propyl-*N*-methyl-2-oxopyrrolidinium salicylate given below:

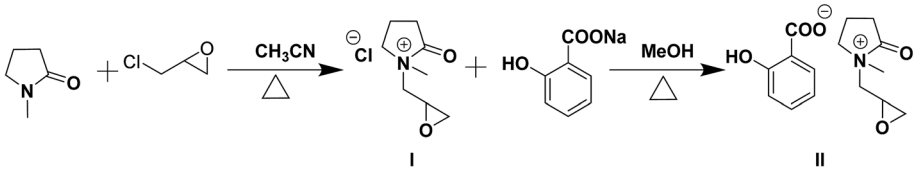

Scheme for synthesis of 2′, 3′-epoxy propyl - N-methyl-2- oxopyrrolidinium salicylate

2.5. Characterization of *N*-(2′,3′-epoxypropyl)-*N*-methyl-pyrrolidonium salicylate

The $[EPPY]^+[SAL]^-$ was characterized by the following methods: NMR (^1H and ^{13}C), elemental analysis and FTIR. The structure of $[EPMpyr]^+[SAL]^-$ is as shown in Fig. 1. FTIR ($\nu = cm^{-1}$): 3442, 2995, 1621, 1501, 1403, 1332, 1256, 1113, 967, 856, 756, 679, 561, 479. $[EPPYR]^+[SAL]^-$ ^1H NMR (400 MHz, DMSO): δ 1.9–2.0 (M, 2H), 2.15–2.3 (t, 2H), 2.7–2.8 (s, 3H), 3.3–3.4 (m, 3H), 3.5–3.65 (d, 2H), 3.66–3.90 (m, 1), 4.0–4.2 (m, 1), 6.75–6.85 (t, 1H), 6.86–7.00 (m, 1H), 7.10–7.30 (t, 1H), 7.40–7.60 (m, 1H), 7.65–7.95 (d–d, 1H). ^{13}C NMR (100 MHz, DMSO): δ 18, 30, 33, 51, 65, 72, 75, 115, 120, 122, 132, 134, 138, 163 and 178. Elemental analysis (in %) Theoretical calculation for: $C_{15}H_{21}NO_4$: C, 64.50; H, 7.58; N, 5.01; O, 22.91; the values found (in %) are C, 64.95; H, 7.10; N, 5.28; O, 23.36.

2.6. Apparatus and procedure

Anton Parr DSA 5000 M vibrating tube digital densitometer and speed of sound analyzer were used to determine the density and speed of sound of IL and their binary mixtures simultaneously. Temperature and pressure are important parameters to affecting physical properties, and were controlled to ±0.01 K and 101 kPa respectively. Doubly distilled ultra-pure water was used to calibrate the instrument according to the method of Lagourette *et al.*[60] The {IL (1) + methanol or water (2)} binary mixture samples were prepared by weighing on a Mettler Toledo AG245, which has a precision of 0.0001 g. The estimated uncertainty in density and speed of sound was less than $\pm 2 \times 10^{-4}$ g cm^{-3} and ±0.09 m s^{-1}, respectively.

3. Result and discussion

The density ρ, and speed of sound u, are interesting volumetric properties which are important for industrial processes and development. Fig. 2 to 5, show the investigated values of density and speed of sound data, the volumetric properties of pure ionic liquid (IL) $[EPMpyr]^+[SAL]^-$ and their binary mixtures with methanol or water, were measured under atmospheric pressure from $T = (293.15–313.15)$ K.

Tables 2 and 3, show the experimental values of density, ρ, speed of sound u, excess molar volume V_m^E, isentropic compressibility k_s, deviation in isentropic compressibility Δk_s and intermolecular free length L_f corresponding to several mole fractions of IL systems.

Those systems are formed by ionic liquids and it's binary mixtures of methanol or water, *viz.* {$[EPMpyr]^+[SAL]^-$ (1) + methanol (2)}; {$[EPMpyr]^+[SAL]^-$ (1) + water (2)} at (293.15, 298.15, 303.15, 308.15 and 313.15) K, respectively. All

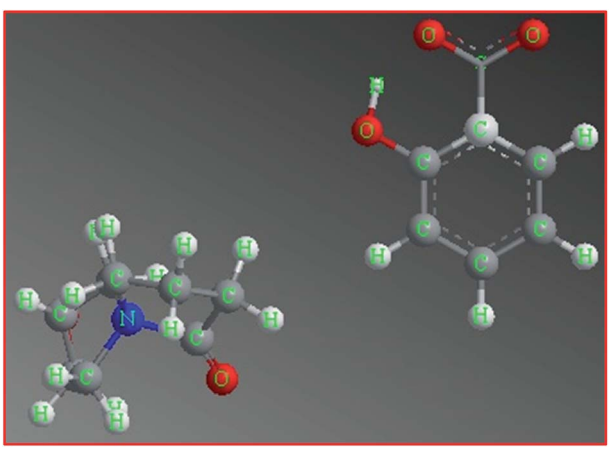

Fig. 1 Structure of the ionic liquid $[EPMpyr]^+[SAL]^-$.

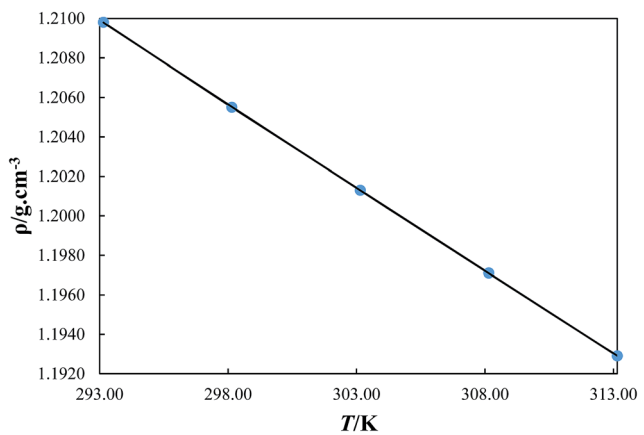

Fig. 2 Density, ρ, of $[EPMpyr]^+[SAL]^-$ at temperatures from (293.15 to 313.15) K. The solid line represents the smoothness of these data.

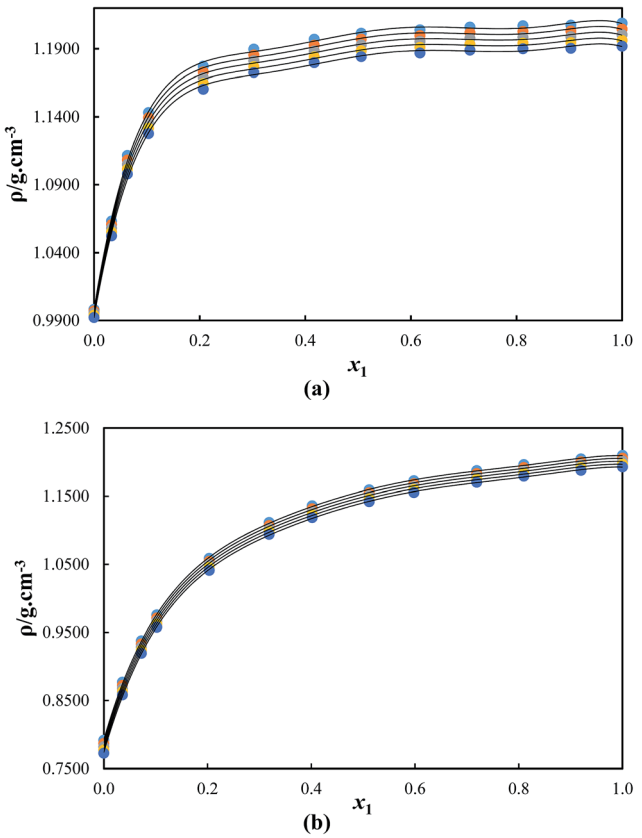

Fig. 3 Density, ρ, for the mixture of (a) {[EPMpyr]$^+$[SAL]$^-$ (1) + water (2)} and (b) {[EPMpyr]$^+$[SAL]$^-$ (1) + methanol (2)} as function of the composition expressed in the mole fraction of {[EPMpyr]$^+$[SAL]$^-$} at T = 293.15 K (●), T = 298.15 K (●), T = 303.15 K (●), T = 308.15 K (●) and T = 313.15 K (●). The solid line represents the smoothness of these data.

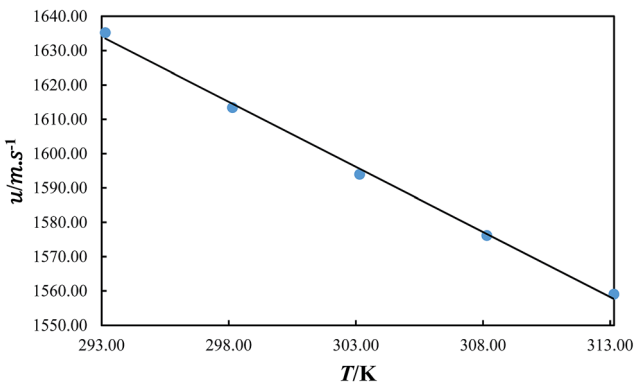

Fig. 4 Speed of sound velocity of {[EPMpyr]$^+$[SAL]$^-$} at temperatures from (293.15 to 313.15) K. The solid line represents the smoothness of these data.

combinations were mixed well to give a homogeneous solution across the entire mole fraction range.

The measured data of ρ and u of pure [EPMpyr]$^+$[SAL]$^-$, methanol, water, and their binary mixtures are display in Tables 2 and 3 as a function of IL mole fraction (x_1) for entire composition range at temperature from (293.15 to 313.15) K in

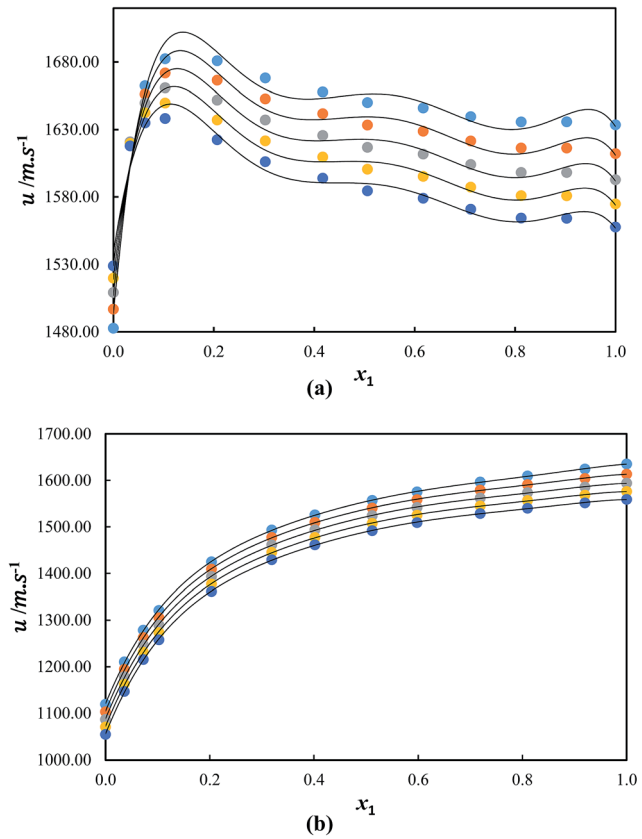

Fig. 5 Speed of sound, u, for the mixture of (a) {[EPMpyr]$^+$[SAL]$^-$ (1) + water (2)} and (b) {[EPMpyr]$^+$[SAL]$^-$ (1) + methanol (2)} as function of the composition expressed in the mole fraction of {[EPMpyr]$^+$[Cl]$^-$} at T = 293.15 K (●), T = 298.15 K (●), T = 303.15 K (●), T = 308.15 K (●) and T = 313.15 K (●). The solid line represents the smoothness of these data.

steps of 5 K under atmospheric pressure. The Fig. 6 to 8 were plotted based on the investigated values and these are V_m^E, Δk_s, and L_f as a function of the IL mole fraction at different temperatures of binary mixtures.

Here see the figures, in water with IL binary mixtures graphs, look like waves, that mean its accelerating due to initially, at the time of mixing pyrrolidonium salicylate IL interact with water to forms slight white precipitates, after shaking it becomes homogeneous liquids in every mole fraction of combinations. These are because of anionic effect, here salicylate anion plays a major role in that interaction.

In addition, the curves obtained with the parameters listed in Tables 2 and 3, have also been included. Normally, ILs is completely miscible with solvents, which have more dielectric constants otherwise ILs are not completely miscible.[61–63] The Fig. 2 and 3 shows the temperature dependent density values. From the measured data, the density of pure IL was greater then it's starting organic compound. Additionally, the densities of the binary mixture or pure ILs decreases with increase the temperature.

The excess molar volume, V_m^E was calculated from the investigated density data list by using the following eqn (1):

Table 2 Density, (ρ) speed of sound, (u) excess molar volume, (V_m^E) isentropic compressibility (k_s), intermolecular free length, (L_f) and deviation in isentropic compressibility, (Δk_s) with mole fraction of *N*-(2′,3′-epoxypropyl)-*N*-methyl-2-oxopyrrolidinium salicylate in the binary mixture of {[EPMpyr]$^+$[SAL]$^-$ (1) + methanol (2)} at (293.15 to 313.15) K and at pressure $P = 0.1$ MPa

x_1	ρ/g cm^{-3}	u/m s^{-1}	V_m^E/ cm^3 mol^{-1}	k_s/10^8 Pa^{-1}	L_f/ 10^7 m	Δk_s/ 10^8 Pa^{-1}
***T* = 293.15 K**						
0.0000	0.7914	1119.30	0.000	100.86	2.047	0.00
0.0360	0.8769	1210.33	−0.488	77.84	1.798	−20.50
0.0724	0.9377	1278.51	−0.768	65.24	1.646	−30.56
0.1023	0.9756	1320.95	−0.910	58.74	1.562	−34.96
0.2034	1.0587	1424.91	−1.106	46.52	1.390	−40.11
0.3189	1.1115	1493.34	−1.103	40.34	1.294	−38.21
0.4018	1.1360	1525.85	−1.023	37.81	1.253	−34.95
0.5117	1.1592	1556.94	−0.861	35.59	1.216	−29.48
0.5978	1.1726	1575.19	−0.692	34.37	1.195	−24.67
0.7189	1.1874	1596.43	−0.510	33.04	1.171	−17.53
0.8099	1.1962	1609.51	−0.370	32.27	1.158	−11.94
0.9201	1.2046	1624.27	−0.151	31.47	1.143	−5.04
1.0000	1.2098	1635.20	0.000	30.91	1.133	0.00
T = 298.15 K						
0.0000	0.7867	1103.13	0.000	104.46	2.102	0.00
0.0360	0.8723	1194.56	−0.502	80.34	1.844	−21.51
0.0724	0.9332	1262.85	−0.791	67.19	1.686	−32.02
0.1023	0.9711	1305.29	−0.936	60.44	1.599	−36.60
0.2034	1.0543	1409.15	−1.137	47.77	1.422	−41.93
0.3189	1.1071	1477.40	−1.134	41.38	1.323	−39.93
0.4018	1.1317	1509.76	−1.051	38.77	1.281	−36.53
0.5117	1.1549	1540.54	−0.885	36.48	1.242	−30.83
0.5978	1.1682	1558.46	−0.712	35.24	1.221	−25.82
0.7189	1.1831	1579.01	−0.530	33.90	1.198	−18.37
0.8099	1.1919	1590.91	−0.391	33.14	1.184	−12.53
0.9201	1.2003	1604.17	−0.160	32.37	1.170	−5.30
1.0000	1.2055	1613.45	0.000	31.87	1.161	0.00
***T* = 303.15 K**						
0.0000	0.7820	1086.78	0.000	108.27	2.160	0.00
0.0360	0.8676	1178.57	−0.515	82.97	1.891	−22.58
0.0724	0.9286	1247.02	−0.811	69.25	1.727	−33.56
0.1023	0.9666	1289.44	−0.959	62.22	1.637	−38.33
0.2034	1.0499	1393.18	−1.164	49.07	1.454	−43.84
0.3189	1.1027	1461.27	−1.158	42.47	1.353	−41.72
0.4018	1.1273	1493.52	−1.072	39.77	1.309	−38.16
0.5117	1.1506	1524.09	−0.900	37.42	1.270	−32.22
0.5978	1.1639	1541.79	−0.721	36.14	1.248	−26.99
0.7189	1.1789	1561.88	−0.534	34.77	1.224	−19.21
0.8099	1.1877	1573.56	−0.395	34.00	1.210	−13.11
0.9201	1.1961	1585.61	−0.162	33.25	1.197	−5.54
1.0000	1.2013	1593.94	0.000	32.76	1.188	0.00
***T* = 308.15 K**						
0.0000	0.7772	1070.51	0.000	112.28	2.292	0.00
0.0360	0.8630	1162.62	−0.533	85.73	1.939	−23.72
0.0724	0.9240	1231.23	−0.837	71.39	1.770	−35.20
0.1023	0.9620	1273.61	−0.987	64.08	1.731	−40.15
0.2034	1.0454	1377.25	−1.194	50.43	1.536	−45.85
0.3189	1.0984	1445.22	−1.186	43.59	1.428	−43.61
0.4018	1.1230	1477.38	−1.097	40.80	1.382	−39.88
0.5117	1.1463	1507.82	−0.919	38.37	1.340	−33.66
0.5978	1.1596	1525.37	−0.734	37.06	1.317	−28.19
0.7189	1.1746	1545.16	−0.539	35.66	1.292	−20.07
0.8099	1.1834	1556.54	−0.397	34.88	1.277	−13.70
0.9201	1.1919	1568.38	−0.162	34.11	1.263	−5.80
1.0000	1.1971	1576.18	0.000	33.62	1.254	0.00
***T* = 313.15 K**						
0.0000	0.7724	1054.36	0.000	116.46	2.301	0.00
0.0360	0.8583	1146.78	−0.550	88.59	2.036	−24.95
0.0724	0.9194	1215.52	−0.861	73.61	1.856	−36.99
0.1023	0.9575	1257.88	−1.015	66.01	1.732	−42.17
0.2034	1.0410	1361.41	−1.225	51.83	1.535	−48.16
0.3189	1.0940	1429.29	−1.214	44.74	1.426	−45.90
0.4018	1.1186	1461.37	−1.122	41.86	1.379	−42.07
0.5117	1.1419	1491.75	−0.938	39.35	1.337	−35.67
0.5978	1.1553	1509.20	−0.749	38.00	1.314	−30.05
0.7189	1.1703	1528.79	−0.546	36.56	1.289	−21.69
0.8099	1.1792	1539.98	−0.399	35.58	1.272	−15.30
0.9201	1.1877	1551.55	−0.160	34.98	1.261	−6.99
1.0000	1.1929	1559.03	0.000	35.49	1.270	0.00

$$V_m^E = \sum_{i=1}^{2} x_i M_i \left(\rho^{-1} - \rho_i^{-1}\right) \quad (1)$$

According to Fig. 6(a) and (b), the excess molar volume values are negative for all temperatures over entire composition range, so the volume of the solution was contracted due to the interaction between the IL and their binary mixture of water or methanol and are significant. Furthermore, the Fig. 6(a) and (b) indicates, the greater negative values of excess molar volume occurs when the temperatures increases. Higher temperature has been helpful to reduce the distance between unlike molecules, so the molecules are interacted more strongly. Moreover, Fig. 6(a) and (b) indicates the excess molar volume, minima occurs with water and methanol at $x_1 = 0.3026$ and at $x_1 = 0.2034$, respectively. The quasi-clathrates perhaps occurred in the mixture of an IL with organic components are reported in Wang *et al.*[64,65] In this case, it may happen in our binary mixtures such as [EPMpyr]$^+$[SAL]$^-$ with methanol in the nearby [EPMpyr]$^+$[SAL]$^-$ at $x_1 = 0.2034$. Similar results were also investigated for binary mixtures of [EPMpyr]$^+$[SAL]$^-$ with water at $x_1 = 0.3026$. Fig. 6(a) and (b), the excess molar volume graph indicates that 0.2000 and 0.3000 mole fraction of IL has low values and all binary mixture have negative excess molar values. In addition, the value of V_m^E is fully based on the effect of the hydrogen bond, polarity and interstitial accommodation in entire compositions. The packing/filling effect of methanol or water molecules in the interstices of IL, ion–dipole interactions between water and methanol with the pyrrolidonium ring of IL, all contributes to the negative values of V_m^E. The excess molar volume V_m^E, decreases with increasing temperature for both binary systems. The Tables 2 and 3 show that the result of excess molar volume data summaries for binary mixtures of IL with methanol or water. The results suggest the presence of the competing effect. These competing effect could be used to better understand the partial molar volumes of corresponding mixtures at infinite dilution.

Table 3 Density, (ρ) speed of sound, (u) excess molar volume (V_m^E) isentropic compressibility (k_s), intermolecular free length, (L_f) and deviation in isentropic compressibility (Δk_s) of *N*-(2′,3′-epoxypropyl)-*N*-methyl-2-oxopyrrolidinium salicylate in the binary liquid mixture of {[EPMpyr]$^+$[SAL]$^-$ (1) + water (2)} from at (293.15 to 313.15) K and at pressure $P = 0.1$ MPa

x_1	ρ/g cm^{-3}	u/m s^{-1}	V_m^E/ cm^3 mol^{-1}	k_s/ $10^8 \times$ Pa^{-1}	L_f/10^7 m	Δk_s/ $10^8 \times$ Pa^{-1}
$T = 293.15$ K						
0.0000	0.9982	1482.63	0.000	45.57	1.376	0.00
0.0332	1.0633	1620.29	0.034	35.82	1.220	−9.27
0.0630	1.1115	1662.43	−0.384	32.55	1.163	−12.10
0.1031	1.1432	1682.43	−0.616	30.90	1.133	−13.16
0.2067	1.1772	1680.87	−0.828	30.07	1.118	−12.49
0.3026	1.1897	1668.20	−0.849	30.20	1.120	−10.96
0.4170	1.1970	1657.88	−0.747	30.39	1.123	−9.10
0.5059	1.2014	1650.02	−0.756	30.57	1.127	−7.63
0.6171	1.2040	1645.98	−0.582	30.66	1.128	−5.92
0.7118	1.2060	1639.62	−0.493	30.84	1.132	−4.36
0.8123	1.2070	1635.67	−0.291	30.97	1.134	−2.77
0.9029	1.2073	1635.80	−0.039	30.95	1.134	−1.46
1.0000	1.2089	1633.54	0.000	31.00	1.135	0.00
T = 298.15 K						
0.0000	0.9971	1496.81	0.000	44.76	1.376	0.00
0.0332	1.0607	1620.01	0.047	35.92	1.233	−8.42
0.0630	1.1082	1656.29	−0.365	32.89	1.180	−11.06
0.1031	1.1394	1671.86	−0.589	31.40	1.153	−12.04
0.2067	1.1730	1666.47	−0.797	30.70	1.140	−11.41
0.3026	1.1855	1652.74	−0.819	30.88	1.143	−10.00
0.4170	1.1927	1641.78	−0.720	31.11	1.147	−8.31
0.5059	1.1972	1633.35	−0.736	31.31	1.151	−6.97
0.6171	1.1997	1628.78	−0.570	31.42	1.153	−5.43
0.7118	1.2017	1621.52	−0.490	31.65	1.157	−3.99
0.8123	1.2027	1616.27	−0.291	31.83	1.160	−2.52
0.9029	1.2031	1616.32	−0.042	31.82	1.160	−1.37
1.0000	1.2046	1612.10	0.000	31.94	1.162	0.00
$T = 303.15$ K						
0.0000	0.9957	1509.18	0.000	44.10	1.378	0.00
0.0332	1.0581	1620.83	0.060	35.97	1.245	−7.75
0.0630	1.1048	1649.66	−0.344	33.26	1.197	−10.13
0.1031	1.1355	1660.90	−0.562	31.92	1.173	−11.02
0.2067	1.1688	1651.82	−0.763	31.36	1.162	−10.42
0.3026	1.1812	1637.14	−0.785	31.59	1.167	−9.11
0.4170	1.1884	1625.65	−0.687	31.84	1.171	−7.57
0.5059	1.1929	1616.81	−0.706	32.07	1.175	−6.34
0.6171	1.1954	1611.80	−0.544	32.20	1.178	−4.95
0.7118	1.1975	1604.08	−0.472	32.45	1.182	−3.63
0.8123	1.1985	1598.17	−0.279	32.67	1.186	−2.29
0.9029	1.1989	1598.15	−0.031	32.66	1.186	−1.28
1.0000	1.2003	1592.76	0.000	32.84	1.189	0.00
$T = 308.15$ K						
0.0000	0.9941	1519.86	0.000	43.55	1.427	0.00
0.0332	1.0553	1619.78	0.068	36.12	1.259	−7.11
0.0630	1.1014	1642.56	−0.326	33.65	1.215	−9.28
0.1031	1.1316	1649.65	−0.536	32.76	1.238	−9.77
0.2067	1.1645	1637.15	−0.730	32.04	1.224	−9.48
0.3026	1.1769	1621.61	−0.752	32.31	1.229	−8.26
0.4170	1.1841	1609.66	−0.655	32.59	1.235	−6.85
0.5059	1.1885	1600.53	−0.677	32.85	1.240	−5.73
0.6171	1.1911	1595.26	−0.518	32.99	1.242	−4.49
0.7118	1.1932	1587.27	−0.451	33.26	1.247	−3.28
0.8123	1.1943	1580.93	−0.263	33.50	1.252	−2.06
0.9029	1.1946	1580.83	−0.019	33.50	1.252	−1.17
1.0000	1.1961	1574.75	0.000	33.71	1.256	0.00
$T = 313.15$ K						
0.0000	0.9922	1528.91	0.000	43.115	1.400	0.00
0.0332	1.0525	1617.85	0.077	36.299	1.303	−6.53
0.0630	1.0979	1634.94	−0.308	34.074	1.263	−8.50
0.1031	1.1277	1638.19	−0.511	33.042	1.225	−9.19
0.2067	1.1603	1622.49	−0.699	32.739	1.220	−8.61
0.3026	1.1726	1606.13	−0.720	33.058	1.226	−7.48
0.4170	1.1797	1593.86	−0.625	33.367	1.231	−6.19
0.5059	1.1842	1584.48	−0.649	33.635	1.236	−5.16
0.6171	1.1868	1578.98	−0.493	33.796	1.239	−4.05
0.7118	1.1889	1570.82	−0.429	34.088	1.245	−2.95
0.8123	1.1900	1564.25	−0.246	34.343	1.249	−1.84
0.9029	1.1903	1564.09	−0.003	34.341	1.249	−1.07
1.0000	1.1919	1557.61	0.000	34.581	1.254	0.00

Tables 2 and 3, shows that the increasing concentration of IL results in decreases the intermolecular free length, L_f of binary mixture. The Fig. 7(a) and (b), and Tables 2 and 3 indicates that as the speed of sound increases as corresponding decrease in

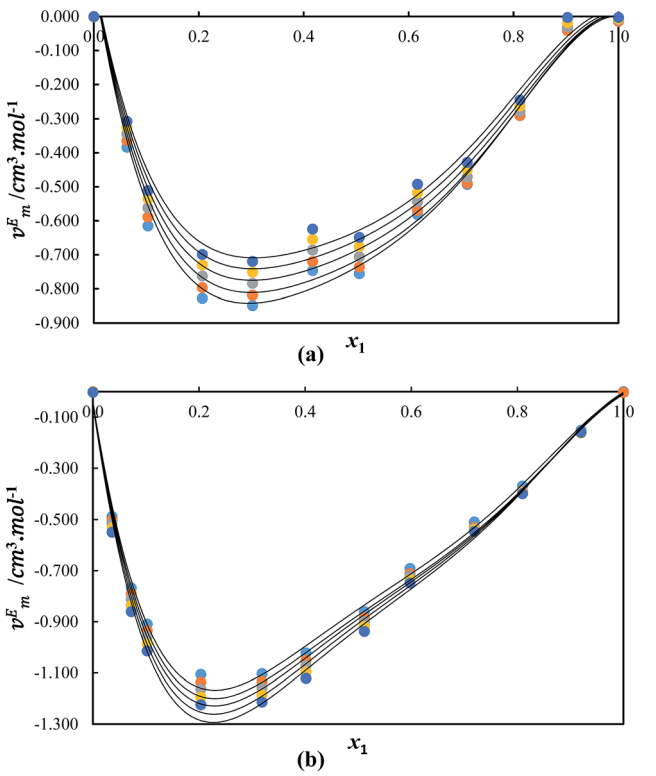

Fig. 6 Excess molar volumes, for the mixture of (a) {[EPMpyr]$^+$[SAL]$^-$ (1) + water (2)} and (b) {[EPMpyr]$^+$[SAL]$^-$ (1) + methanol (2)} as function of the composition expressed in the mole fraction of {[EPMpyr]$^+$[SAL]$^-$} at $T = 293.15$ K (●), $T = 298.15$ K (●), $T = 303.15$ K (●), $T = 308.15$ K (●) and $T = 313.15$ K (●). The solid lines were generated using Redlich–Kister curve-fitting.

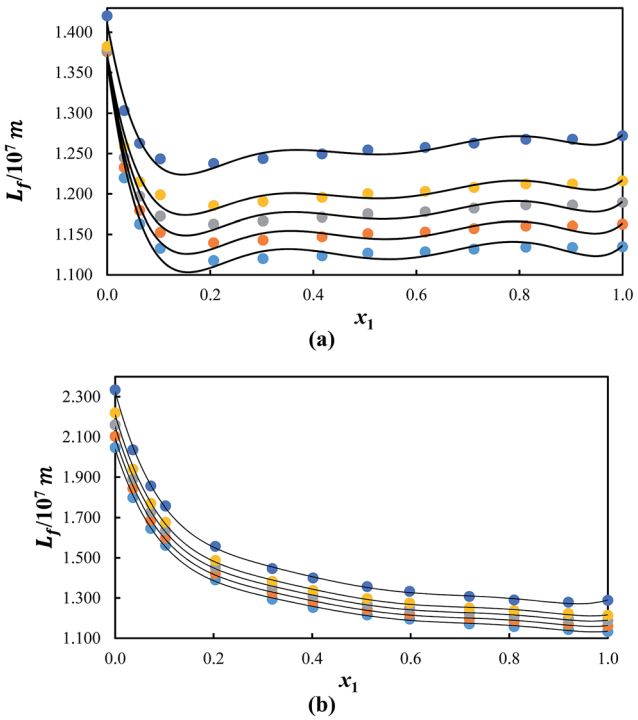

Fig. 7 Intermolecular free length, L_f, for the mixture of (a) {[EPMpyr]$^+$[SAL]$^-$ (1) + water (2)} and (b) {[EPMpyr]$^+$[SAL]$^-$ (1) + methanol (2)} as function of the composition expressed in the mole fraction of {[EPMpyr]$^+$[SAL]$^-$} at $T = 293.15$ K (●), $T = 298.15$ K (●), $T = 303.15$ K (●), $T = 308.15$ K (●) and $T = 313.15$ K (●). The solid lines were generated using Redlich–Kister curve-fitting.

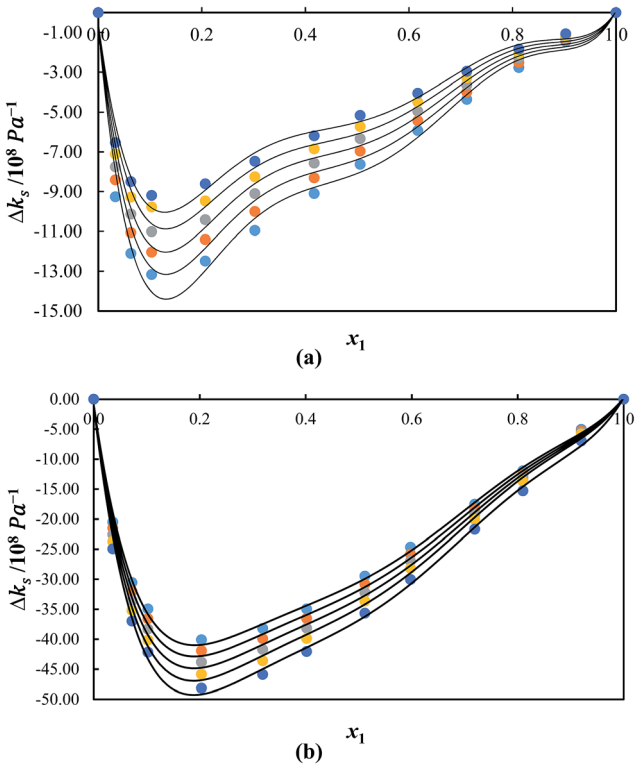

Fig. 8 Deviation of isentropic compressibility, Δk_s, for the mixture of (a) {[EPMpyr]$^+$[SAL]$^-$ (1) + water (2)} and (b) {[EPMpyr]$^+$[SAL]$^-$ (1) + methanol (2)} as function of the composition expressed in the mole fraction of {[EPMpyr]$^+$[SAL]$^-$} at $T = 293.15$ K (●), $T = 298.15$ K (●), $T = 303.15$ K (●), $T = 308.15$ K (●) and $T = 313.15$ K (●). The solid lines were generated using Redlich–Kister curve-fitting.

intermolecular free length and the intermolecular free length also increases with increasing temperature. Moreover intermolecular free length explains the greater distances between the surfaces of the two molecules, and this behavior leads to a corresponding decrease in the speed of sound.

Intermolecular free length (L_f) has been calculated from the eqn (2)

$$L_f = k_j(k_s)^{1/2} \quad (2)$$

where k_j is the Jacobson's constant and is a temperature dependent constant. Its value is $(93.875 + 0.375T) \times 10^{-8}$.

Isentropic compressibility (k_s) defined as eqn (3)

$$k_s = \rho^{-1}u^{-2} \quad (3)$$

The deviation in isentropic compressibility (Δk_s) can be defined from the isentropic compressibility as illustrated in eqn (4)

$$\Delta k_s = k_s - \sum_i^2 x_i k_{s,i} \quad (4)$$

This property is related to density and speed of sound by the Newton–Laplace equation.

Generally, the speed of sound increases with an increase in mole fraction of the mixture but decreases with temperature. The molar fractions increase linearly with temperatures and decays the isentropic compressibility exponentially. This performance elucidated due to the isentropic compressibility has been well defined as the inverse of the product of the density and square of the speed of sound. The free space was decreased due to the interaction between the molecules in binary mixtures, and in this way contributing to the negative deviation in isentropic compressibility. Fig. 8(a) and (b) display, the negative value of deviation in isentropic compressibility occurs over the entire composition of {[EPMpyr]$^+$[SAL]$^-$ + methanol or water} at all temperatures. The minimum value of deviation in isentropic compressibility of the binary mixtures was -40.11×10^8 Pa^{-1} and -13.16×10^8 Pa^{-1} with methanol and water are occurring at $x_1 = 0.2034$ and 0.1031, respectively. The ideal mixtures are more compressible then these mixtures due to the performance of deviation in isentropic compressibility. In this case, the unlike molecules approach closely and a stronger interaction between methanol or water with [EPMpyr]$^+$[SAL]$^-$ mixtures that lead to a decrease in compressibility. Normally, the deviation in isentropic compressibility values decreases with an increasing temperature for both binary systems at a several composition of [EPMpyr]$^+$[SAL]$^-$ as shown in Fig. 8(a) and (b). The compressibility decreases because of the unlike molecules are contiguity, due to the mixture of components have strongly interacted.

Table 4 Coefficients A_i, and standard deviations, σ, obtained for the binary systems {[EPMPYR]$^+$[SAL]$^-$ (1) + water or methanol (2)} at different temperatures for the Redlich–Kister equation

	T/K	A_0	A_1	A_2	A_3	A_4	σ
{[EPMpyr]$^+$[SAL]$^-$ (1) + methanol (2)}							
V_m^E/(cm^3 mol^{-1})	293.15	−3.513	−2.855	−1.889	−3.213	−3.655	0.02
	298.15	−3.608	−2.903	−2.060	−3.284	−3.688	0.03
	303.15	−3.669	−3.013	−2.098	−3.335	−3.386	0.03
	308.15	−3.749	−3.118	−2.056	−3.479	−4.109	0.03
	313.15	−3.831	−3.207	−2.067	−3.662	−4.260	0.03
L_f	293.15	5.331	−0.980	−6.602	7.909	39.533	0.9
	298.15	5.449	−1.008	−6.782	8.116	40.536	0.9
	303.15	5.571	−1.039	−6.976	8.344	41.567	0.9
	308.15	5.855	−0.963	−6.772	8.302	42.519	0.9
	313.15	5.886	−1.175	−7.752	9.912	44.780	0.9
Δk_s/(10^8 × Pa^{-1})	293.15	−121.99	−88.49	−47.92	−175.78	−201.65	1.0
	298.15	−127.59	−91.93	−49.65	−184.93	−212.81	1.0
	303.15	−133.35	−95.64	−51.45	−194.88	−224.49	1.1
	308.15	−139.35	−99.81	−53.13	−204.97	−237.44	1.2
	313.15	−147.59	−102.88	−56.59	−207.97	−258.37	1.3
{[EPMpyr]$^+$[SAL]$^-$ (1) + water (2)}							
V_m^E/(cm^3 mol^{-1})	293.15	−2.770	−1.762	−4.611	−2.374	6.514	0.08
	298.15	−2.685	−1.625	−4.639	−2.283	6.674	0.09
	303.15	−2.561	−1.544	−4.665	−2.226	6.917	0.09
	308.15	−2.444	−1.478	−4.586	−2.192	6.991	0.09
	313.15	−2.330	−1.416	−4.521	−2.193	7.139	0.09
L_f	293.15	4.823	−1.054	−4.048	3.691	28.909	0.60
	298.15	4.922	−1.060	−4.029	3.638	29.277	0.70
	303.15	5.022	−1.062	−4.007	3.591	29.632	0.70
	308.15	5.272	−1.011	−3.669	3.332	29.957	0.70
	313.15	5.283	−1.124	−4.230	3.728	31.158	0.70
Δk_s/(10^8 × Pa^{-1})	293.15	−32.53	−19.15	9.05	−102.12	−151.96	0.80
	298.15	−29.73	−17.46	8.36	−93.11	−139.15	0.70
	303.15	−27.09	−15.87	8.22	−85.31	−128.94	0.70
	308.15	−24.57	−14.48	8.12	−76.83	−117.74	0.70
	313.15	−22.17	−12.81	7.86	−72.15	−110.40	0.60

4. Correlation of derived properties

The derived properties have been correlated by Redlich–Kister equation[66] as below in eqn (5):

$$X = x_1 x_2 \sum_{i=1}^{k} A_j (1 - 2x_1)^{i-1} \quad (5)$$

where X is excess molar volumes (V_m^E), deviation in isentropic compressibility (Δk_s) and intermolecular free length, L_f. The least-square method has been used to determine the fitting parameters A_j values. Table 4 shows that the summarized results.

Composed with the corresponding standard deviations, σ. For the correlation as investigated using eqn (6).

$$\sigma(X) = \sum_{i=1}^{n} \left[\frac{X_{expt} - X_{calc}}{(N - K)} \right]^{1/2} \quad (6)$$

where N the number of is experimental points and k is the number of coefficients used in the Redlich–Kister equation. The values of V_m^E and Δk_s, as well as the plots of the Redlich–Kister model. Both binary systems of the standard deviations indicate very low values for both excess molar volumes and deviations in isentropic compressibility at all inspected temperatures.

5. Conclusions

In this study, the synthesis, characterization and investigation of important physical parameters of novel pure ionic liquid and their binary mixtures with water or methanol at (293.15 to 313.15) K in steps of 5 K under atmospheric pressure are presented. The physical parameters such as density and speed of sound for pure ionic liquid and their binary mixtures of {[EPMpyr]$^+$[SAL]$^-$ with methanol or water} were measured. The excess molar volume, V_m^E isentropic compressibility, k_s, deviation in isentropic compressibility, Δk_s and intermolecular free length, L_f were calculated and discussed. The above calculated parameters of excess molar volume, V_m^E and deviation in isentropic compressibility's, Δk_s shows negative values. These indicate strong intermolecular interactions occurring between unlike molecules; the compacting effect is a major role in these binary mixtures because of the strong interaction between pyrrolidonium cation and salicylate anion. The binary combination of IL mixtures has strong attractive interaction, readjustments in structure and packing effect due to the great negative values of Δk_s. The methanol with [EPMpyr]$^+$[SAL]$^-$ has more effective packing arrangement than water due to their more negative values in Δk_s and V_m^E as well as ion–dipole

interactions between methanol and $[EPMpyr]^{+}[SAL]^{-}$. The salicylate anion has carboxylate as well as hydroxyl groups so it can form hydrogen bonds easily. Acceptable correlations for the excess thermodynamic parameters occurred by fitting with the Redlich–Kister polynomial equation.

Acknowledgements

Mr Vasantha Kumar Arumugam is grateful to the Durban University of Technology and the National Research Foundation (NRF) South Africa for the Innovation Doctoral Grant (Grant UID: 101117).

References

1 N. A. Smirnova and E. A. Safonova, *Colloid J.*, 2012, **74**, 273–285.
2 N. V. Plechkova and K. R. Seddon, *Chem. Soc. Rev.*, 2008, **37**, 123–150.
3 P. Wasserscheid and T. Welton, *Synthesis and Purification of Ionic Liquids*, Wiley, Germany, 2003, DOI: 10.1002/3527600701.ch.
4 H. Zhao, S. Xia and P. Ma, *J. Chem. Technol. Biotechnol.*, 2005, **80**, 1089–1096.
5 J. Dupont, R. F. de Souza and P. A. Suarez, *Chem. Rev.*, 2002, **102**, 3667–3692.
6 T. Welton, *Chem. Rev.*, 1999, **99**, 2071–2084.
7 P. Wasserscheid and W. Keim, *Angew. Chem., Int. Ed.*, 2000, **39**, 3772–3789.
8 M. R. Curras, M. F. C. Gomes, P. Husson, A. A. H. Padua and J. Garcia, *J. Chem. Eng. Data*, 2010, **55**, 5504–5512.
9 P. K. Chhotaray, J. Shankar and R. L. Gardas, *J. Chem. Thermodyn.*, 2014, **74**, 255–262.
10 V. K. Sharma, S. Solanki and S. Bhagour, *J. Therm. Anal. Calorim.*, 2015, **1191**, 293–1302.
11 A. Stoppa, O. Zech, W. Kunz and R. Buchner, *J. Chem. Eng. Data*, 2010, **55**, 1768–1773.
12 A. Heintz, *J. Chem. Thermodyn.*, 2005, **37**, 525–535.
13 J. G. Huddleston, H. D. Willauer, R. P. Swatloski, A. E. Visser and R. D. Rogers, *Chem. Commun.*, 1998, 1765–1766.
14 M. S. Selvan, M. D. McKinley, R. H. Dubois and J. L. Atwood, *J. Chem. Eng. Data*, 2000, **45**, 841–845.
15 E. Vercher, P. J. Miguel, F. J. Llopis, A. V. Orchilles and A. Martinez-Andreu, *J. Chem. Eng. Data*, 2012, **57**, 1953–1963.
16 B. Gonzalez, N. Calvar, I. Dominguez and A. Dominguez, *J. Chem. Eng. Data*, 2009, **54**, 1353–1358.
17 J. D. Holbrey, R. D. Rogers, R. A. Mantz, P. C. Trulove, V. A. Cocalia, A. E. Visser, J. L. Anderson, J. L. Anthony, J. F. Brennecke, E. J. Maginn, T. Welton and R. A. Mantz, *Ionic Liquids in Synthesis*, Wiley-VCH Verlag GmbH and Co., KGaA, Weinheim, 2008, p. 57.
18 P. Bonhote, A. P. Dias, N. Papageorgiou, K. Kalyanasundaram and M. Gratzel, *Inorg. Chem.*, 1996, **35**, 1168–1178.
19 M. Pucheault and M. Vaultier, *Top. Curr. Chem.*, 2010, **290**, 83–126.
20 M. Smiglak, W. M. Reichert, J. D. Holbrey, J. S. Wilkes, L. Sun, J. S. Thrasher, K. Kirichenko, S. Singh, A. R. Katritzky and R. D. Rogers, *Chem. Commun.*, 2006, 2554–2556.
21 M. Moniruzzaman and M. Goto, *J. Chem. Eng. Jpn.*, 2011, **44**, 370–381.
22 M. E. Zakrzewska, E. Bogel-Lukasik and R. Bogel-Lukasik, *Energy Fuels*, 2010, **24**, 735–737.
23 L. J. A. Conceicao, E. Bogel-Lukasik and R. A. Bogel-Lukasik, *RSC Adv.*, 2013, **21**, 846–1855.
24 Q. Xin, K. Pfeiffer, J. Prausnitz, D. Clark and H. Blanch, *Biotechnol. Bioeng.*, 2012, **109**, 346–352.
25 Z. Lei, C. B. Dai and B. Chen, *Chem. Rev.*, 2014, **114**, 1289–1326.
26 G. W. Meindersma, A. R. Hansmeier and A. B. de Haan, *Ind. Eng. Chem. Res.*, 2010, **49**, 7530–7540.
27 M. J. Earle and K. R. Seddon, *Pure Appl. Chem.*, 2000, **72**, 1391–1398.
28 M. J. Earle, J. M. Esperanca, S. S. Gilea, M. A. Canongia, J. N. Lopes, L. P. N. Rebelo, J. W. Magee, K. R. Seddon and A. J. Widegren, *Nature*, 2006, **439**, 831–834.
29 J. H. An and W. S. Kim, *Cryst. Growth Des.*, 2013, **13**, 31–39.
30 J. H. An, J. M. Kim, S. M. Chang and W. S. Kim, *Cryst. Growth Des.*, 2010, **10**, 44–3050.
31 P. D. McCrary, P. A. Beasley, G. Gurau, A. Narita, P. S. Barber, O. A. Cojocaru and R. D. Rogers, *New J. Chem.*, 2013, **37**, 2196–2202.
32 B. D. Ribeiro, M. A. Z. Coelho, L. P. N. Rebelo and I. M. Marrucho, *Ind. Eng. Chem. Res.*, 2013, **52**, 12146–12153.
33 N. Grinberg, F. Albu, K. Fandrick, E. Iorgulescu and A. Medvedovici, *J. Pharm. Biomed. Anal.*, 2013, **75**, 1–6.
34 S. Ferrari, E. Quartarone, P. Mustarelli, A. Magistris, S. Protti, S. Lazzaroni, M. Fagnoni and A. Albini, *J. Power Sources*, 2009, **194**, 45–50.
35 G. B. Appetecchi, M. Montanino, M. Carewska, M. Moreno, F. Alessandrini and S. Passerini, *Electrochim. Acta*, 2011, **56**, 1300–1307.
36 A. R. Ferreira, M. G. Freire, J. C. Ribeiro, F. M. Lopes, J. G. Crespo and J. A. P. Coutinho, *Ind. Eng. Chem. Res.*, 2012, **51**(8), 3483–3507.
37 A. Kamankesh, M. Vossoughi, A. Shamloo, S. A. Mirkhani and J. Akbari, *Fluid Phase Equilib.*, 2012, **332**, 48–57.
38 M. T. G. Jongmans, B. Schuur and A. B. de Haan, *J. Chem. Thermodyn.*, 2012, **47**, 229–234.
39 J. Garcia, S. Garcia, J. S. Torrecilla and F. Rodriguez, *Fluid Phase Equilib.*, 2011, **301**, 62–67.
40 B. Mokhtarani, J. Musavi and M. Parvini, *Fluid Phase Equilib.*, 2014, **363**, 41–49.
41 I. Bahadur, S. Erlin, S. Singh, E. E. Ebenso and G. G. Redhi, *ACS Sustainable Chem. Eng.*, 2016, **4**, 601–608.
42 N. Deenadayalu, I. Bahadur and T. Hofman, *J. Chem. Thermodyn.*, 2010, **42**, 726–733.
43 N. Deenadayalu, I. Bahadur and T. Hofman, *J. Chem. Eng. Data*, 2010, **55**, 2636–2642.
44 N. Deenadayalu, I. Bahadur and T. Hofman, *J. Chem. Eng. Data*, 2011, **56**, 1682–1686.

45 I. Bahadur and N. Deenadayalu, *J. Solution Chem.*, 2011, **40**, 1528–1543.
46 I. Bahadur, N. Deenadayalu, Z. Tywabi, S. Sen and T. Hofman, *J. Chem. Thermodyn.*, 2012, **49**, 24–38.
47 I. Bahadur and N. Deenadayalu, *Thermochim. Acta*, 2013, **566**, 77–83.
48 I. Bahadur and N. Deenadayalu, *S. Afr. J. Chem.*, 2013, **66**, 200–206.
49 V. Govinda, P. M. Reddy, I. Bahadur, P. Attri, P. Venkatesu and P. Venkateswarlu, *Thermochim. Acta*, 2013, **556**, 75–88.
50 I. Bahadur, T. M. Letcher, S. Singh, G. G. Redhi, P. Venkatesu and D. Ramjugernath, *J. Chem. Thermodyn.*, 2015, **82**, 34–46.
51 S. Singh, I. Bahadur, G. G. Redhi, D. Ramjugernath and E. E. Ebenso, *J. Mol. Liq.*, 2014, **200**, 160–167.
52 S. Singh, I. Bahadur, G. G. Redhi, E. E. Ebenso and D. Ramjugernath, *J. Chem. Thermodyn.*, 2015, **89**, 104–111.
53 S. Singh, I. Bahadur, G. G. Redhi, E. E. Ebenso and D. Ramjugernath, *J. Mol. Liq.*, 2014, **199**, 518–523.
54 M. Singh and S. Kumar, *J. Appl. Polym. Sci.*, 2003, **87**, 1001–1015.
55 C. Yang, H. Lai, Z. Liu and P. Ma, *J. Chem. Eng. Data*, 2006, **51**, 584–589.
56 F. Comelli and R. Francesconi, *J. Chem. Eng. Data*, 1997, **42**, 705–709.
57 W. Fan, Q. Zhou, S. Zhang and R. Yan, *J. Chem. Eng. Data*, 2008, **53**, 1836–1840.
58 H. Djojoputro and S. Ismadji, *J. Chem. Eng. Data*, 2005, **50**, 1343–1347.
59 A. C. Gomez Marigliano and H. N. Solimo, *J. Chem. Eng. Data*, 2002, **47**, 796–800.
60 B. Lagourette, C. Boned, H. Saint-Guirons, P. Xans and H. Zhou, *Meas. Sci. Technol.*, 1992, **3**, 699–701.
61 M. Freemantle, *An Introduction to Ionic Liquids*, RSC Publishing, Cambridge, UK, 2010.
62 P. Bonhote, A. P. Dias, N. Papageorgiou, K. Kalyanasundaram and M. Gratzel, *Inorg. Chem.*, 1996, **35**, 1168–1178.
63 P. Wassercheid and W. Keim, *Angew. Chem., Int. Ed.*, 2000, **39**, 3772–3789.
64 J. Wang, A. Zhu, Y. Zhao and K. Zhuo, *J. Solution Chem.*, 2005, **34**, 585–596.
65 Y. Zhong, H. Wang and K. Diao, *J. Chem. Thermodyn.*, 2007, **39**, 291–296.
66 O. Redlich and A. T. Kister, *Ind. Eng. Chem.*, 1948, **40**, 345–348.

10.2 Critical review for 2nd Publication

Synthesis, characterization of 2', 3'-epoxy propyl - N-methyl-2- oxopyrrolidinium salicylate ionic liquid and study of its interaction with water or methanol.

This article describes the synthesis and characterization of a novel N-2′, 3′-epoxypropyl-N-methyl-2-oxopyrrolidinium salicylate $[Epmpyr]^+[SAL]^-$ IL. The chemical structure of the IL was identified by FTIR, ^1H NMR, ^{13}C NMR and elemental analysis techniques. In addition, investigation of the thermophysical and thermodynamic properties and its related binary mixtures with either water or methanol in mole fraction ranges from 0.1 to1.0 at temperatures (293.15 to 313.15) K, in interval of 5 K under atmospheric pressure were undertaken. The required combinations of binary liquid mixtures were prepared to make a homogeneous solution across the entire mole fraction range. Both ρ and u were found to be decrease with increasing temperatures, whereas both increases with increasing mole fraction of the IL. Particularly, the temperature has a significant effect on the interaction among the presiding molecules present in the liquid mixtures, and this could be the reason for decreases in ρ and u with increasing temperature. Density (ρ) and speed of sound (u) are significant volumetric properties which are essential for research and development processes in industries.

This IL was completely soluble in water which is a useful in industrial applications because water is a universal cheap solvent and easy to use, recoverable, reusable and cost effective as well. In addition, this type of water soluble ILs are easily separated from organic solvents. Nowadays ILs are used as a dilute solution in industrial applications because of their fascinating physical properties and also economic viability. In particular, this strong solubility nature is indicative of the high dielectric constant values. According to the experimental data, it was found that the density of the IL was low due to the source of starting organic compound.

Furthermore, the thermodynamic properties for example V_m^E, k_s, $\Delta k_s$and L_f were computed from the measured experimental thermophysical properties. It was found that V_m^E gives negative values for both liquid mixtures across the entire mole fraction ranges at all temperatures, and this further confirms, the "contraction or competing effect" occurred, due to significant attraction among the molecules in the liquid mixtures. The high temperature affects the interactions between uneven molecules which implies that the shape and structure of IL and molecular solvents are different, resulting in more negative values for V_m^E and Δk_s. The minima value of $V_{m,min}^E$ = -0.849 (cm^3

mol^{-1}) for binary mixtures with water at the x_1 = 0.3026 and $V^E_{m,min}$ = -1.106 (cm^3 mol^{-1}) for mixtures with methanol at x_1= 0.2034. In particular, V^E_m has depended on inter and intramolecular hydrogen bonds, polarity of the solution and interstitial accommodation of molecules in whole compositions for binary mixtures. These negative values of V^E_m clearly indicate the strong packing/filling effects obtained with either water or methanol molecules upon mixing with the 2-oxopyrrolidinium ring in this IL. Ion-dipole interactions also influence the negative deviations in V^E_m.

The excess molar volumes for binary mixtures at infinite dilution is obviously better understood by examining these competing effects. The intermolecular free length also increases with increasing temperature due to temperature influence on the interactions to increase the bond length among the uneven solute and solvent molecules. The molecules in the binary mixtures acquired more energy while increase the temperature, these energies influence to create some repulsion to get away each other, this is the reason for more L_f values. Generally, k_s is defined as the square root of u and inverse value of the ρ. The free space in the liquid mixtures was reduced because the strong interactions amongst the molecules contribute to making the Δk_s negative. The deviation in isentropic compressibility minima for binary mixtures were $\Delta k_{s,min}$ = -40.11 (cm^3 mol^{-1}) with methanol and $\Delta k_{s,min}$ = -13.16 (cm^3 mol^{-1}) with water were obtained at mole fraction x_1 = 0.2034 and x_1 = 0.1031, respectively for each system. In these binary mixtures, unlike molecules are approached closely to make a strong interaction among the water or methanol with IL, and this leads to a decrease in compressibility.

10.3 3rd Publication

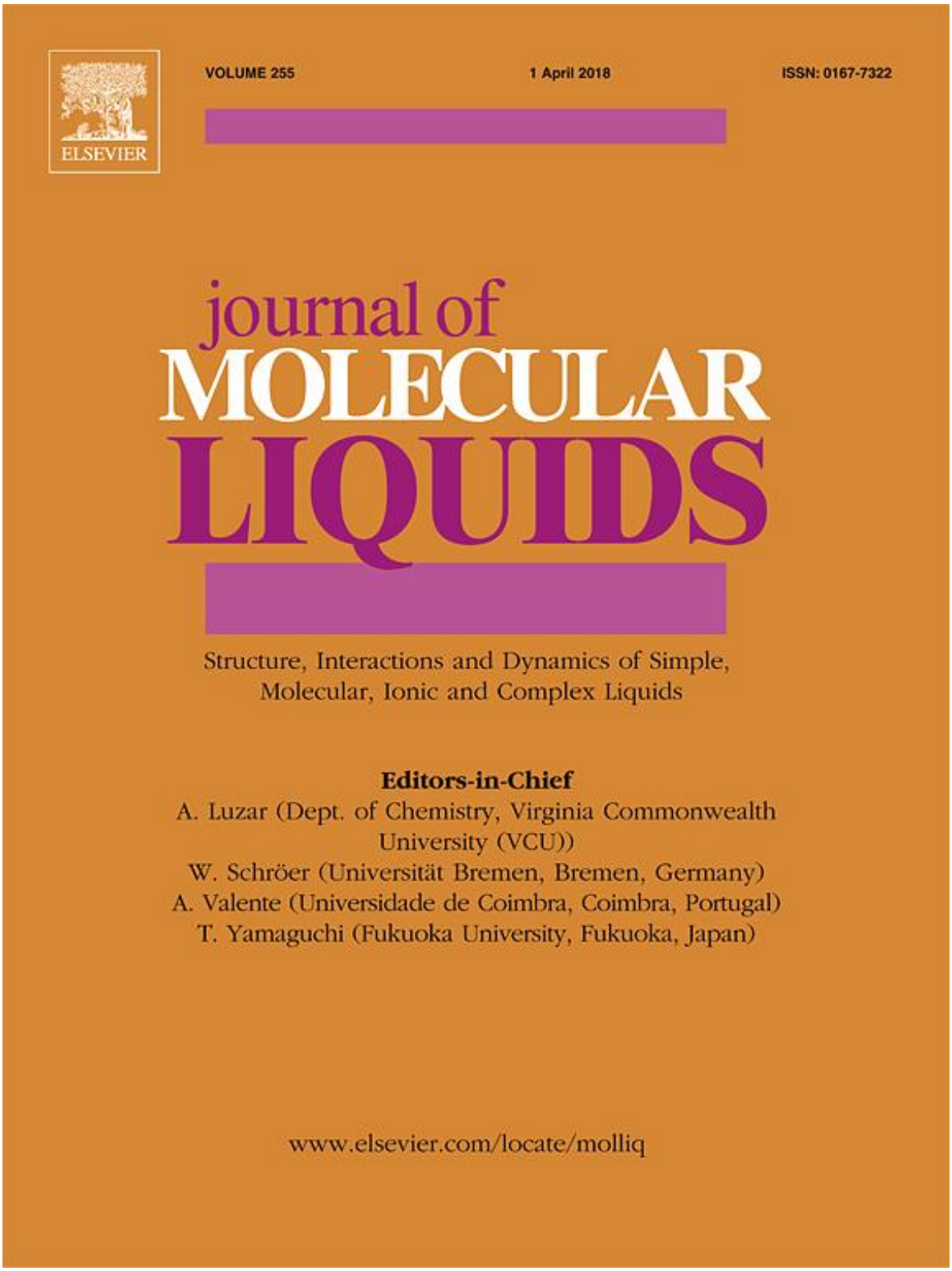

Graphical abstract

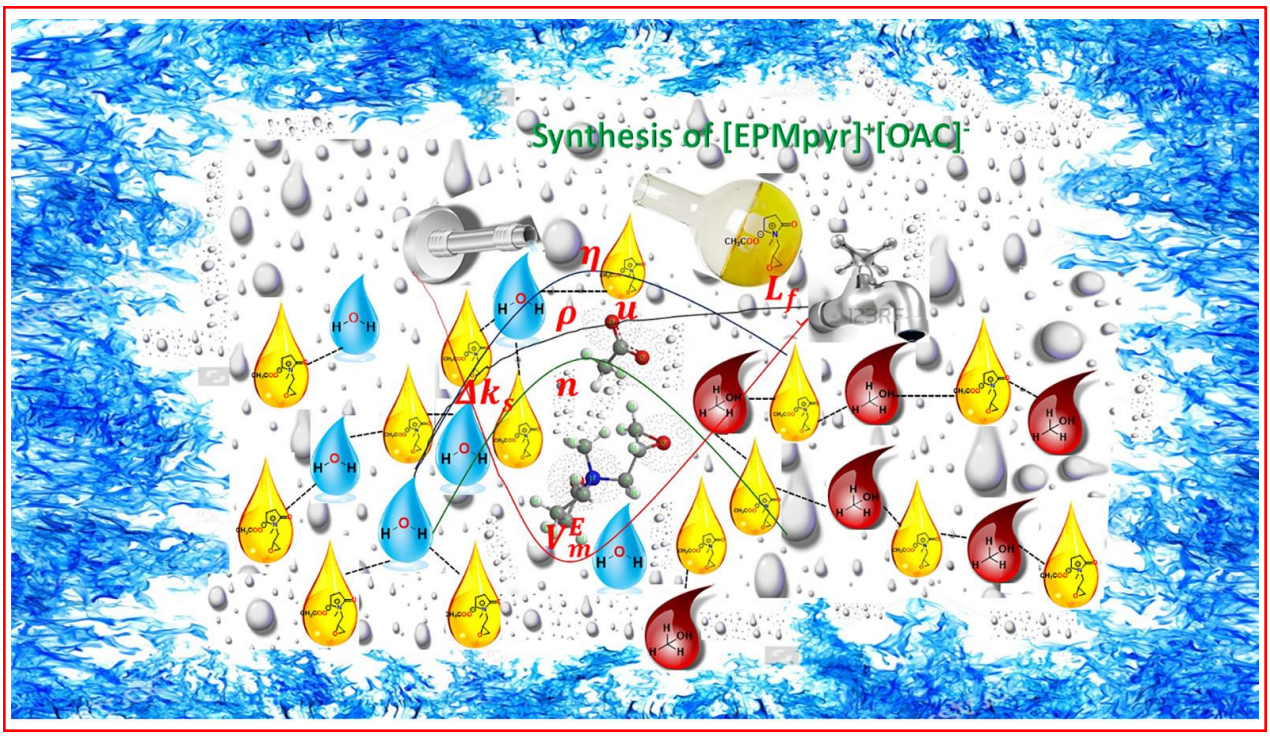

Journal of Molecular Liquids 242 (2017) 1215–1227

Contents lists available at ScienceDirect

Journal of Molecular Liquids

journal homepage: www.elsevier.com/locate/molliq

Synthesis, characterization and thermophysical properties of novel 2′, 3′-N-epoxypropyl- *N*-methyl-2-oxopyrrolidinium acetate ionic liquid and their binary mixtures with water or methanol

Vasanthakumar Arumugam, G.G. Redhi *, R.M. Gengan

Department of Chemistry, Durban University of Technology, Durban-4001, South Africa

ARTICLE INFO

Article history:
Received 28 March 2017
Received in revised form 20 July 2017
Accepted 24 July 2017
Available online 26 July 2017

Keywords:
Oxopyrrolidinium
Intermolecular free length
Isentropic compressibility
Excess molar volume
Epoxy propyl

ABSTRACT

Novel 2′, 3′-N-epoxypropyl-*N*-methyl-2-oxopyrrolidinium acetate ($[EPMpyr]^+[OAC]^-$) ionic liquid (IL) was successfully synthesized and characterized by FTIR, ^1H NMR, ^{13}C NMR and elemental analysis. This ionic liquid was utilized to produce binary mixtures with water or methanol, and their density (ρ), viscosity (η), velocity of sound (u) and refractive index (n_D) were measured at varied temperatures from 288.15 to 313.15 K, at atmospheric pressure of $P = 0.1$ MPa. This investigation resulted in significant thermophysical data being measured for pure IL, water, methanol and its binary mixtures of water or methanol over the entire range of mole fractions at fixed temperature and atmospheric pressure. Thermodynamic physicochemical properties of excess molar volume (V_m^E), isentropic compressibility (k_s), deviation in isentropic compressibilities (Δk_s), and intermolecular free length (L_f), were computed from the resulting experimental data of density and speed of sound. Furthermore, the calculated thermodynamic properties from these experimental data were successfully correlated using the Redlich-Kister equation. The obtained data were analyzed and interesting information about the influence of the functional group interactions and hydrogen bonds between IL and solvents were studied. The correlations and resulting data gave insight about the molecular interactions of binary mixtures as well as possible new applications for pyrrolidonium based ILs.

1. Introduction

Nowadays, the most interesting term “ionic liquids” (ILs) is generally assigned to molten organic salts [1]. The composed combination of organic cations with different anions which may be organic or inorganic in nature and having lower melting points below 373 K, are known as room temperature ILs [2–5] Owing to their unique physical properties such as low melting points, low flammability, negligible vapor pressures, high ionic density, significant tuneability, high electrochemical and thermal stability, good conductivity and favorable solubility in both organic and inorganic compounds, research on ILs is growing tremendously [2,6]. Moreover, the major advantage of the IL is, that their physical properties can be tuned simply by changing the cation or anion, for instance, change in substituting groups of cations or anions will yield the required designer solvent [7–9].

The intermolecular forces exhibited between the components of molecules in the liquid mixtures are directly related to their density and speed of sound [10]. Furthermore, the better understanding about theoretical interactions, modeling and technological applications of ILs can be provided by the thermo-physical properties of IL and its binary mixtures [11]. Currently, scientific communities and the chemical and applied industries are focused on the room temperature stable, environment-friendly ILs due to their unique physicochemical properties and extraordinary applications [2,12,13]. The physiochemical properties also help in analyzing structural properties and enhanced predictive modeling by providing the details about hydrogen bonds [14,15].

The study about binary mixture of RTILs with water is very important for industrial applications, and it is necessary to understand the nature of the interaction between RTIL with water [16,17]. It is found that most of these RTILs are highly hygroscopic in nature. The industrial applications of ILs are also significantly influenced by their viscosities. Some industries are not able to utilize RTILs as they are too viscous. The partial amphiphilic nature of RTILs plays an important role in these more straightforward interactions [18]. Viscosity and conductivity may change when the addition of small amount of water cause significant effects [19,20].

* Corresponding author.
E-mail address: redhigg@dut.ac.za (G.G. Redhi).

http://dx.doi.org/10.1016/j.molliq.2017.07.099
0167-7322/

Table 1
Density of water, methanol and ionic liquids data at various temperatures (293.15 K to 313.15 K) from literature.

Component	Supplier	% Mass purity	T/K	ρ/gcm^{-3}		
				Exp.	Lit.	
Water			293.15	0.9982	0.9998	[45]
					0.9996	
			298.15	0.9971		
			303.15	0.9957	0.9974	[45]
			308.15	0.9941	0.9940	[45]
			313.15	0.9922		
Methanol	Fluka	≥99.0				
			29,315	0.7914	0.7915	[46]
					0.7912	[47]
					0.7910	[49]
					0.7912	[48]
			298.15	0.7867	0.7868	[46]
					0.7866	[47]
					0.7865	[48]
					0.7866	[50]
			303.15	0.7820	0.7821	[46]
					0.7818	[47]
					0.7819	[49]
					0.7817	[48]
					0.7819	[50]
			308.15	0.7772	0.7770	[48]
					0.7772	[50]
			313.15	0.7724	0.7726	[46]
					0.7726	[47]
					0.7720	[49]
					0.7722	[48]
					0.7727	[52]
$[EPMPYR]^+[Cl]^-$			293.15	1.0685	1.0685	[44]
			298.15	1.0637	1.0637	[44]
			303.15	1.0590	1.0589	[44]
			308.15	1.0542	1.0572	[44]
			313.15	1.0495	1.0494	[44]
$[EPMPYR]^+[OAC]^-$			288.15	1.0677	–	
			293.15	1.0634	–	
			298.15	1.0590	–	
			303.15	1.0547	–	
			308.15	1.0503	–	
			313.15	1.0459	–	

Due to their significant characteristic properties, ILs have been applicable in the development of most important industries involved in solar cells, capacitors, chromatography, synthesis, catalysis, biotechnology and liquid-liquid extractions [2,21–24]. The alternative designer solvent to conventional organic volatile solvents, ILs have been used in a wide range of applications such as solvent effects [2,3] [2,3] electrochemistry [25–27] pharmaceutical [28–30] separation technologies [2,31–33]and modern advanced catalytic reactions [34]. Currently, global research is moving towards greener sustainable development processes and the usage of ILs in chemical industries is growing rapidly due to their biodegradability, low toxicity and their outstanding thermo-physical properties, particularly negligible vapor pressure, [32] good thermal stability and high conductivity [33]. In the last decade, researchers began to investigate the important physicochemical properties such as density, speed of sound, viscosity, conductivity, surface tension and refractive index of pure ILs and their mixtures with water or molecular solvents. The most important IL groups investigated include imidazolium, pyrrolidinium, pyridinium, piperidinium, ammonium and phosphonium-based ILs, however industries still require more information about newly synthesized novel ILs. The investigation of physicochemical properties of aqueous solutions of synthesized ILs are a continuation of our systematic research on IL mixtures.

In the present work, the synthesized novel IL was used to make binary mixtures with water or methanol, and their physicochemical properties were determined. The investigation

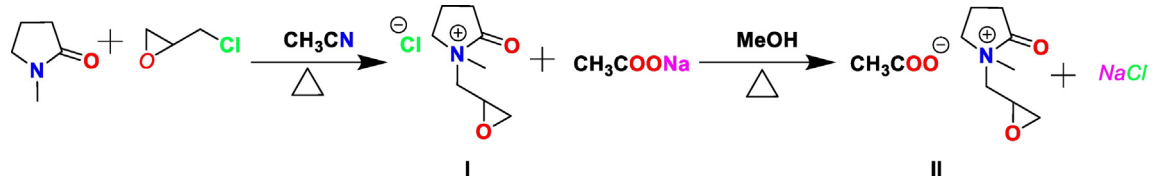

Scheme 1. Synthesis of 2′,3′-N-epoxypropyl-*N*-methyl- pyrrolidonium acetate.

Table 2
Density,(ρ) Speed of sound,(u) viscosity, (η) and refractive index, (n_D) with mole fraction (x_1) of N-(2′,3′-epoxypropyl)-*N*-methyl-2-oxopyrrolidinium acetate in the binary liquid mixture of {[EPMpyr]$^+$[OAC]$^-$ (1) + water (2)} from T/K = 288.15 to 313.15 at pressure P = 0.1 MPa.

x_1	ρ/(g·cm^{-3})	u/(m·s^{-1})	η(mpa·s)	n_D
288.15 K				
0.0000	0.9991	1466.4	1.03	1.3330
0.0346	1.0316	1653.1	2.67	1.3735
0.0775	1.0538	1726.6	5.19	1.4022
0.1028	1.0611	1735.6	6.62	1.4131
0.2008	1.0715	1712.4	9.75	1.4361
0.3054	1.0727	1675.2	10.40	1.4470
0.4045	1.0722	1648.8	10.09	1.4517
0.5113	1.0713	1628.4	9.60	1.4557
0.6049	1.0701	1614.2	9.08	1.4575
0.7052	1.0693	1603.0	8.66	1.4589
0.8048	1.0686	1594.3	8.31	1.4602
0.9047	1.0682	1587.6	8.04	1.4617
1.0000	1.0677	1582.0	7.80	1.4619
293.15 K				
0.0000	0.9982	1482.3	0.91	1.3330
0.0346	1.0293	1651.3	2.26	1.3728
0.0775	1.0503	1715.8	4.27	1.4010
0.1028	1.0573	1722.6	5.40	1.4117
0.2008	1.0673	1696.2	7.75	1.4346
0.3054	1.0684	1658.4	8.32	1.4446
0.4045	1.0678	1631.8	8.17	1.4500
0.5113	1.0669	1611.3	7.82	1.4539
0.6049	1.0658	1597.0	7.47	1.4559
0.7052	1.0650	1585.8	7.16	1.4572
0.8048	1.0643	1580.0	6.92	1.4581
0.9047	1.0639	1570.2	6.73	1.4593
1.0000	1.0634	1564.5	6.55	1.4602
298.15 K				
0.0000	0.9971	1496.5	0.81	1.3339
0.0346	1.0268	1648.8	1.94	1.3724
0.0775	1.0467	1704.5	3.56	1.4000
0.1028	1.0535	1709.1	4.45	1.4104
0.2008	1.0630	1679.6	6.28	1.4329
0.3054	1.0641	1641.1	6.76	1.4431
0.4045	1.0635	1614.3	6.70	1.4487
0.5113	1.0626	1593.7	6.47	1.4519
0.6049	1.0614	1579.3	6.23	1.4542
0.7052	1.0606	1568.0	6.01	1.4555
0.8048	1.0599	1559.3	5.83	1.4565
0.9047	1.0595	1552.5	5.68	1.4577
1.0000	1.0590	1546.7	5.55	1.4584
303.15 K				
0.0000	0.9957	1508.9	0.73	1.3332
0.0346	1.0241	1645.6	1.67	1.3715
0.0775	1.0427	1693.0	3.01	1.3990
0.1028	1.0496	1695.4	3.71	1.4092
0.2008	1.0587	1662.8	5.18	1.4313
0.3054	1.0597	1623.7	5.57	1.4413
0.4045	1.0591	1596.8	5.56	1.4466
0.5113	1.0582	1576.2	5.41	1.4501
0.6049	1.0571	1561.7	5.23	1.4524
0.7052	1.0563	1550.4	5.10	1.4534
0.8048	1.0556	1541.6	4.97	1.4549
0.9047	1.0552	1534.7	4.87	1.4559
1.0000	1.0547	1528.9	4.77	1.4563
308.15 K				
0.0000	0.9941	1519.6	0.69	1.3332
0.0346	1.0214	1641.6	1.46	1.3709
0.0775	1.0384	1681.3	2.60	1.3978
0.1028	1.0457	1681.6	3.13	1.4079
0.2008	1.0543	1646.0	4.33	1.4296
0.3054	1.0553	1606.3	4.67	1.4393
0.4045	1.0547	1579.3	4.69	1.4449
0.5113	1.0538	1558.6	4.60	1.4481
0.6049	1.0527	1544.1	4.47	1.4504
0.7052	1.0519	1532.7	4.38	1.4515
0.8048	1.0512	1523.9	4.28	1.4527
0.9047	1.0508	1517.1	4.21	1.4543
1.0000	1.0503	1511.2	4.13	1.4549

(continued on next page)

Table 2 (*continued*)

x_1	$\rho/(g\cdot cm^{-3})$	$u/(m\cdot s^{-1})$	η(mpa·s)	n_D
313.15 K				
0.0000	0.9922	1528.7	0.65	1.3336
0.0346	1.0185	1637.0	1.29	1.3706
0.0775	1.0336	1669.5	2.28	1.3967
0.1028	1.0417	1667.7	2.67	1.4068
0.2008	1.0497	1629.1	3.63	1.4280
0.3054	1.0509	1588.9	3.95	1.4380
0.4045	1.0503	1561.4	4.00	1.4430
0.5113	1.0494	1541.0	3.94	1.4471
0.6049	1.0483	1526.6	3.85	1.4483
0.7052	1.0475	1515.1	3.79	1.4502
0.8048	1.0468	1506.3	3.72	1.4503
0.9047	1.0464	1499.4	3.67	1.4530
1.0000	1.0459	1493.6	3.62	1.4520

of thermodynamically derived properties elucidated the molecular interaction between IL and water or methanol. Calculated thermodynamic properties data are fitted to Redlich-Kister equations. Our previous work was also related with 2′,3′-epoxypropyl-*N*-methyl-2-Oxopyrrolidinium cation with chloride anion [35,36].

2. Experimental Section

2.1. Materials and methods

Materials: *N*-methyl-2-pyrrolidone, epichlorohydrin, sodium acetate, acetonitrile, methanol, acetone, and hexane were purchased from Fluka Chemicals with purity of ≥99%. The purity and density of the pure compounds in comparison with literature [34–45] values are presented in Table 1. Ultra-pure deionized water was used in all the experiments. The water content using a Metrohm Karl Fischer coulometer (model KF Titrando) was found to be 0.065% in 2′,3′-N-epoxypropyl-*N*-methyl-2-Oxopyrrolidinium $[EPMpyr]^+[OAC]^-$ IL. The thermophysical properties of density are shown in Table 1 and compared with literature data as well.

2.1.1. Synthesis of 2′,3′-N-epoxypropyl-N-methyl-2-Oxopyrrolidinium acetate

2.1.1.1. Step I: synthesis of 2′, 3′- N-epoxypropyl-N-methyl-2-oxopyrrolidinium chloride $[EPMpyr]^+[Cl]^-$. Synthesis of 2′,3′-N-epoxypropyl-*N*-methyl-2-oxopyrrolidinium chloride $[EPMpyr]^+[Cl]^-$ IL was reported previously and the methodology of synthesizing and characterization was also described [35,44,45]. The structure of the IL given in the Scheme (1) compound (I).

2.1.2. Characterization of 2′,3′-N-epoxypropyl-N-methyl-2-oxopyrrolidinium chloride $[EPMpyr]^+[Cl]^-$

The structure of the $[EPMpyr]^+[Cl]^-$ IL was confirmed by the following characterizations ^{1}HNMR, ^{13}CNMR, FTIR and elemental analysis of CHN was reported in previous publications [35,44,45].

2.1.2.1. Step II: synthesis of 2′,3′-N-epoxypropyl-N-methyl-2-oxo pyrrolidinium acetate. The 2′,3′-N-epoxypropyl-*N*-methyl-2-oxopyrrolidinium acetate $[EPMpyr]^+[OAC]^-$ was synthesized by dissolving the desired quantity 1.12 mol of sodium acetate separately in methanol to make a clear solution in round-bottomed flask. Then, the above synthesized intermediate I, IL 2′,3′-N-epoxypropyl-*N*-methyl-2-oxopyrrolidium chloride was added to exchange the acetate anion. The reaction temperature was kept at 80 to 90 °C for 10 h with constant stirring. The product was purified by a solvent wash with acetone, petroleum ether, and hexane to remove unwanted starting materials and sodium chloride, then distilled again at 60 °C for 48 h to get pure moisture-free IL. The product

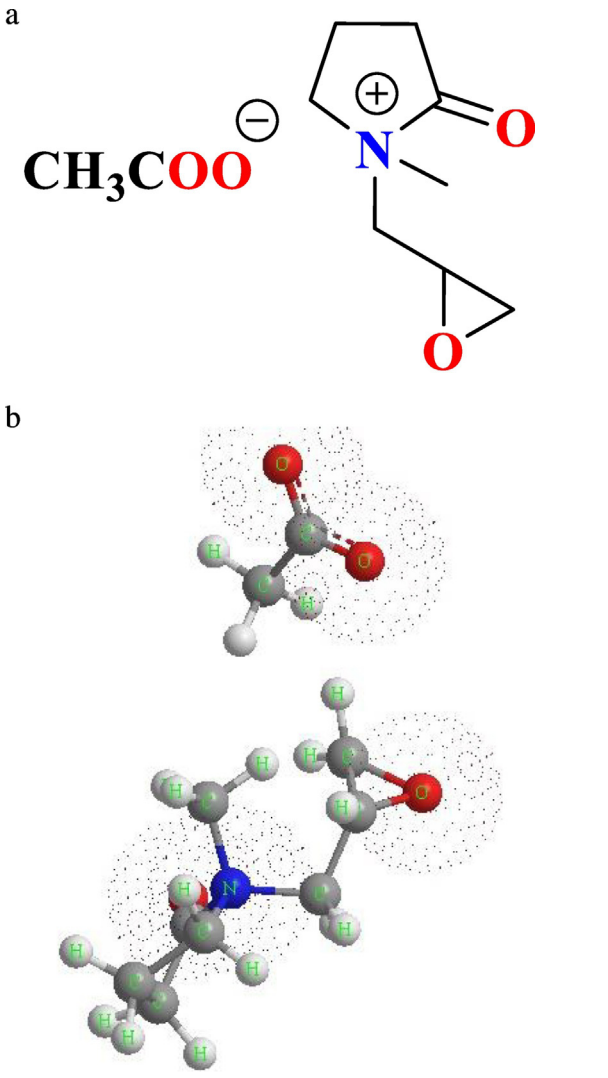

Fig. 1. a: Structure of the ionic liquid $[EPMpyr]^+[OAC]^-$. b: 3D Structure of the ionic liquid $[EPMpyr]^+[OAC]^-$.

identity was established with FTIR, NMR (^{1}H and^{13}C) and elemental analysis.

2.1.3. Characterization of 2′,3′-N-epoxypropyl-N-methyl- pyrrolidonium acetate

The $[EPMpyr]^+[OAC]^-$ was characterized by the following methods: NMR (^{1}H and^{13}C) (shown in Figs. SI:2a, SI:2b, SI:3a and SI:3b), elemental analysis and FTIR (see Fig. SI: 1). The structure of $[EPMpyr]^+[OAC]^-$ is confirmed by the following techniques as shown in FTIR ($\nu = cm^{-1}$): 3442, 2995, 1621, 1501, 1403, 1332, 1256, 1113, 967, 856, 756, 679, 561, 479. $[EPMpyr]^+[OAC]^-$ ^{1}H NMR (400 MHz, DMSO): δ1.08–1.12(t, 2H), 2.00 (s, 3H), 2.05–2.08(q, 2H), 2.28–2.32(t, 2H), 2.35–2.39(t, 2H), 2.83 (s, 3H), 3.44–3.48 (t, 2H), 5.39 (s, 1H) ^{13}C NMR (100 MHz, DMSO): δ9, 18, 20, 28, 30, 31, 49, 50, 177.4 and 177.77. Elemental Analysis (in %) Theoretical calculation for: $C_{10}H_{17}NO_4$: C, 55.80; H, 7.96; N, 6.51; O, 22.91; the values found (in %) are C, 55.24; H, 7.86; N, 6.28.

2.2. Measurements

Mettler AB 204-N balance was used to prepare the binary mixtures of the sample for measurements, at the time of doing investigation. This balance maintained the uncertainty $\pm 1.10^{-7}$ kg for the mass measurements. Anton Paar DSA 5000 M oscillating U-tube densitometer, speed of sound analyzer with automatic micro-viscometer were used to determine the density, speed of sound and viscosity simultaneously at different investigated temperatures from 288.15 to 313.15 K under atmospheric pressure. The temperature and pressure are an important parameter for the determination of physico-chemical properties, so both properties are maintained at 0.01 K temperature and 101 kPa atmospheric pressure. Doubly distilled freshly degassed water and dry air were used to calibrate the instruments before the start experiment. The important thermo-physical properties of refractive index (n_D) was measured for pure compounds and their binary mixtures using the Bellingham and Stanley instrument, RFM 340+ refractometer which maintains the uncertainty less than $\pm 2.10^{-4}$ units. The specification of the instruments clearly informs one about the accuracy and repeatability, therefore ρ, u and η were estimated and their errors found to be less than $\pm 2.0 \times 10^{-4}$ g·cm^{-3}, ± 1.0 m·s^{-1}, and ± 1.0 mPa·s respectively. The estimated uncertainty in V_m^E, k_s, and Δk_s was ± 0.05 cm^3·mol^{-1}, $\pm 0.40 \times 10^{-8}$ Pa^{-1} and $\pm 1.00 \times 10^{-8}$ Pa^{-1}, respectively. The investigation of the physicochemical properties of the pure $[EPMpyr]^+[OAC]^-$ IL and their binary mixtures with concentration from 0.0 to 1.0 mol fraction was undertaken. The special stoppered glass tubes were used to prepare the samples for the measurements at the time of the investigation. The IL which is used in these experiments will be recycled, purified and reused. The method of procedure for measurements has been described previously [35,44,45].

3. Result and discussion

The experimental density (ρ), speed of sound (u), viscosity (η) and refractive index (n_D) of the pure IL $[EPMpyr]^+[OAC]^-$, water, methanol and their binary mixtures were measured respectively. Those physicochemical properties were investigated as a function of IL mole fraction (x_1), for the whole composition ranges at temperatures from 288.15 to 313.15 K, in steps of 5 K under atmospheric pressure. The results obtained for the thermophysical properties are presented in Table 2 and related graphs were shown in the Figs. SI: 8a, SI: 8b, SI: 9a, SI: 9b, SI: 10a, SI: 10b, SI: 11a and SI: 11b. The values of ρ and u is directly proportional to mole fraction at all investigated temperatures and inversely proportional to the temperature. This means that both ρ and u values are gradually increasing while mole fraction of $[EPMpyr]^+[OAC]^-$ (x_1) increases, Fig. SI: 8a, SI: 8b, SI: 9a and SI: 9b shows that the ρ of the pure IL decreases with an increase in temperature. Fig. SI: 4a indicate that the u for the mixtures of IL with water initially increases and thereafter decreases with mole fraction (x_1) whilst Fig. SI: 9a shows u increases with mole fraction (x_1). Solvent-solvent, solute-solvent and solute-solute interactions occur in the investigated binary mixtures, and the u is important to understand these interactions [46,47]. Dielectric constant significantly influences the miscibility of ILs with solvents [48]. Moreover, solvents which have strong dielectric constants are completely miscible with solvents, while low dielectric constant solvents are not completely miscible [12,49,50]. The nature of the thermodynamic properties of binary mixtures is difficult to understand due to the fact that they depend on many parameters. The nature of the components mostly related to shape, size and chemical nature of the components used for the investigated binary systems [51,52]. Interstitial accommodation influence in the structural effects occurs, primarily because of the difference in molar volumes of the binary mixtures [53].

The refractive index (n_D) can reflect the molecule electronic polarizability and provide useful information about the interaction forces in solution systems. Refractive index (n_D) increases with increasing concentration of IL for the binary systems shown in Figs. SI: 11a, SI: 11b

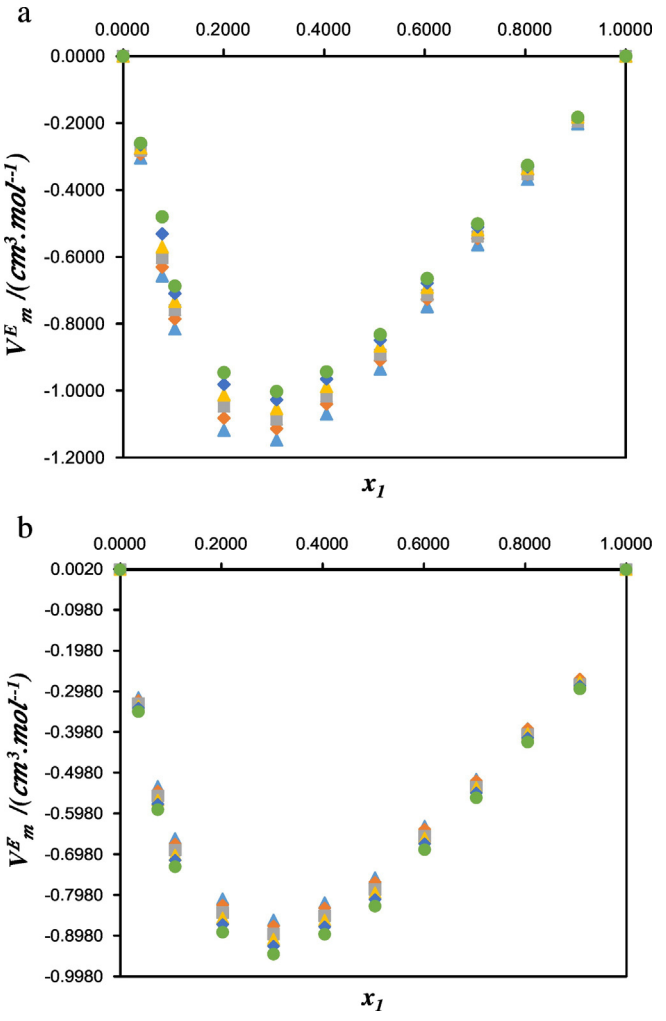

Fig. 2. a: 2Excess molar volumes, V_m^E, for the mixture of {$[EPMpyr]^+[OAC]^-$ (1) + water (2)} as function of the composition expressed in the mole fraction of $[EPMpyr]^+[OAC]^-$ at T = 288.15 K (▲),T = 293.15 K (◆), T = 298.15 K (■), T = 303.15 K (▲), T = 308.15 K (◆) and T = 313.15 K (●). b: Excess molar volumes, V_m^E, for the mixture of {$[EPMpyr]^+[OAC]^-$ (1) + methanol (2)} as function of the composition expressed in the mole fraction of $[EPMpyr]^+[OAC]^-$ at T = 288.15 K (▲),T = 293.15 K (◆), T = 298.15 K (■), T = 303.15 K (▲), T = 308.15 K (◆) and T = 313.15 K (●).

Table 3
Excess molar volume,(V_m^E) Isentropic compressibility (k_s), Intermolecular free length,(L_f) Deviation in isentropic compressibility, (Δk_s) with mole fraction (x_1) of N-(2′,3′-epoxypropyl)-*N*-methyl-2-oxopyrrolidinium acetate in the binary liquid mixture of {[EPMpyr]$^+$[OAC]$^-$(1) + water (2)} from T/K = 288.15 to 313.15 at pressure $P = 0.1$ MPa.

x_1	V_m^E/(cm^3·mol^{-1})	k_s/(10^8 Pa^{-1})	Δk_s/(10^{8}Pa^{-1})	L_f/(10^{-7}m)
288.15 K				
0.0000	0.00	46.5	0.0	1.38
0.0346	−0.30	35.5	−10.7	1.20
0.0775	−0.66	31.8	−13.5	1.14
0.1028	−0.82	31.3	−14.3	1.13
0.2008	−1.12	31.8	−13.1	1.14
0.3054	−1.15	33.2	−10.4	1.16
0.4045	−1.07	34.3	−9.0	1.18
0.5113	−0.94	35.2	−6.5	1.20
0.6049	−0.75	35.9	−5.6	1.21
0.7052	−0.56	36.4	−4.0	1.22
0.8048	−0.37	36.8	−2.7	1.23
0.9047	−0.20	37.1	−1.1	1.23
1.0000	0.00	37.4	0.0	1.24
293.15 K				
0.0000	0.00	45.6	0.0	1.38
0.0346	−0.29	37.2	−8.1	1.24
0.0775	−0.63	32.3	−12.1	1.16
0.1028	−0.79	31.9	−13.0	1.15
0.2008	−1.08	32.6	−11.8	1.16
0.3054	−1.11	34.0	−9.3	1.19
0.4045	−1.04	35.2	−8.0	1.21
0.5113	−0.91	36.1	−5.6	1.22
0.6049	−0.73	36.8	−4.9	1.24
0.7052	−0.55	37.3	−3.4	1.25
0.8048	−0.35	37.6	−2.5	1.25
0.9047	−0.19	38.1	−0.9	1.26
1.0000	0.00	38.4	0.0	1.26
298.15 K				
0.0000	0.00	44.8	0.0	1.38
0.0346	−0.28	35.8	−8.7	1.23
0.0775	−0.60	32.9	−10.9	1.18
0.1028	−0.76	32.5	−11.8	1.17
0.2008	−1.05	33.4	−10.6	1.19
0.3054	−1.09	34.9	−8.2	1.22
0.4045	−1.02	36.8	−6.3	1.25
0.5113	−0.89	37.1	−4.8	1.25
0.6049	−0.71	37.8	−4.3	1.26
0.7052	−0.54	38.4	−2.9	1.27
0.8048	−0.35	38.8	−2.0	1.28
0.9047	−0.20	39.2	−0.7	1.29
1.0000	0.00	39.5	0.0	1.29
303.15 K				
0.0000	0.00	44.1	0.0	1.38
0.0346	−0.27	36.1	−7.9	1.25
0.0775	−0.57	33.5	−9.8	1.20
0.1028	−0.73	33.2	−10.6	1.20
0.2008	−1.01	34.2	−9.5	1.21
0.3054	−1.05	35.8	−7.1	1.24
0.4045	−0.99	37.0	−6.1	1.26
0.5113	−0.87	38.0	−4.0	1.28
0.6049	−0.69	38.8	−3.7	1.29
0.7052	−0.52	39.4	−2.5	1.30
0.8048	−0.34	39.9	−1.7	1.31
0.9047	−0.18	40.2	−0.6	1.32
1.0000	0.00	40.6	0.0	1.32
308.15 K				
0.0000	0.00	43.6	0.0	1.38
0.0346	−0.27	36.3	−7.1	1.26
0.0775	−0.53	34.1	−8.7	1.22
0.1028	−0.71	33.8	−9.6	1.22
0.2008	−0.98	35.0	−8.4	1.24
0.3054	−1.03	36.7	−6.1	1.27
0.4045	−0.97	38.0	−5.3	1.29
0.5113	−0.85	39.1	−3.3	1.31
0.6049	−0.68	39.8	−3.1	1.32
0.7052	−0.51	40.5	−2.1	1.33
0.8048	−0.33	41.0	−1.4	1.34
0.9047	−0.18	41.4	−0.4	1.35
1.0000	0.00	41.7	0.0	1.35

Table 3 (*continued*)

x_1	V_m^E/(cm^3·mol^{-1})	k_s/(10^8 Pa^{-1})	Δk_s/(10^8Pa^{-1})	L_f/(10^{-7}m)
313.15 K				
0.0000	0.00	43.1	0.0	1.42
0.0346	−0.26	36.6	−6.4	1.31
0.0775	−0.48	34.7	−7.8	1.27
0.1028	−0.69	34.5	−8.6	1.27
0.2008	−0.95	35.9	−7.4	1.30
0.3054	−1.00	37.7	−5.2	1.33
0.4045	−0.94	39.1	−4.5	1.35
0.5113	−0.83	40.1	−2.6	1.37
0.6049	−0.66	40.9	−2.6	1.38
0.7052	−0.50	41.6	−1.6	1.39
0.8048	−0.33	42.1	−1.1	1.40
0.9047	−0.18	42.5	−0.3	1.41
1.0000	0.00	42.9	0.0	1.42

Standard uncertainties for $V_m^E = \pm 0.05$ cm^3·mol^{-1}, $k_s = \pm 0.4 \times 10^{-8}$ Pa^{-1} and $\Delta k_s \pm 1.0 \times 10^{-8}$ Pa^{-1}.

and SI:7. The viscosity of the binary mixtures for $[EPMpyr]^+[OAC]^-$ with the water combination initially increases with increasing mole fraction but it reaches a certain maximum concentration of IL, then decreases thereafter with increasing IL concentration. The above mentioned two physicochemical properties decrease with increasing temperatures for both systems. The viscosity (η) of the IL and its binary mixtures are shown in Figs. SI: 10a, SI: 10b and SI:6. The binary mixture plot of $[EPMpyr]^+[OAC]^-$ IL with methanol differs when compared with IL with water, since the viscosity of the methanol is very low, and the competing effect is less pronounced compared to the water mixture. The addition of IL to methanol makes a significant change to the nature of the viscosity plot. The viscosity of the binary mixtures exponentially increase due to the crowding of solute ions which enhance the interactions among ions of anion-anion, cation-anion, and cation-cation. Generally, hydrogen bonds are influential in increasing the viscosity of the binary systems. The spatial structure clearly shows the different H-bonding interactions in the liquid mixtures including intra and intermolecular H-bonding.

3.1. Excess molar volume

The calculated thermodynamic properties of excess molar volumes (V_m^E) were derived from the experimental density data of the pure components (ρ_1 and ρ_2) and binary mixture (ρ) using the equation as below:

$$V_m^E = \sum_{i=1}^{2} x_i M_i (\rho^{-1} - \rho_i^{-1}) \quad (1)$$

The experimental density data was used to calculate V_m^E and the results are tabulated in Table 2. The V_m^E increases with increasing mole fraction and decreases with increasing temperature as indicated in Fig. 2(a) and (b) as well as Table 2 and 3 respectively. The results show that the competing effects plays an important role in this binary mixture, due to the presence of stronger interactions. Here the volume contraction "negative" effect is possibly due to the ion-polar interaction between the molecules of IL and water or methanol, gathering varied species closer together. The small molecules fitting in between the larger molecules may happen in this composition and the negative effects are due to the ill-fitting molecules mixed together. Observation and interpretation of the resulting data shows the competing effects in the investigated binary mixtures as indicated in Tables 2 and 3, could be better understood in terms of the partial molar volumes at infinite dilution. The intermolecular interaction between IL moieties and water or methanol also to suggest self-association between the moieties of IL which has been considered as the ion + ion association, and weak force of Van der Waals associations among the bulky alkyl group and other part of the ILs, as well as the strong H-bond of water molecules influence in that interactions. ILs are peculiar solvents, which interact with solvents such as water or methanol through ionic interactions, inter- and intramolecular hydrogen bonding, and dipolar interactions. The results indicate a particularly strong association between the IL and H_2O probably via H-bonding between the negative COO^- group and the relatively H^+ of H_2O. The size of the ions in the ILs strongly influences and decides the association of ion + ion in the binary mixture. (See Fig. 1.)

The charge effect of the ion varies inversely with its surface area. Cations in the IL significantly influence the polarity of ILs, and as a result the polarity of the ILs is largely dependent on the cations, this being confirmed by the spectroscopic studies. The reason is the substituted floppy alkyl groups in cations are more significantly influenced compared with anions. Negative V_m^E values are seen for the ILs involving pyrrolidinium cations with hydrophilic anions containing electronegative oxygen atoms in $[CH_3COO]^-$. The effect is manifests itself at both ends of the concentration scale. The combination of $[EPMpyr]^+[OAC]^-$ (1) + water (2) or methanol (2) gave a negative value for the whole mole fraction range of composition, and Fig. 2(a) and (b) show plots which virtually symmetrical with a maximum around $x_1 \approx 0.5$ and initially decreases then increases with increasing temperature from (288.15 to 313.15) K. The values of $V_{m,\ \min}^E$ are −40.53 cm^3 mol^{-1}(for water), and −33.56 cm^3 mol^{-1}(for methanol) obtained at $x_1 = 0.4894$ and 0.5489, respectively for the binary systems of {$[EPMpyr]^+[OAC]^-$ (1) + water or methanol (2)} at all investigated temperatures [see Fig. 2(a) and (b)].

3.2. Isentropic compressibility (k_s) and deviation in isentropic compressibility (Δk_s)

Newton-Laplace equation (Eq. 2) was used to calculate the isentropic compressibility, k_s from experimental resulting data.

$$k_s = \rho^{-1} u^{-2} \quad (2)$$

The deviations in isentropic compressibility,Δk_s, were calculated using Eq. (3):

$$\Delta k_s = k_s - \sum_{i}^{2} x_i k_{s,i} \quad (3)$$

The chemical composition, temperature, and pressure are fixed for the investigated binary mixtures in order to determine the thermodynamic

Table 4
Density,(ρ) Speed of sound,(u) viscosity, (η) and refractive index, (n_D) with mole fraction (x_1) of N-(2′,3′-epoxypropyl)-*N*-methyl-2-oxopyrrolidinium acetate in the binary liquid mixture of {[EPMpyr]$^+$[OAC]$^-$ (1) + methanol (2)} from T/K = 288.15 to 313.15 at pressure P = 0.1 MPa.

x_1	ρ/(g·cm^{-3})	u/(m·s^{-1})	η (mPa·s)	n_D
288.15 K				
0.0000	0.7961	1136.2	0.64	1.3307
0.0360	0.8446	1210.4	0.77	1.3538
0.0744	0.8830	1271.0	1.01	1.3725
0.1088	0.9095	1313.9	1.23	1.3851
0.2024	0.9587	1395.5	1.88	1.4091
0.3033	0.9919	1451.8	2.67	1.4248
0.4042	1.0138	1489.2	3.46	1.4354
0.5040	1.0295	1516.4	4.46	1.4429
0.6015	1.0408	1535.6	4.99	1.4481
0.7036	1.0501	1551.8	5.78	1.4529
0.8051	1.0576	1564.6	6.52	1.4561
0.9086	1.0639	1575.5	7.28	1.4589
1.0000	1.0677	1582.0	7.80	1.4613
293.15 K				
0.0000	0.7914	1120.0	0.60	1.3287
0.0360	0.8400	1194.2	0.71	1.3523
0.0744	0.8784	1254.6	0.92	1.3713
0.1088	0.9049	1297.5	1.12	1.3845
0.2024	0.9542	1378.8	1.69	1.4077
0.3033	0.9874	1434.9	2.35	1.4235
0.4042	1.0094	1472.2	3.02	1.4344
0.5040	1.0251	1499.2	3.68	1.4413
0.6015	1.0364	1518.4	4.28	1.4467
0.7036	1.0458	1534.5	4.91	1.4516
0.8051	1.0532	1547.4	5.51	1.4547
0.9086	1.0596	1558.2	6.14	1.4574
1.0000	1.0634	1564.5	6.55	1.4599
298.15 K				
0.0000	0.7867	1103.5	0.55	1.3273
0.0360	0.8353	1177.7	0.66	1.3508
0.0744	0.8738	1238.0	0.85	1.3702
0.1088	0.9004	1280.7	1.03	1.3831
0.2024	0.9497	1361.7	1.52	1.4063
0.3033	0.9829	1417.5	2.09	1.4218
0.4042	1.0049	1454.7	2.66	1.4326
0.5040	1.0207	1481.6	3.22	1.4396
0.6015	1.0320	1500.7	3.71	1.4449
0.7036	1.0414	1516.8	4.23	1.4495
0.8051	1.0489	1529.6	4.72	1.4531
0.9086	1.0552	1540.3	5.21	1.4559
1.0000	1.0590	1546.7	5.55	1.4582
303.15 K				
0.0000	0.7820	1087.3	0.51	1.3257
0.0360	0.8307	1161.3	0.62	1.3499
0.0744	0.8692	1221.4	0.78	1.3690
0.1088	0.8958	1264.0	0.94	1.3812
0.2024	0.9452	1344.6	1.38	1.4046
0.3033	0.9784	1400.3	1.87	1.4208
0.4042	1.0005	1437.4	2.36	1.4305
0.5040	1.0162	1464.2	2.83	1.4379
0.6015	1.0276	1483.2	3.25	1.4433
0.7036	1.0370	1499.2	3.68	1.4475
0.8051	1.0445	1511.9	4.09	1.4509
0.9086	1.0508	1522.6	4.49	1.4546
1.0000	1.0547	1528.9	4.77	1.4567
308.15 K				
0.0000	0.7773	1071.4	0.47	1.3245
0.0360	0.8260	1145.2	0.57	1.3492
0.0744	0.8645	1205.1	0.72	1.3672
0.1088	0.8911	1247.5	0.87	1.3795
0.2024	0.9406	1327.7	1.26	1.4030
0.3033	0.9739	1383.3	1.69	1.4184
0.4042	0.9960	1420.2	2.10	1.4297
0.5040	1.0118	1447.0	2.51	1.4364
0.6015	1.0231	1466.0	2.86	1.4424
0.7036	1.0326	1481.9	3.23	1.4454
0.8051	1.0401	1494.4	3.57	1.4495
0.9086	1.0465	1505.1	3.90	1.4525
1.0000	1.0503	1511.2	4.14	1.4545

Table 4 (*continued*)

x_1	ρ/(g·cm^{-3})	u/(m·s^{-1})	η (mPa·s)	n_D
313.15 K				
0.0000	0.7725	1055.8	0.43	1.3231
0.0360	0.8212	1129.3	0.52	1.3474
0.0744	0.8598	1189.0	0.73	1.3664
0.1088	0.8865	1231.2	0.80	1.3786
0.2024	0.9360	1311.0	1.15	1.4008
0.3033	0.9694	1366.3	1.53	1.4164
0.4042	0.9915	1403.2	1.89	1.4280
0.5040	1.0073	1429.8	2.24	1.4341
0.6015	1.0187	1448.9	2.54	1.4400
0.7036	1.0282	1464.6	2.85	1.4437
0.8051	1.0357	1477.1	3.14	1.4475
0.9086	1.0421	1487.6	3.42	1.4500
1.0000	1.0459	1493.6	3.62	1.4531

properties of k_s. Tables 3 and 4 indicates the isentropic compressibility (k_s) and deviation in isentropic compressibility (Δk_s) data for {[EPMpyr]$^+$[OAC]$^-$ (x_1) + water or methanol (x_2)} binary systems at temperatures 288.15 to 313.15 K under atmospheric pressure.

Generally, increasing the temperature of the solution will help to increase the k_s values due to the thermal agitation creating more compression in the binary mixtures [54]. From the results, the k_s increases with increasing investigated temperatures for both binary systems as shown in Tables 3 and 5. The negative Δk_s occurs because of the increased interactions between the molecules in the binary mixtures. The free space in binary mixtures was decreased by the interaction of both mixtures, and this is most probably why the deviation in isentropic compressibility becomes more negative. In the binary mixtures of [EPMpyr]$^+$[OAC]$^-$ with water or methanol, negative Δk_s over the whole range of compositions at all investigated temperature, is obtained as given by Fig.3a and b. Comparing both binary mixtures the [EPMpyr]$^+$[OAC]$^-$ with water gave a stronger interaction, and this was confirmed from the plot (Fig. 3a) that the values of $\Delta k_{s,\min}$ is −14.3 at mole fraction $x_1 = 0.2990$, and for [EPMpyr]$^+$[OAC]$^-$ with methanol system give Δk_s, min is −31.6 at $x_1 = 02847$. The Δk_svalues slightly differ for the two binary systems; {[EPMpyr]$^+$[OAC]$^-$ (1) + water (2)} is more compressible than {[EPMpyr]$^+$[OAC]$^-$ (1) + methanol (2)} due to the presence of both epoxy and carboxylic groups are strongly interacted with water via hydrogen bonds. The compressibility of the investigated binary mixtures were decreased due to the closer approach of unlike molecules and a stronger interaction between water or methanol with [EPMpyr]$^+$[OAC]$^-$ IL. In these binary mixtures, H-bond plays an important role due to the presence of water or methanol. Water has a higher dielectric constant and increased possibilities of high H-bonding, so the water binary system is more compressible compared with the methanol binary systems. The order of the Δk_s values for both the mixtures {[EPMpyr]$^+$[OAC]$^-$ (x_1) + water (x_2)} > {[EPMpyr]$^+$[OAC]$^-$ (x_1) + methanol (x_2)} showing that there is a compressibility decrease from water to methanol due to water having higher number of hydrogen bonds. One of the reasons for decreasing compressibility is because of greater interactions among the components of mixtures due to the proximity of unlike molecules. The resulting data indicate that the negative V_m^E and Δk_s values due to the chemical effects include the specific interactions such as ion dipole interactions, formation of H-bonds, strong dipole − dipole interactions, and donor − acceptor complexes between solute and solvent molecules. The structural effects also play an important role in the binary mixtures.

Intermolecular free length (L_f) was calculated from the Jacobson derived equations (see Eq. 4) which helps to better understand the intermolecular interactions.

$$L_f = k_j(k_s)^{1/2} \tag{4}$$

Table 3 indicates the intermolecular free length for both binary systems of [EPMpyr]$^+$[OAC]$^-$ + water or methanol was investigated over several temperatures at fixed compositions. From Fig. 4a and b, it is evident that the decrease of intermolecular free length with increasing mole fraction of IL, and increases with increasing temperature given as in Table 3 occurs. The intermolecular free length is inversely proportion to the experimental speed of sound as shown in Fig. 4a and b and Tables 4 and 5. As L_f increases with increasing temperatures due to the temperature influence affecting the molecular interaction, the bonding between the unlike molecules are get weaker. The distance between the centre of the molecules and surface of the molecules increases when increase the temperatures, which leads to decrease in u. The L_f values significantly explain the distance between the two molecules, and this information helps to understand the forces among the molecules in the binary mixture, indicating whether it can be attractive or repulsive forces. These are important in the properties of fluid consistency. These forces are numerically similar but they have opposite directions under external conditions. The distance between the centres of attraction of the molecules decides the attraction forces, while the distance between the surfaces of the molecules decides the repulsive forces. Normally, geometrical centres of the molecules in liquids do not coincide those counters, so it is very difficult to define the distance between the centres of attraction. Moreover, the experimental sound velocity is a predominant factor to investigate the intermolecular free length in liquid mixtures. Jacobson's empirical relation is one of the best methods to calculate and understand the intermolecular free length using k_s [54].

3.3. FTIR discussion

The comparison of the FTIR spectrum of pure [EPMpyr]$^+$[OAC]$^-$ IL and its combination of [EPMpyr]$^+$[OAC]$^-$ with water or methanol give some information about their interactions. Furthermore, these spectra will be explained to some extent regarding hydrogen bonds and molecular interactions. Fig. 5 shows FTIR spectrum of pure IL and their binary interactions; here mole fraction 0.2 for both binary mixtures gave more negative values of V_m^E and Δk_s so FTIR also gave some extra peaks; and these are due to hydrogen bonds and interaction of IL with solvents. The FTIR spectrum of pure IL [EPMpyr]$^+$[OAC]$^-$ is shown in Fig. 5, The peaks are at 2934 cm^{-1} and 2886 cm^{-1} and are C—H stretching vibration for aliphatic asymmetry and symmetry respectively. The bending vibration of the methyl group appeared at peaks 1195 cm^{-1} and 1114 cm^{-1}. Quaternary amine salt obtained peaks at 3502 and 3371 cm^{-1}. Respectively broad shoulders of peaks indicated the presence of C—C and C—N stretching's at 1508 cm^{-1} and 1458 cm^{-1} respectively. The broad peaks at 1664 cm^{-1} indicate the presence of –C = O in the cyclic amide group in cation of IL.

Fig. 5 shows the binary mixture of [EPMpyr]$^+$[OAC]$^-$ with water or methanol for FTIR spectrum. The C=O stretching vibration of the IL was decreased from 1680 cm^{-1} to 1640 cm^{-1} in the binary mixtures due to the ion-dipole interactions between [EPMpyr]$^+$[OAC]$^-$ and water or methanol. The spatial ion-dipole interactions influence in the C=C

Table 5
Excess molar volume,(V_m^E) Isentropic compressibility (k_s), Intermolecular free length,(L_f) Deviation in isentropic compressibility, (Δk_s) with mole fraction (x_1) of N-(2′,3′-epoxypropyl)-*N*-methyl-2-oxopyrrolidinium acetate in the binary liquid mixture of {[EPMpyr]$^+$[OAC]$^-$ (1) + methanol (2)} from T/K = 288.15 to 313.15 at pressure P = 0.1 MPa.

x_1	V_m^E/(cm^3·mol^{-1})	k_s/(10^8 Pa^{-1})	Δk_s/(10^{8}Pa^{-1})	L_f/(10^{-7}m)
288.15 K				
0.0000	0.00	97.3	0.00	1.99
0.0360	−0.31	80.8	−14.3	1.82
0.0744	−0.53	70.1	−22.7	1.69
0.1088	−0.66	63.7	−27.1	1.61
0.2024	−0.81	53.6	−31.6	1.48
0.3033	−0.86	47.8	−31.3	1.40
0.4042	−0.82	44.5	−28.6	1.35
0.5040	−0.76	42.2	−24.9	1.31
0.6015	−0.63	40.8	−20.5	1.29
0.7036	−0.51	39.6	−15.6	1.27
0.8051	−0.39	38.6	−10.5	1.25
0.9086	−0.27	37.9	−5.0	1.24
1.0000	0.00	37.4	0.0	1.24
293.15 K				
0.0000	0.00	100.7	0.0	2.05
0.0360	−0.32	83.5	−15.0	1.86
0.0744	−0.54	72.3	−23.8	1.73
0.1088	−0.67	65.6	−28.3	1.65
0.2024	−0.82	55.1	−33.0	1.51
0.3033	−0.87	49.2	−32.7	1.48
0.4042	−0.83	45.7	−29.8	1.38
0.5040	−0.77	43.4	−25.9	1.34
0.6015	−0.64	41.9	−21.4	1.32
0.7036	−0.52	40.6	−16.3	1.30
0.8051	−0.39	39.7	−10.9	1.28
0.9086	−0.27	38.9	−5.2	1.27
1.0000	0.00	38.4	0.0	1.26
298.15 K				
0.0000	0.00	104.4	0.0	2.10
0.0360	−0.33	86.3	−15.7	1.91
0.0744	−0.56	74.7	−24.9	1.78
0.1088	−0.69	67.7	−29.6	1.69
0.2024	−0.84	56.8	−34.5	1.55
0.3033	−0.89	50.6	−34.1	1.46
0.4042	−0.85	47.0	−31.1	1.41
0.5040	−0.79	44.6	−27.0	1.37
0.6015	−0.65	43.0	−22.3	1.35
0.7036	−0.53	41.7	−17.0	1.33
0.8051	−0.40	40.8	−11.4	1.31
0.9086	−0.28	39.9	−5.5	1.30
1.0000	0.00	39.5	0.0	1.29
303.15 K				
0.0000	0.00	108.2	0.0	2.16
0.0360	−0.33	89.3	−16.5	1.96
0.0744	−0.57	77.1	−26.0	1.82
0.1088	−0.70	69.9	−31.0	1.73
0.2024	−0.85	58.5	−36.0	1.59
0.3033	−0.91	52.1	−35.5	1.50
0.4042	−0.86	48.4	−32.5	1.44
0.5040	−0.79	45.9	−28.2	1.41
0.6015	−0.66	44.2	−23.3	1.38
0.7036	−0.53	42.9	−17.7	1.36
0.8051	−0.40	41.9	−11.8	1.34
0.9086	−0.28	41.1	−5.7	1.33
1.0000	0.00	40.6	0.0	1.32
308.15 K				
0.0000	0.00	112.1	0.0	2.22
0.0360	−0.34	92.3	−17.2	2.01
0.0744	−0.58	79.7	−27.2	1.87
0.1088	−0.71	72.1	−32.3	1.78
0.2024	−0.87	60.3	−37.5	1.63
0.3033	−0.92	53.7	−37.1	1.53
0.4042	−0.88	49.8	−33.8	1.48
0.5040	−0.81	47.2	−29.4	1.44
0.6015	−0.67	45.5	−24.3	1.41
0.7036	−0.55	44.1	−18.5	1.39
0.8051	−0.41	43.1	−12.4	1.37
0.9086	−0.28	42.2	−5.9	1.36
1.0000	0.00	41.7	0.0	1.35

Table 5 (*continued*)

x_1	V^E_m/(cm^3·mol^{-1})	k_s/(10^8 Pa^{-1})	Δk_s/(10^{8}Pa^{-1})	L_f/(10^{-7}m)
313.15 K				
0.0000	0.00	116.1	0.0	2.33
0.0360	−0.35	95.5	−18.0	2.11
0.0744	−0.59	82.3	−28.4	1.96
0.1088	−0.73	74.4	−33.7	1.87
0.2024	−0.89	62.2	−39.1	1.71
0.3033	−0.94	55.3	−38.7	1.61
0.4042	−0.89	51.2	−35.3	1.55
0.5040	−0.83	48.6	−30.6	1.51
0.6015	−0.69	46.8	−25.3	1.48
0.7036	−0.56	45.3	−19.2	1.46
0.8051	−0.42	44.3	−12.9	1.44
0.9086	−0.29	43.4	−6.2	1.42
1.0000	0.00	42.9	0.0	1.42

Standard uncertainties for $V^E_m = \pm 0.05$ cm^3·mol^{-1}, $k_s = \pm 0.4 \times 10^{-8}$ Pa^{-1} and $\Delta k_s \pm 1.0 \times 10^{-8}$ Pa^{-1}.

stretching, resulting in a decrease from 1664 cm^{-1} to 1658 cm^{-1} respectively. The quaternary amine in IL peak values were changed from 3508 cm^{-1} to 3441 cm^{-1} due to solvent interactions. From the FTIR investigation it is evident that the addition of solvents to IL [EPMpyr]$^+$[OAC]$^-$ does influence (i) C—H vibrations in [EPMpyr]$^+$[OAC]$^-$ (ii) Hydrogen bonding between epoxy group in cation and anion group to solvents, (iii) C—O vibration in cation; (iv) C, N

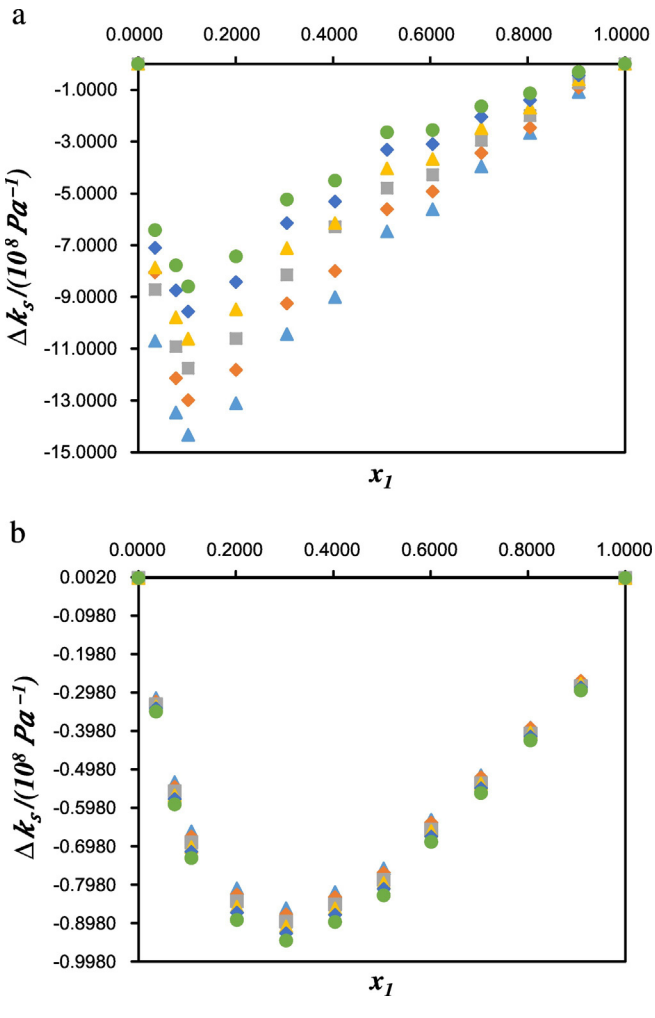

Fig. 3. a: Deviation of isentropic compressibility for the mixture of {[EPMpyr]$^+$[OAC]$^-$ (1) + water (2)} as function of the composition expressed in the mole fraction of [EPMpyr]$^+$[OAC]$^-$ at T = 288.15 K (▲),T = 293.15 K (◆), T = 298.15 K (■), T = 303.15 K (▲), T = 308.15 K (◆) and T = 313.15 K (●). b: Deviation of isentropic compressibility for the mixture of {[EPMpyr]$^+$[OAC]$^-$ (1) + methanol (2)} as function of the composition expressed in the mole fraction of [EPMpyr]$^+$[OAC]$^-$ at T = 288.15 K (▲),T = 293.15 K (◆), T = 298.15 K (■), T = 303.15 K (▲), T = 308.15 K (◆) and T = 313.15 K (●).

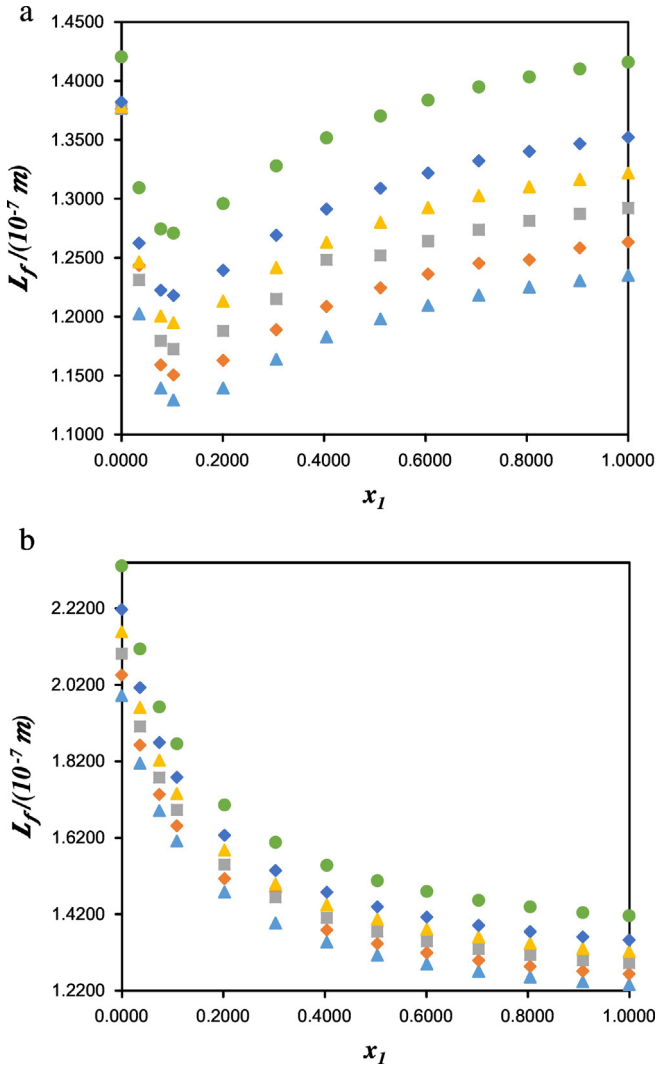

Fig. 4. a: Intermolecular free length, L_f, for the mixture of {[EPMpyr]$^+$[OAC]$^-$ (1) + water (2)} as function of the composition expressed in the mole fraction of [EPMpyr]$^+$[OAC]$^-$ at T = 288.15 K (▲),T = 293.15 K (◆), T = 298.15 K (■), T = 303.15 K (▲), T = 308.15 K (◆) and T = 313.15 K (●). b: Intermolecular free length, L_f, for the mixture of {[EPMpyr]$^+$[OAC]$^-$ (1) + methanol (2)} as function of the composition expressed in the mole fraction of [EPMpyr]$^+$[OAC]$^-$ at T = 288.15 K (▲),T = 293.15 K (◆), T = 298.15 K (■), T = 303.15 K (▲), T = 308.15 K (◆) and T = 313.15 K (●).

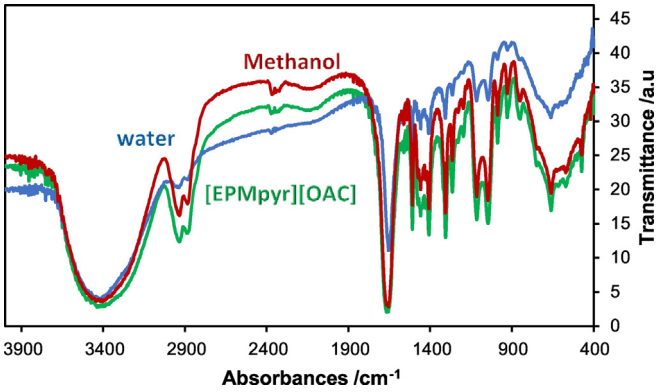

Fig. 5. FTIR spectrum of $[EPMpyr]^+[OAC]^-$ IL and its binary mixture of water or methanol.

stretching in cation of $[EPMpyr]^+[OAC]^-$ IL, Overall the FTIR study indicates the ion-dipole interactions in binary mixture of $[EPMpyr]^+[OAC]^-$.

3.4. Correlation of derived properties

The Redlich-Kister equation as shown below Eq. (5) was used to correlate the derived properties:

$$X = x_1 x_2 \sum_{i=1}^{k} A_j (1-2x_1)^{i-1} \quad (5)$$

where X is excess molar volumes (V_m^E) and deviation in isentropic compressibility (Δk_s), the least-squares method has been used to determine the fitting parameters A_j values. Table 4 shows the summarized results, and the corresponding standard deviations σ,for the correlation as investigated using Eq. 6.

$$\sigma(X) = \sum_{i=1}^{n} \left[\frac{X_{expt} - X_{calc}}{(N-K)}\right]^{1/2} \quad (6)$$

Where N the number of is experimental points and k is the number of co-efficient used in the Redlich-Kister equation. The values of V_m^E and Δk_s, as well as the plots of the Redlich-Kister model. Both binary systems have very low standard deviation values for V_m^E, Δk_s and L_f case at all temperatures (Table 6).

4. Conclusion

This article reports on the experimental results of densities (ρ), speed of sound (u), viscosity (η), and refractive index (n_D) for novel IL and their mixtures. From the measured values their derived properties of excess molar volumes (V_m^E), isentropic compressibility (k_s), intermolecular free length (L_f), and deviation in isentropic compressibility (Δk_s) of binary mixtures with water or methanol where calculated. This investigation experimental data for temperatures from 288.15 to 313 K in steps of 5 under atmospheric pressure at fixed compositions across the mole fraction ranges. The resulting data shows the dissociation of self-associated IL and solvents such as water and methanol causes negative excess molar volume and negative deviation in isentropic compressibility; this information confirm the presence of competing effect, which explains the strong molecular interaction between IL with water or methanol. FTIR studies also support these arguments due to peaks related to the hydrogen bond and interaction being obtained. The experimental investigation conforms the strong interactions, self-ionization, and hydrogen bonding. It has been confirmed that the IL $[EPMpyr]^+[OAC]^-$ with water binary system have strongly interaction and greater competing effect. The binary mixture of $[EPMpyr]^+[OAC]^-$ with methanol, showed less interaction than water, due to strong hydrogen bond and high dielectric constant of water. The derived thermodynamic properties were successfully correlated by Redlich-Kister equation.

Table 6
Coefficients A_i, and standard deviations, σ, obtained for the binary systems {$[EPMpyr]^+[OAC]^-$ (1) + water or methanol (2)} at different temperatures for the Redlich-Kister equation.

Derived properties	T/K	A_0	A_1	A_2	A_3	σ
{$[EPMpyr]^+[OAC]^-$ (1) + water (2)}						
$V_m^E/(cm^3 \cdot mol^{-1})$	288.15	−3.730	−3.327	−2.664	−1.167	0.014
	293.15	−3.629	−3.245	−2.486	−1.086	0.013
	298.15	−3.560	−3.142	−2.385	−0.900	0.013
	303.15	−3.459	−3.085	−2.185	−0.807	0.012
	308.15	−3.393	−3.018	−2.048	−0.571	0.013
	313.15	−3.328	−2.964	−1.866	−0.282	0.018
$L_f/(10^{-7}m)$	288.15	4.156	−1.745	12.714	5.252	0.520
	293.15	4.247	−1.794	12.974	5.399	0.527
	298.15	4.365	−1.738	13.172	5.167	0.531
	303.15	4.452	−1.794	13.453	5.236	0.537
	308.15	4.556	−1.812	13.715	5.233	0.543
	313.15	4.773	−1.873	14.314	5.355	0.563
$\Delta k_s/(10^8 \times Pa^{-1})$	288.15	−24.300	−14.068	−89.145	−134.497	1.143
	293.15	−21.452	−14.774	−79.593	−113.461	0.756
	298.15	−17.429	−8.889	−75.829	−115.663	0.86
	303.15	−15.468	−9.740	−67.656	−101.607	0.829
	308.15	−12.831	−8.334	−61.696	−92.77	0.751
	313.15	−10.315	−6.912	−56.282	−84.897	0.682
{$[EPMpyr]^+[OAC]^-$ (1) + methanol (2)}						
$V_m^E/(cm^3 \cdot mol^{-1})$	288.15	−2.887	−1.773	−3.001	−1.260	0.023
	293.15	−2.930	−1.818	−3.028	−1.362	0.024
	298.15	−2.999	−1.841	−3.142	−1.351	0.025
	303.15	−3.03	−1.894	−3.144	−1.453	0.024
	308.15	−3.091	−1.921	−3.223	−1.445	0.025
	313.15	−3.154	−1.953	−3.318	−1.486	0.026
$L_f/(10^{-7}m)$	288.15	4.392	−2.185	16.73	12.442	0.675
	293.15	4.520	−2.033	17.155	12.418	0.692
	298.15	4.595	−2.303	17.563	13.152	0.71
	303.15	4.700	−2.365	18.001	13.525	0.729
	308.15	4.808	−2.427	18.447	13.909	0.748
	313.15	5.034	−2.55	19.352	14.637	0.785
$\Delta k_s/(10^8 \times Pa^{-1})$	288.15	−96.86	−69.537	−115.023	−125.763	0.816
	293.15	−100.926	−72.368	−120.594	−132.228	0.863
	298.15	−105.215	−75.401	−126.403	−139.072	0.908
	303.15	−109.680	−78.577	−132.325	−146,002	0.957
	308.15	−114.319	−81.82	−138.377	−152.896	1.007
	313.15	119.168	−85.135	−144.785	−160.417	1.058

Standard uncertainties for $V_m^E = \pm 0.05\ cm^3 \cdot mol^{-1}$, $k_s = \pm\ 0.4 \times 10^{-8}\ Pa^{-1}$ and $\Delta k_s \pm 1.0 \times 10^{-8}\ Pa^{-1}$.

Appendix A. Supplementary data

Supplementary data to this article can be found online at http://dx.doi.org/10.1016/j.molliq.2017.07.099.

References

[1] M. Freemantle, An Introduction to Ionic Liquids, RSC Publishing, London, 2009.
[2] T. Welton, Chem. Rev. 99 (1999) 2071–2083.
[3] J.P. Hallett, T. Welton, Chem. Rev. 111 (2011) 3508–3576.
[4] J. Flieger, E.B. Grushka, A. Czajkowska-Żelazko, Austin J. Anal. Pharm. Chem. 1 (2) (2014) 1009–1016.
[5] M. Freemantle, Cambridge: Royal Society of Chemistry Chapter, 1, 2010 1–10.
[6] U. Domańska, A. Marciniak, M. Krolikowska, M. Arasimowicz, J. Chem. Eng. Data 55 (2010) 2532–2536.
[7] F.S. Voth, Fluid Phase Equilib. 294 (2010) 148–156.
[8] M.N. Garaga, M. Nayeri, A. Martinelli, J. Mol. Liq. 210 (2015) 169–177.
[9] A. Nazet, S. Sokolov, T. Sonnleitner, T. Makino, M. Kanakubo, R. Buchner, J. Chem. Eng. Data 60 (2015) 2400–2411.
[10] G. Nath, Chem. Sci. Trans. 1 (2012) 516–521.
[11] T. Kavitha, T. Vasantha, P. Venkatesu, R.S.R. Devi, T. Hofman, J. Mol. Liq. 198 (2014) 11–20.
[12] P. Wasserscheid, W. Keim, Angew. Chem. Int. Ed. 39 (2000) 3772–3789.
[13] D.S. Silvester, Analyst 136 (2011) 4871–4882.
[14] L.E. Barrosse-Antle, A.M. Bond, R.G. Compton, A.M.O. Mahony, E.I. Rogers, D.S. Silvester, Chem. Asian. J. 5 (2010) 202–230.

[15] J.M. Crosthwaite, M.J. Muldoon, S.N.V.K. Aki, E.J. Maginn, J.F. Brennecke, J. Phys. Chem. B 110 (2006) 9354–9361.
[16] J. Jacquemin, P. Husson, A.A.H. Padua, V. Majer, Green Chem. 8 (2006) 172–180.
[17] G.R. Chaudhary, S. Bansal, S.K. Mehta, A.S. Ahluwalia, J. Solution Chem. 43 (2014) 340–359.
[18] E.P. Grishina, L.M. Ramenskaya, M.S. Gruzdev, O.V. Kraeva, J. Mol. Liq. 177 (2013) 267–272.
[19] E. Rilo, J. Vila, J. Pico, S. Garcia-Garabal, L. Segade, L.M. Varela, O. Cabeza, J. Chem. Eng. Data 55 (2010) 639–644.
[20] R. Hayes, G.G. Warr, R. Atkin, Chem. Rev. 115 (2015) 6357–6426.
[21] Q. Zhou, L.S. Wang, H.P. Chen, J. Chem. Eng. Data 51 (2006) 905–908.
[22] A.E. Visser, R.D. Rogers, J. Solid State Chem. 171 (2003) 109–113.
[23] P. Wasserscheid, T. Welton, Wiley-Verlag, Weinheim, 2003.
[24] J.S. Wilkes, J. Mol. Catal. A 214 (2004) 11–17.
[25] J.F. Brennecke, E.J. Maginn, AIChE J 47 (2001) 2384–2389.
[26] R. Palm, H. Kurig, K. Tõnurist, A. Jänes, E. Lust, Electrochem. Commun. 22 (2012) 203–206.
[27] P. Yang, Y. Zhao, C. Su, K. Yang, B. Yan, Acta, 88, 2013 203–207.
[28] P.D. McCrary, P.A. Beasley, G. Gurau, A. Narita, P.S. Barber, O.A. Cojocaru, R.D. Rogers, New J. Chem. 37 (2013) 2196–2202.
[29] O.A. Cojocaru, K. Bica, G. Gurau, A. Narita, P.D. McCrary, J.L. Shamshina, P. Barber, R.D. Rogers, Med. Chem. Commun. 4 (2013) 559–563.
[30] A. Dimitrijevic, T. Trtic-Petrovic, M. Vraneš, S. Papovic, A. Tot, S. Dozic, S. Gadzuric, J. Chem. Eng. Data 61 (2016) 549–555.
[31] D. Coleman, N. Gathergood, Chem. Soc. Rev. 39 (2010) 600–637.
[32] V.I. Parvulescu, C. Hardacre, Chem. Rev. 107 (2007) 2615–2665.
[33] L. Chen, J. Chen, Z. Song, G. Cui, Y. Xu, X. Wang, J. Liu, J. Chem. Thermodyn. 91 (2015) 292–300.
[34] J. Chen, L. Chen, Y. Lu, Y. Xu, J. Mol. Liq. 197 (2014) 374–380.
[35] A. Vasanthakumar, I. Bahadur, G.G. Redhi, R.M. Gengan, K. Anand, J. Mol. Liq. 219 (2016) 685–693.
[36] I. Bahadur, S. Erlin, S. Singh, E.E. Ebenso, G.G. Redhi, ACS Sustain. Chem. Eng. 4 (2) (2016) 601–608.
[37] M. Singh, S. Kumar, J. Appl. Polym. Sci. 87 (2003) 1001–1015.
[38] C. Yang, H. Lai, Z. Liu, P. Ma, J. Chem. Eng. Data 51 (2006) 584–589.
[39] F. Comelli, R. Francesconi, J. Chem. Eng. Data 42 (1997) 705–709.
[40] W. Fan, Q. Zhou, S. Zhang, R. Yan, J. Chem. Eng. Data 53 (2008) 1836–1840.
[41] H. Djojoputro, S. Ismadji, J. Chem. Eng. Data 50 (2005) 1343–1347.
[42] A.C. Gomez Marigliano, H.N. Solimo, J. Chem. Eng. Data 47 (2002) 796–800.
[43] B. Lagourette, C. Boned, H. Saint-Guirons, P. Xans, H. Zhou, Meas. Sci. Technol. 3 (1992) 699–701.
[44] A. Vasanthakumar, G.G. Redhi, R.M. Gengan, ACS Sustain. Chem. Eng. 4 (2016) 4951–4964.
[45] M.N. Roy, D. Ekka, R. Dewan, Acta Chim. Slov. 58 (2011) 792–796.
[46] J. A. Riddick, W. B. Bunger, T. K. Sakano, Wiley-Inter Science: New York, (1986).
[47] M. Freemantle, RSC Publishing: Cambridge, UK, (2010).
[48] P. Bonhote, A.P. Dias, N. Papageorgiou, K. Kalyanasundaram, M. Gratzel, Inorg. Chem. 35 (1996) 1168–1178.
[49] I.M. Abdulagatov, A. Tekin, J. Safarov, A. Shahverdiyev, E. Hassel, J. Chem. Thermodyn. 40 (2008) 1386–1401.
[50] I.M. Abdulagatov, A. Tekin, J. Safarov, A. Shahverdiyev, E. Hassel, Int. J. Thermophys. 29 (2008) 505–533.
[51] Y. Li, H. Ye, P. Zeng, F. Qi, Volumetric properties of binary mixtures of the Ionic Liquid 1-butyl-3-methylimidazolium tetrafluoroborate with aniline, J. Solution Chem. 39 (2010) 219–230.
[52] I. Bahadur, T.M. Letcher, S. Singh, G.G. Redhi, P. Venkatesu, D. Ramjugernath, J. Chem. Thermodyn. 82 (2015) 34–46.
[53] M.T. Zafarani-Moattar, H. Shekaari, J. Chem. Thermodyn. 37 (2005) 1029–1035.
[54] M. Gowrisankar, P. Venkateswarlu, K. Sivakumar, S. Sivarambabu, J. Solut. Chem. 42 (2013) 916–935.

Synthesis, characterization and thermophysical properties of novel 2′, 3′-N-epoxypropyl- N-methyl-2-oxopyrrolidinium acetate ionic liquid and their binary mixture with water or methanol

Vasanthakumar Arumugam,[a] G. G. Redhi, [a] R. M. Gengan.[a]*

[a]Department of Chemistry, Durban University of Technology, Durban-4001

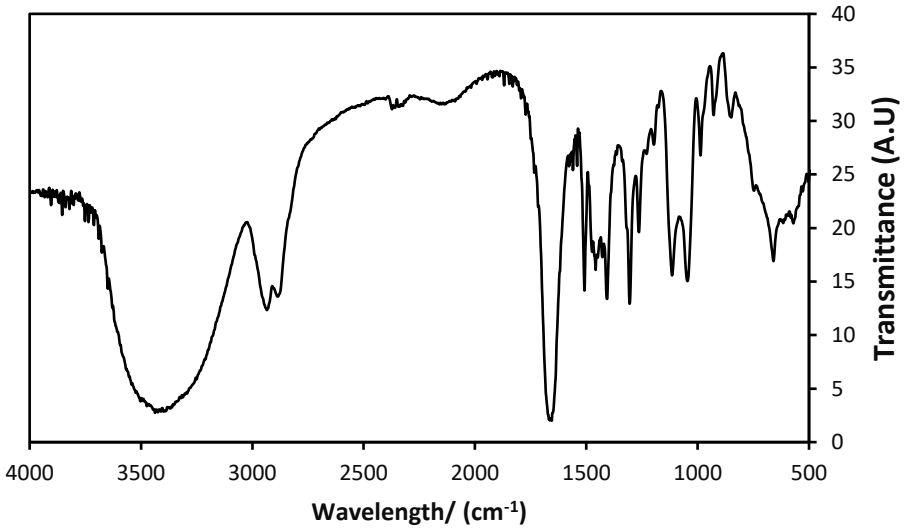

Figure SI: 1. FTIR spectra of synthesized $[EPMpyr]^+[OAC]^-$ IL

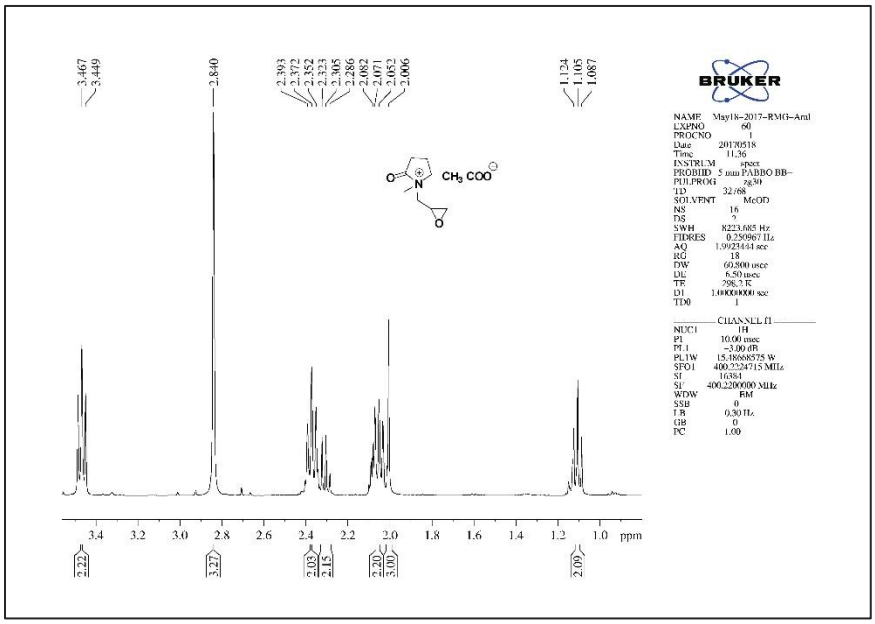

Figure SI: 2a ^{1}HNMR spectra of $[EPMpyr]^{+}[OAC]^{-}$

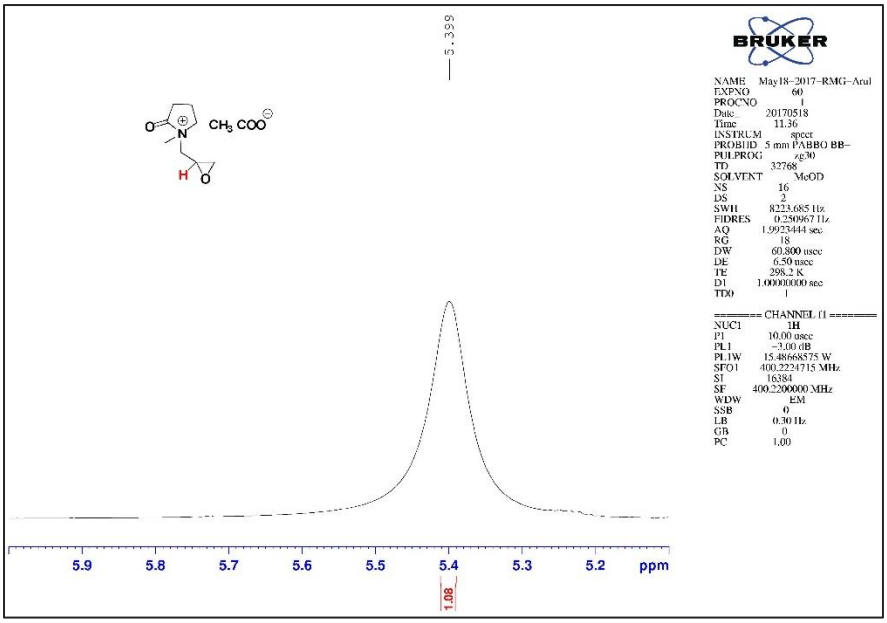

Figure SI: 2b Figure SI:3 ^{1}HNMR spectra of $[EPMpyr]^{+}[OAC]^{-}$

Table SI:1 Integral values, peak area and peak purity of the 1HNMR spectra.

Peaks	Integral Values (δ)	Peak area	Peak purity
	Cations		
N-CH3	2.8398	0.02	0.0070
C3	2.3621	0.05	0.0212
	2.3722	0.05	0.0211
C4	1.0080	0.08	0.0794
	1.1319	0.08	0.0707
C5	2.0785	0.07	0.0337
	2.0570	0.07	0.0340
C1'	3.6196	0.06	0.0166
	3.6073	0.06	0.0166
C2'	3.6873	0.08	0.0217
C3'	4.1428	0.07	0.0169
	Anion		
CH_3-	2.0058	0.03	0.00863

Note: The above ^{1}HNMR spectra confirms the structure of $[EPMpyr]^+[OAC]^-$ IL as well as its purity. The Table SI:1 which explains the peak purity of the compound using peak area and integral values. In the cationic group –N-CH_3 at (δ2.8398) peak singlet with three protons and –CH_2 next to carbonyl group with at (δ2.3621) triplet, two protons which are explain the N-methyl group substituted five membered oxopyrrolidinium cationic group. Furthermore the singlet at δ 5.4 with a single proton shows the –CH next to ether group (–CH-C-O), actually it supposed to be multiplet but in this case, the peak indicates broad singlet like –OH group due to this proton interacted with oxygen via hydrogen bond formation and the resulting like hydroxyl group, it might be the reason for that. The singlet around at δ 2.0 with three protons represent the anionic group.

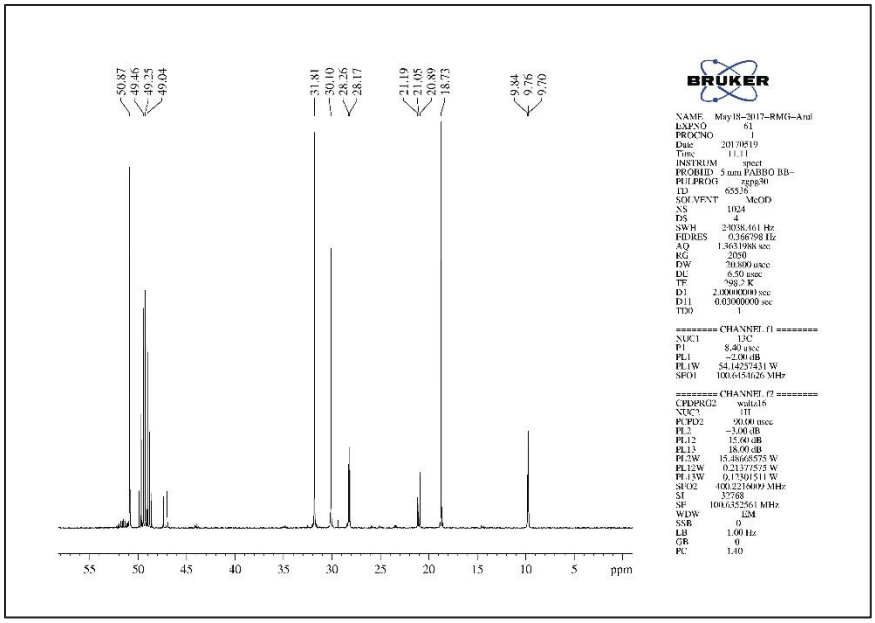

Figure SI: 3a ^{13}CNMR spectra of [EPMpyr]$^{+}$[OAC]$^{-}$

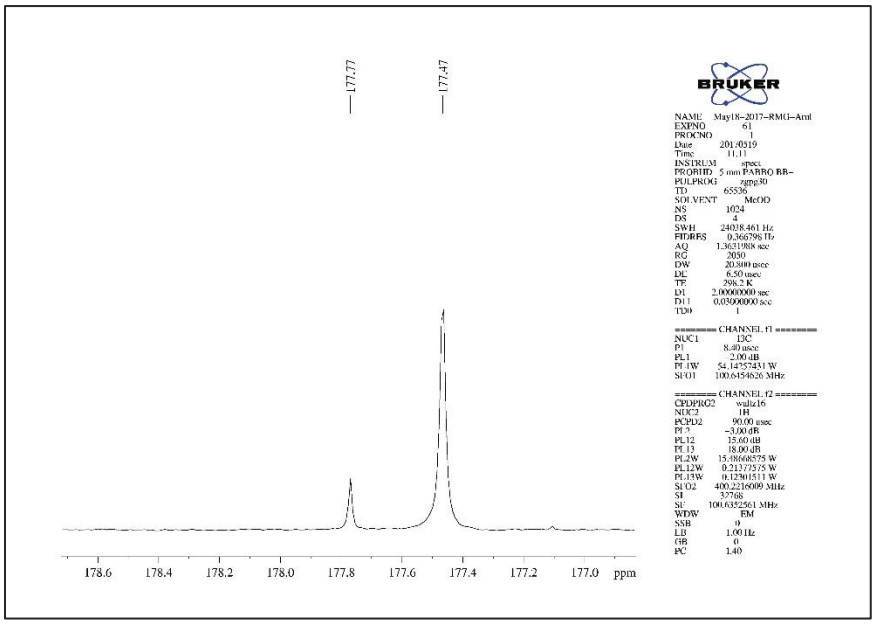

Figure SI: 3b ^{13}CNMR spectra of [EPMpyr]$^{+}$[OAC]$^{-}$

Table SI:2 Peak purity and integral values of ^{13}CNMR spectra.

Peaks	Integral Values (δ)	Peak area	Peak purity
	Cations		
N-CH3	73.9807	0.07	0.0009
C_2=O	177.47	0.03	0.0002
C3	24.8253	0.06	0.0024
C4	18.6960	0.04	0.0021
C5	64.3719	0.19	0.0030
C1'	59.5380	0.05	0.0008
C2'	50.8355	0.07	0.0014
C3'	31.8151	0.13	0.0041
	Anions		
C=O	177.77	0.03	0.0002

Note: From the ^{13}CNMR clearly explain the carbonyl groups which are present in cationic and anionic group. The two peaks at δ 177 confirms the acetate anion and oxo group in pyrrolidinium cation. Overall the peak area and integral values further explain the whole structure of the $[EPMpyr]^+[OAC]^-$ IL.

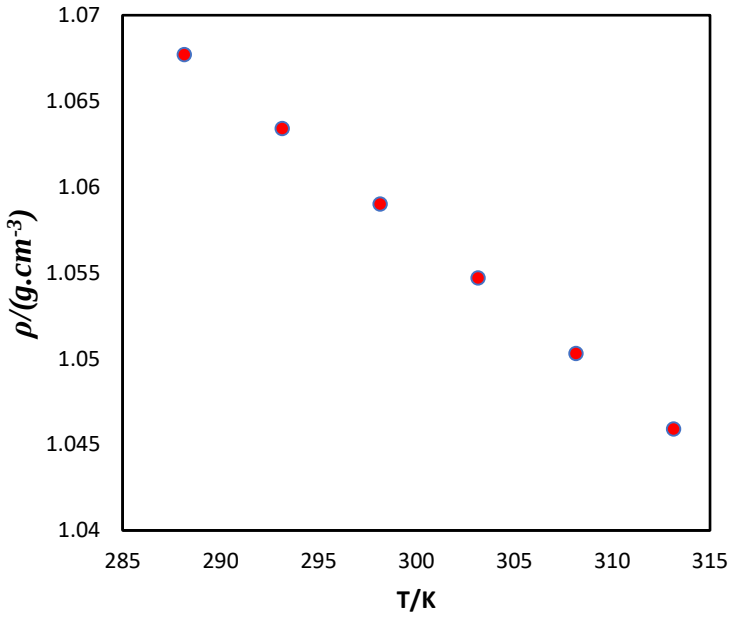

Figure SI:4. Density, ρ, of [EPMpyr]⁺[OAC]⁻ at temperatures from (288.15 to 313.15) K.

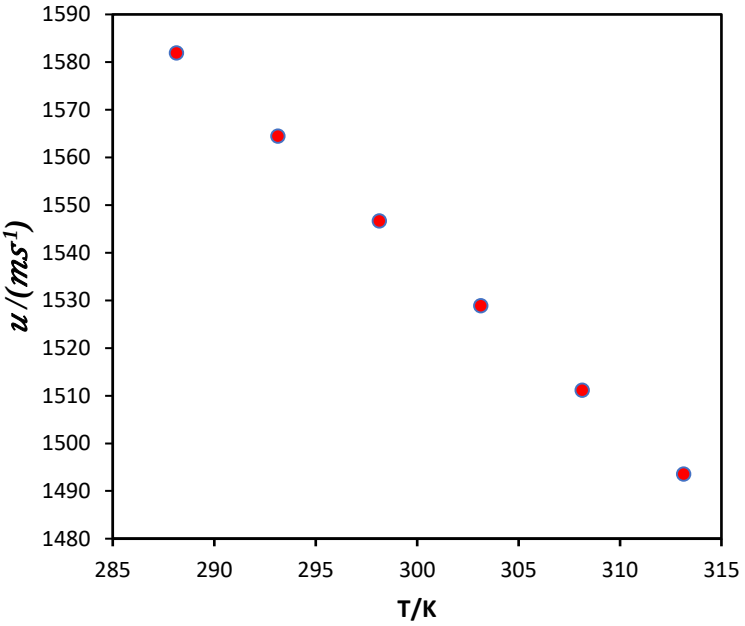

Figure SI:5. Speed of sound velocity of {[EPMpyr]⁺[OAC]⁻ at temperatures from (288.15 to 313.15) K

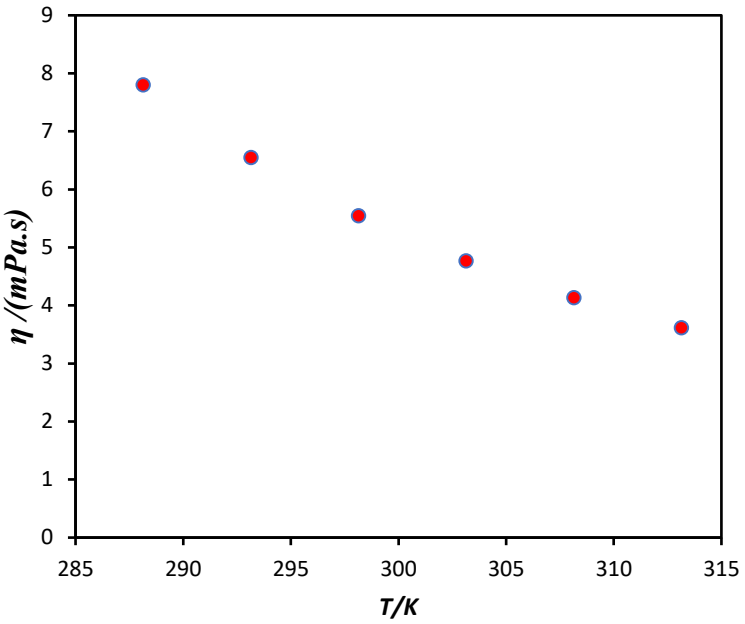

Figure SI:6. Viscosity, η, of [EPMpyr]⁺[OAC]⁻ at temperatures from (288.15 to 313.15) K.

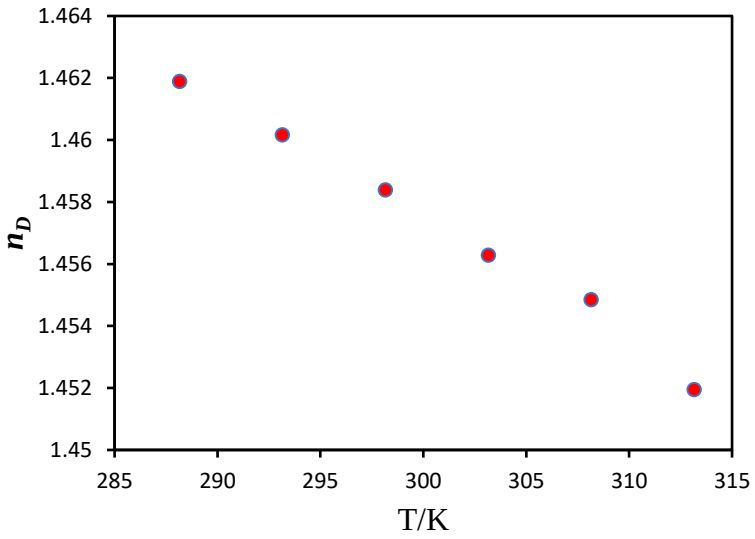

Figure .SI:7. Refractive index, (n_D) , of [EPMpyr]⁺[OAC]⁻ at temperatures from (288.15 to 313.15) K.

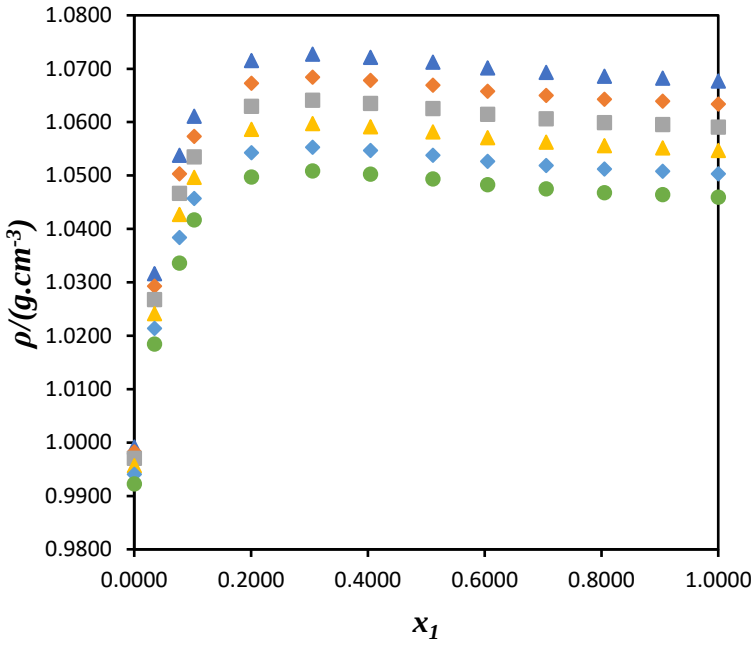

Figure.SI: 8a. Density, ρ, for the mixture of {[EPMpyr]⁺[OAC]⁻ (1) + water (2)} as function of the composition expressed in the mole fraction of {[EPMpyr]⁺[OAC]⁻at T = 288.15 K ( ),T = 293.15 K ( ), T = 298.15 K ( ), T = 303.15 K ( ), T = 308.15 K ( ) and T = 313.15 K (●).

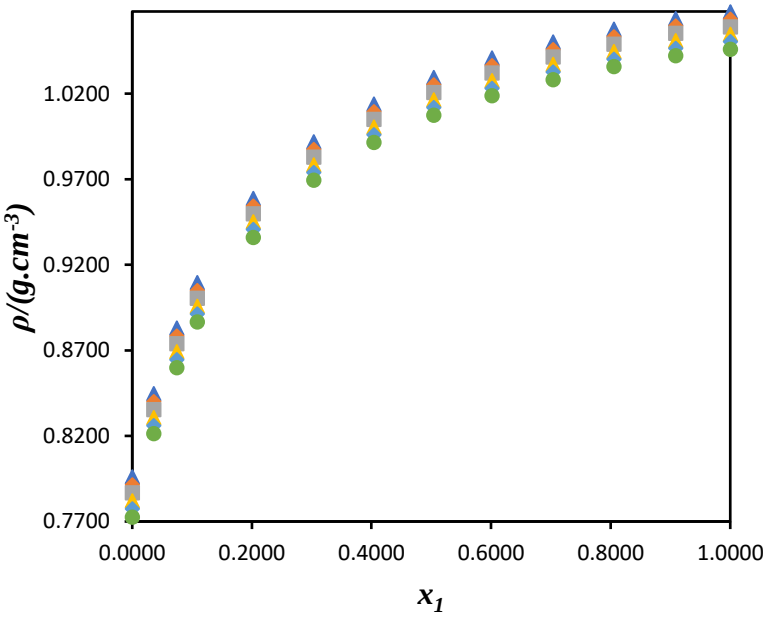

Figure SI: 8b. Density, ρ, for the mixture of {[EPMpyr]⁺[OAC]⁻ (1) + methanol (2)} as function of the composition expressed in the mole fraction of {[EPMpyr]⁺[OAC]⁻at T = 288.15 K ( ),T = 293.15 K ( ), T = 298.15 K ( ), T = 303.15 K ( ), T = 308.15 K ( ) and T = 313.15 K (●).

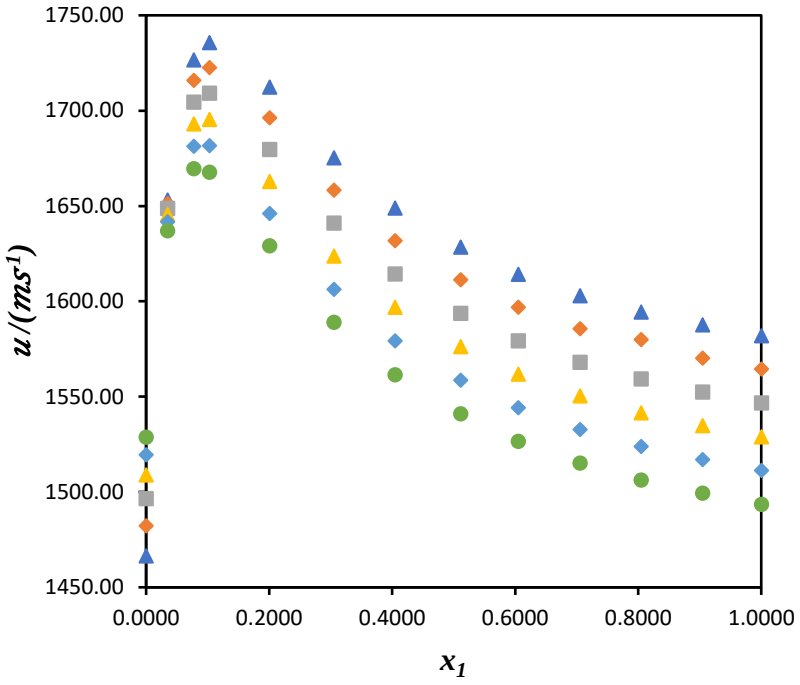

Figure. SI: 9a. Speed of sound, u, for the mixture of {[EPMpyr]$^+$[OAC]$^-$ (1) + water (2)} } as function of the composition expressed in the mole fraction of {[EPMpyr]$^+$[OAC]$^-$at T = 288.15 K (△),T = 293.15 K (◆), T = 298.15 K (■), T = 303.15 K (▲), T = 308.15 K (◆) and T = 313.15 K (●).

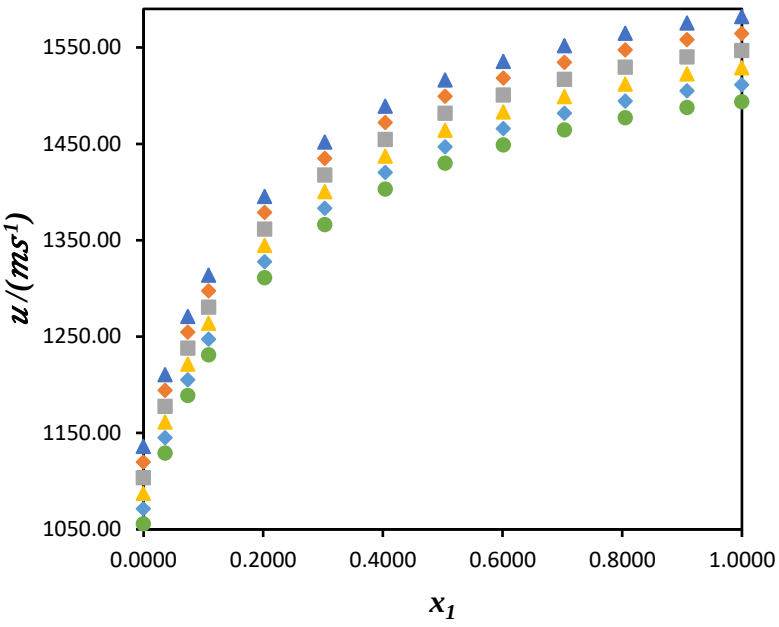

Figure. SI: 9b. Speed of sound, u, for the mixture of {[EPMpyr]$^+$[OAC]$^-$ (1) + methanol (2)} as function of the composition expressed in the mole fraction of {[EPMpyr]$^+$[OAC]$^-$ at T = 288.15 K ( ),T = 293.15 K ( ), T = 298.15 K ( ), T = 303.15 K ( ), T = 308.15 K ( ) and T = 313.15 K (●).

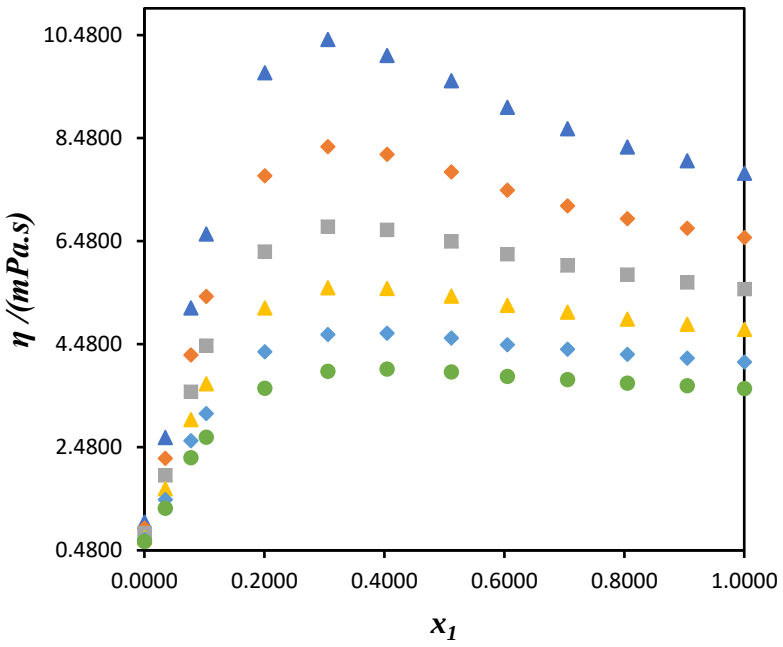

Figure. SI: 10a. Viscosity, η for the mixture of {[EPMpyr]⁺[OAC]⁻ (1) + water (2)} as function of the composition expressed in the mole fraction of {[EPMpyr]⁺[OAC]⁻at T = 288.15 K ( ),T = 293.15 K ( ), T = 298.15 K ( ), T = 303.15 K ( ), T = 308.15 K ( ) and T = 313.15 K (●).

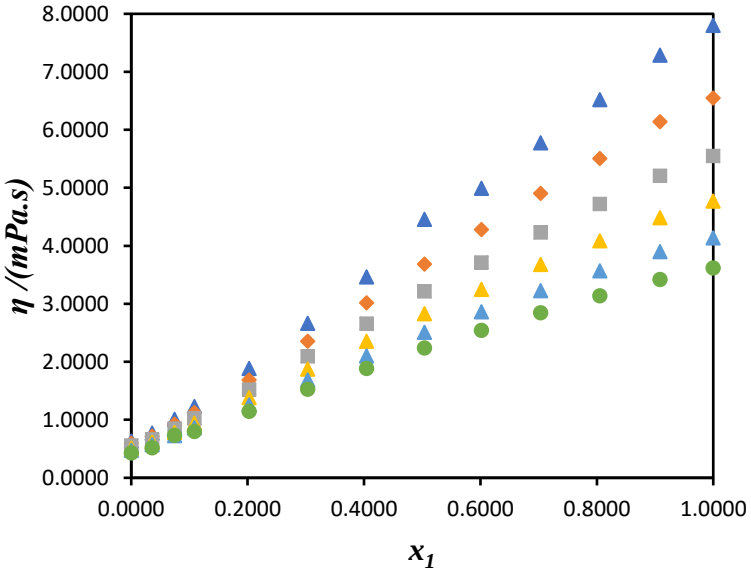

Figure. SI: 10b. Viscosity, η for the mixture of {[EPMpyr]⁺[OAC]⁻ (1) + methanol (2)} as function of the composition expressed in the mole fraction of {[EPMpyr]⁺[OAC]⁻at T = 288.15 K ( ),T = 293.15 K ( ), T = 298.15 K ( ), T = 303.15 K ( ). T = 308.15 K ( ) and T = 313.15 K (●).

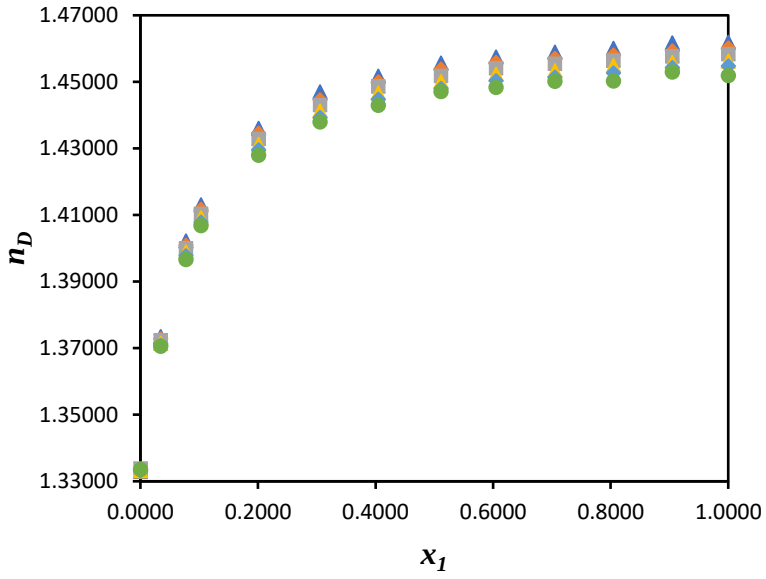

Figure. SI: 11a. Refractive index, (n_D) , for the mixture of {[EPMpyr]⁺[OAC]⁻ (1) + water (2)} as function of the composition expressed in the mole fraction of {[EPMpyr]⁺[OAC]⁻at T = 288.15 K ( ),T = 293.15 K ( ), T = 298.15 K ( ), T = 303.15 K ( ), T = 308.15 K ( ) and T = 313.15 K (●).

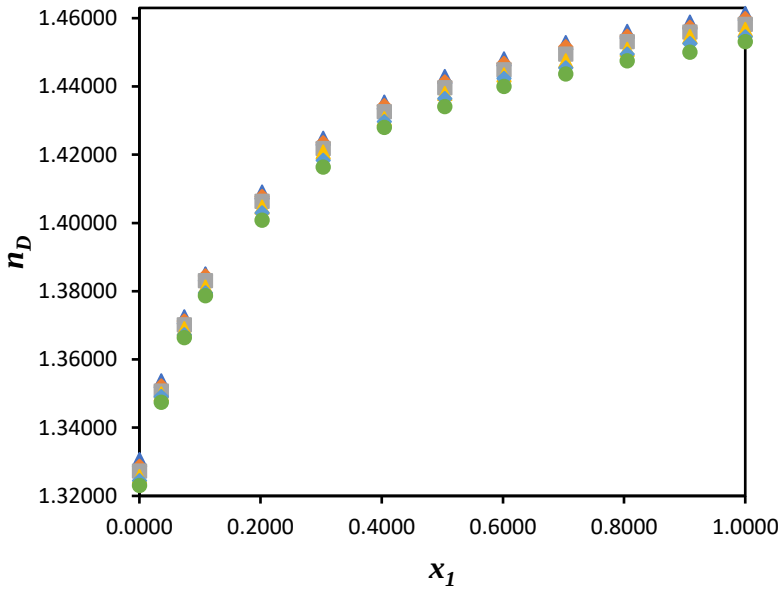

Figure. SI: 11b. Refractive index, (n_D) , for the mixture of {[EPMpyr]⁺[OAC]⁻ (1) + methanol (2)} as function of the composition expressed in the mole fraction of {[EPMpyr]⁺[OAC]⁻at T = 288.15 K ( ),T = 293.15 K ( ), T = 298.15 K ( ), T = 303.15 K ( ), T = 308.15 K ( ) and T = 313.15 K (●).

10.4 Critical review for 3rd Publication

Synthesis, characterization and thermophysical properties of novel 2', 3'- N-epoxypropyl- N-methyl-2-oxopyrrolidinium acetate ionic liquid and their binary mixture with water or methanol

In this research article, a novel N-2′,3′-epoxypropyl-N-methyl-2-oxopyrrolidinium acetate $[Epmpyr]^+[OAC]^-$ IL was synthesize and characterized by FTIR, ^1H NMR, ^{13}C NMR as well as by elemental analysis to identify their chemical structure. The experimental physicochemical properties like ρ, u, η and n were measured. These physicochemical properties were determined for IL and their binary mixtures with either water or methanol in the desired mole fractions of 0.1 to 1.0 at fixed temperatures from 288.15 to 313.15 K in interval of 5 K under atmospheric pressure. These properties and data are very important in industrial applications and research development processes when using this IL. The above mentioned thermophysical properties were found to increase with increasing mole fraction of the IL and decreases with increasing temperature of both binary systems. Density (ρ) and speed of sound (u) are temperature dependent properties.

Generally, the dielectric constant decides the degree of solubility: the ILs which have high dielectric constant values are highly soluble in solvents or vice versa. The thermodynamic properties and their behaviour for binary mixtures are hard to understand fully because they are dependent on many parameters. Primarily, they depend on the nature of the chemical compounds and the significant interactions that occur in the desired composition of binary mixtures. Normally, the nature of the components is typically correlated with the shape, size and chemical activity of the chemical components used for the investigated binary mixtures. In particular, the viscosity of the binary mixtures initially increases and after the saturation tends to decrease with the mole fraction of the IL. Both η and n decreases with increasing temperature. The viscosity of the binary mixtures with methanol is different from that with water due to the fact that the η of methanol is very low compared with water. The η of the binary mixtures of methanol increases exponentially due to the crowding of the solute ions to improve the attractions among the ions namely, anion-anion, cation-anion, and cation-cation. Commonly, the influence of the hydrogen bonds plays a vital role in the resulting viscosities for binary mixtures.

The computed thermodynamic properties of V_m^E, was derived from experimental density data of IL and binary mixtures of the solution. The V_m^E increases with increasing mole fraction but decreases with increasing temperature. The negative values for V_m^E confirmed the presence of filling or packing effects occurring as a result of the strong interactions between the molecules which are present in the binary mixtures. Furthermore, volume constriction represents the obtained negative effect due to the ion-polar interaction between the molecules present in the liquid mixture and unlike species getting closer together. The small molecules fitting in between the larger molecules may also happen in these compositions and the negative effects are due to the ill-fitting molecules mixed together. Effective interactions among the IL moieties with water or methanol suggest that the self-association between the IL which could be considered as the ion + ion association and weak Van der Waals forces between the bulky alkyl substituted group of the IL, and of course the strong H-bond contributions to the interactions. The size of the ions in the ILs strongly influences and decides the association of ion + ion in the binary mixture.

The polarity of the IL is mostly dependent on the cation present in the IL and could be confirmed and represented by spectroscopic techniques. In this case, the floppy alkyl substitution group in the cation is significantly influenced by the anion. The thermodynamic properties gave negative values for the entire mole fraction ranges of the binary mixtures, and the resulting data shows that these values initially decreases, but after mole fraction of 0.5, it was increases at all investigated temperatures. The values of $V_{m,mim}^E$= -40.53 cm^3 mol^{-1}(for water), and $V_{m,mim}^E$= -33.56 cm^3 mol^{-1} (for methanol) were obtained at x_1 = 0.4894 and x_1 = 0.5489, respectively for the binary systems of {[Epmpyr]$^+$[OAC]$^-$ (x_1) + water or methanol (x_2)} at all examined temperatures.

The k_s is derived from experimental u data at desired mole fractions at all examined temperatures under atmospheric pressure for both binary systems. The isentropic compressibility increases with increasing temperature due to the increased compressibility which occurs, resulting from increased thermal agitation in the binary mixtures. In contrast, k_s decreases with increasing mole fraction of the IL at all investigated temperatures for both binary systems. The negative Δk_s occurred since strong interactions create a strong packing effect for both binary mixtures. Comparing both binary mixtures, the [Epmpyr]$^+$[OAC]$^-$ with water gave stronger interactions. The values of $\Delta k_{s,min}$= -14.3 (10^8 Pa^{-1}) at mole fraction x_1 = 0.2990 and [Epmpyr]$^+$[OAC]$^-$ with the methanol system gave $\Delta k_{s,min}$= -31.6 (10^8 Pa^{-1}) $\Delta k_{s,min}$ at x_1 = 0.2847. Generally, when comparing both binary systems,

the one that containing water was more compressible than methanol in IL binary mixtures, due to the dielectric constant and more possibilities of H-bonding among water and IL molecules. The decreasing order of Δk_s for binary systems is as follows {[Epmpyr]$^+$[OAC]$^-$ (x_1) + water (x_2)} > {[Epmpyr]$^+$[OAC]$^-$(x_1) + methanol (x_2)} which indicates that, the compressibility decreases from water to methanol.

The L_f was computed from the experimental speed of sound data for both binary systems, in fixed mole fractions at temperatures from 288.15 to 313.15 K at 5 K intervals under atmospheric pressure. Intermolecular free length increases with increasing temperature and decreases with increasing mole fraction of the IL. The L_f is inversely proportion to the u and it is strongly influenced by temperature due to the bonding or interactions between unlike molecules becoming weaker, and this is a reason for the surface of the molecules to migrate from the centre of other molecules. The distance between the centre and surface of the adjoining molecules could be increased and L_f also explains the forces between the molecules present in the liquid mixtures, whether it can be attractive or repulsive forces. The magnitude of the forces is similar however directions are different. The numerical sign of the forces is same but in opposite directions under external conditions. Jacobson's Empirical relation is one of the best methods to calculate and understand the L_f using k_s.

The FTIR spectra of IL and its corresponding binary mixtures were compared to get further information about the interactions studies. The spectrum of the IL confirms the functional groups present in the IL moiety and the spectrum for IL with water or methanol binary system revealed the occurrence of some interaction among the molecules in liquid mixtures. The FTIR was examined for both binary system at the mole fraction of 0.2, due to the fact that both thermodynamic properties of V_m^E and Δk_s gave higher negative values at the 0.2 mole fraction. FTIR also showed extra peaks due to hydrogen bonds and interaction of the IL with solvents. The C = O stretching vibration decreased from 1680 cm^{-1} to 1640 cm^{-1} in the binary mixtures due to the ion-dipole interactions between [Epmpyr]$^+$[OAC]$^-$ and water or methanol. The spatial ion-dipole interactions influence the C = O stretching so it was decreased from 1664 cm^{-1} to 1658 cm^{-1}. The quaternary amine in IL peak values shifted from 3508 cm^{-1} to 3441 cm^{-1} due to solvent interactions. From the investigation of FTIR, it is evident that the addition of solvents to [Epmpyr]$^+$[OAC]$^-$ does influence (i) C-H vibrations in [Epmpyr]$^+$[OAC]$^-$, (ii) Hydrogen bonding

between epoxy group in cation and anion group to solvents, (iii) C-O vibration in cation; (iv) C-N stretching in cation of $[Epmpyr]^+[OAC]^-$ Overall the FTIR study confirms the ion-dipole interactions in binary mixture of $[Epmpyr]^+[OAC]^-$.

The Redlich-Kister polynomial equation was used to correlate the derived thermodynamic properties such as V_m^E, Δk_s, and L_f at all investigated temperatures.

11 Chapter 7

11.1 4th Publication

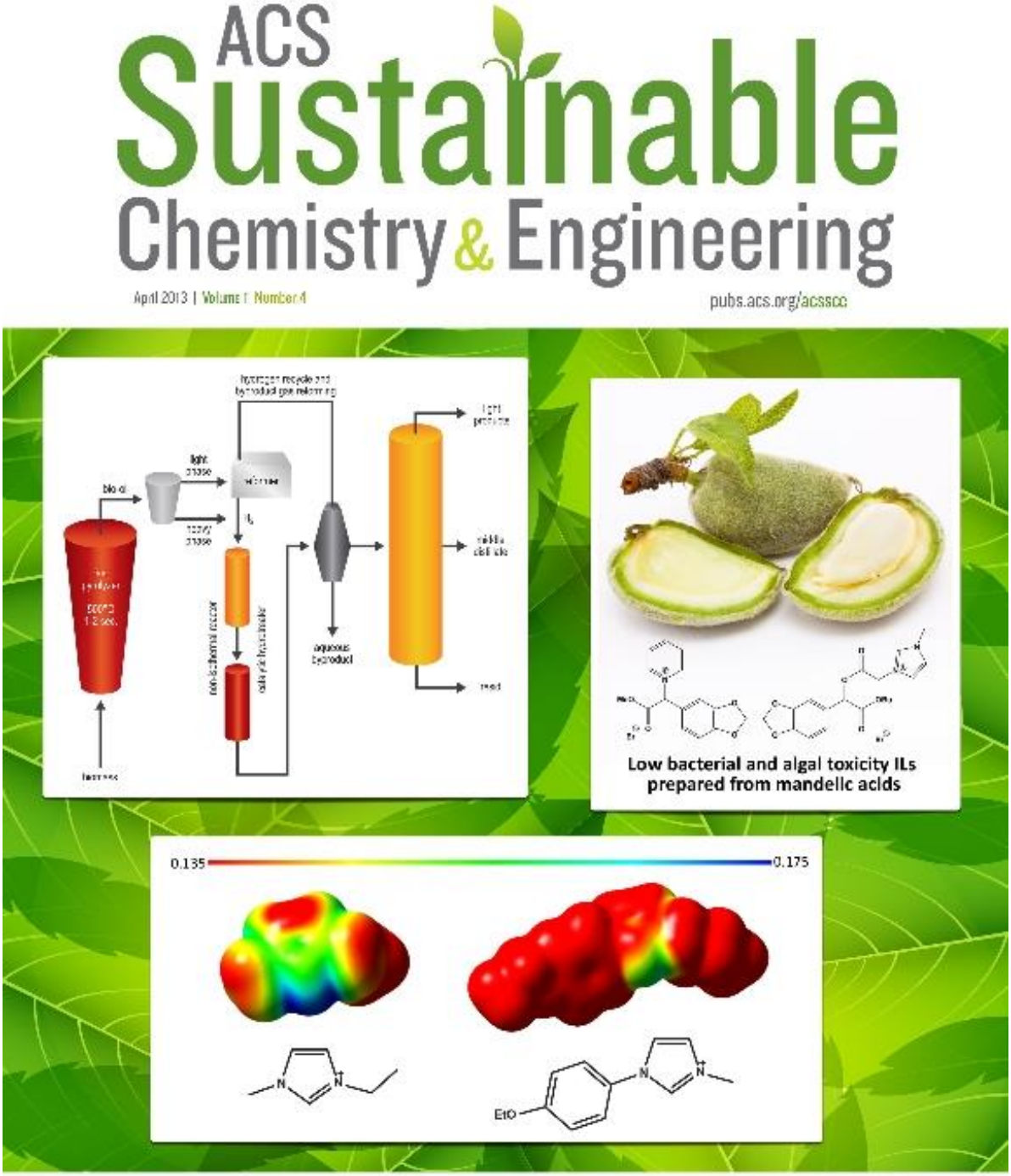

Graphical abstract

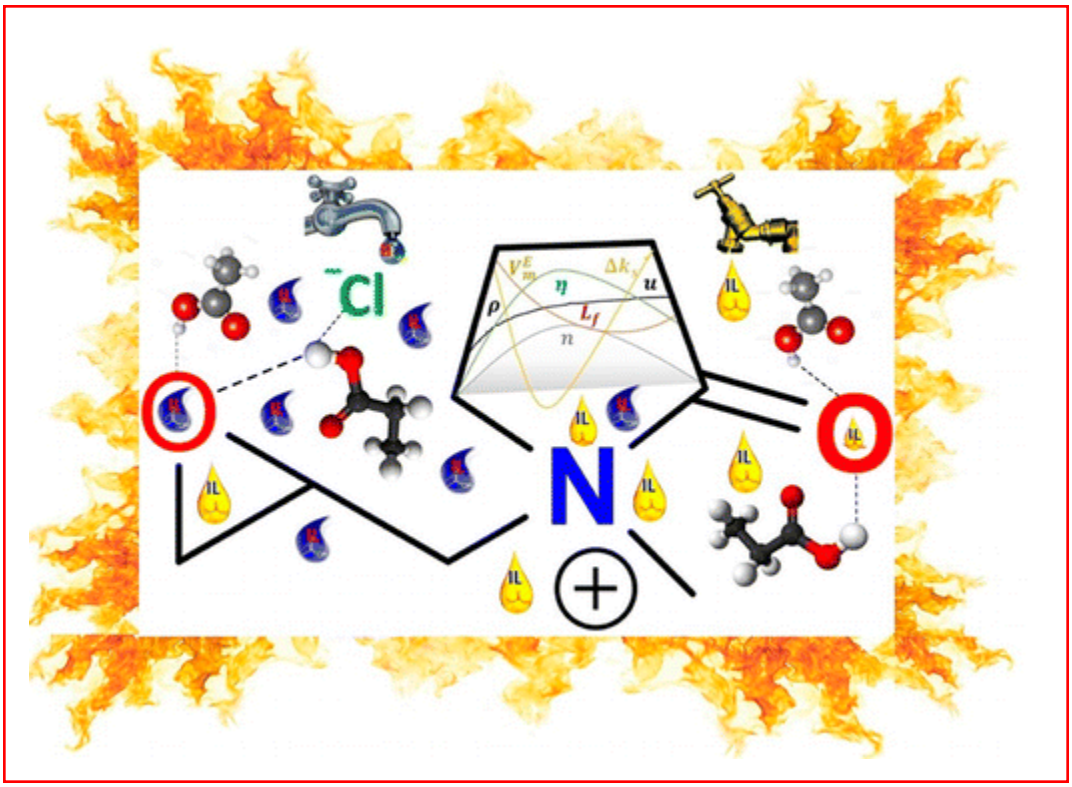

ACS Sustainable Chemistry & Engineering

Research Article

pubs.acs.org/journal/ascecg

Influence of Epoxy Group in 2-Pyrrolidonium Ionic Liquid Interactions and Thermo-Physical Properties with Ethanoic or Propanoic Acid at Various Temperatures

Arumugam Vasantha Kumar,[†] G. G. Redhi,*[,†] and R. M. Gengan[†]

[†]Department of Chemistry, Durban University of Technology, P. O. Box 1334, Durban 4000, South Africa

ABSTRACT: In this present study, the interaction between a carboxylic acid and ionic liquids, in terms of their binary mixtures and corresponding thermo-physical properties, was investigated. Here, the novel ionic liquid (IL) $[EPMpyr]^+[Cl]^-$ was synthesized, and it has been mixed with ethanoic or propanoic acids. The influence of the epoxy group in this ionic liquid was more strongly affected with the acids, and their physicochemical properties at varied temperatures are discussed in term of density (ρ), viscosity (η), speed of sound (u), and refractive index (n) measurements. The density (ρ), speed of sound (u), viscosity (η), and refractive index (n) of the IL, ethanoic acid, propanoic acid, and their corresponding binary mixtures {[([EPMpyr]$^+$[Cl]$^-$ (1) + ethanoic or propanoic acid (2)} have been measured at T = (293.15−313.15) K and at P = 0.1 MPa. The theoretical thermodynamic properties of excess molar volumes (V_m^E), isentropic compressibility (k_s), deviation in isentropic compressibility (Δk_s), and intermolecular free length (L_f) are calculated using experimental density and speed of sound data. The V_m^E and Δk_s values for both binary mixtures were found to be negative over the entire mole fraction range of composition at all the investigated temperatures. These results suggest the existence of specific interactions between components in the molecules. The experimental data could be helpful to understand the molecular interactions between the IL and carboxylic acid combinations. The experimental data were fitted to the Redlich−Kister polynomial equation.

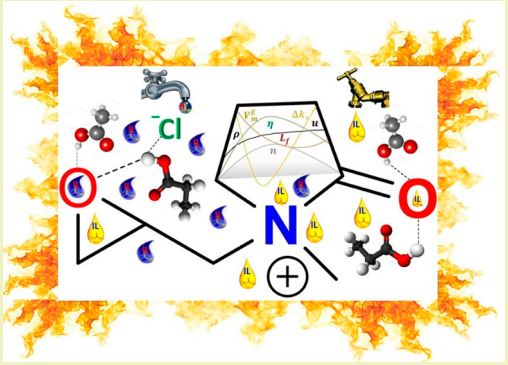

KEYWORDS: *Density, Speed of sound, Viscosity, Refractive index, N-(2′,3′-epoxypropyl)-N-methyl-2-oxopyrrolidinium chloride, Redlich−Kister equation*

INTRODUCTION

Ionic liquids are emerging new materials of molten state organic salts which contain a combination of cations and anions. The cations are normally organic molecules, while the anions may be inorganic or organic molecules.[1] In many cases, ILs are distinguished as newly generated solvents or greener solvents, which are liquid at room temperature and are composed totally of ions.[2] ILs are generally viscous and have boiling points below 100 °C.[3] Generally, cations of ILs have a low degree of symmetry due to the large difference in size of the cations and anions in the ionic liquid.[3] During the past decade, most researchers concentrated their attention on the creation of novel room-temperature ionic liquids (RTILs) because of their unique properties as well as significant applications.[4,5] The new generation of stable room temperature ionic liquids (RTILs) have been applicable in both industrial and academic communities due to their fascinating properties such as a large liquid range, good electrical conductivity, and low volatilities.[6−11] The glass transition temperature of an IL is one of the most attractive properties, which strongly defines the electrolyte nature of the IL, and it may also change the derived thermodynamic properties and is apparently related to the combination of the structure of the cations and anions,[12,13] The scientific society needs a better understanding of the intermolecular interactions in binary and ternary mixtures of the ionic liquids which is obviously related to the molecular structure and thermo-physical properties of ILs.[14]

The main advantages of ILs are flexibility of their physicochemical properties by appropriately creating novel ionic liquid architectures, for example, changing the side chain length or substitution group of cations/anions or introducing novel functional groups in the cation/anion structure.[15,16] The thermo-physical properties are important to investigate interactions between molecules in liquid mixtures as well as those interactions that depend on the molecular geometry and charge distribution of the solvents.[17] The extraordinary properties of ILs are high conductivity,[6] negligible vapor pressure,[18] high thermal and chemical stability,[19] and low flammabilities.[20] For use of ILs as solvents, a good understanding of the thermo-physical properties of ionic liquids and its liquid mixtures, such as density, sound velocity, refractive index, and viscosity, is necessary.

Carboxylic acids are an important family of chemicals which are used in several industries for the manufacture of

Received: June 7, 2016
Revised: July 29, 2016
Published: August 1, 2016

DOI: 10.1021/acssuschemeng.6b01262
ACS Sustainable Chem. Eng. 2016, 4, 4951−4964

Table 1. Comparison of Experimental Density and Speed of Sound of Pure Liquids with Literature Values at Temperatures from 293 K to 313 K

components	T (K)	ρ (g cm^{-3}) exp	ρ (g cm^{-3}) lit	ref	u (ms^{-1}) exp	u (ms^{-1}) lit	ref
ethanoic acid	293.15	1.0524	1.0497	49	1168.3	1152.7	49
			1.0493	51		1149.0	51
			1.0492	52		1150.0	56
	298.15	1.0468	1.0441	49	1152.4	1135.7	49
			1.0440	53		1132.0	51
			1.0437	51			
	303.15	1.0412	1.0385	49	1135.5	1118.4	49
			1.0380	51		1115.0	51
	308.15	1.0299	1.0328	49	1118.5	1101.2	49
			1.0326	53			
	313.15		1.0272	49	1101.4	1084.0	49
propanoic acid	293.15	0.9915	0.9933	49	1171.5	1164.7	49
			0.9938	54		1165.6	54
			0.9939	55		1165.0	55
	298.15	0.9861	0.9879	49	1153.4	1146.0	49
			0.9884	54		1127.7	54
			0.9885	55		1147.0	55
	303.15	0.9808	0.9825	49	1134.8	1127.1	49
			0.9831	54		1127.7	54
			0.9831	55		1128.0	55
	308.15	0.9754	0.9771	49	1116.3	1108.3	49
			0.9776	54		1108.9	54
			0.9777	55		1109.0	55
	313.15	0.9701	0.9717	49	1097.8	1089.0	49
			0.9722	54		1090.2	54
			0.9723	55		1090.0	55
N-methyl-*N*-(2′,3′-epoxypropyl)-2-oxopyrrolidinium chloride	293.15	1.0694	1.0685	57	1502.2	1502.4	57
	298.15	1.0646	1.0637	57	1483.6	1483.6	57
	303.15	1.0598	1.0589	57	1464.4	1464.6	57
	308.15	1.0550	1.0572	57	1445.5	1487.2	57
	313.15	1.0502	1.0494	57	1426.8	1427.2	57

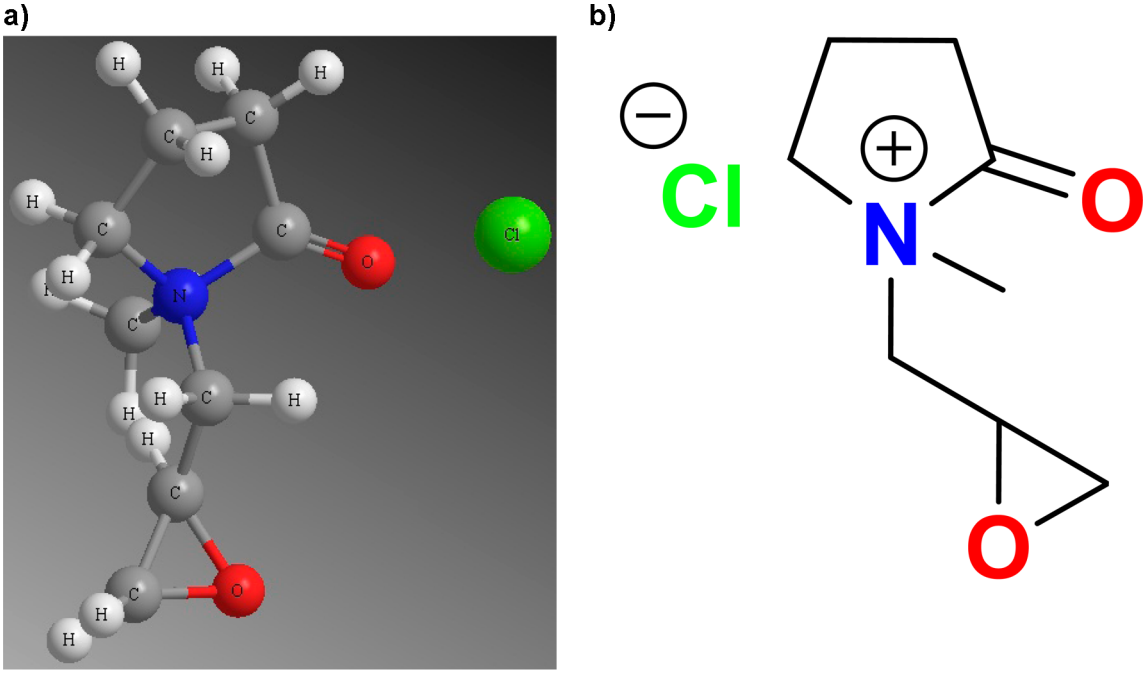

Figure 1. (a) 3D structure of the ionic liquid [EPMpyr]$^+$[Cl]$^-$. (b) Structure of the ionic liquid [EPMpyr]$^+$[Cl]$^-$.

pharmaceutical products, cleaning agents, separation processes, polyesters resins, and food preservatives, and they are also used in beverages as an acidulant and as buffers, flavoring agents, fungicides, insecticides, catalysts, and in other chemical industries. Indeed, the combination of acid with ionic liquid makes for more effective usages in the future.[21−25] Generally,

DOI: 10.1021/acssuschemeng.6b01262
ACS Sustainable Chem. Eng. 2016, 4, 4951−4964

Table 2. Density (ρ), Speed of Sound (u), Viscosity (η), and Refractive Index (n), with Mole Fraction (x_1) of *N*-(2′,3′-Epoxypropyl)-*N*-methyl-2-oxopyrrolidinium Chloride in a Binary Liquid Mixture of {[EPMpyr]$^+$[Cl]$^-$ (1) + Ethanoic Acid (2)} from T (K) = 293.15 to 313.15 at Pressure P = 0.1 MPa

x_1	ρ (g cm^{-1})	u (m s^{-1})	η (mPa s)	n
		293.15 K		
0.0000	1.0524	1168.32	1.2875	1.3737
0.0373	1.0593	1219.71	1.5920	1.3908
0.0644	1.0633	1253.04	1.8300	1.3991
0.1087	1.0697	1296.59	2.2336	1.4048
0.2041	1.0765	1368.77	2.7282	1.4221
0.3022	1.0788	1415.20	2.8028	1.4336
0.4053	1.0783	1443.58	2.5868	1.4414
0.5054	1.0769	1461.31	2.3239	1.4470
0.6050	1.0750	1474.31	2.1072	1.4512
0.7073	1.0723	1484.01	1.9194	1.4547
0.8065	1.0718	1493.03	1.8169	1.4583
0.9047	1.0719	1501.20	1.7517	1.4606
1.0000	1.0710	1506.65	1.6765	1.4636
		298.15 K		
0.0000	1.0468	1152.40	1.1805	1.3722
0.0373	1.0538	1202.53	1.4480	1.3892
0.0644	1.0579	1235.65	1.6520	1.3976
0.1087	1.0645	1278.66	1.9999	1.4032
0.2041	1.0715	1350.94	2.4253	1.4204
0.3022	1.0738	1397.40	2.4924	1.4317
0.4053	1.0734	1425.76	2.3139	1.4394
0.5054	1.0721	1443.37	2.0946	1.4450
0.6050	1.0702	1456.22	1.9080	1.4491
0.7073	1.0675	1465.74	1.7465	1.4525
0.8065	1.0670	1474.64	1.6574	1.4561
0.9047	1.0672	1482.71	1.6018	1.4592
1.0000	1.0662	1488.04	1.5368	1.4616
		303.15 K		
0.0000	1.0412	1135.48	1.0853	1.3708
0.0373	1.0483	1185.11	1.3220	1.3874
0.0644	1.0526	1218.06	1.5000	1.3957
0.1087	1.0593	1260.49	1.8022	1.4015
0.2041	1.0665	1332.91	2.1724	1.4185
0.3022	1.0689	1379.32	2.2345	1.4299
0.4053	1.0686	1407.64	2.0867	1.4375
0.5054	1.0673	1425.16	1.9000	1.4431
0.6050	1.0654	1437.85	1.7379	1.4471
0.7073	1.0627	1447.22	1.5968	1.4505
0.8065	1.0622	1455.99	1.5213	1.4539
0.9047	1.0624	1463.94	1.4729	1.4572
1.0000	1.0615	1469.17	1.4154	1.4595
		308.15 K		
0.0000	1.0355	1118.48	1.0016	1.3691
0.0373	1.0429	1167.68	1.2130	1.3862
0.0644	1.0474	1200.41	1.3710	1.3944
0.1087	1.0540	1242.41	1.6324	1.3998
0.2041	1.0615	1314.96	1.9585	1.4167
0.3022	1.0640	1361.31	2.0176	1.4281
0.4053	1.0637	1389.57	1.8920	1.4356
0.5054	1.0624	1406.98	1.7308	1.4412
0.6050	1.0606	1419.52	1.5911	1.4452
0.7073	1.0579	1428.73	1.4691	1.4484
0.8065	1.0575	1437.37	1.4022	1.4519
0.9047	1.0576	1445.22	1.3603	1.4548
1.0000	1.0567	1450.37	1.3089	1.4573
		313.15 K		
0.0000	1.0299	1101.41	0.9283	1.3677
0.0373	1.0374	1150.19	1.1150	1.3842
0.0644	1.0418	1182.27	1.2560	1.3927
0.1087	1.0488	1224.57	1.4893	1.3981
0.2041	1.0565	1297.19	1.7761	1.4151
0.3022	1.0591	1343.42	1.8313	1.4263
0.4053	1.0588	1371.57	1.7234	1.4337
0.5054	1.0576	1388.88	1.5859	1.4393
0.6050	1.0557	1401.28	1.4646	1.4431
0.7073	1.0531	1410.32	1.3559	1.4465
0.8065	1.0527	1418.85	1.2974	1.4498
0.9047	1.0529	1426.60	1.2606	1.4531
1.0000	1.0519	1431.64	1.2147	1.4551

ionic liquids are basic in nature and more viscous due to the nitrogenous compounds present there, so their basicity and viscosity makes them less attractive to use in some applications. This research focuses on assisting in solving these problems. The attention of the scientific community and chemical industry is now more than ever focused on exploring new applications of ILs due to their interesting properties, which makes them more useful as greener solvents. The application of ILs includes, among others, use as green solvents, heterogeneous catalysts, synthesis of organometallics,[26] nanocomposite synthesis,[27] and biocatalysis.[28] An important application of ILs as working fluids is in different electrochemical industries, such as for batteries,[29,30] solar cells,[31] transistors,[32] capacitors,[33] chemical sensors,[34] and fuel cells.[35] Moreover, they have also been used in separation and extraction technologies[36,37] and in thermal fluids,[38] liquid crystals,[39] lubricants, and fuel additives,[40] along with the generation of high conductivity materials[41] and in preparation of polymer gel catalytic membranes. The important industries, such as catalysis,[42] electrochemistry,[6] biotechnology,[43] nanotechnology,[44] and energy generation,[45] have been using ILs to promote research and development in order to make novel functional materials in efficient and cost-effective ways by using various technologies. The capturing of CO_2 and separation processes are advanced applications of ILs. These alternative technologies take into account their low volatility and highly tunable nature, which permit the creation of task-specific ILs with notable affinity for CO_2 over other gases.[46]

Another popular family of ILs which are relatively less expensive and have wide electrochemical windows of great interest in electrochemical applications are the pyrrolidonium group of ILs.[47] However, the physical properties especially melting points are significantly higher than the corresponding imidazolium ILs with same anion and equivalent cationic substituent groups. The separation of aromatic from aliphatic hydrocarbons and the extraction of sulfur compounds from hydrocarbon mixtures, are possible and favorable with pyrrolidinium based ionic liquids due to their greater selectivity.[48] Pyrrolidinium and piperidinium based ILs exhibit greater cathodic stability and lower viscosities compared to other groups of ILs and ultimately these are the important and attractive properties required for use in the field of electrochemistry.[49] N-butyl-*N*-methylpyrrolidinium bis(trifluoro methansulfonyl) imide has been used as electrolytes for metal/air battery systems due to

DOI: 10.1021/acssuschemeng.6b01262
ACS Sustainable Chem. Eng. 2016, 4, 4951−4964

Table 3. Excess Molar Volume (V_m^E), Isentropic Compressibility (k_s), Intermolecular Free Length (L_f), Deviation in Isentropic Compressibility (Δk_s) with Mole Fraction (x_1) of *N*-(2′,3′-Epoxypropyl)-*N*-methyl-2-oxopyrrolidinium Chloride in a Binary Liquid Mixture of {[EPMpyr]$^+$[Cl]$^-$ (1) + Ethanoic Acid (2)} from T (K) = 293.15 to 313.15 at Pressure P = 0.1 MPa

x_1	V_m^E (cm^3 mol^{-1})	k_s (10^8 Pa^{-1})	Δk_s (10^8 Pa^{-1})	L_f(10^7 m)
		293.15 K		
0.0000	0.0000	69.6130	0.0000	1.7003
0.0373	−0.2841	63.4550	−5.0932	1.6235
0.0644	−0.4639	59.8980	−7.8792	1.5773
0.1087	−0.7989	55.6070	−10.9078	1.5197
0.2041	−1.2056	49.5820	−14.2164	1.4350
0.3022	−1.3621	46.2830	−14.7204	1.3864
0.4053	−1.3072	44.5010	−13.5663	1.3595
0.5054	−1.1412	43.4850	−11.7302	1.3440
0.6050	−0.8743	42.7970	−9.5836	1.3332
0.7073	−0.4684	42.3450	−7.1198	1.3262
0.8065	−0.3087	41.8550	−4.7859	1.3185
0.9047	−0.2391	41.3960	−2.4488	1.3113
1.0000	0.0000	41.1320	0.0000	1.3070
		298.15 K		
0.0000	0.0000	71.9330	0.0000	1.7440
0.0373	−0.2880	65.6220	−5.2056	1.6661
0.0644	−0.4724	61.9100	−8.1171	1.6183
0.1087	−0.8177	57.4570	−11.2594	1.5591
0.2041	−1.2340	51.1370	−14.7590	1.4708
0.3022	−1.3944	47.6900	−15.3040	1.4203
0.4053	−1.3381	45.8290	−14.1165	1.3924
0.5054	−1.1699	44.7720	−12.2123	1.3762
0.6050	−0.8990	44.0630	−9.9782	1.3652
0.7073	−0.4863	43.6030	−7.4108	1.3581
0.8065	−0.3228	43.0980	−4.9838	1.3503
0.9047	−0.2519	42.6220	−2.5567	1.3427
1.0000	−0.0000	42.3570	−0.0000	1.3386
		303.15 K		
0.0000	0.0000	74.4910	0.0000	1.7913
0.0373	−0.2972	67.9190	−5.4212	1.7104
0.0644	−0.4831	64.0320	−8.4733	1.6606
0.1087	−0.8348	59.4150	−11.7234	1.5998
0.2041	−1.2603	52.7760	−15.4209	1.5078
0.3022	−1.4221	49.1730	−15.9972	1.4553
0.4053	−1.3631	47.2280	−14.7628	1.4263
0.5054	−1.1901	46.1300	−12.7724	1.4096
0.6050	−0.9129	45.4000	−10.4329	1.3984
0.7073	−0.4922	44.9280	−7.7475	1.3912
0.8065	−0.3231	44.4090	−5.2085	1.3831
0.9047	−0.2489	43.9200	−2.6698	1.3754
1.0000	0.0000	43.6450	−0.0000	1.3712
		308.15 K		
0.0000	−0.0000	77.1950	−0.0000	1.8401
0.0373	−0.3007	70.7040	−5.2951	1.7610
0.0644	−0.4941	66.2690	−8.8582	1.7049
0.1087	−0.8592	61.4650	−12.2345	1.6419
0.2041	−1.2951	54.4820	−16.1453	1.5458
0.3022	−1.4599	50.7150	−16.7512	1.4915
0.4053	−1.3980	48.6870	−15.4585	1.4613
0.5054	−1.2223	47.5480	−13.3719	1.4441
0.6050	−0.9394	46.7910	−10.9231	1.4325
0.7073	−0.5109	46.3070	−8.1094	1.4252
0.8065	−0.3374	45.7700	−5.4526	1.4168
0.9047	−0.2607	45.2700	−2.7904	1.4091
1.0000	0.0000	44.9870	−0.0000	1.4047
		313.15 K		
0.0000	0.0000	80.0390	−0.0000	1.9351
0.0373	−0.3109	72.8640	−5.9211	1.8463
0.0644	−0.5095	68.6720	−9.2018	1.7924
0.1087	−0.8796	63.5820	−12.7999	1.7247
0.2041	−1.3272	56.2500	−16.9214	1.6222
0.3022	−1.4949	52.3160	−17.5520	1.5645
0.4053	−1.4307	50.2050	−16.1929	1.5326
0.5054	−1.2516	49.0170	−14.0100	1.5144
0.6050	−0.9638	48.2400	−11.4369	1.5023
0.7073	−0.5273	47.7410	−8.4898	1.4945
0.8065	−0.3499	47.4870	−5.4062	1.4905
0.9047	−0.2708	46.6660	−2.9226	1.4776
1.0000	−0.0000	46.3820	0.0000	1.4730

their low vapor pressure, high gas affinity and great conductivity in nature.[50]

Generally the anions of ILs such as bis(trifluoromethylsulfonyl)imide (Tf_2N) and PF_6 are hydrophobic in nature due to their highly delocalized charged molecules and other types of ILs like halide anions and carboxylate (COO^-), while alkyl phosphate R_2PO_4 is hydrophilic in nature as reported by Anouti et al.[51] Anouti et al.[52] reports that pyrrolidinium alkyl carboxylates protic ILs have been used as surfactants in aqueous media because of their aggregation behavior.[53] The present work is related to our investigation of thermo-physical properties of liquid mixtures of ILs.[54,55] The combination of *N*-2′,3′-epoxypropyl-*N*-methyl-2-oxopyrrolidinium chloride with water or ethanol was investigated to determine its physicochemical properties.,[55,62] In the present work, the thermo-physical properties of *N*-2′,3′-epoxypropyl-*N*-methyl-2-oxopyrrolidinium chloride with ethanoic or propanoic acid at several temperatures are investigated. The present research may create new applications for ionic liquids in other industries because these experiments clearly tell us about how to reduce the basicity and viscosity of ionic liquids simultaneously by using a simple mixing of acids, without affecting the nature of the ionic liquids.

EXPERIMENTAL SECTION

Materials. *N*-Methyl pyrrolidone, epichlorohydrin, ethanoic acid, propanoic acid, methanol, acetonitrile, hexane, and acetone were purchased from Fluka Chemicals with purity of ≥99% by mass. The densities and speed of sound of the pure ethanoic acid, propanoic acid, and ionic liquids were compared with literature at 298.15 K and are presented in Table 1.[56−62] The percentage of moisture content was found to be 0.05% in [EPMpyr]$^+$[Cl]$^-$ using Karl Fischer instrument.

Synthesis of N-2′,3′-Epoxypropyl-N-methyl-2-oxopyrrolidinium chloride [EPMpyr]$^+$[Cl]$^-$. *N*-2′,3′-Epoxypropyl-*N*-methyl-2-oxopyrrolidinium chloride [EPMpyr]$^+$[Cl]$^-$ ionic liquid was synthesized[57] in our previous publication, and the methodology of synthesis and characterization was also described.[62,63] The synthesized ionic liquid was purified by using different solvent washing and redistillation methods. The structure of the IL is given in the Figure 1a and b.

Characterization of N-2′,3′-Epoxypropyl-N-methyl-2-oxopyrrolidinium chloride [EPMpyr]$^+$[Cl]$^-$. The structure of the [EPMpyr]$^+$[Cl]$^-$ was confirmed by the following characterizations ^{1}HNMR, ^{13}CNMR, FTIR, and elemental analysis of CHN was reported in our previous paper.[62,63]

DOI: 10.1021/acssuschemeng.6b01262
ACS Sustainable Chem. Eng. 2016, 4, 4951−4964

Table 4. Density (ρ), Speed of Sound (u), Viscosity (η), and Refractive Index (n), with Mole Fraction (x_1) of *N*-(2′,3′-Epoxypropyl)-*N*-methyl-2-oxopyrrolidinium Chloride in a Binary Liquid Mixture of {[EPMpyr]$^+$[Cl]$^-$ (1) + Propanoic Acid (2)} from T (K) = 293.15 to 313.15 at Pressure P = 0.1 MPa

x_1	ρ (g cm^{-3})	u (m s^{-1})	η (mPa s)	n
		293.15 K		
0.0000	0.9915	1171.53	1.0697	1.3885
0.0325	1.0014	1207.70	1.3050	1.3980
0.0638	1.0102	1242.11	1.5770	1.4055
0.1089	1.0193	1279.79	1.8356	1.4102
0.2050	1.0353	1348.53	2.3329	1.4240
0.3036	1.0462	1396.90	2.5435	1.4340
0.4076	1.0538	1432.50	2.5365	1.4414
0.5049	1.0580	1448.42	2.2882	1.4463
0.6079	1.0614	1464.19	2.0880	1.4507
0.7037	1.0640	1475.94	1.9353	1.4541
0.8065	1.0661	1487.14	1.8080	1.4577
0.9028	1.0687	1489.89	1.6425	1.4603
1.0000	1.0694	1502.21	1.6227	1.4625
		298.15 K		
0.0000	0.9861	1153.40	0.9963	1.3866
0.0325	0.9962	1189.23	1.2090	1.3963
0.0638	1.0051	1223.86	1.4500	1.4038
0.1089	1.0143	1261.94	1.6730	1.4084
0.2050	1.0304	1330.76	2.1043	1.4221
0.3036	1.0414	1379.07	2.2846	1.4320
0.4076	1.0490	1414.70	2.2775	1.4394
0.5049	1.0532	1430.51	2.0691	1.4444
0.6079	1.0567	1446.12	1.8952	1.4486
0.7037	1.0592	1457.72	1.7628	1.4521
0.8065	1.0614	1468.77	1.6503	1.4556
0.9028	1.0640	1471.46	1.5074	1.4582
1.0000	1.0646	1483.61	1.4894	1.4603
		303.15 K		
0.0000	0.9808	1134.81	0.9294	1.3848
0.0325	0.9910	1170.77	1.1200	1.3944
0.0638	1.0000	1205.63	1.3350	1.4018
0.1089	1.0093	1243.84	1.5330	1.4066
0.2050	1.0255	1312.72	1.9086	1.4202
0.3036	1.0366	1360.95	2.0638	1.4301
0.4076	1.0442	1396.62	2.0588	1.4375
0.5049	1.0485	1412.33	1.8818	1.4424
0.6079	1.0519	1427.80	1.7293	1.4467
0.7037	1.0544	1439.24	1.6129	1.4500
0.8065	1.0566	1450.13	1.5164	1.4535
0.9028	1.0592	1452.40	1.3898	1.4561
1.0000	1.0598	1464.36	1.3733	1.4584
		308.15 K		
0.0000	0.9754	1116.26	0.8692	1.3831
0.0325	0.9858	1152.43	1.0410	1.3929
0.0638	0.9949	1187.47	1.2330	1.4004
0.1089	1.0043	1225.77	1.4100	1.4048
0.2050	1.0206	1294.71	1.7383	1.4185
0.3036	1.0318	1342.89	1.8758	1.4283
0.4076	1.0394	1378.53	1.8704	1.4356
0.5049	1.0437	1394.18	1.7183	1.4404
0.6079	1.0472	1409.50	1.5859	1.4447
0.7037	1.0497	1420.81	1.4846	1.4479
0.8065	1.0518	1431.54	1.3991	1.4515
0.9028	1.0544	1433.69	1.2860	1.4540
1.0000	1.0550	1445.50	1.2703	1.4563
		313.15 K		
0.0000	0.9701	1097.77	0.8166	1.3812
0.0325	0.9806	1134.18	0.9710	1.3909
0.0638	0.9898	1169.39	1.1440	1.3984
0.1089	0.9993	1207.77	1.3009	1.4033
0.2050	1.0158	1276.76	1.5919	1.4164
0.3036	1.0269	1324.90	1.7120	1.4268
0.4076	1.0347	1360.55	1.7068	1.4332
0.5049	1.0389	1376.09	1.5776	1.4394
0.6079	1.0424	1391.29	1.4619	1.4414
0.7037	1.0449	1402.45	1.3715	1.4462
0.8065	1.0471	1413.04	1.2955	1.4488
0.9028	1.0496	1415.09	1.1937	1.4526
1.0000	1.0502	1426.78	1.1801	1.4531

Apparatus and Procedure. Density, speed of sound, viscosity, and refractive index are significant physicochemical properties and were analyzed by using a vibrating tube digital densitometer, speed of sound, and viscosity analyzer, Vis., Anton Parr DSA 5000 M. To determine the density, sound velocity, viscosity, and refractive index of pure ethanoic acid, propanoic acid, ionic liquid, and its binary mixture have been measured simultaneously at different temperatures. Physical properties are most sensitive with pressure and temperature, which were controlled to ±0.01 K and 101 kPa, respectively. The refractive index of the pure components and its binary liquid mixtures were investigated at varied temperature by the Anton Parr refractometer with a digital display with accuracy of 0.01 K in temperature. An airtight syringe was used carefully to transfer the pure liquids into stoppered bottles. The airtight glass stoppered 10 cm^3 glass vials were used to fill ILs and to weigh. The pure components and its binary mixtures [IL (1) + ethanoic or propanoic acid (2)] were prepared by weighing, with the help of OHAUS analytical mass balance with 0.0001 g of precision to measure the weight of each component of the liquid mixtures. The experimental procedure has been reported in detail elsewhere.[64] The determination of physicochemical properties of density and speed of sound with temperatures tolerant limits was as follows: less than ±2 × 10^{-5} g cm^{-3}, ±0.6 ms^{-1}, and ± 0.02 K, respectively.

RESULTS AND DISCUSSION

The industrially useful properties of density, viscosity, speed of sound, and refractive index were investigated at temperatures from T = 293.15 to 313.15 K at P = 0.1 MPa for IL [EPMpyr]$^+$[Cl]$^-$, ethanoic acid, propanoic acid, and their corresponding binary systems. {[EPMpyr]$^+$[Cl]$^-$(1) + ethanoic or propanoic acid (2)} experimental data are given in Tables 2–5. Each property of the pure components and their binary mixtures was plotted against mole fraction of IL at experimental temperatures and are given in Figures 3, 5, 7, 9–12. Tables 2 and 4 show that the properties of density, sound velocity, viscosity and refractive index values decreases when the temperature for both binary systems and pure components is increased as indicated in Figures 2, 4, 6, and 8. Density increases with increasing concentration, which is due to the strong interaction of [EPMpyr]$^+$[Cl]$^-$ with propanoic acid.[65]

It is very difficult to understand the interactions in the liquid mixtures; sound velocity clearly describes the interaction among the solvent−solvent, solute−solute, and solute−solvent in liquid mixtures.[66] The refractive index is also an important property which helps to better understand the molecular interactions of like and unlike molecules. The speed of sound

DOI: 10.1021/acssuschemeng.6b01262
ACS Sustainable Chem. Eng. 2016, 4, 4951−4964

Table 5. Excess Molar Volume (V_m^E), Isentropic Compressibility (k_s), Intermolecular free length (L_f), Deviation in Isentropic Compressibility (Δk_s) with Mole Fraction (x_1) of *N*-(2′,3′-Epoxypropyl)-*N*-methyl-2-oxopyrrolidinium Chloride in a Binary Liquid Mixture of {[EPMpyr]$^+$[Cl]$^-$ (1) + Propanoic Acid (2)} from T (K) = 293.15 to 313.15 at Pressure P = 0.1 MPa

x_1	V_m^E (cm^3 mol^{-1})	k_s (10^8 Pa^{-1})	Δk_s (10^8 Pa^{-1})	L_f (10^7 m)
		293.15 K		
0.0000	0.0000	73.49	−0.0000	1.7471
0.0325	−0.3207	68.47	−3.9829	1.6864
0.0638	−0.6241	64.16	−7.2826	1.6324
0.1089	−0.8579	59.90	−10.1007	1.5773
0.2050	−1.3007	53.11	−13.8066	1.4852
0.3036	−1.5145	48.98	−14.7758	1.4263
0.4076	−1.5330	46.24	−14.1825	1.3858
0.5049	−1.3497	45.05	−12.2546	1.3678
0.6079	−1.1105	43.95	−10.0616	1.3510
0.7037	−0.8617	43.14	−7.7925	1.3385
0.8065	−0.5681	42.41	−5.2291	1.3272
0.9028	−0.4245	42.15	−2.4038	1.3231
1.0000	0.0000	41.44	−0.0000	1.3119
		298.15 K		
0.0000	−0.0000	76.23	−0.0000	1.7957
0.0325	−0.3357	70.98	−4.1620	1.7328
0.0638	−0.6487	66.42	−7.6636	1.6763
0.1089	−0.8890	61.91	−10.6669	1.6183
0.2050	−1.3415	54.80	−14.5511	1.5226
0.3036	−1.5587	50.49	−15.5529	1.4614
0.4076	−1.5774	47.63	−14.9210	1.4195
0.5049	−1.3904	46.40	−12.8897	1.4010
0.6079	−1.1455	45.25	−10.5808	1.3836
0.7037	−0.8900	44.43	−8.1885	1.3709
0.8065	−0.5888	43.67	−5.4943	1.3593
0.9028	−0.4385	43.41	−2.5312	1.3551
1.0000	0.0000	42.68	0.0000	1.3436
		303.15 K		
0.0000	0.0000	79.17	0.0000	1.8467
0.0325	−0.3438	73.62	−4.4115	1.7808
0.0638	−0.6664	68.80	−8.1294	1.7215
0.1089	−0.9136	64.04	−11.3030	1.6609
0.2050	−1.3781	56.59	−15.3741	1.5613
0.3036	−1.5988	52.08	−16.4105	1.4978
0.4076	−1.6178	49.10	−15.7387	1.4542
0.5049	−1.4272	47.81	−13.6003	1.4351
0.6079	−1.1772	46.63	−11.1611	1.4173
0.7037	−0.9151	45.79	−8.6380	1.4043
0.8065	−0.6073	45.01	−5.8008	1.3923
0.9028	−0.4507	44.76	−2.6672	1.3884
1.0000	−0.0000	44.00	0.0000	1.3767
		308.15 K		
0.0000	−0.0000	82.28	−0.0000	1.8997
0.0325	−0.3597	76.38	−4.6996	1.8303
0.0638	−0.6925	71.28	−8.6417	1.7682
0.1089	−0.9464	66.27	−11.9894	1.7048
0.2050	−1.4216	58.45	−16.2604	1.6011
0.3036	−1.6451	53.74	−17.3283	1.5352
0.4076	−1.6626	50.63	−16.6033	1.4901
0.5049	−1.4678	49.29	−14.3457	1.4703
0.6079	−1.2117	48.07	−11.7713	1.4520
0.7037	−0.9424	47.19	−9.1085	1.4386
0.8065	−0.6272	46.39	−6.1103	1.4264
0.9028	−0.4633	46.14	−2.8104	1.4225
1.0000	−0.0000	45.36	0.0000	1.4105
		313.15 K		
0.0000	0.0000	85.54	0.0000	2.0004
0.0325	−0.3682	79.28	−5.0016	1.9259
0.0638	−0.7118	73.88	−9.1820	1.8592
0.1089	−0.9728	68.60	−12.7157	1.7915
0.2050	−1.4602	60.39	−17.2016	1.6808
0.3036	−1.6869	55.48	−18.2937	1.6111
0.4076	−1.7037	52.21	−17.5271	1.5629
0.5049	−1.5050	50.83	−15.1351	1.5421
0.6079	−1.2430	49.56	−12.4160	1.5227
0.7037	−0.9668	48.66	−9.6036	1.5088
0.8065	−0.6448	47.83	−6.4449	1.4959
0.9028	−0.4737	47.58	−2.9667	1.4920
1.0000	−0.0000	46.78	0.0000	1.4794

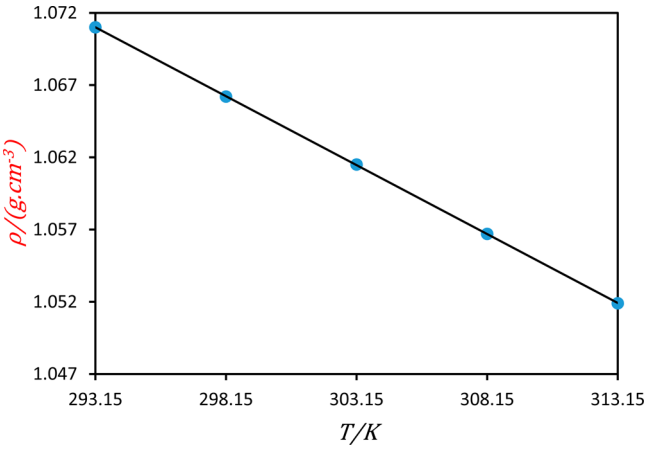

Figure 2. Density (ρ) of [EPMpyr]$^+$[Cl]$^-$ at temperatures from 293.15 to 313.15 K.

and refractive index decreases with an increasing temperature for both binary liquid mixtures of {[EPMpyr]$^+$[Cl]$^-$(1) + ethanoic or propanoic acid (2)} as given in Tables 2 and 4. These properties of sound velocity and refractive index are inversely proportional to temperature plots (Figures 4 and 8), but both properties show an increase with mole fraction of IL as shown in Figures 5 and 9.

Derived Properties. *Excess Molar Volume.* The excess molar volumes are important thermo-physical properties which are calculated from experimental density data. Equation 1 is used to calculate the excess molar volume V_m^E as follows:

$$V_m^E = \sum_{i=1}^{2} x_i M_i (\rho^{-1} - \rho_i^{-1}) \quad (1)$$

where x_1 and x_2 denote mole fractions; M_1 and M_2 represent molar masses; ρ_1 and, ρ_2 indicate the densities of IL and their binary mixtures of acid, and ρ is the density of their binary mixtures.

The calculated excess molar volume data for the binary mixtures of {[EPMpyr]$^+$[Cl]$^-$(1) + ethanoic or propanoic acid (2)} are shown in Tables 3 and 5. The plots of excess molar volumes versus mole fraction of ILs for both systems are given in Figure 10a and b. The Tables 3 and 5 indicate the derived values of V_m^E for [EPMpyr]$^+$[Cl]$^-$ with ethanoic or propanoic acid. The V_m^E are negative for both binary systems for the entire composition range at all investigated temperatures. Ionic liquids

DOI: 10.1021/acssuschemeng.6b01262
ACS Sustainable Chem. Eng. 2016, 4, 4951−4964

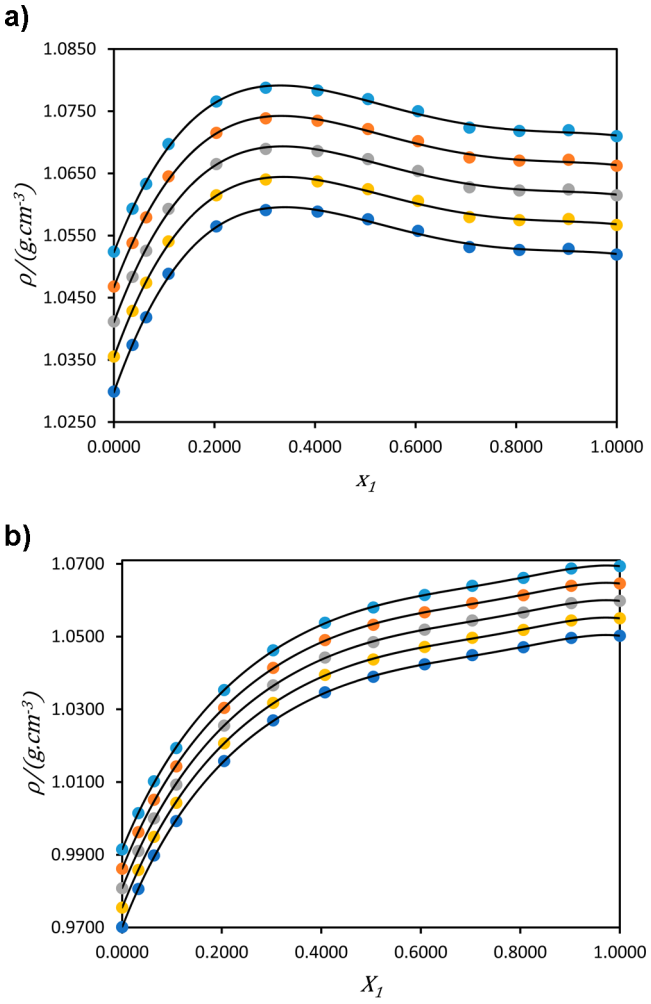

Figure 3. Density (ρ) for the mixture of (a) {[EPMpyr]$^+$[Cl]$^-$ (1) + ethanoic (2)} and (b) {[EPMpyr]$^+$[Cl]$^-$ (1) + propanoic (2)} as a function of the composition expressed in the mole fraction of {[EPMpyr]$^+$[Cl]$^-$ at T = 293.15 K (light blue circle), T = 298.15 K (orange circle), T = 303.15 K (gray circle), T = 308.15 K (yellow circle), and T = 313.15 K (dark blue circle).

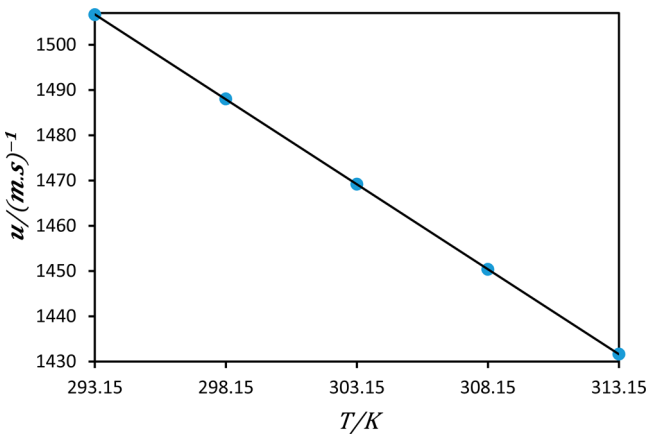

Figure 4. Speed of sound velocity of {[EPMpyr]$^+$[Cl]$^-$ at temperatures from 293.15 to 313.15) K.

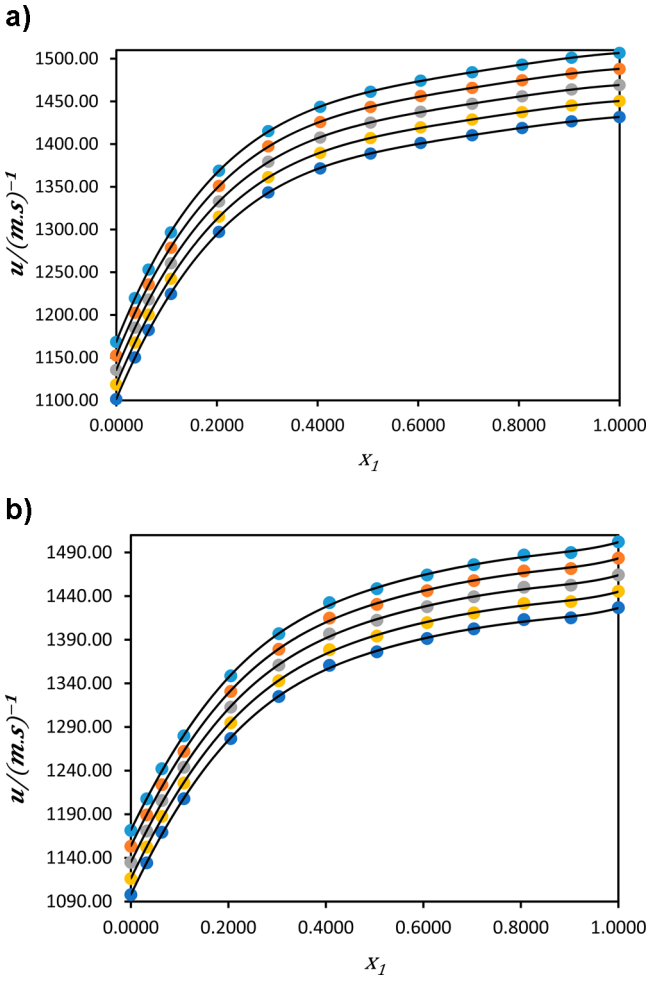

Figure 5. Speed of sound (u) for the mixture of (a) {[EPMpyr]$^+$[Cl]$^-$ (1) + ethanoic (2)} and (b) {[EPMpyr]$^+$[Cl]$^-$ (1) + propanoic acid (2)} as a function of the composition expressed in the mole fraction of {[EPMpyr]$^+$[Cl]$^-$ at T = 293.15 K (light blue circle), T = 298.15 K (orange circle), T = 303.15 K (gray circle), T = 308.15 K (yellow circle), and T = 313.15 K (dark blue circle).

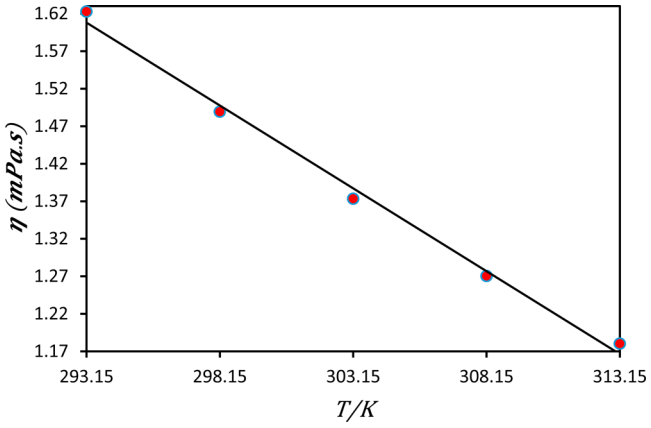

Figure 6. Viscosity (η) of [EPMpyr]$^+$[Cl]$^-$ at temperatures from 293.15 to 313.15 K.

are peculiar solvents, which interact with acids such as ethanoic or propanoic acid via ionic interactions, inter- and intramolecular hydrogen bonding, and dipolar interactions.[67] The higher negative values of V_m^E for both binary systems confirms efficient packing or competing effects that occur in the binary system of IL with acid due to the strong interaction between [EPMpyr]$^+$[Cl]$^-$ and ethanoic or propanoic acids[68] or the

DOI: 10.1021/acssuschemeng.6b01262
ACS Sustainable Chem. Eng. 2016, 4, 4951−4964

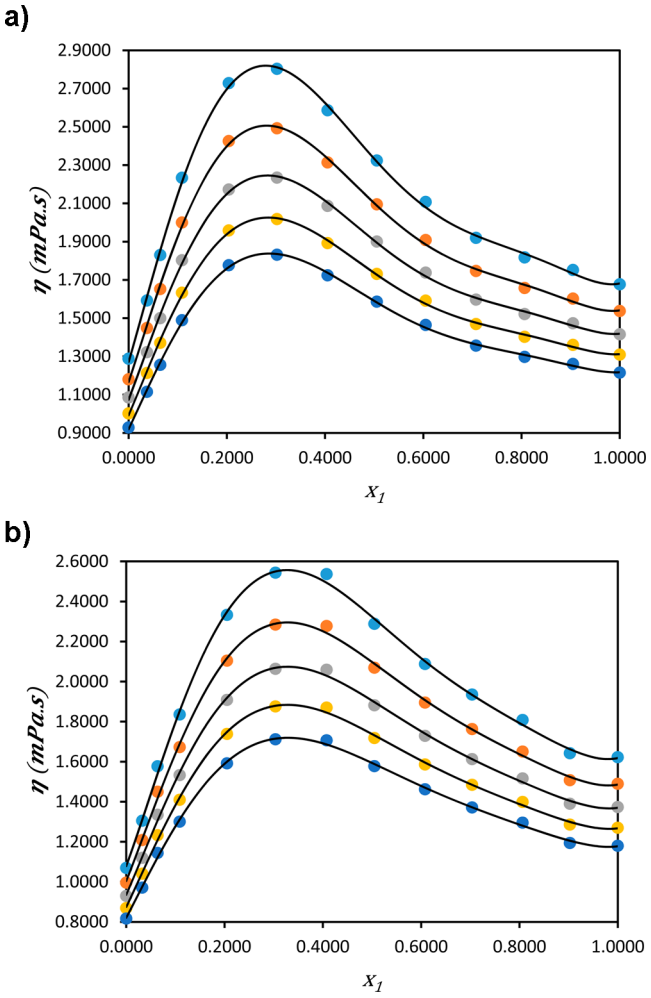

Figure 7. Viscosity (η) for the mixture of (a) {[EPMpyr]$^+$[Cl]$^-$ (1) + ethanoic acid (2)} and (b) {[EPMpyr]$^+$[Cl]$^-$ (1) + propanoic acid (2)} as a function of the composition expressed in the mole fraction of {[EPMpyr]$^+$[Cl]$^-$ at T = 293.15 K (light blue circle), T = 298.15 K (orange circle), T = 303.15 K (gray circle), T = 308.15 K (yellow circle), and T = 313.15 K (dark blue circle).

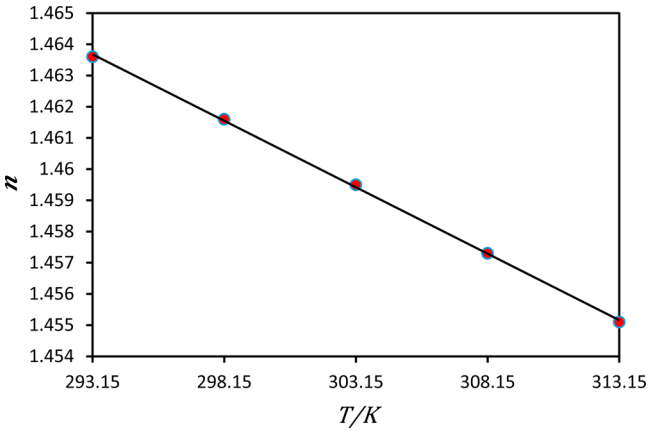

Figure 8. Refractive index (n) of [EPMpyr]$^+$[Cl]$^-$ at temperatures from 293.15 to 313.15 K.

negative excess molar volumes due to the contribution (ion + dipole) interaction of IL [EPMpyr]$^+$[Cl]$^-$ with ethanoic or propanoic acid, and in addition, the interaction interstices of [EPMpyr]$^+$[Cl]$^-$ give some space for ethanoic or propanoic

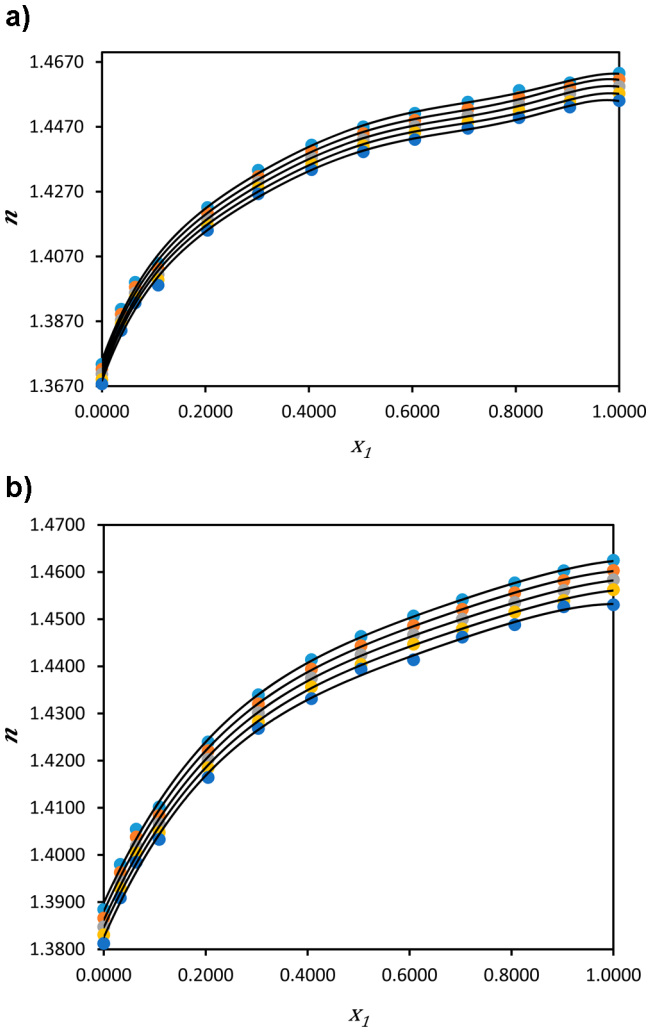

Figure 9. Refractive index (n) for the mixture of (a) {[EPMpyr]$^+$[Cl]$^-$ (1) + ethanoic acid (2)} and (b) {[EPMpyr]$^+$[Cl]$^-$ (1) + propanoic acid (2)} as a function of the composition expressed in the mole fraction of {[EPMpyr]$^+$[Cl]$^-$ at T = 293.15 K (light blue circle), T = 298.15 K (orange circle), T = 303.15 K (gray circle), T = 308.15 K (yellow circle), and T = 313.15 K (dark blue circle).

acid to fulfill the structural alignment.[69] The V_m^E minima values occur at x_1 = 0.3022 and 0.4076 for the IL + ethanoic or propanoic acid binary mixture, respectively, and V_m^E is negative over the entire mole fraction range of compositions at all investigated temperature.

The negative values of V_m^E also disclose the unlike molecular interactions, formation of hydrogen bond, and charge transfer complexes. The values of V_m^E the minima decrease with an increase in the temperature of the binary systems. Moreover, the minima goes toward the lower mole fraction of IL [EPMpyr]$^+$[Cl]$^-$ for the ethanoic acid and propanic acid binary systems due to the asymmetric curves of binary systems. Actually, the occurrences of the asymmetric nature of excess molar volume curves, because of the components present in the binary mixtures, have a large molar volume difference. Furthermore, the present investigation gives the negative V_m^E curves at higher mole fraction of IL [EPMpyr]$^+$[Cl]$^-$ and may be ascribed because of the superior fitting effect in the molecules of carboxylic acid in the ionic liquid interstices. Related work of binary mixtures IL with ethanoic or propanoic acid was also reported.[53]

DOI: 10.1021/acssuschemeng.6b01262
ACS Sustainable Chem. Eng. 2016, 4, 4951−4964

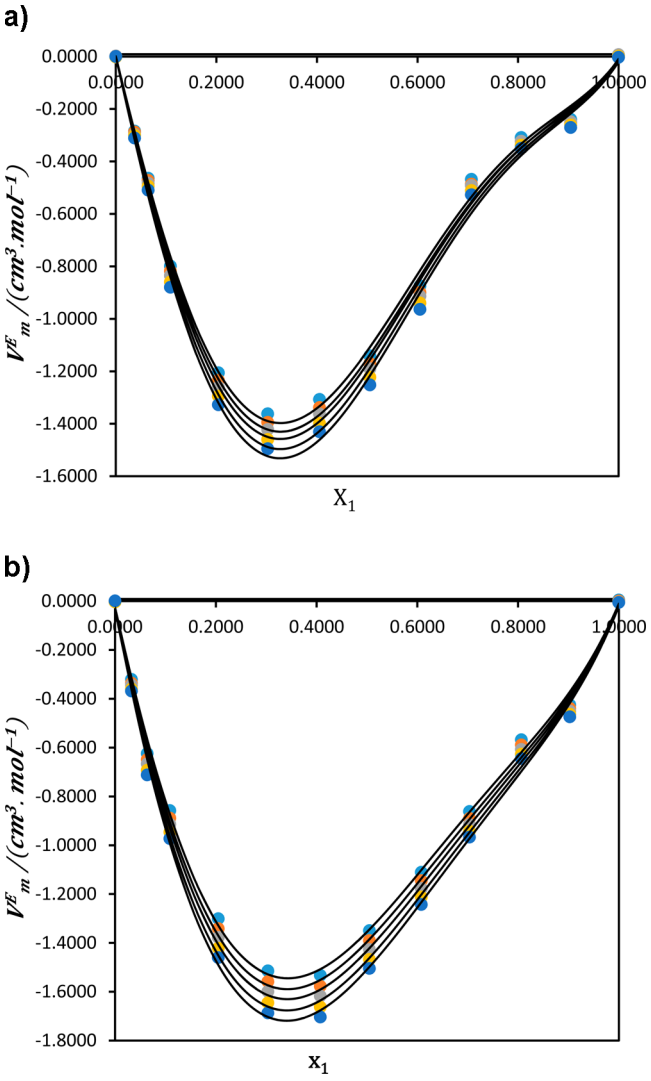

Figure 10. Excess molar volumes (V^E_m) for the mixture of (a) {[EPMpyr]$^+$[Cl]$^-$ (1) + ethanoic acid (2)} and (b) {[EPMpyr]$^+$[Cl]$^-$ (1) + propanoic acid (2)} as a function of the composition expressed in the mole fraction of {[EPMpyr]$^+$[Cl]$^-$ at T = 293.15 K (light blue circle), T = 298.15 K (orange circle), T = 303.15 K (gray circle), T = 308.15 K (yellow circle), and T = 313.15 K (dark blue circle).

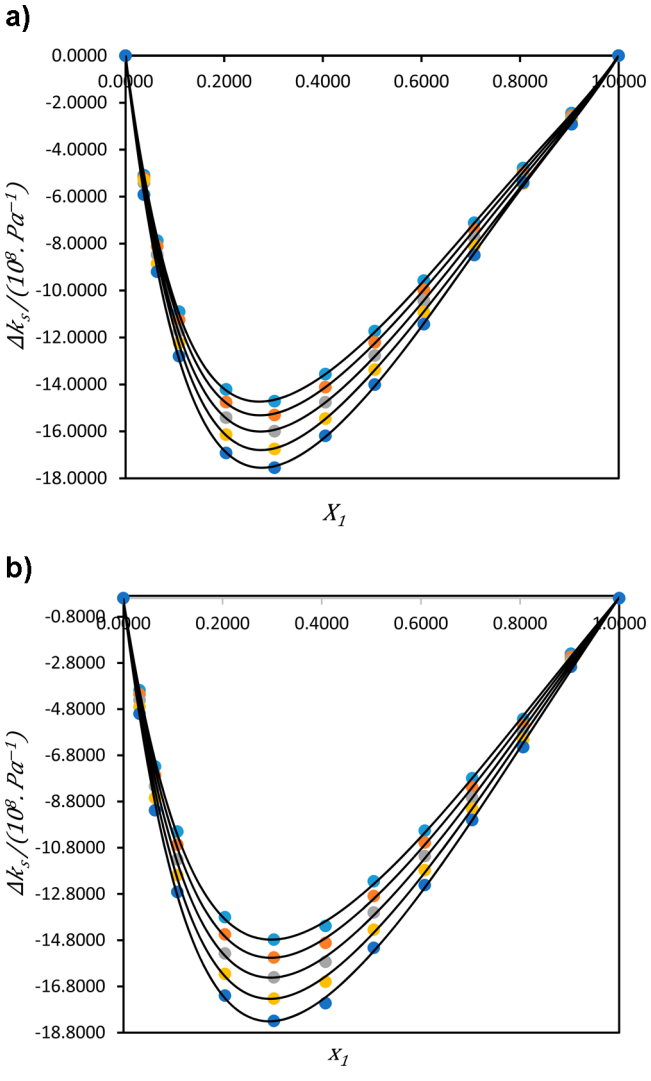

Figure 11. Intermolecular free length (L_f) for the mixture of (a) {[EPMpyr]$^+$[Cl]$^-$ (1) + ethanoic acid (2)} and (b) {[EPMpyr]$^+$[Cl]$^-$ (1) + propanoic acid (2)} as a function of the composition expressed in the mole fraction of {[EPMpyr]$^+$[Cl]$^-$ at T = 293.15 K (light blue circle), T = 298.15 K (orange circle), T = 303.15 K (gray circle), T = 308.15 K (yellow circle), and T = 313.15 K (dark blue circle).

Isentropic Compressibility and Deviation in Isentropic Compressibility. The Newton−Laplace eq 2 was used to calculate the isentropic compressibility's (k_s) as below:

$$k_s = \rho^{-1}u^{-2} \tag{2}$$

$$\Delta k_s = k_s - \sum_i^2 x_i k_{s,i} \tag{3}$$

where k_s represents the isentropic compressibility and i and x_i denote the mole fractions of the pure component and binary liquid mixtures, respectively.

Tables 3 and 5 show the calculated results of isentropic compressibility (k_s) and deviation in isentropic compressibility (Δk_s) for the binary system of {[EPMpyr]$^+$[Cl]$^-$ (1) + ethanoic or propanoic acid (2)} over the entire composition range for both binary mixtures at investigated temperatures. From the above tables, it is also evident that increases in k_s values with increasing temperature over the entire composition range for both binary mixtures are due to an increase in the thermal agitation of solution making the solution more compressible.[70] The free space in binary mixtures was decreased by the interaction among the mixtures, and this is most probably why the deviation in isentropic compressibility become more negative.[71] Figure 11 indicates the deviation in isentropic compressibility (Δk_s) of the binary system for [EPMpyr]$^+$[Cl]$^-$ with ethanoic or propanoic acid are negative over the whole composition range of IL for all investigated temperatures. The mole fractions x_1 = 0.3022 and 0.3036 gives the minima values of Δk_s as −17.5520 (10^8 Pa^{-1}) and −18.2937 (10^8 Pa^{-1}), which occurs correspondingly for both ethanoic and propanoic acid binary systems. These values of Δk_s suggest that the unlike molecules approach closely, and strong interactions are formed among the ethanoic or propanoic acids with [EPMpyr]$^+$[Cl]$^-$ mixtures that contribute to a decrease in compressibility.

As shown in Figure 11 the values of Δk_s decrease with an increase in temperature for both binary systems for all compositions of [EPMpyr]$^+$[Cl]$^-$. The Δk_s values slightly differ for

DOI: 10.1021/acssuschemeng.6b01262
ACS Sustainable Chem. Eng. 2016, 4, 4951−4964

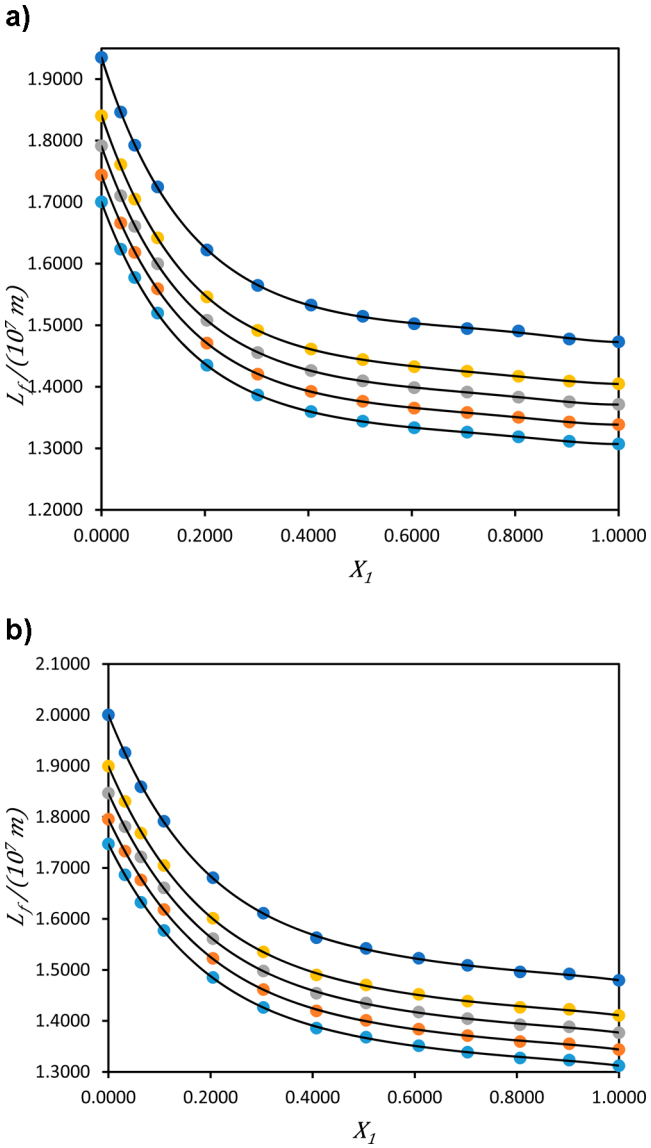

Figure 12. Deviation of isentropic compressibility ($\Delta\kappa_S$) for the mixture of (a) {[EPMpyr]$^+$[Cl]$^-$ (1) + ethanoic acid (2)} and (b) {[EPMpyr]$^+$[Cl]$^-$ (1) + propanoic acid (2)} as a function of the composition expressed in the mole fraction of {[EPMpyr]$^+$[Cl]$^-$ at T = 293.15 K (light blue circle), T = 298.15 K (orange circle), T = 303.15 K (gray circle), T = 308.15 K (yellow circle), and T = 313.15 K (dark blue circle).

the two binary systems; {[EPMpyr]$^+$[Cl]$^-$ (1) + propanoic acid (2)} is more compressible than {[EPMpyr]$^+$[Cl]$^-$ (1) + ethanoic acid (2)} due to the presence of an additional alkyl and epoxy group. These groups strongly interacted with a similar structure of propionic acid. The theoretical interactions in between the molecules are shown in Figure 13, and this may help to better understand the nature of the interaction. There is a slight difference in the term of interactions between the two acids. The unlike molecules are closer together in the binary mixtures due to the strong interaction among the components of mixtures, and this is why the compressibility has been decreasing.[72] The order of compressibility increases for the binary mixtures as follows {[EPMpyr]$^+$[Cl]$^-$ (1) + ethanoic acid (2)} < {[EPMpyr]$^+$[Cl]$^-$ (1) + propanoic acid (2)}.

The important points which are established from the above thermo-physical properties, interactions, and structural effects are follows. The resulting data show that the negative V_m^E and Δk_s values due to the chemical effects include the specific interactions such as ion dipole interactions, formation of H-bonds, strong dipole−dipole interactions, and donor−acceptor complexes between solute and solvent molecules. The structural effects play an important role in the binary mixtures because the unlike molecules interact closer together. The sizes of the molecules are different, but the skeletal fitting for component molecules into cavities of others results in negative V_m^E and Δk_s values.

Intermolecular Free Length. Jacobson's empirical relation and isentropic compressibility's were used to calculate the thermo-physical property of the intermolecular free length (L_f) from Equation 4 as follows:

$$L_f = k_j(k_s)^{1/2} \tag{4}$$

where k_j is the temperature-dependent Jacobson's constant, and its value is (93.875 + 0.375 T)10^{-8}.

Tables 3 and 5 show the resulting data of intermolecular free length (L_f) for {[EPMpyr]$^+$[Cl]$^-$ (1) + ethanoic or propanoic acid (2)} binary mixtures across the entire mole fraction of the liquid mixtures at investigated temperatures seen in the L_f versus x_1 of IL plot in Figure 12. The properties of fluids consist of attractive and repulsive forces and were investigated by using the intermolecular free length. It helps to determine the distance among the centers between the two molecules in the liquid mixtures, which is called intermolecular forces, that is the great significance of the intermolecular free length. The values of forces are numerically equal but in opposite directions under given external conditions. The center of attraction of the molecules plays a vital role in the attractive forces, and it depends on the distance among the molecules, while the distance between the surfaces of the molecules describes clearly the repulsive forces and is dependent on them.

The important properties of the distance among the centers of attraction is enormously hard to define because the centers cannot coincide with the structural centers of the molecules in the liquid. Additionally, the sound velocity variations in liquid mixtures play an important role in determining the intermolecular free length. Figure 12 and Tables 3 and 5 indicate that the intermolecular free length and speed of sound are related in an inverse manner. The large distance among the surfaces of the two molecules is clearly identified by the increasing intermolecular free length, as well as a decrease in the speed of sound. This is a useful method for investigating the nature of molecular interactions between the components in the liquid mixtures.

FTIR Studies for Liquid Mixtures. Figure 14 shows the FTIR spectrum of the IL and binary mixture of IL + ethanoic or propanoic acids. These spectrum explain the interaction of ILs with acids. The FTIR characteristic vibrations for ILs at 3443 cm^{-1} is for the ammonium group. The vibration peaks at 2931 and 2881 cm^{-1} stretching are for the C−H bond, and the peak at 1508 cm^{-1} is for the bending vibration for C−H. The vibration bands of C−N and C−O obtained peaks at 1404 and 1303 cm^{-1}, and chlorine stretching appeared at 666 cm^{-1}. The FTIR spectrum of binary mixture {[EPMpyr]$^+$[Cl]$^-$ (1) + ethanoic acid (2)} represents the violet color in Figure 13. The characteristic vibrations at 3453 and 3405 cm^{-1} denotes the −OH and ammonium group, respectively. The bands at 2954 and 2879 cm^{-1} indicate the stretching vibrations for C−H bonding, and the band at 1508 cm^{-1} is for C−H bending

DOI: 10.1021/acssuschemeng.6b01262
ACS Sustainable Chem. Eng. 2016, 4, 4951−4964

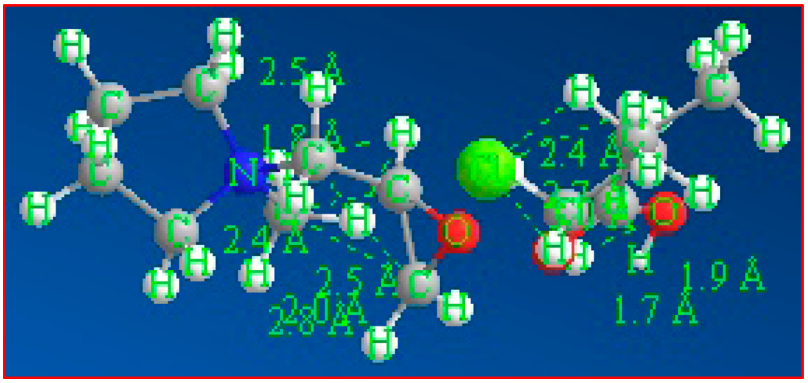

Figure 13. Chemical structure and theoretical interaction of ionic liquid with propanoic acid.

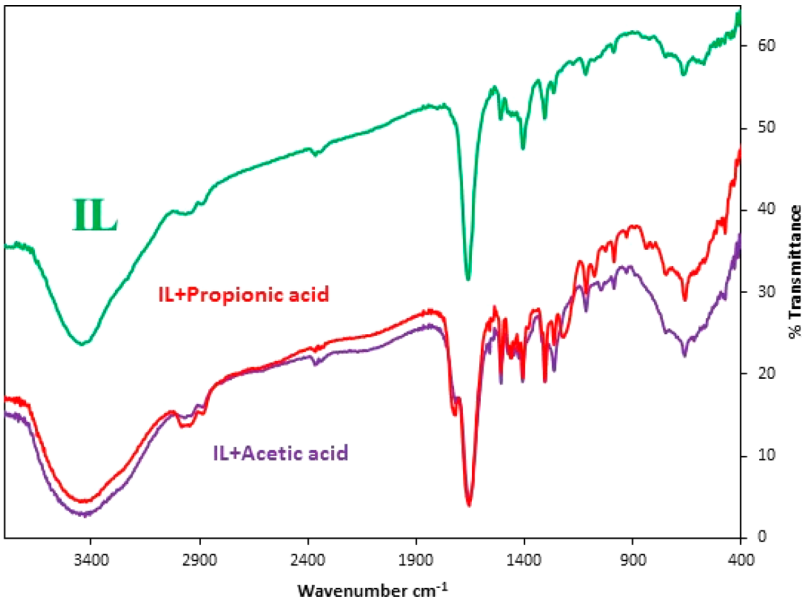

Figure 14. FTIR spectra of ionic liquid (green), ionic liquid with acetic acid (blue), and ionic liquid with propanoic acid (red).

vibration. Peaks at 1719 and 1655 cm^{-1} represent the C═O group of ethanoic acid and IL, respectively. Thepeaks at 1409, 1472, and 1447 cm^{-1} tell us about the C−N vibrations. The C−O bond gives the peak at 1306 cm^{-1}, and chloride appeared at 661 cm^{-1}. FTIR for binary mixtures of {[EPMpyr]$^+$[Cl]$^-$ (1) + propanoic acid (2)} shows the red color spectrum in Figure 13. Characteristic vibrations at 3453 cm^{-1} are for the −OH and ammonium group. The C−H stretching vibrations are at 2966 and 2903 cm^{-1}, and the bending vibration of C−H is at 1508 cm^{-1}. Carbonyl groups appeared at 1724 and 1657 cm^{-1}. Stretching vibrations at 1408 and1464 cm^{-1} represent the C−N vibrations, and 1432 cm^{-1} represents the C−N bending vibrations. The C−O vibration is at 1306 cm^{-1}, and the chloride peak is shown at 660 cm^{-1}. FTIR indicates that the addition of acid to IL does influence (1) C−H and C−N vibrations of the cation in ILs, (2) C−O vibrations of ILs and acid, and (3) C═O vibrations of ILs and acid. Thus, the FTIR spectra analysis gave an explanation about the interaction of ion + dipole and the interaction between ILs and acids in a binary mixture of {[EPMpyr]$^+$[Cl]$^-$ (1) + ethanoic or propanoic acid (2)}.

Correlation of Derived Properties. Tables 3 and 5 show the calculated thermo-physical properties of excess/deviation of the {[EPMpyr]$^+$[Cl]$^-$ (1) + ethanoic or propanoic acid (2)}. The Redlich−Kister equation[67] (eq 5) given below was used to fit those properties such as V_m^E, Δk_s, η, and L_f:

$$X = x_1 x_2 \sum_{i=1}^{k} A_j (1 - 2x_1)^{i-1} \tag{5}$$

where X is an excess molar volume (V_m^E), deviation in isentropic compressibility (Δk_s), and intermolecular free length (L_f), and viscosity (η). The least-squares method has been used to determine the corresponding fitting parameters A_j values. Table 6 shows the summarized results as well as including corresponding standard deviations. Here, σ as given by eq 6.

$$\sigma(X) = \sum_{i=1}^{n} \left[\frac{X_{expt} - X_{calc}}{(N - K)} \right]^{1/2} \tag{6}$$

where N denotes the number of experimental points and K represents the number of coefficients in the Redlich−Kister equation. The plots of the Redlich−Kister model together with the experimental V_m^E, Δk_s, L_f, and η data are displayed in Table 6. For both binary systems, the standard deviations indicate very low values for both excess molar volumes and deviations in isentropic compressibility at all investigated temperatures.

DOI: 10.1021/acssuschemeng.6b01262
ACS Sustainable Chem. Eng. 2016, 4, 4951−4964

Table 6. Coefficients (A_i) and Standard Deviations (σ) Obtained for Binary Systems {[EPMpyr]$^+$[Cl]$^-$ (1) + Ethanoic or Propanoic Acid (2)} at Different Temperatures for the Redlich−Kister Equation

	T (K)	A_0	A_1	A_2	A_3	σ
		{[EPMpyr]$^+$[Cl]$^-$ (1) + ethanoic acid (2)}				
V_m^E(cm^{3}mol^{-1})	293.15	−4.489	−5.432	−0.848	2.87	0.032
	298.15	−4.602	−5.534	−0.905	2.99	0.033
	303.15	−4.685	−5.656	−0.898	2.968	0.033
	308.15	−4.812	−5.787	−0.966	3.084	0.034
	313.15	−4.928	−5.895	−1.04	3.126	0.035
L_f (10^7 m)	293.15	4.542	−2.367	16.237	11.202	0.6
	298.15	4.65	−2.432	16.653	11.523	0.6
	303.15	4.761	−2.499	17.084	11.856	0.6
	308.15	4.875	−2.576	17.537	12.231	0.6
	313.15	5.111	−2.712	18.431	12.856	0.6
Δk_s ($10^8 \times$ Pa^{-1})	293.15	−46.857	−39.438	−38.068	−25.646	0.1
	298.15	−48.817	−41.246	−38.902	−25.169	0.1
	303.15	−51.067	−43.189	−40.374	−25.882	0.1
	308.15	−53.551	−45.88	−41.472	−24.594	0.1
	313.15	−56.079	−48.081	−42.646	−27.875	0.1
η (mPa s)	293.15	8.744	4.332	18.947	1.643	0.5
	298.15	8.967	0.053	14.332	8.922	0.5
	303.15	7.093	2.938	15.661	1.816	0.4
	308.15	6.446	2.446	14.363	1.821	0.4
	313.15	5.891	2.045	13.219	1.804	0.4
		{[EPMpyr]$^+$[Cl]$^-$ (1) + propanonic acid (2)}				
V_m^E (cm^3 mol^{-1})	293.15	−5.41	−4.131	−1.935	1.618	0.029
	298.15	−5.569	−4.208	−2.057	1.542	0.031
	303.15	−5.716	−4.299	−2.131	1.556	0.031
	308.15	−5.875	−4.392	−2.262	1.47	0.032
	313.15	−6.024	−4.493	−2.338	1.466	0.032
L_f(10^7 m)	293.15	4.609	−2.432	16.704	12.158	0.6
	298.15	4.719	−2.502	17.141	12.523	0.6
	303.15	4.831	−2.574	17.594	12.898	0.6
	308.15	4.947	−2.648	18.059	13.286	0.6
	313.15	5.186	−2.789	18.978	14.012	0.7
Δk_s ($10^8 \times$ Pa^{-1})	293.15	−49.618	−37.956	−28.478	−18.515	0.1
	298.15	−52.186	−40.099	−30.134	−19.371	0.1
	303.15	−55.03	−42.202	−32.16	−21.135	0.1
	308.15	−58.019	−44.479	−34.452	−23.225	0.1
	313.15	−61.185	−46.921	−36.907	−25.305	0.1
η (mPa s)	293.15	8.722	2.977	15.133	0.545	0.5
	298.15	7.849	2.422	14.007	0.983	0.4
	303.15	7.108	1.987	13.004	1.245	0.4
	308.15	6.47	1.625	12.105	1.439	0.4
	313.15	5.92	1.319	11.294	1.605	0.3

CONCLUSIONS

In this study, a synthesized ionic liquid was used to make a binary mixture of {[EPMpyr]$^+$[Cl]$^-$ (1) + ethanoic or propanoic acid (2)}, and physicochemical properties such as density, viscosity, speed of sound, and refractive index across the entire mole fraction ranges from 0.03 to 1.0 at temperatures from T = 293.15 to 313.15 K in steps of 5 K under atmospheric pressure were determined. From the resulting data, derived properties of excess molar volume, isentropic compressibility, deviation in isentropic compressibility, and intermolecular free length have been calculated and discussed. The negative values of excess molar volume and deviation in isentropic compressibility indicates the presence of strong interactions between unlike molecules. Comparing propanoic acid and ethanoic acid, ethanoic acid interacted weakly because of the extra methyl group present in the propanoic acid and the epoxy propyl group strongly interacted with propanoic acid. The propanoic acid binary system has more negative values in V_m^E and Δk_s as well as ion−dipole interactions between propanoic acid and [EPMPyr]$^+$[Cl]$^-$. L_f has been calculated for both binary systems from experimental isentropic compressibility data and is discussed as well. The Redlich−Kister polynomial equation was used to correlate the excess thermodynamic parameters obtained from the results. Good correlation was obtained in all cases.

AUTHOR INFORMATION

Corresponding Author

*E-mail: redhigg@dut.ac.za. Tel.: +27 (31) 373 2936. Fax: +27 0866741159.

Notes

The authors declare no competing financial interest.

DOI: 10.1021/acssuschemeng.6b01262
ACS Sustainable Chem. Eng. 2016, 4, 4951−4964

■ ACKNOWLEDGMENTS

Vasantha Kumar Arumugam is grateful to the Durban University of Technology, National Research Foundation (NRF) South Africa, for the Innovation Doctoral Grant (Grant UID: 101117).

■ REFERENCES

(1) Flieger, J.; Grushka, E. B.; Czajkowska-Zelazko, A. Ionic Liquids as Solvents in Separation Processes. *Austin J. Anal. Pharm. Chem.* **2014**, *1*, 1−8.
(2) Wasserscheid, P.; Welton, T. *Ionic Liquids in Synthesis*, 2nd ed.; Wiley-VCH: Weinheim, 2007.
(3) Arco, S. D.; Laxamana, R. T.; Giron, O. D.; Obliosca, J. M. Synthesis of [RMIM] Acetate Halogen-Free Ionic Liquids for Use as Greener Solvents in Diels-Alder Reaction. *Philipp. J. Sci.* **2009**, *138*, 133−139.
(4) Welton, T. Room-Temperature Ionic Liquids. Solvents for Synthesis and Catalysis. *Chem. Rev.* **1999**, *99*, 2071−2084.
(5) Armand, M.; Endres, F.; MacFarlane, D. R.; Ohno, H.; Scrosati, B. Ionic iquid Materials for the Electrochemical Challenges of the Future. *Nat. Mater.* **2009**, *8*, 621−629.
(6) Wasserscheid, P.; Keim, W. Ionic Liquids-New "Solutions" for Transition Metal Catalysis. *Angew. Chem., Int. Ed.* **2000**, *39*, 3772−3789.
(7) Silvester, D. S. Recent advances in the use of ionic liquids for electrochemical sensing. *Analyst* **2011**, *136*, 4871−4882.
(8) Bonhote, P.; Dias, A. P.; Papageorgiou, N.; Kalyanasundaram, K.; Grätzel, M. Hydrophobic. Highly Conductive Ambient Temperature Molten Salts. *Inorg. Chem.* **1996**, *35*, 1168−1178.
(9) MacFarlane, D. R.; Meakin, P.; Sun, J.; Amini, N.; Forsyth, M. Pyrrolidinium Imides: A New Family of Molten Salts and Conductive Plastic Crystal Phases. *J. Phys. Chem. B* **1999**, *103*, 4164−4170.
(10) Barrosse-Antle, L. E.; Bond, A. M.; Compton, R. G.; O'Mahony, A. M.; Rogers, E. I.; Silvester, D. S. Voltammetry in Room Temperature Ionic Liquids: Comparisons and Contrasts with Conventional Electrochemical Solvents. *Chem. - Asian J.* **2010**, *5*, 202−230.
(11) Cao, Y.; Wu, J.; Zhang, J.; Li, H.; Zhang, Y.; He, J. Room temperature ionic liquids (RTILs): A new and versatile platform for cellulose processing and derivatization. *Chem. Eng. J.* **2009**, *147*, 13−21.
(12) Lazzús, J. A. Hybrid method to predict melting points of organic compounds using group contribution + neural network + particle swarm algorithm. *Ind. Eng. Chem. Res.* **2009**, *48*, 8760−8766.
(13) Lazzus, J. A. A group contribution method to predict the melting point of ionic liquids. *Fluid Phase Equilib.* **2012**, *313*, 1−6.
(14) Kavitha, T.; Vasantha, T.; Venkatesu, P.; Devi, R. S. R.; Hofman, T. Thermophysical properties for the mixed solvents of N-methyl-2-pyrrolidone with some of the imidazolium-based ionic liquids. *J. Mol. Liq.* **2014**, *198*, 11−20.
(15) Appetecchi, G. B.; Montanino, M.; Zane, D.; Carewska, M.; Alessandrini, F.; Passerini, S. Effect of the alkyl group on the synthesis and the electrochemical properties of N-alkyl-N-methyl-pyrrolidinium bis(trifluoromethanesulfonyl)imide ionic liquids. *Electrochim. Acta* **2009**, *54*, 1325−1332.
(16) Appetecchi, G. B.; Montanino, M.; Carewska, M.; Moreno, M.; Alessandrini, F.; Passerini, S. Chemical-physical properties of bis (perfluoroalkylsulfonyl) imide-based ionic liquids. *Electrochim. Acta* **2011**, *56*, 1300−1307.
(17) Gardas, R. L.; Freire, M. G.; Carvalho, P. J.; Marrucho, I. M.; Fonseca, I. M. A.; Ferreira, A. G. M.; Coutinho, J. A. P. PρT Measurements of Imidazolium-Based Ionic Liquids. *J. Chem. Eng. Data* **2007**, *52*, 1881−1888.
(18) Earle, M. J.; Esperanca, J. M. S. S.; Gilea, M. A.; Canongia Lopes, J. N.; Rebelo, L. P. N.; Magee, J. W.; Seddon, K. R.; Widegren, J. A. The distillation and volatility of ionic liquids. *Nature* **2006**, *439*, 831−834.
(19) Maton, C.; De Vos, N.; Stevens, C. V. Ionic liquid thermal stabilities: decomposition mechanisms and analysis tools. *Chem. Soc. Rev.* **2013**, *42*, 5963−5977.
(20) Smiglak, M.; Reichert, W. M.; Holbrey, J. D.; Wilkes, J. S.; Sun, L.; Thrasher, J. S.; Kirichenko, K.; Singh, S.; Katritzky, A. R.; Rogers, R. D. Combustible ionic liquids by design: is laboratory safety another ionic liquid myth? *Chem. Commun.* **2006**, *24*, 2554−2556.
(21) King, C. J. Amine-based systems for carboxylic acid recovery: tertiary amines and the proper choice of diluent allow extraction and recovery from water. *Chemtech.* **1992**, *5*, 285−291.
(22) Clifford, S. L.; Ramjugernath, D.; Raal, J. D. Subatmospheric vapor pressure curves for propionic acid, butyric acid, isobutyric acid, valeric acid, isovaleric acid, hexanoic acid and heptanoic acid. *J. Chem. Eng. Data* **2004**, *49*, 1189−1192.
(23) Kumar, S.; Babu, B. V. http://discovery.bits-pilani.ac.in/~bvbabu/Susheel_Babu_JFET_Carboxylic%20acids_Review.pdf.
(24) Hong, Y. K.; Hong, W. H.; Han, D. H. Application of reactive extraction to recovery of carboxylic acids, Biotechnol. *Biotechnol. Bioprocess Eng.* **2001**, *6*, 386−394.
(25) Lotero, E.; Liu, Y.; Lopez, D. E.; Suwannakarn, K.; Bruce, D. A.; Goodwin, J. G. Synthesis of biodiesel via acid catalysis. *Ind. Eng. Chem. Res.* **2005**, *44*, 5353−5363.
(26) Wasserscheid, P.; Welton, T., Eds.; *Ionic Liquids in Synthesis*; Wiley-VCH Verlag: Weinheim, 2003; pp41−126.
(27) Zhou, Y.; Antonietti, M. Synthesis of Very Small TiO_2 Nanocrystals in a Room-Temperature Ionic Liquid and Their Self-Assembly toward Mesoporous Spherical Aggregates. *J. Am. Chem. Soc.* **2003**, *125*, 14960−14961.
(28) Liu, Y.; Wang, M. J.; Li, J.; Li, Z. Y.; He, P.; Liu, H. T.; Li, J. H. Synthesis of Very Small TiO_2 Nanocrystals in a Room-Temperature Ionic Liquid and Their Self-Assembly toward Mesoporous Spherical Aggregates. *Chem. Commun.* **2005**, 1778−1780.
(29) Katayama, Y.; Oshino, Y.; Ichihashi, N.; Tachikawa, N.; Yoshii, K.; Toshima, K. Electrochemical preparation of palladium nanoparticles in bis (trifluoromethylsulfonyl) amide ionic liquids consisting of pyrrolidinium cations with different alkyl chain lengths. *Electrochim. Acta* **2015**, *183*, 37.
(30) Theivaprakasam, S.; MacFarlane, D. R.; Mitra, S. Electrochemical studies of N-Methyl N-Propyl Pyrrolidinium bis (trifluoromethanesulfonyl) imide ionic liquid mixtures with conventional electrolytes in $LiFePO_4$/Li cells. *Electrochim. Acta* **2015**, *180*, 737−745.
(31) Kuang, D.; Wang, P.; Ito, S.; Zakeeruddin, S. M.; Gratzel, M. Stable Mesoscopic Dye-Sensitized Solar Cells Based on Tetracyanoborate Ionic Liquid Electrolyte. *J. Am. Chem. Soc.* **2006**, *128*, 7732−7733.
(32) Lee, J.; Panzer, M. J.; He, Y.; Lodge, T. P.; Frisbie, C. D. Ion Gel Gated Polymer Thin-Film Transistors. *J. Am. Chem. Soc.* **2007**, *129*, 4532−4533.
(33) Ue, M.; Takeda; Takahashi, M. T.; Takehara, M. Ionic Liquids with Low Melting Points and Their Application to Double-Layer Capacitor Electrolytes. *Electrochem. Solid-State Lett.* **2002**, *5*, A119−A121.
(34) Wei, D.; Ivaska, A. Applications of ionic liquids in electrochemical sensors. *Anal. Chim. Acta* **2008**, *607*, 126−135.
(35) Noda, A.; Susan, M. A. B. H.; Kudo, K.; Mitsushima, S.; Hayamizu, K.; Watanabe, M. Brønsted Acid-Base Ionic Liquids as Proton-Conducting Nonaqueous Electrolytes. *J. Phys. Chem. B* **2003**, *107*, 4024−4033.
(36) Scovazzo, P.; Kieft, J.; Finan, D. A.; Koval, C.; DuBois, D.; Noble, R. Gas separations using non-hexafluorophosphate $[PF6]^-$ anion supported ionic liquid membranes. *J. Membr. Sci.* **2004**, *238*, 57−63.
(37) Jork, C.; Seiler, M.; Beste, Y. A.; Arlt, W. Influence of Ionic Liquids on the Phase Behavior of Aqueous Azeotropic Systems. *J. Chem. Eng. Data* **2004**, *49*, 852−857.
(38) Wu, B.; Reddy, R. G.; Rogers, R. D. Novel ionic liquid thermal storage for solar thermal electric power systems. *Proceedings of Solar Forum.* **2001**.

DOI: 10.1021/acssuschemeng.6b01262
ACS Sustainable Chem. Eng. 2016, 4, 4951−4964

(39) Holbrey, J. D.; Seddon, K. R. The phase behavior of 1-alkyl-3-methylimidazolium tetrafluoroborates; ionic liquids and ionic liquid crystals. *J. Chem. Soc., Dalton Trans.* **1999**, *13*, 2133−2139.
(40) Wang, H.; Lu, Q.; Ye, C.; Liu, W.; Cui, Z. Friction and wear behaviors of ionic liquid of alkylimidazolium hexafluorophosphates as lubricants for steel/steel contact. *Wear* **2004**, *256*, 44−48.
(41) Keskin, S.; Kayrak-Talay, D.; Akman, U.; Hortacsu, O. A review of ionic liquids towards supercritical fluid applications. *J. Supercrit. Fluids* **2007**, *43*, 150−180.
(42) Hallett, J. P.; Welton, T. Room-temperature ionic liquids: solvents for synthesis and catalysis. *Chem. Rev.* **2011**, *111*, 3508−3576.
(43) Roosen, C.; Müller, P.; Greiner, L. Ionic liquids in biotechnology: applications and perspectives for biotransformations. *Appl. Microbiol. Biotechnol.* **2008**, *81*, 607−614.
(44) Dupont, J.; Scholten, J. D. On the structural and surface properties of transition metal nanoparticles in ionic liquids. *Chem. Soc. Rev.* **2010**, *39*, 1780−1804.
(45) MacFarlane, D. R.; Tachikawa, N.; Forsyth, M.; Pringle, J. M.; Howlett, P. C.; Elliott, G. D.; Davis, J. H.; Watanabe, M.; Simon, P.; Angell, C. A. Energy applications of ionic liquids. *Energy Environ. Sci.* **2014**, *7*, 232−250.
(46) Wang, C.; Luo, X.; Zhu, X.; Cui, G.; Jiang, D.-E.; Deng, D.; Li, H.; Dai, S. The strategies for improving carbon dioxide chemisorption by functionalized ionic liquids. *RSC Adv.* **2013**, *3*, 15518−15527.
(47) Trulove, P. C.; Mantz, R. A. Electrochemical properties of ionic liquids. In *Ionic Liquids in Synthesis*; Wasserscheid, P., Welton, T., Eds.; 2nd ed.; Wiley: Wenheim, 2008; pp 141−174.
(48) Domanska, U.; Redhi, G. G.; Marciniak, A. Activity coefficients at infinite dilution measurements for organic solutes and water in the ionic liquid 1-butyl-1-methylpyrrolidinium trifluoromethanesulfonate using GLC. *Fluid Phase Equilib.* **2009**, *278*, 97−102.
(49) Pont, A. L.; Marcilla, R.; De Meatza, I.; Grande, H.; Mecerreyes, D. Pyrrolidiniumbased polymeric ionic liquids as mechanically and electrochemically stable polymer electrolytes. *J. Power Sources* **2009**, *188*, 558−563.
(50) Grande, L.; Paillard, E.; Kim, G. T.; Monaco, S.; Passerini, S. Ionic Liquid Electrolytes for Li-Air Batteries: Lithium Metal Cycling. *Int. J. Mol. Sci.* **2014**, *15*, 8122−8137.
(51) Anouti, M.; Jones, J.; Boisset, A.; Jacquemin, J.; Caillon-Caravanier, M.; Lemordant, D. Aggregation behavior in water of new imidazolium and pyrolidinium alkycarboxylates protic ionic liquids. *J. Colloid Interface Sci.* **2009**, *340*, 104−111.
(52) Anouti, M.; Vigeant, A.; Jacquemin, J.; Brigouleix, C.; Lemordant, D. Volumetric Properties, viscosity and refractive index of the protic ionic liquid, pyrrolidinium octanoate, in molecular solvents. *J. Chem. Thermodyn.* **2010**, *42*, 834−845.
(53) Singh, S.; Bahadur, I.; Redhi, G.; Ebenso, E. E.; Ramjugernath, D. Density and speed of sound of 1-ethyl-3-methylimidazolium ethyl sulphate with acetic or propionic acid at different temperatures. *J. Mol. Liq.* **2014**, *199*, 518−523.
(54) Bhanuprakash, P.; Narasimha Rao, C.; Sivakumar, K. Evaluation of molecular interactions by volumetric and acoustic studies in binary mixtures of the ionic liquid $[EMIM]^+[MeSO4]^-$ with ethanoic and propanoic acid at different temperatures. *J. Mol. Liq.* **2016**, *219*, 79−87.
(55) Bahadur, I.; Sapei, E.; Singh, S.; Ebenso, E. E.; Redhi, G. G. Physicochemical properties of N-butyl-N-methyl-2-oxopyrrolidonium bromide and its binary mixtures with water or methanol. *ACS Sustainable Chem. Eng.* **2016**, *4* (2), 601−608.
(56) Gonzalez, B.; Domınguez, A.; Tojo, J. Dynamic Viscosities, Densities, and Speed of Sound and Derived Properties of the Binary Systems Acetic Acid with Water, Methanol, Ethanol, Ethyl Acetate and Methyl Acetate at T = (293.15, 298.15, and 303.15) K at Atmospheric Pressure. *J. Chem. Eng. Data* **2004**, *49*, 1590−1596.
(57) Levichev, S. A. Oberflächenspannung, Dichte und Exzessvolumina in binären und ternären Lösungen. *Fiziko-chimiceskie Svojstva Rastvorov.* **1964**, *J.80*, 219−226.
(58) Krestov, G. A. Volum- und Viskosität-Charakteristiken von Tetraphenylporfirin-Lösungen bei verschiedenen Temperaturen. *Viniti* **1986**, 1−17.
(59) Bahadur, I.; Deenadayalu, N.; Naidoo, P.; Ramjugernath, D. Density, speed of sound, and refractive index measurements for the binary systems (butanoic acid + propanoic acid, or 2-methyl-propanoic acid) at T = (293.15 to 313.15) K. *J. Chem. Thermodyn.* **2013**, *57*, 203−211.
(60) Bahadur, I.; Naidoo, P.; Singh, S.; Ramjugernath, D.; Deenadayalu, N. Effect of temperature on density, sound velocity, refractive index and their derived properties for the binary systems (heptanoic acid + propanoic or butanoic acids). *J. Chem. Thermodyn.* **2014**, *78*, 7−15.
(61) Schaaffs, W.; Teil, I. Die Schallgeschwindigkeit in organischen Flüssigkeiten. *Z. Phys. Chem.(Leipzig)* **1944**, *194*, 28−38.
(62) Vasanthakumar, A.; Bahadur, I.; Redhi, G. G.; Gengan, R. M.; Anand, K. Synthesis, characterization and thermophysical properties of ionic liquid N-methyl-N-(2′,3′-epoxypropyl)-2-oxopyrrolidinium chloride and its binary mixtures with water or ethanol at different temperatures. *J. Mol. Liq.* **2016**, *219*, 685−693.
(63) Vasanthakumar, A.; Bahadur, I.; Redhi, G.; Gengan, R. M. Synthesis, characterization of 2′,3′-epoxy propyl - N-methyl-2-oxopyrrolidinium salicylate ionic liquid and study of its interaction with water or methanol. *RSC Adv.* **2016**, *6*, 61566.
(64) Bahadur, I.; Deenadayalu, N.; Naidoo, P.; Ramjugernath, D. Volumetric, Acoustic and Refractive Index for the Binary System (Butyric acid + Hexanoic acid) at Different Temperatures. *J. Solution Chem.* **2014**, *43*, 787−803.
(65) Deosarkar, S. D.; Pandhare, V. V.; Kattekar, P. S. Densities and Refractive Indices of Potassium Salt Solutions in Binary [ethanol +water] Mixture of Different Compositions. *J. Eng.* **2013**, *2013*, 1−4.
(66) Roy, M. N.; Ekka, D.; Dewan, R. Physico-chemical studies of some bioactive solutes in pure ethanoic acid. *Acta Chim. Slov.* **2011**, *58*, 792−796.
(67) Deenadayalu, N.; Bhujrajh, P. Excess molar volumes and partial molar volumes for (propionitrile + an alkanol) at T = 298.15 K and p = 0.1 MPa. *J. Chem. Thermodyn.* **2006**, *38*, 278−282.
(68) Ahluwalia, R.; Wanchoo, R. K.; Sharma, S. K.; Vashisht, J. L. Density, viscosity, and surface tension of binary liquid systems: ethanoic acid, propanoic acid, and butanoic acid with nitrobenzene. *J. Solution Chem.* **1996**, *25*, 905−917.
(69) Zafarani-Moattar, M. T.; Shekaari, H. Apparent molar volume and isentropic compressibility of ionic liquid 1-butyl-3-methylimidazolium bromide in water, methanol, and ethanol at T = (298.15 to 318.15) K. J. Chem. *J. Chem. Thermodyn.* **2005**, *37*, 1029−1035.
(70) Gowrisankar, M.; Venkateswarlu, P.; Sivakumar, K.; Sivarambabu, S. Ultrasonic Studies on Molecular Interactions in Binary Mixtures of N-Methyl Aniline with Methyl Isobutylketone, + 3-Pentanone, and + Cycloalkanones at 303.15 K. *J. Solution Chem.* **2013**, *42*, 916−935.
(71) Zafarani-Moattar, M. T.; Shekaari, H. Volumetric and Speed of Sound of Ionic Liquid, 1-Butyl-3- methylimidazolium Hexafluorophosphate with Acetonitrile and Methanol at T = (298.15 to 318.15) K. *J. Chem. Eng. Data* **2005**, *50*, 1694−1699.
(72) Redlich, O.; Kister, A. T. Algebraic Representation of Thermodynamic Properties and the Classification of Solutions. *Ind. Eng. Chem.* **1948**, *40*, 345−348.

DOI: 10.1021/acssuschemeng.6b01262
ACS Sustainable Chem. Eng. 2016, 4, 4951−4964

11.2 Critical review for 4th Publication

Influence of epoxy group in 2-pyrrolidonium ionic liquid interactions and thermo-physical properties with ethanoic or propanoic acid at various temperatures.

This paper study the thermophysical properties of N-2′,3′-epoxypropyl-N-methyl-2-oxopyrrolidinium chloride $[EPMpyr]^+[Cl]^-$ IL, and its corresponding binary mixtures with either ethanoic or propanoic acid at temperatures from 288.15 to 313.15 K, intervals of 5 K at atmospheric pressure for the whole mole fraction ranges of both binary systems. Specifically, investigation for the influence of the epoxypropyl group substitution in the cation of this IL reveals a significant contribution in both binary mixtures. Density(ρ), sound velocity (u), viscosity (η) and refractive index (n) for the IL binary mixtures have been measured experimentally. The experimental data of these properties were evaluate and useful information was obtained on how the chemical structures are related to these thermophysical properties, and these in turn provide valuable insights on how to synthesize the targeted ILs. Moreover, these physicochemical properties were decreased with increasing temperature or increases with increasing mole fraction of the IL. In addition, this thermophysical property data of ILs could be useful for industrial applied research and developments, as many industries and researchers are trying to use eco-friendly solvents to replace traditional volatile solvents. The resulting data were plotted against entire mole fraction ranges for both binary systems. The thermodynamic properties of liquid mixtures play an important role in understanding the specific interaction, geometrical effects, molecular arrangements and molecular modelling in the binary mixtures. The molecular interactions between the unlike molecules were also comprehended using n data.

The thermodynamic properties, for instance V_m^E, k_s, $\Delta k_s$and $L_f$were computed from experimental ρ and u data. Furthermore, the V_m^E data decreases with increasing temperature, but increases with increasing mole fraction of the IL. The negative V_m^E represents the strong competing or filling effects between components of molecules in this liquid mixture. This also implies that the IL is completely miscible with acids due to its high dielectric constant values and strong interaction occurs between the unlike molecules across the entire range of composition in the liquid mixtures of both binary systems at the inspected temperatures. In addition, the excess properties gave more detailed information about ionic interactions, inter and intramolecular H-bonding and dipole-dipole interactions.

The strong interaction of ion-dipole in $[EPMpyr]^+[Cl]^-$ with ethanoic or propanoic acid contribute significantly to the negative V_m^E. The interaction interstices and the functional group in the IL structure gave a free space for ethanoic or propanoic acid to fill through structural alignment. The minima values for $V_{m,min}^E$ were obtained at x_1 = 0.3022 and x_1=0.4076 for the (IL + ethanoic or propanoic acid) binary mixtures, respectively. In addition, the negative values of V_m^E also reveals the unlike molecular interactions and charge transfer complexes.

The k_s increases with increasing temperature over the whole range of mole fraction for both binary systems, which means the solutions become more compressible while increasing the thermal agitation of the solution. The increased interactions among the molecules reduces the free space in the solution of binary liquid mixtures which accounts for a greater negative Δk_s. The Δk_s gave a higher negative value for the entire mole fraction ranges of both binary systems at all examined temperatures. The minimum values of Δk_s occurs at mole fraction of x_1 = 0.3022 and 0.3036 and gives Δk_s values of $\Delta k_{s,min}$ = -17.5520 $(10^8 Pa^{-1})$ and $\Delta k_{s,min}$ = -18.2937 $(10^8 Pa^{-1})$ respectively.

In both binary systems, Δk_s values of the binary mixture {$[Epmpyr]^+[Cl]^-$ (x_1) + propanoic acid (x_2)} is more compressible than {$[Epmpyr]^+[Cl]^-$ (x_1) + ethanoic acid (x_2)} due to the epoxypropyl group interacting more strongly with propanoic acid than ethanoic acid, resulting in a slight difference in the molecules of the Δk_s value for ethanoic acid mixture. Thermodynamic properties such as V_m^E and Δk_s gives negative values due to significant effects and exact interactions such as H-bonds, strong dipole-dipole interactions, ion-dipole interactions and donor-acceptor complexes among the solute and solvent molecules. The higher V_m^E values observed for the {$[Epmpyr]^+[Cl]^-$ (x_1) + propanoic acid (x_2)} system compared with the {$[Epmpyr]^+[Cl]^-$ (x_1) + ethanoic acid (x_2)} system is due to the higher electron donating capacity of propionic acid relative to acetic acid. This accounts for interactions such as structural effects and size of the molecules. It could also be the reason for the attraction of unlike molecules becoming closer together, and skeletal fitting for both molecules in the liquid mixtures.

Another important thermodynamic property is intermolecular free length (L_f) which evaluates the fluid consisting of attractive and repulsive forces in the liquid mixtures. In addition, it could also be used to investigate the distance between the centres from two adjoining molecular surfaces. The L_f is found to be inversely proportional to the u , and temperature predominantly influences the L_f.

Heat gives some additional energies to these molecules resulting in increased separation. This is one of the important tools used to investigate the molecular distances, forces operating in the liquid mixtures and interactions.

FTIR in particular, also establishes the molecular solute and solvent interactions for the binary mixtures of IL + ethanoic or propanoic acids. The FTIR spectrum indicates that the addition of acid to IL does influence the bonding of C-H and C-N bands of the cation in IL, C-O vibrational bands in IL and acid as well as C=O band in IL and acid. Therefore, the evaluation of FTIR spectra gave better clarification about the interaction among the ion + dipole interaction between IL and acids in the binary mixture of {$[Epmpyr]^+[Cl]^-$ (x_1) + ethanoic or propanoic acid (x_2)}.

Derived thermodynamic properties of V_m^E, Δk_s and L_f was correlated with the Redlich-Kister polynomial equation. For both binary systems the standard deviations indicate very low values for both V_m^E, and Δk_s, at all experimental temperatures.

12 Chapter 8

12.1 5th Publication

Graphical abstract

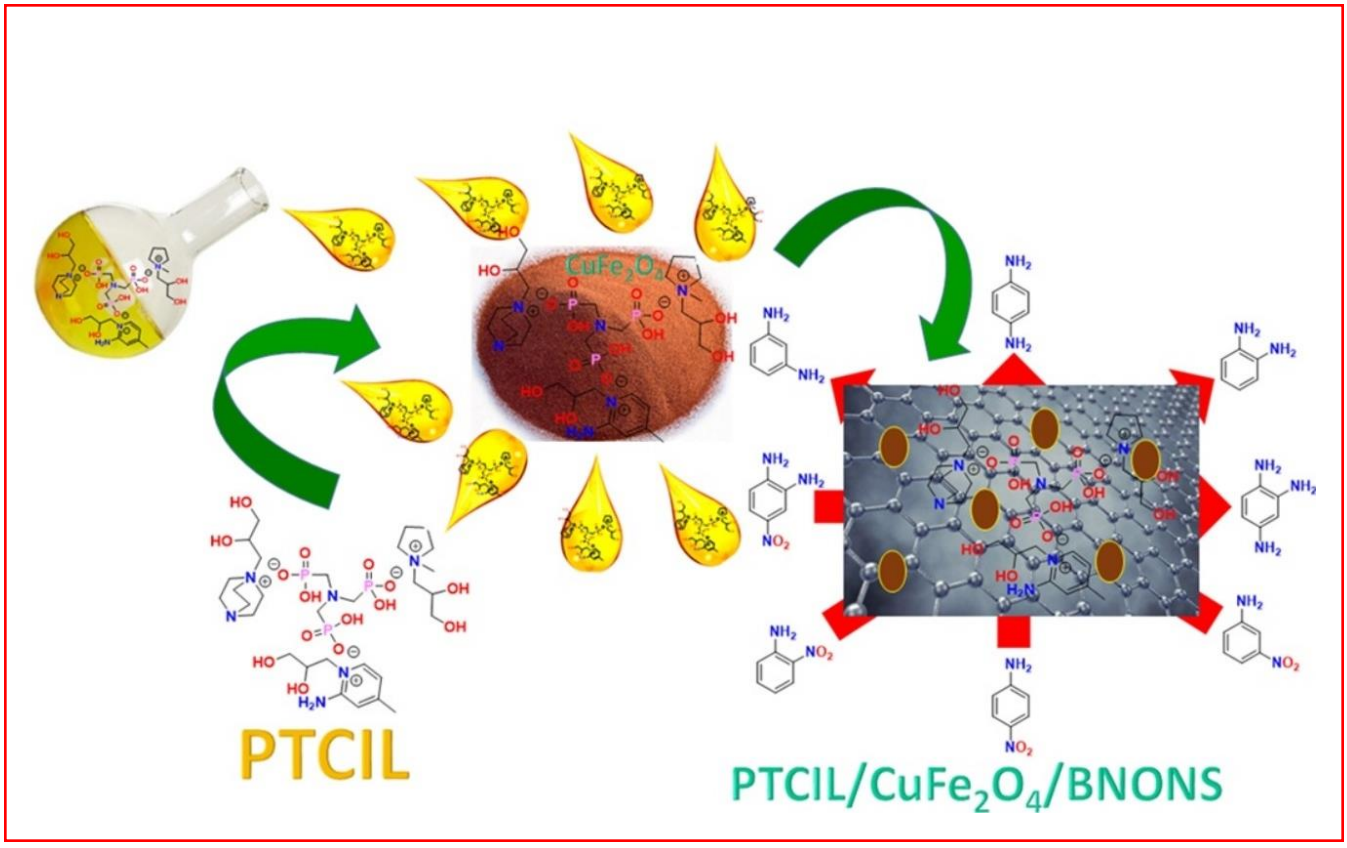

Applied Catalysis B: Environmental 222 (2018) 99–114

Contents lists available at ScienceDirect

Applied Catalysis B: Environmental

journal homepage: www.elsevier.com/locate/apcatb

Nano-material as an excellent catalyst for reducing a series of nitroanilines and dyes: triphosphonated ionic liquid- $CuFe_2O_4$-modified boron nitride

Vasanthakumar Arumugam[a], Pavithra Sriram[b], Ta-Jen Yen[b], Gyanasivan Govindsamy Redhi[a], Robert Moonsamy Gengan[a,*]

[a] Department of Chemistry, Faculty of Applied Sciences, Durban University of Technology, Durban, South Africa
[b] Department of Materials Science and Engineering, National Tsing Hua University, Hsinchu 30013, Taiwan, ROC

ARTICLE INFO

Keywords:
copper ferrite nanoparticle
phosphonate tri-cationic ionic liquid
partially oxidized boron nitride
nitroaniline

ABSTRACT

In this study a nanomaterial containing a novel tri-cationic phosphonate ionic liquid (TCPIL), copper ferrite magnetic nanoparticles ($CuFe_2O_4$ NP) and partially oxidized modified boron nitride nanosheet (BNONS) was synthesized, characterized and used as an efficient catalyst to reduce a series of nitro-anilines (NAs), and dyes. Three different ionic liquids (ILs) $[DABCO]^+[PDOL]^-$, $[APIC]^+[PDOL]^-$ and $[PYR]^+[PDOL]^-$ were synthesized separately, characterized and used to prepare a novel TCPIL {[DABCO, PYR, APIC-PDOL]$^+$[ATMP]$^-$}ionic liquid. Thereafter $CuFe_2O_4$ NPs and BNONS were used to synthesize the nanomaterial (TCPIL/$CuFe_2O_4$/BNONS): spectroscopic, microscopic and surface morphological studies were undertaken. The catalytic reduction of a series of NAs such as 2-nitroaniline (2-NA), 3-nitroaniline (3-NA), 4-nitroaniline (4-NA) and 4-nitro-2-phenylenediamine (4-NPDA) and dyes methylene blue (MB) and allura red (AR) in aqueous solution at ambient temperature were effective in all compounds tested: the order of reduction, based on reaction time, was 4-NPD > 4-NA > 3-NA > 2-NA. Kinetic studies indicated either zero order or pseudofirst order. The rate constant, order of the reaction, activation energy and constant ratio were also calculated for each substrate. Furthermore kinetic studies at various temperatures showed that an increase in temperature speeded the reaction whilst by increasing the amount of catalyst the reaction occurred faster. In addition, the nanomaterial was easily recovered and re-used for more than seven times with negligible loss of its catalytic activity. Moreover, it is possible to make different nanomaterial by combining different d-block metals such Zn, Pd, Pt and Mn with BNONSs for potential applications in biomedical, sensors and catalytic fields.

1. Introduction

Ionic liquids (ILs) are low melting salts which are a combination of cations and anions. They are used in various fields due to their outstanding physical and chemical properties such as having low melting point, zero vapor pressure, high solubility and either low or high viscosities depending on its structure. ILs are used in various applications such as a leading solvent for the green synthesis of nanomaterials [1,2], battery electrolytes [3], absorption of CO_2 [4,5] lignocellulosic biomass [6], biopharmaceutical applications [7], and catalyst in synthetic organic chemistry [8–10]. Recently, multi-cationic and multi-anionic compounds for the development of supramolecular ionic networks have been reported [11–13], whilst liquid exfoliated h-BN nanosheets (BNNS) have been stabilized using ILs [14]. It is reported that a combination of magnetic iron oxide NPs and ILs supported by BNNS have displayed better chemical activity than the IL's or NPs used alone [15,16]. This is because of their higher surface area, extraordinary stability of monolayer's and the significant role of BNNS in preventing the aggregation and conductivity of NPs in ILs [15,16]. A multi-ionic ionic liquid is one that contains more than one cation linked to the same type of anion and is usually a mixture of ILs. This is commonly prepared by mixing pre-existing ILs. A 4th generation IL (4-ILs) is a new concept and is described as one that contains more than one cation linked to a single substrate that contains multiple anionic sites.

Copper NPs has received significant attention owing to their exceptional and interesting applications in catalysis, photonics, and electronics [17–19] whilst magnetic iron oxide (Fe_3O_4) and (Fe_2O_3) NPs exhibit an excellent properties in water treatment, magnetic imaging, biosensor, cell labelling and drug delivery because of their low toxicity and low cost, high chemical stability and saturation in magnetization and easy manipulation in low magnetic field [20].

Graphene and hexagonal boron nitride (h-BN) are the two most

* Corresponding author.
E-mail address: genganrm@dut.ac.za (R.M. Gengan).

http://dx.doi.org/10.1016/j.apcatb.2017.08.059
Received 15 April 2017; Received in revised form 1 August 2017; Accepted 17 August 2017
Available online 25 August 2017

important members of the layered materials family possessing hexagonal lattice structures with virtually similar physicochemical properties. However in the last decade h-BN has attracted greater attention because of its fascinating features such as wide energy band gap [21], chemical inertness [22], electrical insulating properties [23], high surface area [24], and high thermal conductivity [25]. Furthermore, h-BN is more suitable for fabrication of hybrids due to its unique physicochemical properties [26–29] and can promote organic reactions such as the adsorption of CO which is catalyzed by Pd (III) loaded onto h-BN [30]. Recent reports shows that h-BN serves as a good platform to stabilize and disperse the noble metal NPs and their oxides [31–34] whilst tannic acid and ferric ion complex modified with h-BN exhibit exceptional catalytic activity for the reduction of 4-NA. Also h-BN is used in industries for various applications such as sensors [29,35,36], energy [37,38], catalysts [39–43], antibacterial agents [44,45] and biomedical fields [31].

h- Boron nitride nanosheets and nanotubes have better chemical stability than their carbon analogues. A recent report indicated that the formation of B—N—O bond by slow and strong oxidation at high temperatures shortened the BN nanosheets [28]. Recently, researchers [46,47] have investigated the oxidized structure of 2D h-BN by a chemical oxidation method and studied the electronic properties of h-BNONS. They found that chemisorption of oxygen plays an important role in the oxidation process of h-BN sheets and in modifying the properties of h-BN [48]. Although, these approaches have shown a feasible pathway for the preparation of h-BNONS, further improvement in their electronic properties are desirable for catalytic applications. Herein, we propose the use of novel TCPILs for improving their conductivity and stability of $CuFe_2O_4$ NP and h-BNONS nanosheets.

Generally, NAs are an important intermediate in organic synthesis, pharmaceuticals and dyeing industries. Many industries dispose of untreated effluent containing NAs thereby polluting the environment and ground-water [49]. Recently public health and environmental pollution issues are reported on low concentration of 2-NA especially in contaminated water [50–52]. The Unites States Environmental Protection Agency have listed the NAs as dangerous wastes and toxic pollutants [51,52]. Hence better protocols are required to convert the NAs to less toxic and more useful products. One such methodology is to use catalysts which could be effective in ambient reaction conditions and preferably in aqueous solution [53]. Such methodology is based on reduction of NAs to their corresponding amines derivatives [54,55] Recently, researchers developed an immobilized iron metal containing IL which was used as an effective and versatile heterogeneous catalyst for the chemoselective hydrogenation of nitroarenes into anilines [56].

The present study describes the facile synthesis and full characterization of three ILs, a unique TCPILs and their utility in the preparation of the nanomaterial containing $CuFe_2O_4$ and BNONS. Furthermore, the catalytic activity of the nanomaterial was assessed for the reduction of a series of NAs to their respective amino aromatics whilst two dyes were also included in this study. The kinetic studies of reduction reaction at different temperature and various quantity of catalyst (TCPIL/$CuFe_2O_4$/BNONS) was investigated and data were plotted.

2. Experimental

2.1. Materials and Method

Boron nitride (99.8% purity), copper sulphate (99.5% purity), ferric chloride (99.8% purity), ferrous sulpate (99.9% purity), liquid ammonia (30% solution), amino trimethylene triphosphonic acid (ATMP) (98% purity), 1-methyl-2-pyrrolidinone (99.8% purity), 3-chloro-1,2-propanediol (99.8% purity), 1,4-diazobicyclo[2.2.2]octane, 2-amino pyridine, methanol, ethanol, acetonitrile, sodium nitrite (99.9%), potassium permanganate (99% purity), sulphuric acid (98% purity), hydrogen peroxide (98% purity), 2-nitroaniline (98% purity), 3-nitroaniline (98% purity), 4-nitroaniline (99% purity), 4-nitro-2-phenylenediamine, methylene blue dye (95% purity) and allura red dye (80% purity) were purchased from Sigma Aldrich, South Africa.

The surface morphology of the composite was investigated by JSM-6701F (JEOL, Japan) scanning electron microscope (SEM): the sample was coated with gold. The energy dispersive X-ray spectrometry (EDS) analysis was carried out using a JEM-2100F at an accelerating voltage of 200 k. The sample was dissolved in ethanol and sonicated for 10 min to disperse the NPs and to make a stable dispersion (0.1 mg/mL). A D5000 Siemens diffractometer with copper source (K = 154.18) was used for recording XRD spectra. During XRD analysis, 100 mg sample was weighed and degassed at 110 °C for 2 hrs under 140 mbar pressure. XPS spectra were obtained using an ESCALAB 250 spectrometer operated in a fixed analyzer transmission mode (pass energy 150 eV) and Al-K (1486.6 eV) excitation. Prior to AFM analysis, the composite was dissolved in ethanol and further deposited onto mica substrates and dried. Shimadzu UV-2600 instrument was calibrated and fix the required parameters then run the blank solutions before start the experiment.

2.1.1. Synthesis of ionic liquids

2.1.1.1. I, Synthesis of [DABCO-PDO]$^+$[Cl]$^-$. N-2′, 3′ dihydroxy propyl 1,4-diazobicyclo [2.2.2]octanium chloride [DABCO-PDO]$^+$[Cl]$^-$ **(I)** IL was synthesized, characterized and purified by known protocol [57] (Scheme 1).

2.1.1.2. II, Synthesis of [PYR-PDO]$^+$[Cl]$^-$. In a 100 mL three-necked round bottom flask, fitted with a thermometer and water condenser, was added 1-methyl-2-pyrrolidinone (4.45 g, 50 mmol) in ethanol (50 mL). Thereafter 3-chloro-1,2-propanediol (6.0819 g, 55 mmol) was added slowly in an ice box set-up at the temperature of 8–10 °C with constant stirring and thereafter the content was brought to a moderate reflux to 90–100 °C on an oil bath, with constant stirring for 24 hrs. The flask was cooled and any volatile and unreacted materials were removed *in vacuo* to give a yellow colored liquid identified as N-2′,3′-dihydroxy propyl-1-methyl-2-pyrrolidonium chloride [PYR-PDO]$^+$[Cl]$^-$ **(compound II)**: reaction Scheme 2. The yield of the product was 98.20% and it was characterized by techniques such as FTIR, ^{1}HNMR, ^{13}CNMR and elemental analyses. [PYR-PDO]$^+$[Cl]$^-$. FTIR (υ = cm^{-1}): 3309, 2940, 2871, 1644, 1505, 1407, 1304, 1262 and 1036. ^{1}H NMR (400 MHz, $CDCl_3$): δ 4.3 (s, 2H), 3.8 (s, 1H), 3.7 (d, 2H), 3.4-3.6 (m, 2H), 3.3 (d, 2H), 2.7 (s, 3H), 2.2 (t, 2H), (1.9-2.0 (m, 2H). ^{13}C NMR (100 MHz, $CDCl_3$): δ 158, 135, 132, 130, 125, 88, 25, 15. The elemental composition (%) calculated for $C_8H_{16}ClNO_3$ is: C, 45.83; H, 7.69; N, 6.68, which are close to the values found: C, 45.56; H, 7.10; N, 6.29.

2.1.1.3. III, Synthesis of [APIC-PDO]$^+$[Cl]$^-$. In a 100 mL three-necked round bottom flask, fitted with a thermometer and water condenser, was added 2-amino pyridine (APIC) (4.57 g, 50 mmol) in ethanol (50 mL). Thereafter 3-chloro-1,2-propanediol (6.0819 g, 55 mmol) was added slowly in an ice box setup at the temperature of 8–10 °C with constant stirring and the content was brought to a moderate reflux to 90–100 °C on an oil bath, with constant stirring for 24 hrs. The flask was cooled and volatile unreacted materials were removed *in vacuo* to give a yellow colored N-2′,3′- dihydroxy propyl 2-amino pyridinium chloride [APIC-PDO]$^+$[Cl]$^-$ ionic liquid **(compound III)** shown in reaction Scheme 3. The yield of the product was 96% and it was

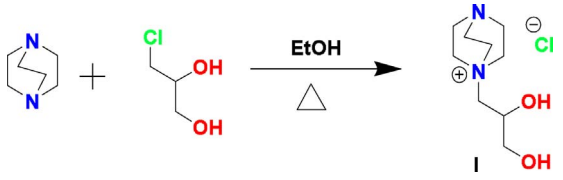

Scheme 1. Synthesis of [DABCO-PDO]$^+$[Cl]$^-$.

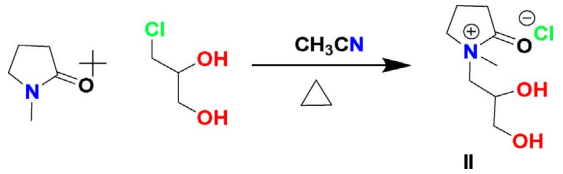

II

Scheme 2. Synthesis of $[PYR\text{-}PDO]^+[Cl]^-$.

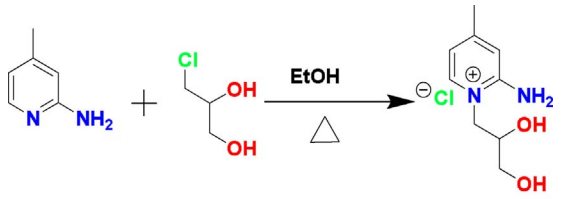

III

Scheme 3. Synthesis of $[APIC\text{-}PDO]^+[Cl]^-$.

characterized by the following techniques FTIR, ^{1}HNMR, ^{13}CNMR and elemental analyses. $[APIC\text{-}PDO]^+[Cl]^-$. FTIR (υ = cm^{-1}): 3323, 3170, 2953, 2884, 1583, 1444, 1373, 1046 and 1034. ^{1}H NMR (400 MHz, CD_3OD): δ 7.8 (d, 1H), 7.0 (s, 1H), 6.8 (d, 1H), 4.5-4.6 (d, 1H), 4.2-4.4 (d, 1H), 4.0-4.1 (d, 1H), 3.5-3.8 (m, 2H), 2.5-3.0 (s, 3H). ^{13}C NMR (100 MHz, CD_3OD): δ 156, 142, 118, 115, 70, 65, 55, 22. The elemental composition (%) calculated for $C_9H_{15}ClN_2O_2$ is: C, 49.43; H, 6.91; N, 12.81, which are close to the values found: C, 49.56; H, 6.60; N, 12.59.

2.1.1.4. IV, Synthesis of [DABCO, PYR, APIC-PDO]$^+$[ATMP]$^-$. In a 100 mL three-necked round bottom flask, fitted with a thermometer and water condenser, was added a sodium hydroxide (0.4 g, 20 mmol) in 50 mL of methanol. Thereafter amino tris (methyl phosphonic acid) (ATMP) (5.981 g, 20 mmol) was added dropwise, with constant stirring, on an ice bath. The reaction mixture was maintained at 8–10 °C for 1 h. Then 20 mmol of each $[DABCO\text{-}PDO]^+[Cl]^-$, $[PYR\text{-}PDO]^+[Cl]^-$ and $[APIC\text{-}PDO]^+[Cl]^-$ IL were added. The flask was transferred into an oil bath and the content was brought to reflux at 120 °C for 24 hrs. The flask was cooled and any volatile and unreacted materials were removed *in vacuo* to give a yellow colored $[DABCO, PYR, APIC\text{-}PDO]^+[ATMP]^-$ ionic liquid **(compound IV)** which was subsequently further purified by solvent washing, reaction Scheme 4. The yield of the product was 85% and it was characterized by the following techniques: FTIR, ^{1}HNMR, ^{13}CNMR, ^{31}PNMR and elemental analysis. $[DABCO, PYR, APIC\text{-}PDO]^+[ATMP]^-$. FTIR (υ = cm^{-1}): 3416, 3323, 2953, 2884, 1744, 1658, 1513, 1453, 1382, 1243, 1182, 1034, 915, 736, 654 and 569 (see Fig. 1b). ^{1}H NMR (400 MHz, D_2O): δ 7.5 (d, 2H), 6.6-6.8 (m, 3H), 4.3-4.4 (s, 2H), 4.0-4.1 (s, 6H), 3.9-4.0 (t, 5H), 3.8-3.9 (m, 10H), 3.5-3.7 (m, 23H), 3.3-3.4 (t, 2H), 3.1-3.2 (s, 3H), 2.2-2.4 (m, 6H), 1.7-2.1 (m, 2H). ^{13}C NMR (100 MHz, D_2O): δ 180, 160, 155, 145, 135, 118, 72, 68, 67, 65, 64, 63, 62, 61, 58, 56, 55, 54, 53, 52, 50, 48, 46, 32, 30, 22, 18.

2.1.2. Synthesis of $CuFe_2O_4$ nanoparticles

Magnetic $CuFe_2O_4$ nanoparticles were synthesized by chemical co-precipitation of Fe^{3+} and Cu^{2+} ions in an alkaline solution, followed by treatment under hydrothermal conditions [58,59].

2.1.3. Preparation of partially oxidized BNONS

The BNONS was prepared by modifying the chemical oxidation method [46,48]. Briefly, h-BN powder (1 g, 40 mmol) was added to a solution of sodium nitrite (0.8 g), in concentrated sulphuric acid (50 mL), on an ice bath. Thereafter potassium permanganate (5.6 g) was added, vigorously stirred and maintained at 10 °C. The reaction vessel was removed from the ice bath, agitated for 3 hrs and heated at 40 °C. Then deionized water (100 mL) was subsequently added, the reaction vessel was transferred to an oil bath and heated at 120–130 °C for 45 minutes. The solution was diluted with 200 mL of deionized water followed by the addition of a 30% solution of hydrogen peroxide (50 mL). The as-obtained partially oxidized BNONS powder (white color) was repeatedly washed with deionized water and dilute HCl to remove sulphate ions. The final washings were tested with $BaCl_2$ solution for sulphate. The as-purified partially oxidized BN (BNONS) powder was filtered and dried at 60 °C for 24 hrs.

2.1.4. Preparation of nanomaterial

The $TCPIL/CuFe_2O_4/BNONS$ nanomaterial (See Fig. 1) was synthesized by co-precipitation of the as-prepared $TCPIL/CuFe_2O_4$ nanoparticles in BNONS aqueous solution. In a typical synthesis, 1 g of T-CPIL {$[(DABCO\text{-}PYR\text{-}APIC)\text{-}PDOL]^+[ATMP]^-$} was dissolved in deionized water (20 mL). Then, $CuFe_2O_4$ (2 g) NPs was added into the above solution and heated at 120 °C for 24 hrs with constant stirring. Thereafter sodium dodecyl lauryl sulfate (0.1 g) was added followed by addition of BNNONS solution (1.0 g in 10 mL) and 30% ammonia solution (25 mL) with vigorous stirring to dissolve all materials. This solution was heated at 150 °C with constant stirring for 12 hrs. Then the pH of the solution was adjusted to 9-10 with dilute ammonia solution. The mixture was stirred for 1 h and cooled to reach ambient temperature. Finally, the mixture was centrifuged and filtered to obtain $TCPIL/CuFe_2O_4/BNONS$ powder (brown). The product was washed several times with deionized water and dried under vacuum at 70 °C. The final product was dispersed in ethanol (20 mL). The mass ratio of $CuFe_2O_4$, IL and BNONS in the $TCPIL/CuFe_2O_4/BNONS$ nanomaterial was calculated as 2:1:1. The outline method of the preparation shown in Fig. 1 as below.

2.1.5. Catalytic reduction of nitroanilines and dyes

The catalytic activity of $TCPIL/CuFe_2O_4/BNONS$ was investigated by the reduction of a series of NAs and dyes (Scheme 5). Briefly, 2-NA (0.5 mL, 0.05 M), 3-NA (0.75 mL, 0.05 M), 4-NA (0.75, 0.01 M), 4-NPDA (0.75, 0.005 M) as well as MB (0.75, 0.01 M)and AR (0.50 mL, 0.05 M) solution was added separately into a quartz cuvette followed by $NaBH_4$ (0.75 mL, 0.5 M) and finally by deionized water (1.485 mL). A smaller quantity of 4-NPDA was used due to its poor solubility. Then an aqueous solution of $TCPIL/CuFe_2O_4/BNONS$ (0.015 mL, 0.2 mg/mL) was added into the quartz cuvette and the reaction was monitored by UV-Vis. The UV–vis absorption spectra were recorded after every five minutes (Fig. 11(a)–(f)). The kinetics of the reaction was investigated to compute the rate constant, order of the reaction and activation energy. In addition, several temperatures such as 298 K, 303 K, 313 K, 323 K, 333 K and different dosage of the catalyst such as 0.015, 0.030 and 0.040 (2 mg/ml) were used for kinetic studies. During the reduction of NAs and dyes, the solution changed to colourless thereby indicating a visual confirmation of the reduction process. After completion of the reaction, small aliquots of NH_4Cl solution was added to neutralize excess $NaBH_4$. The catalyst was recovered by external magnets as shown in Fig. 2.

3. Results and Discussion

The FTIR spectrum of $TCPIL/CuFe_2O_4/BNONS$ nanomaterial (Figure ES-1a (Electronic Supplementary)) showed the characteristic peaks at 3317, 2910, 1762, 1620, 1398, 1058, 808, and 559 cm^{-1}, revealing the presence of functional groups such as $-NH_2$, $-$C-H, $-$C═O, $-$C−N, $-$C−O, $-PO_3$, $-$B−N and FeO. In addition to these peaks, C-H and $-$OH peaks were also observed at 2910 cm^{-1} and 3317 cm^{-1}, respectively. The BNONS (Figure ES-1c) showed surface bonds such as B-N (1446 cm^{-1}), B-OH/B-NH_2 (3325 cm^{-1} and 3190 cm^{-1}), B−N−B (802 cm^{-1}), B−N−O (1107 cm^{-1}), C−O (1045 cm^{-1}), and B-N-O (1026 cm^{-1}) [31]. FTIR results showed that non-covalent functionalization of BNONS occurred via van der Waals forces as consistent with a previous report [60]. When compared to the pristine h-BN, the band at

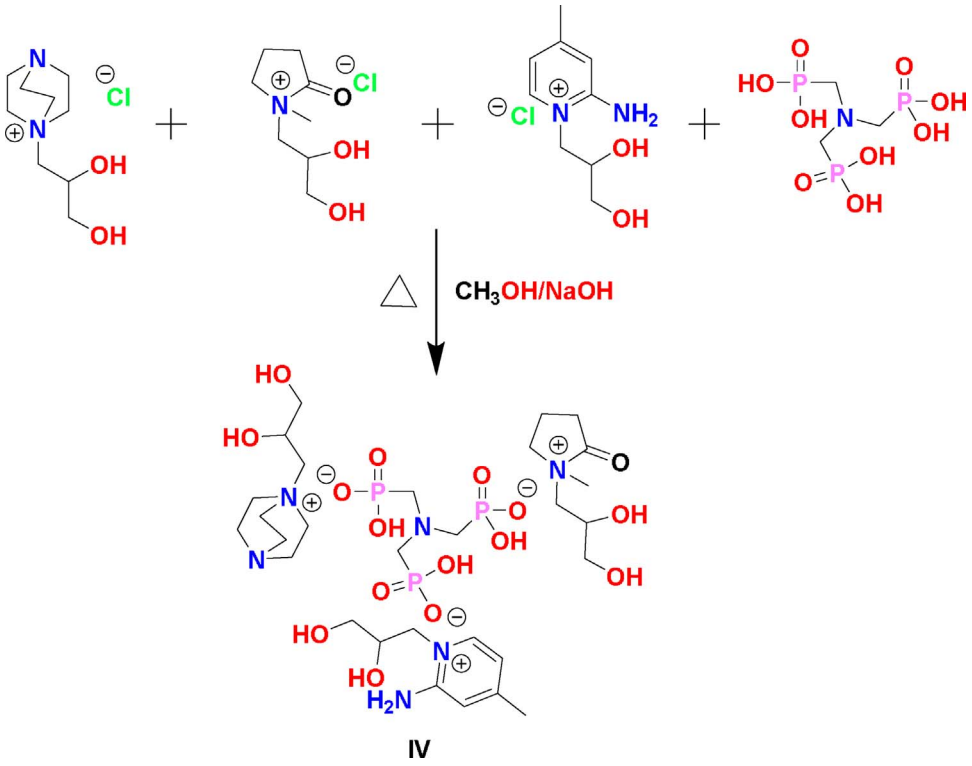

Scheme 4. Synthesis of [DABCO, PYR, APIC-PDO]$^{+}$[ATMP]$^{-}$.

1100 cm^{-1} for OH-BNONS shifted slightly. Furthermore, the absorption peak was assigned to B-O deformation originating from the hydroxyl group of the OH—BNONS [31]. The absorption peaks were in correlation with those reported previously for activated BN [61]. The FTIR of nanomaterial also exhibited typical absorption bands at 925 and 970 cm^{-1} corresponding to the stretching vibrations of the P-OH group in IL shown in (Figure ES-1b and 1d). The characteristic peaks of PO_3H were also observed at 1762, 1620 and 1058 cm^{-1} [61]. The characteristic absorption band of Fe—O in $CuFe_2O_4$ NP were observed at 559 and 466 cm^{-1}. In addition, peaks at 1629, 1539, 1338 and 950 cm^{-1} corresponded to metal-metal and metal oxygen bonds. Regarding the IL to metal and BN-P vibrations, the stretching vibration of the Cu—N bonds were also observed at 456 cm^{-1}.

X-ray diffraction (XRD) analysis was an important technique which provided valuable information for interpretation of the crystalline nature of the metal, metal oxide and BNONS. The typical XRD pattern of the TCPIL/$CuFe_2O_4$/BNONS nanomaterial (Figure ES-2) displayed two characteristic peaks at the 2Θ values of 27.3° and 55.3° for (212), (423) planes, which corresponded to the two crystalline phases such as hexagonal BNONS (JCPDS 45-896) and cubic $CuFe_2O_4$ (JCPDS 77-10). The $CuFe_2O_4$ phase exhibited sharp peaks at 2Θ value of 311, suggesting they were nano-crystalline. The other phases such as copper (JCPDS, no. 851326); copper (I) oxide, Cu_2O (JCPDS, no. 741230); copper (II) oxide, CuO (JCPDS, no. 410254); and magnetite, Fe_3O_4 (JCPDS, no. 751609) were also observed. By using the formula of Debye Scherrer ($D = K\lambda/(\beta \cos\theta)$ and the full width at half maximum of the diffraction peak at the Bragg angle 2θ, the size of $CuFe_2O_4$ was determined to be 20 nm. The crystallinity of $CuFe_2O_4$NP in the composite was confirmed by XRD patterns. Figure ES 2 shows discrete characteristic peaks at the 2Θ values of 27.3°, 28.4 °, 32.9 °, 46.8°, 55.3° and 58.0° which were assigned to the (220), (117), (1114), (311) (552) and (443) crystallographic planes of Fe_3O_4. The XRD peaks of Fe_3O_4 at around 26.8° and 55.6° overlapped with the (220) and (443) facets of the h-BN.

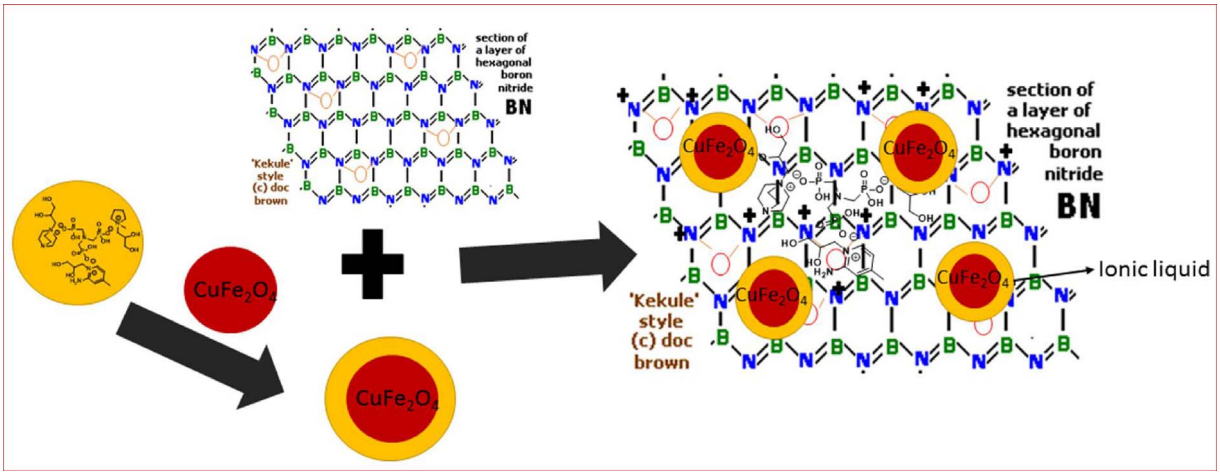

Fig. 1. Preparation of TCPIL/$CuFe_2O_4$/BNONS Nanomaterial.

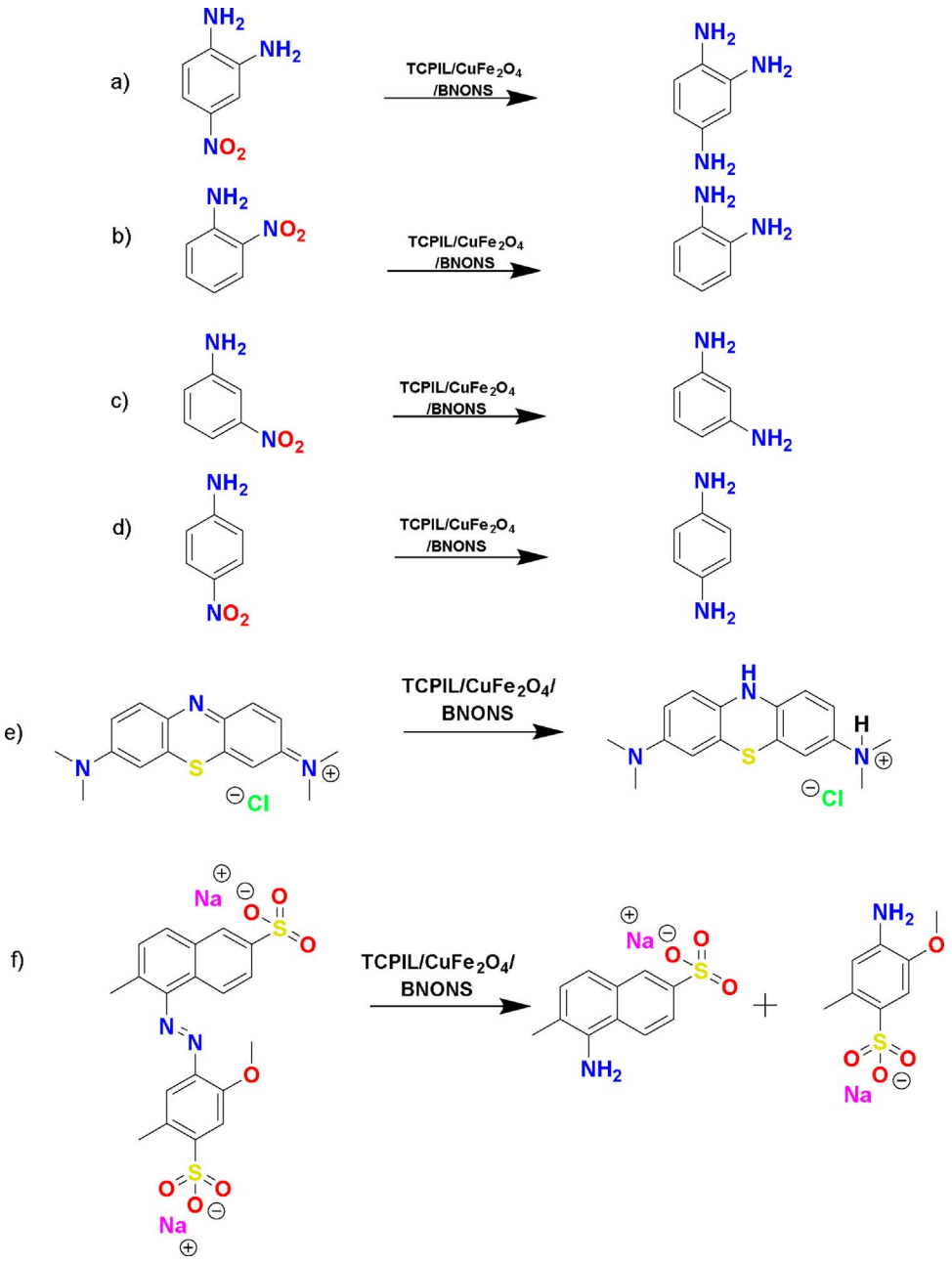

Scheme 5. Reduction of various NAs such as (a) 4-NPDA, (b) 2-NA, (c) 3-NA (d) 4-NA and dyes (e) MB and (f) AR to their amine and corresponding analogues.

Raman spectra provided useful information to identify the bonding states of the h-BN films, thus providing complementary evidence of the successful formation of modified h-BN [31,46,60,62]. The characteristics peaks in the Raman spectra of h-BN were similar to that of the BCN film prior to etching, revealing that B and N atoms were dominating the edge effect. The greatly imperfect SP_2 hybridized graphene-like structure of BN on Cu foil was observed. The E_2g symmetric vibration mode in h-BN indicated the peaks at 1365 and 1872 cm^{-1} which were similar to that of h-BN (Fig. 3b) [63–65]. Subsequently, the additional sharp peak at 1707 cm^{-1} indicated the B-O-N bond. The Raman spectra of h-BNONS (Fig. 3a) exhibited some extra peaks corresponding to oxygen coordinated boron and nitrogen. The intensity of the peak at 1707 cm^{-1} (806) was close to the peak at 1872 cm^{-1} (662.5), providing ample evidence for the formation of h-BNONS. The arrangement of layers of h-BNONS was different from normal h-BN, due to the interaction of oxygen with boron and nitrogen.

Those interactions create an angle strain and some steric hindrances or slight distraction of the electronic cloud of h-BN. As a result, some of the layers were perpendicularly allocated as shown in Fig. 9a and b. Although it does not cause any significant change in the overall structure of the h-BN, slight modification in the surface of the h-BN material occurred. The SEM images (Fig. 9a) showed the multilayers of the material. Further investigation of the SEM images revealed each layer was a single crystal. Thus, Raman spectra results clearly indicated the crystallinity level in the sample and Full Width at Half Maximum (FWHM).

X-ray photoelectron spectroscopy (XPS) was used to investigate the surface chemical composition of the TCPIL/$CuFe_2O_4$/BNONS. Fig. 4 shows the survey scan of the XPS spectrum which evidently indicates the presence of elements such as boron, nitrogen, oxygen, phosphorus, carbon, copper and iron. The exact spectra and peak area intensity were obtained by subtracting the Shirley type backgrounds for all. The deconvoluted B_{1s}, C_{1s} and N_{1s} spectra are displayed in The B_{1s} spectrum (Fig. 4b) has the peaks at the binding energy (B.E) values of 191.0 and 189.9 eV, which were attributed to B-N and B-C bonding, respectively, while the peak at 192.1 eV showed the existence of BNONS. The curve

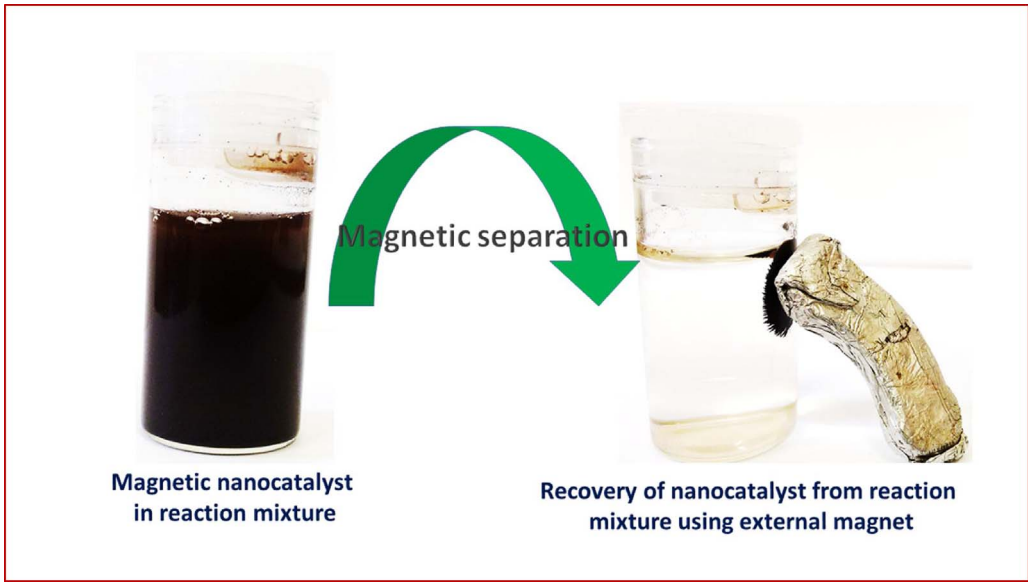

Fig. 2. Magnetic separation of TCPIL/$CuFe_2O_4$/BNONS Nanomaterial.

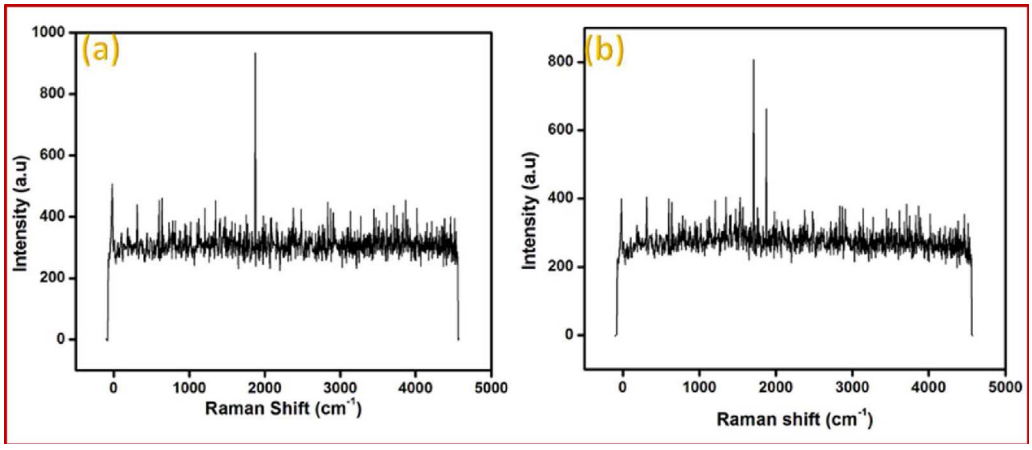

Fig. 3. Raman spectra of pure BN (3a) and partially oxidized slightly modified h-BNONS nanosheet (3b).

fitted C_{1s} spectrum and displayed two main peaks at 284.8 and 285.8 eV, which were ascribed to C-C and C-N, respectively (Fig. 4c) [66–68]. The deconvoluted N_{1s} spectra showed two peaks at 398.4 and 398.9 eV (Fig. 4d). The former one was attributed to N-B bonding and the latter one was ascribed to the N-C bonding [69]. The TEM, XRD and XPS results confirmed that BNONS coating was successfully prepared on the TCPIL/$CuFe_2O_4$ surface via the direct impregnation method. Meanwhile, the surface modification of TCPIL/$CuFe_2O_4$ by BNONS formed rich hydroxyl and phosphonate groups on the surface of the nanomaterials, which improves the surface area and dispersing ability of TCPIL/$CuFe_2O_4$/BNONS matrix.

In general, the BN nanomaterials have thin sheets with less than 8-10 layers and lateral size of the nanosheets ranges from 1.5 to 2 μm. Fig. 5a and b displays the AFM images of TCPIL/$CuFe_2O_4$/BNONS with different height profiles (50 and 500 nm). The height profile of the nano-sheets revealed that they have multilayered nano-sheets and their thickness were ~2.5 nm and this information was further confirmed from literature.[71] It has been reported that there were no wrinkles on the surfaces of the CVD-grown BNONS even after transferring to substrate [70,71].

Fig. 6a and b, shows the characteristic low-magnification TEM images of the TCPIL/$CuFe_2O_4$/BNONS nanomaterials. The $CuFe_2O_4$ NP and TCPIL were uniformly spread over the BN modified partially oxidized BNONS that have fairly rough surfaces. The thickness of the BNONS are ~2.5 nm, which was consistent with our AFM results. The average size of $CuFe_2O_4$ NP is 20 nm. The TCPIL/$CuFe_2O_4$ NPs were anchored on the BNONS without forming any aggregates. TEM images showed that some of the nano layers of BNONS were arranged in parallel in comparison with that of normal h-BN. These arrangements actually give a compact space for nanoparticles and IL binding. The combination of $CuFe_2O_4$ NP, ILs and BNONS should provide good catalytic efficiency.

Fig. 7a and b shows single nanosheets in the composites. The HRTEM images of the nanomaterial revealed that BNONS have multilayered sheets with an outer diameter and thickness of ~20 nm and ~2.5 nm, respectively. Actually, the HRTEM images are not clear due to more electron concentration and ILs interferes while focusing on microscope. However, the diameter of the nanosheets in the BNONS increased to 20–50 nm after IL modification, confirming the coating of IL on the surfaces of BNONS. The thickness of the few layers in the BNONS was around 2.5 nm as confirmed from the height profile AFM image as described previously (Fig. 5a and b). Furthermore, the TCPIL/$CuFe_2O_4$/BNONS retained their perfect crystallization after coating with TCPIL/$CuFe_2O_4$ as observed from TEM images. As shown in Figure. ES-4a the distance between the two lattices fringes in the TCPIL/$CuFe_2O_4$/BNONS nanomaterial were determined to be ~0.5 nm, which corresponds to the 311 plane of the $CuFe_2O_4$ crystal (Fig. 9b). The low accelerating voltage of 60 KV was enough to perform high-angle annular dark-field scanning transmission electron microscopy (STEM) and to avoid the structural damage by the electron beam.

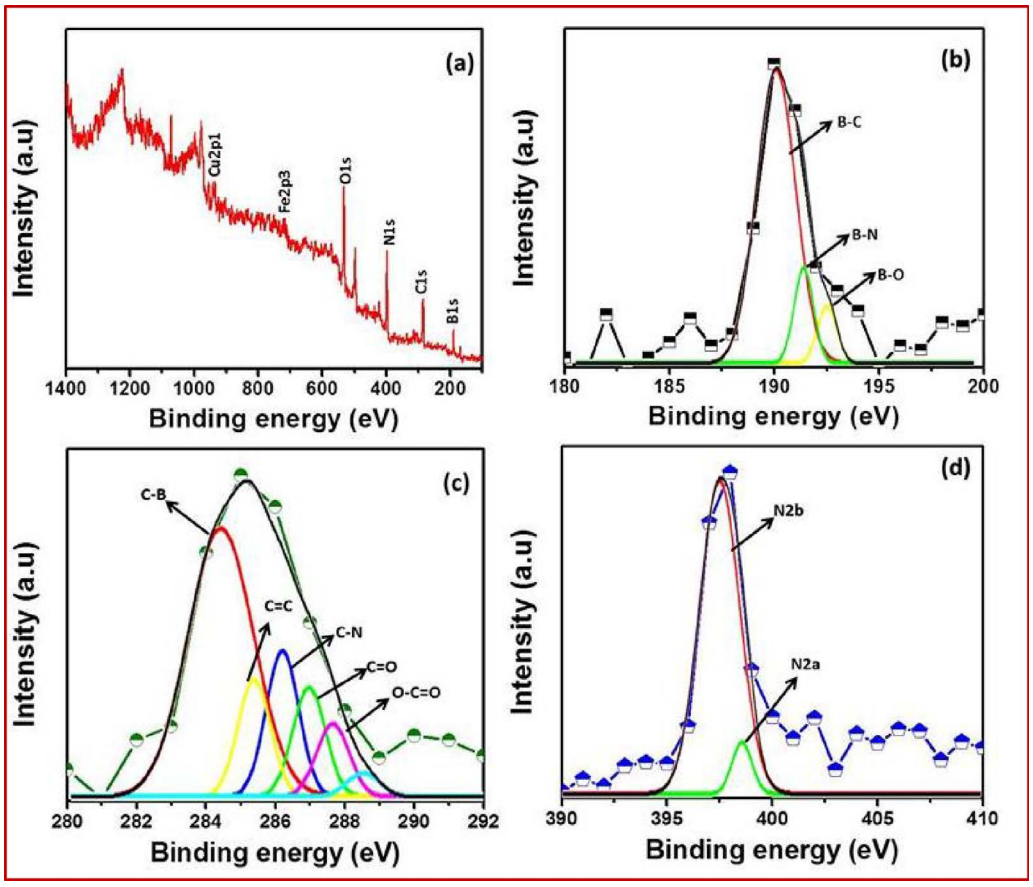

Fig. 4. 4a) XPS spectra of TCPIL/$CuFe_2O_4$/BNONS nanomaterial. 4b) The B1 s spectrum of the peaks at the binding energy (B.E), 4c) C—C and C—N binding energies, 4d) N1 s spectrum of the nanomaterial.

From the representative bright-field image, shown in Fig. 8a, it was clearly observed that the particles are irregular spheres with an average diameter of 20–50 nm. The $CuFe_2O_4$ NPs appear black as indicated by the $CuFe_2O_4$ and Cu NPs in Fig. 8a and b with arrows. Cu NPs appeared as bright dots due to the greater electronic conductivity of Cu than Fe. The AC-STEM images of TCPIL/$CuFe_2O_4$/BNONS and the corresponding elemental distribution of Cu and Fe clearly showed that most of the Cu NPs were grown near the edges of the BNONS where Fe_2O_4 NPs were present. STEM image, displayed in Fig. 8b, confirmed that $CuFe_2O_4$ NP were uniformly modified onto the iron oxide surface.

Fascinatingly, analysis of the selected area electron diffraction (ED) patterns establish the differences between the nanomaterial and two

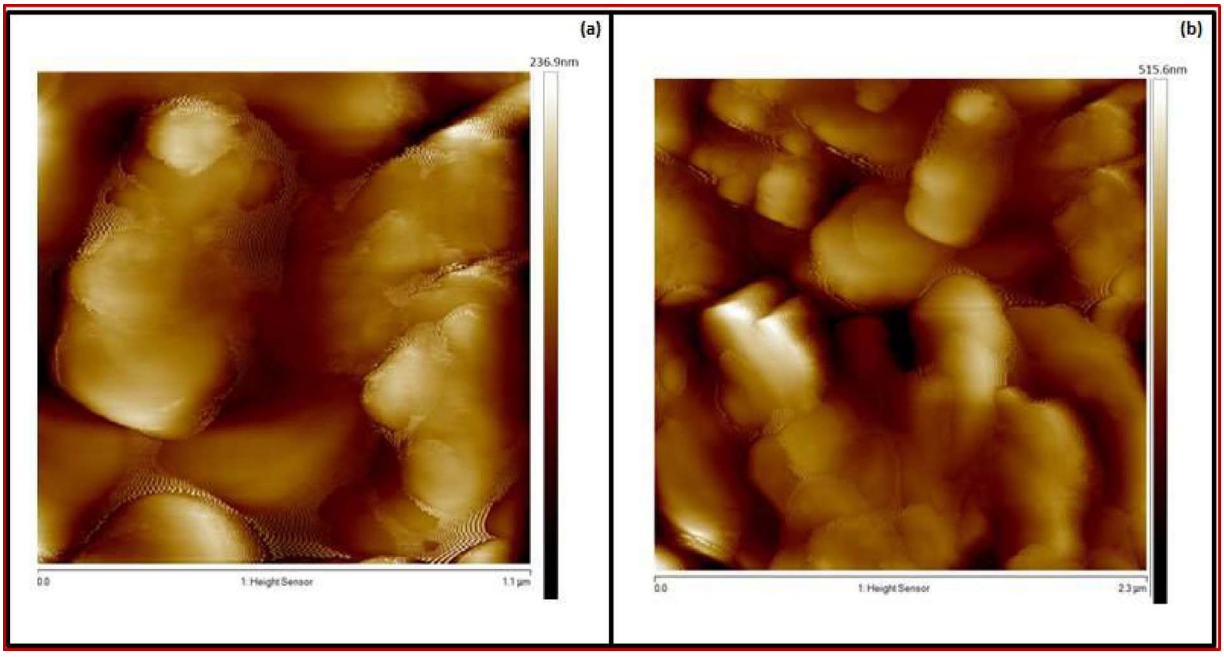

Fig. 5. AFM images of TCPIL/$CuFe_2O_4$/BNONS nanomaterial (4a–4b).

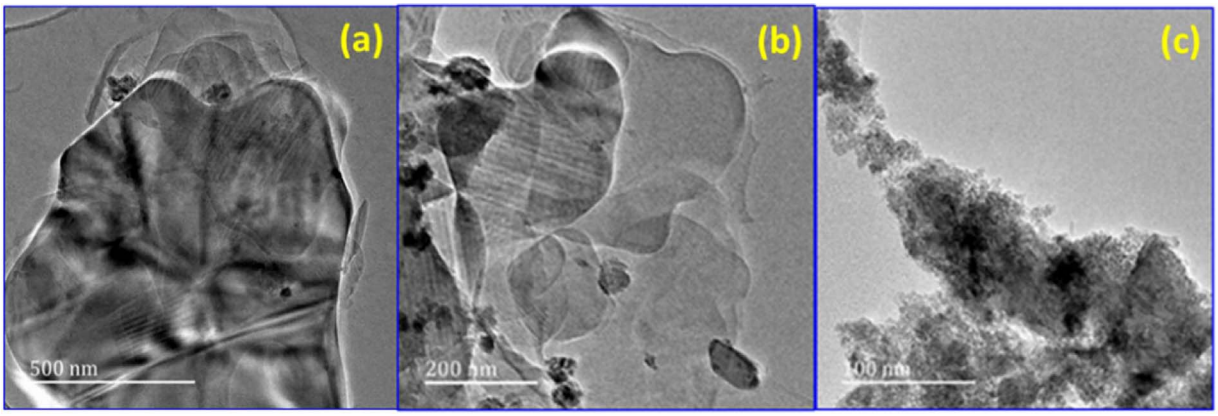

Fig. 6. TEM images of PTCIL/CuFe2O4/BNONS nanomaterial taken at different magnifications (a–b). TEM images of pure $CuFe_2O_4$ nanoparticles (c).

constituents. Figures ES-3a and ES-3b shows the ED patterns of IL/$CuFe_2O_4$/BNONS nanomaterial and the $CuFe_2O_4$ NP, respectively. The presence of rings in ED pattern showed the polycrystalline nature of the $CuFe_2O_4$ NPs. The hexagonal ED pattern of TCPIL/$CuFe_2O_4$/BNONS nanomaterial showed the single crystalline nature. Compared to the $CuFe_2O_4$ NP, ED pattern of the composite showed more bright spots due to greater electronic conductivity resulting from IL and BNONS, revealing the formation of the TCPIL/$CuFe_2O_4$/BNONS nanomaterial.

The surface morphology and particle size of the synthesized nanomaterial were additionally investigated using SEM and EDS, with the results shown in Fig. 9a, b and Fig. 10, respectively. The SEM images of the $CuFe_2O_4$ NPs revealed that the NPs were densely packed with a grain size in the range of 20–30 nm. The BNONS were composed and the sheets have layered thin platelet morphology. The distribution of the $CuFe_2O_4$/IL on the TCPIL/$CuFe_2O_4$/BNONS nanomaterial surface was clearly seen, with the size of the NPs and ILs similar and were uniformly spread over the BNONS layer. This confirmed the presence of the BNONS, IL, and $CuFe_2O_4$ NP in the TCPIL/$CuFe_2O_4$/BNONS nanomaterial. Further investigation of the EDS indicated the presence of elements such as B, N, C, O, P, Fe and Cu in the nanomaterial (Fig. 10). Table 1 lists the amounts of B, N, C, O, P, Fe and Cu in the nanomaterial. The mapping of elements in the nanomaterial using SEM & EDS revealed the distribution of B, N, C, O, P, Fe and Cu (Fig. 9b and c). The thermal stability of the nanomaterial was investigated by TGA analysis as shown in Fig. 11. There was no significant weight loss up to 700 °C, revealing the good thermal stability of the nanomaterial. The decomposition profile of the material was also compared to BN sheets. The nanomaterial exhibited three distinct steps of weight losses upon heating from room temperature to 1000 °C under air flow as displayed in both TG-DTG curves (Fig. 11). The first weight loss (ca. 8.0%) at 100 °C was attributed to the removal of moisture. The second weight loss at 250 °C (ca. 12%) was due to the pyrolysis of the oxygenated functional group on the BNONS surface. Interestingly, compared to normal BN, the decomposition temperature (at 200 °C) of the oxygen functional groups in material increased, suggesting the BNONS and the IL moieties were stabilized mutually. Final weight loss at 700 °C (ca. 12%) was attributed to the decomposition of the IL moiety in the BNONS layer. The results represented indirect proof for the covalent linkage of the Cu ferrite magnetic NPs and BNONS through the phosphonate IL linker.In this study, h-BN surface modified with partially oxidized BN nanosheets were prepared for the first time. This investigation developed the modified graphene oxidized method because BN underwent low and strong oxidation at high temperature to create the interaction between oxygen and the B-N bond and to reduce the electron cloud in-between the B-N. The modified BNONS was confirmed by FTIR, Raman spectroscopy and XRD. Those spectra exhibit different peaks compared to normal hexagonal BN. The physical nature of the material was also different from the normal h-BN due to its smooth texture. The surface morphology of the partially oxidized boron nitride nanosheets was changed from normal h-BN due to the angle and position of some of the sheets were changed to perpendicular. So, random sheets position arrangement perpendicular and the normal surface area could help to increase the stability and it gives some space for IL bound $CuFe_2O_4$ NP and thus it was used as a base material for the nanomaterial. Another important aspect was the synthesis of novel tri-cationic phosphonate ILs, which contains DABCO, amino picoline and pyrrolidonium cations coordinated with triphosphonated amino trimethylene amino phosphonate (ATMP) based anions. The chemical compounds such as heterocyclic compounds, organic components, and substituted propane diol groups does help ILs to bind efficiently with BNONS and

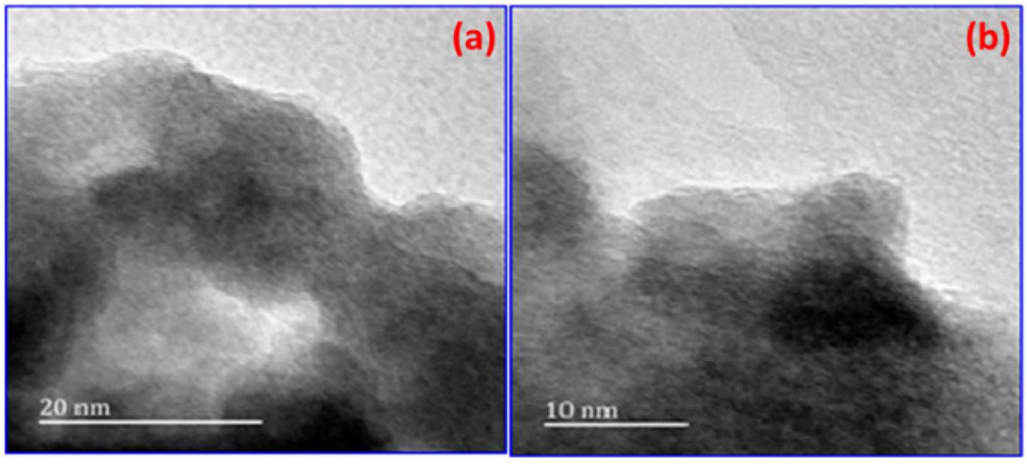

Fig. 7. HRTEM images of PTCIL/$CuFe_2O_4$/BNONS nanomaterial at (a) 20 nm and (b) 10 nm.

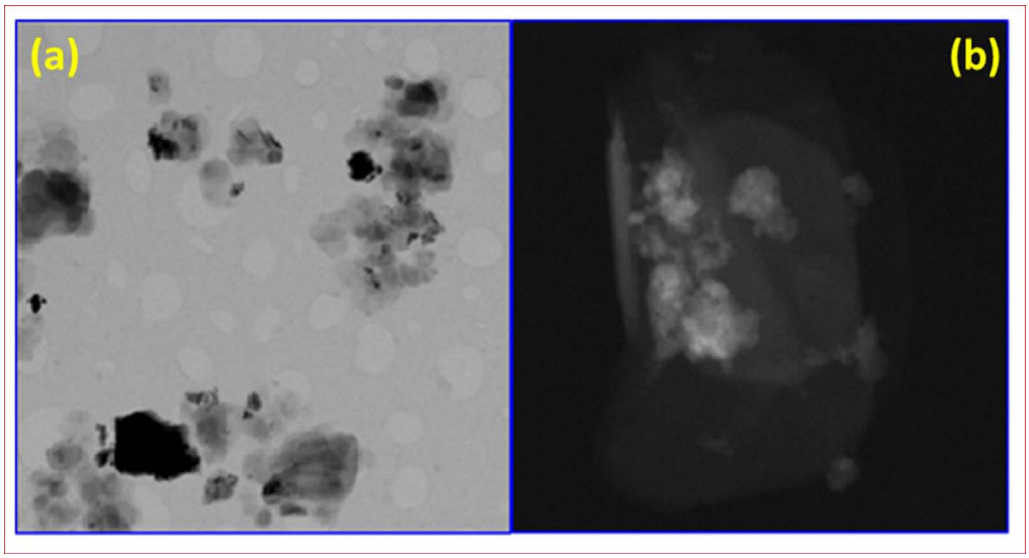

Fig. 8. a) Bright-field STM image for nanomaterial, b) Dark-field STM image for nanomaterial.

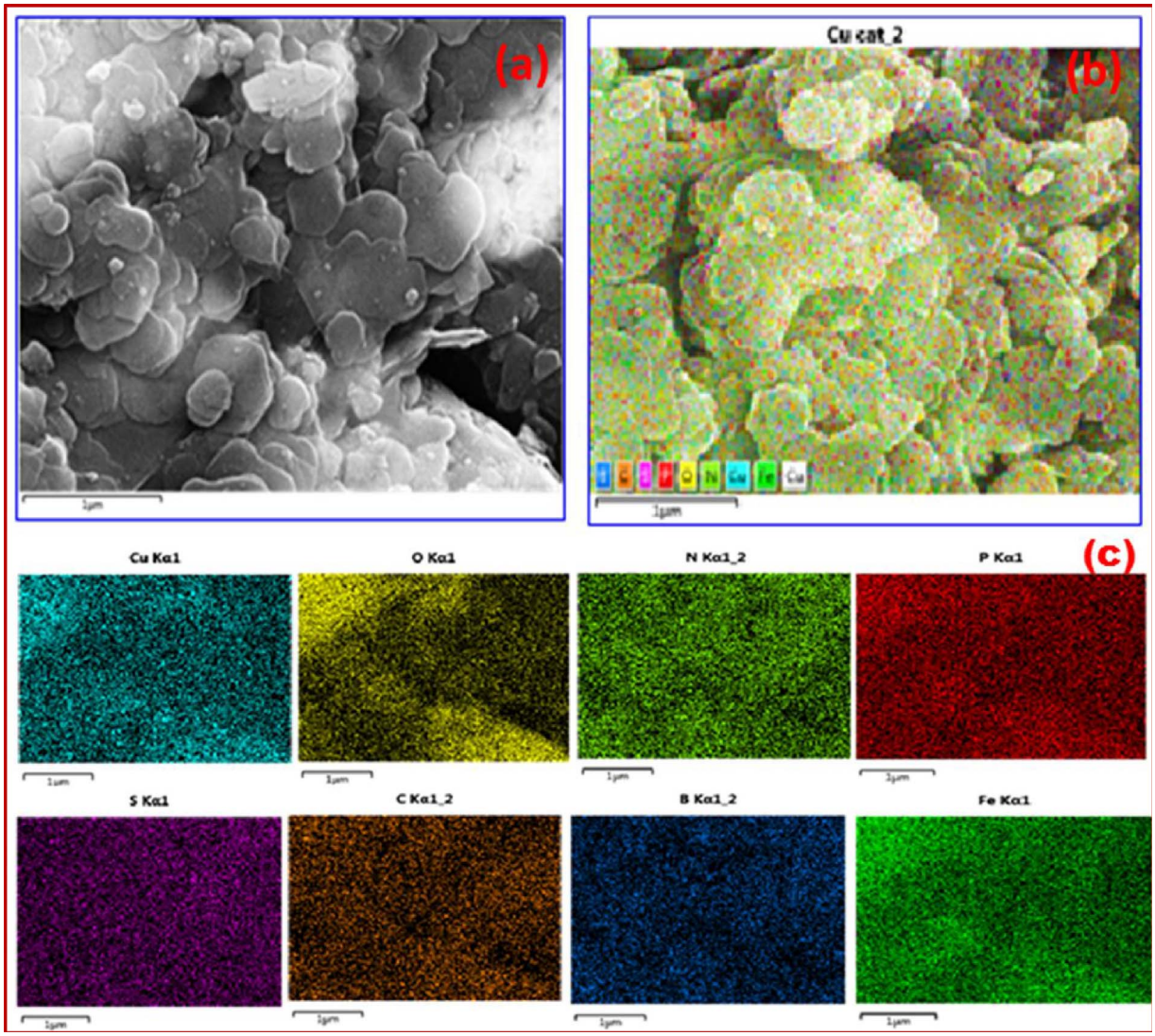

Fig. 9. SEM images of TCPIL/$CuFe_2O_4$/BNONS nanomaterial (9a), mapping of all elements in the nanomaterial (9b) mapping of individual elements.

magnetic NPs, subsequently, cation's and anions were catalytically active in nature. The bimetallic NPs such as $CuFe_2O_4$ magnetic NPs also have great catalytic activity. The co-ordination or binding interactions occur between $CuFe_2O_4$ and ILs. The ILs were coated with $CuFe_2O_4$ NPs as well. These copper and iron particles were strongly interacted with ILs because of its metallic charge, ionic interaction and good chelating

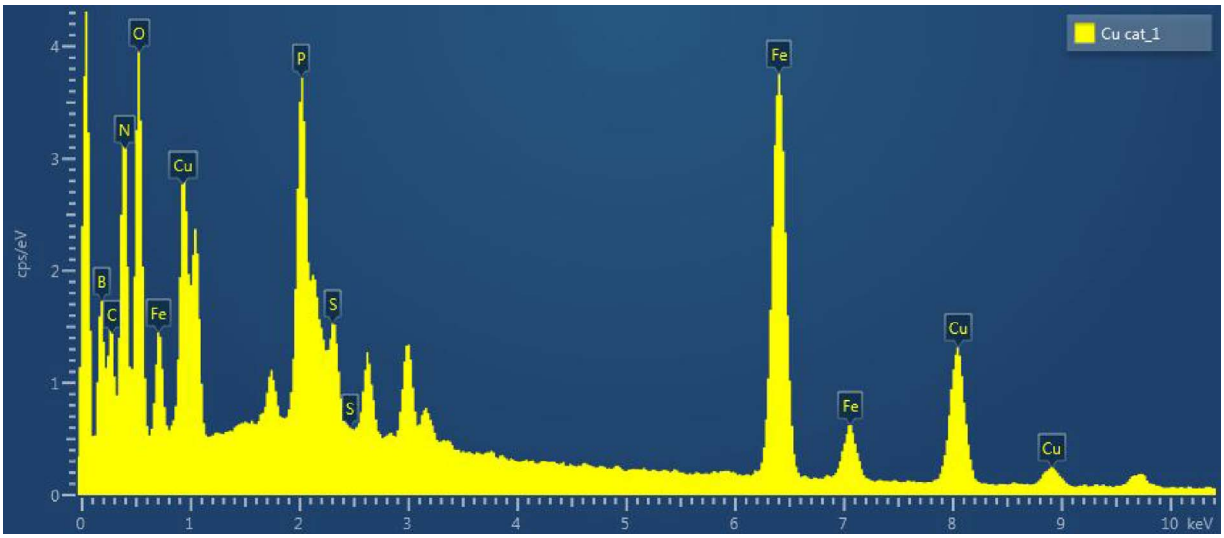

Fig. 10. EDS spectrum of TCPIL/$CuFe_2O_4$/BNONS nanomaterial.

Table 1
The EDS elemental analysis results for the TCPIL/$CuFe_2O_4$/BNONS nanomaterial.

Elements	Weight %	Atomic %
B	26.24	0.98
C	13.31	0.81
N	26.60	0.60
O	16.97	0.36
P	1.70	0.05
S	0.60	0.03
Fe	8.91	0.17
Cu	5.68	0.13
Total	100	

ability of phosphonate groups in ILs. The resulting material was coated with partially oxidized BNONS because of heteroatoms such as oxygen helps to coat BNONS perfectly. This nanomaterial has good physical and chemical properties. The stability, metal identification, compositions, functional groups and morphologies were confirmed by special characterizations as discussed above. The method for preparing TCPIL/$CuFe_2O_4$/BNONS was described in an experimental. The preparation of TCPIL has three active organic molecules DABCO, N-methyl pyrrolidone and amino picoline as cations with the tri-phosphonate anion ATMP. Hence it was hypothesized that this material would expect to have more catalytic activity. The final nanomaterial was made by these ILs capped $CuFe_2O_4$ NPs through noncovalent functionalization of partially oxidized BN nanosheet because it has strong affinity with the basal plane BNONS. The main strategy for uniform and dense assembling of inorganic magnetic NPs and ILs on the BNONS was proposed to be due to the surface functionalization of BNONS with high densities of active heterocyclic compounds and phosphonate groups.The reduction of NAs was investigated with $NaBH_4$ in the absence of nanomaterial. The UV spectrum showed a slow decrease in the typical absorbance peak at 380 nm: only 3% of the NA was reduced even after 24 hrs [72] thereby suggesting that electron transfer from the donor, $NaBH_4$ to the acceptor NA might be prevented by a kinetic barrier. The catalytic activity of the prepared TCPIL/$CuFe_2O_4$/BNONS nanomaterial was evaluated for the reduction of 4-NA to PPD (*para* phenylenediamine) in the presence of $NaBH_4$. The typical absorption peaks of 2-NA to OPD (*ortho* phenylene diamine) is at λ_{max} 410 nm and 240 nm (Fig. 12a), 3-NA to MPD (meta phenylenediamine) is at 360 nm and 300 nm (Fig. 12b), 4-NA and PPD at 380 nm and 240 nm (Fig. 12c) and 4-NPDA to 2, 3, 4-triaminobenzene (Fig. 12d) at 401 nm were monitored. The absorption of MB is at λ_{max} 300 nm, 600 nm as well as 680 nm (Fig. 12e) and AR at 500 nm (Fig. 12f) were monitored: as observed, the absorbance decreased with time corresponding to a recent report [73]. Some of the peaks in the UV spectrum was split at the top of the area due to high concentration of NAs, therefore it further explains about the

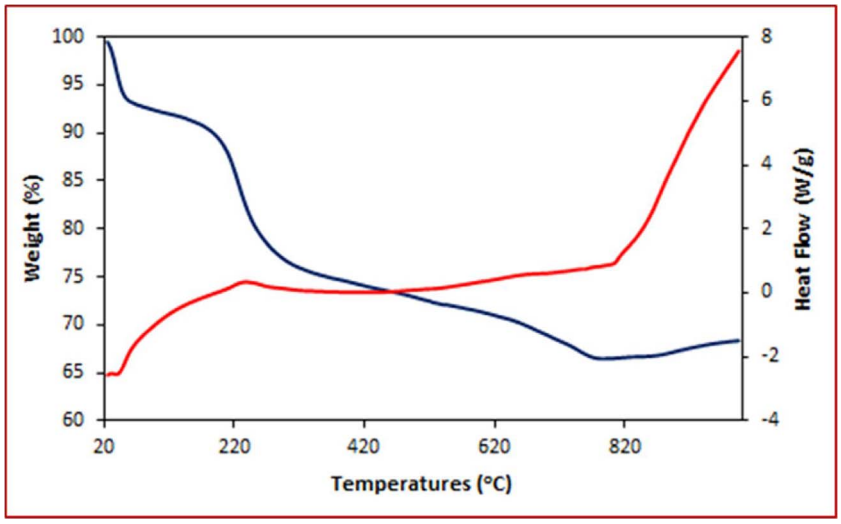

Fig. 11. TGA-DSC curve of the TCPIL/$CuFe_2O_4$/BNONS nanomaterial recorded under air atmosphere.

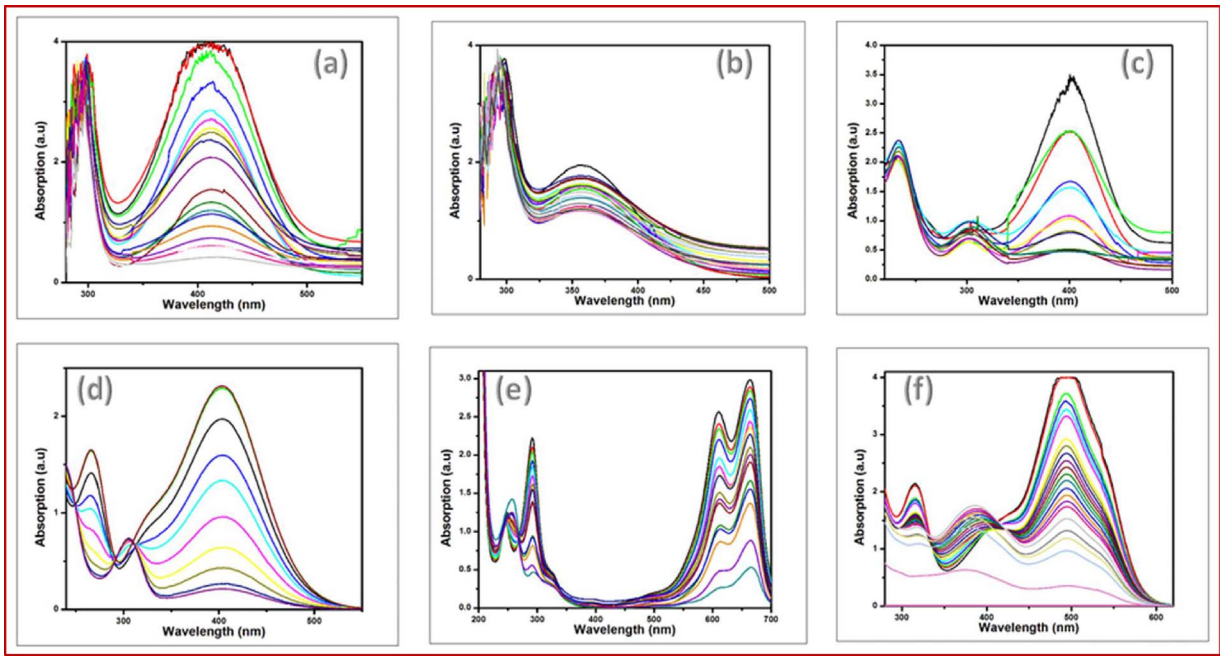

Fig. 12. UV–vis absorption spectrum for reduction reactions by nanomaterial (TCPIL/$CuFe_2O_4$/BNONS): 12a) Reduction of 2-NA to OPD 12b) Reduction of 3-NA to MPD material. 12c) Reduction of 4-NA to PPD 12d) Reduction of 4-nitro-OPD 12e) Reduction of MB dye 12f) Reduction of AR.

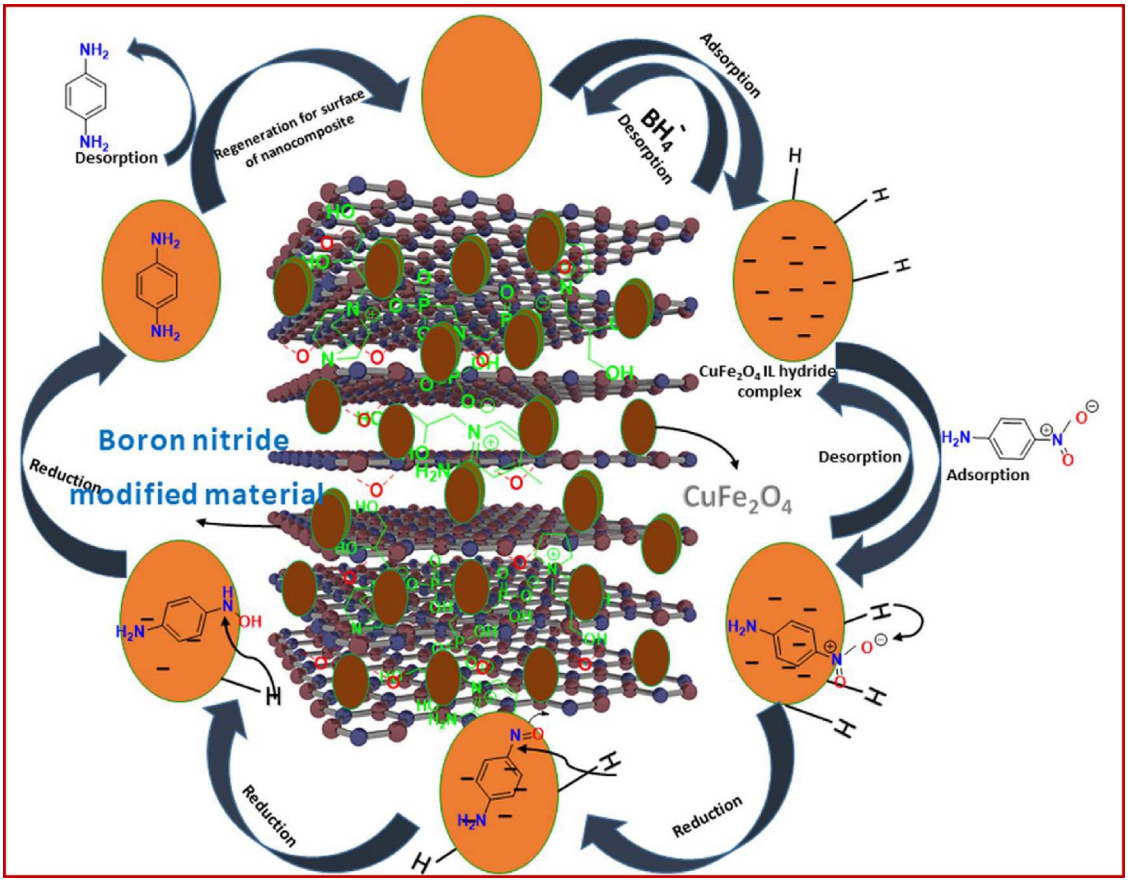

Fig. 13. Proposed mechanism for reduction of p-Nitroaniline to p-Phenylenediamine by TCPIL/$CuFe_2O_4$/BNONS nanomaterial.

catalytic activity of the nanomaterial. The catalytic activity was also compared with other BNNS supported NPs (Table ES-1). It was observed that the reduction of nitroarenes to amino-compounds using the new nanomaterial was equivalent to Pd/BNNS however the latter took a longer reaction time. The use of BNNS/Ag and Ag/BCN was reported to cause slower reduction. To show the conversion of NAs to the amino compounds, the FTIR spectrum (Figure ES-9) was elucidated for the reduction process. Although the absorption at 1400 and 1643 cm^{-1} for the nitro group were observed for the amino product, a significant increase of an additional amino group at 3460 cm^{-1} was observed

thereby confirming the reduction of 4-NA (Figure ES-9).

3.1. Chemical kinetics for reduction reaction of series of nitroanilines and dyes

The nanomaterial IL/$CuFe_2O_4$/BNO was used as an effective catalyst to reduce a series of nitroanilines and dyes as shown in Fig. 12. The progress of the reduction reaction was indicated by the gradual decrease in the intensity in the UV spectrum of each substrate. It is suggested that due to the lower band gap of $CuFe_2O_4$ NPs, the catalyst provides relatively better reduction ability. Therefore the IL most probably acts as a medium for electron movement whereas BNO and $CuFe_2O_4$ can accept as well as transfer the electrons from $NaBH_4$ to the substrate investigated at room temperature. It was observed that the reduction of 2-NA, 3-NA, 4-NA, 4-NPDA, AR and MB, in the presence of the catalyst, was completed within 80, 60, 30, 50, 40 and 120 minutes, respectively. Furthermore, by increasing the temperature of the reaction, it was observed that time decreased which indicated that the reaction occurred faster. The kinetics of the reaction was determined by varying the temperature of the reactions from 25 to 60 °C and concentration of the catalyst from 0.015 to 0.045 ml (2 mg/ml). The concentration of 2-NA, 3-NA, 4-NA, 4-NPDA, AR and MB used was 0.05 M, 0.05 M, 0.05 M, 0.05 M, 0.02 M and 0.02 M, respectively, whilst aqueous $NaBH_4$ was maintained at 0.5 M. The concentration of $NaBH_4$ was significantly higher than the concentration of NAs and dyes and it was maintained constant throughout the series of reaction. The value C/C_0, measured in terms of the relative intensity of UV–vis absorbance at the specific wavelength of the substrate was obtained. The linear correlation $\ln(C/C_0)$ or C/C_0 verses reaction time, as shown in Figs. 14–17, ES.5, ES.6, ES.7 and ES.8, demonstrates the reaction to be zero-order or pseudofirst-order with respect to series of NAs and dyes concentration [75,76]. The kinetic equation for the catalytic reduction is given by $\ln(C/C_0) = -kt$, where k is the apparent pseudofirst-order rate constant (s^{-1}), and t is the reaction time. The rate constant and activation energy of the reduction reaction at several temperature as well as different concentration of catalyst dose was computed and presented in Tables ES-2, ES-3 and ES-4. It was observed that k increased whilst increasing the dosage of the catalyst .The catalyst dosage of 0.015 ml (2 mg/ml) was minimal and it was the optimal dosage for the reduction reaction. For a quantitative comparison, the activity parameter $k_{\_} = k/M$ was introduced, and defined as the ratio of the rate constant k to the weight of the catalyst added, where M is the total mass of the catalyst added in the reaction. Thus, the reaction rate constant per unit mass was calculated as shown in Table 2.

It was observed that the reaction mixture became turbid when higher amount of catalyst was used. This is probably due to less penetration of UV light into reaction mixture and due to light scattering thereby accounting for the decrease in the rate of the reaction. Also there is a possibility that the adsorption of product on the surface of the catalyst might block the active sites of the catalyst [74].

This investigation showed that the nanomaterials produced an excellent reduction profiles for the NAs. These results suggest that an efficient electron transfer from BH_4^- anion to NAs occurs via Fermi level shift of NPs indicting its high catalytic activity [86]. Normally, efficacy of the catalyst depends on its available active surface area and number of active sites on the surface [87]. In addition, the hydride could be formed whilst the nanomaterial reacted with borohydride and this may subsequently interacted with NA molecules which might have been adsorbed onto the metal surface [88]. Furthermore, after quick reaction at the active sites, the reaction was rapidly completed whilst the product desorbed almost immediately from the surface of the nanomaterial. On comparing the NAs used, it was observed that the reduction of 4-NPDA was quicker than 4-NA followed by 3-NA then 2-NA. Interestingly, less amount of the catalyst was used in this study compared to other reported studies. These results also suggest that the amino group might contribute significantly to the reduction reaction.

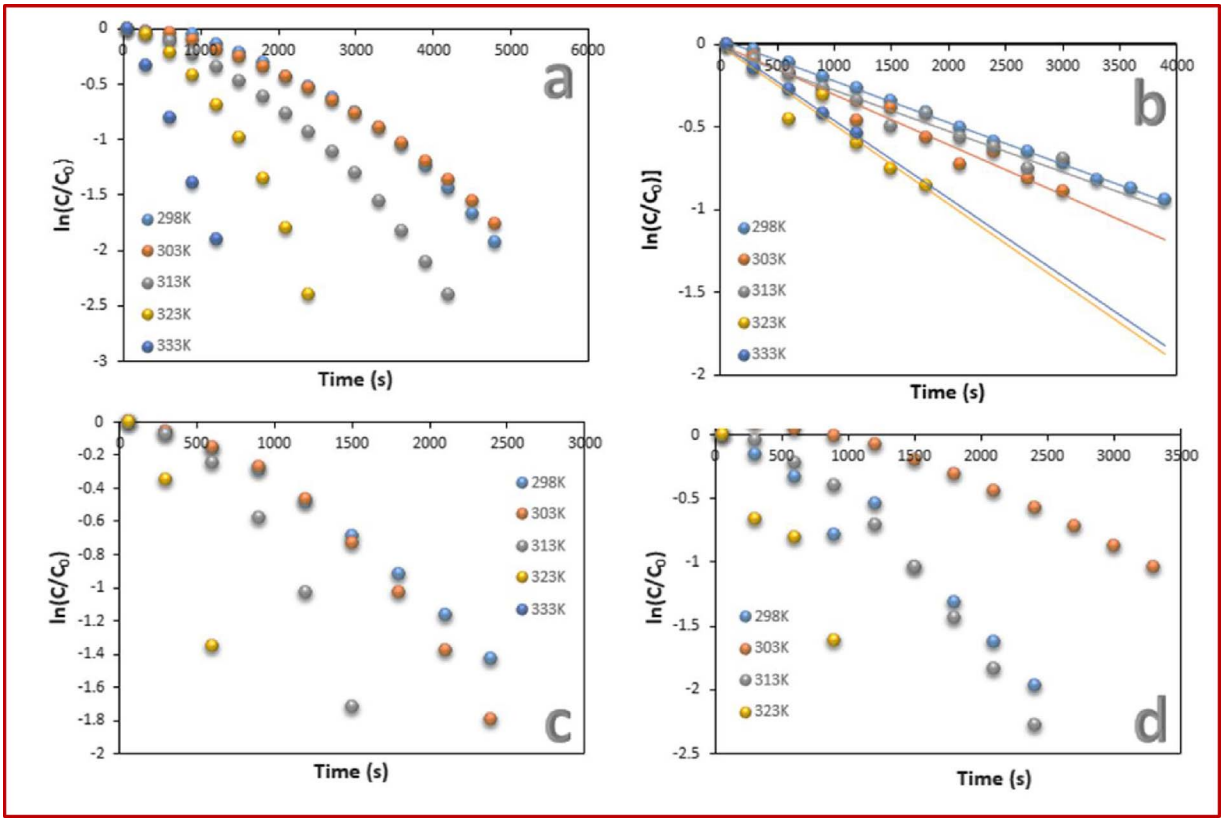

Fig. 14. Kinetic studies for reduction reaction of series of nitroanilines in presence of TCPIL/$CuFe_2O_4$/BNONS at various temperatures such as 25oC, 30oC, 40 °C, 50 °C and 60 °C: a) 2-NA. b) 3-NA c) 4-NA d) 4-NPDA.

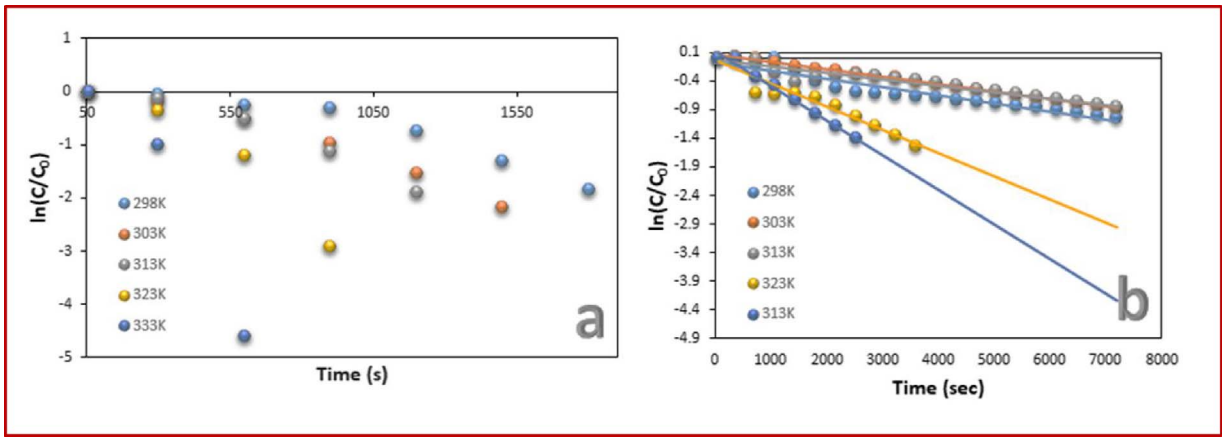

Fig. 15. Kinetic studies for reduction reaction of dyes in presence of TCPIL/$CuFe_2O_4$/BNONS at various temperatures such as 25 °C, 30 °C, 40 °C, 50 °C and 60 °C a) AR. b) MB.

Based on the position of the amino group, electron donating effect is better at the *para* and *meta* position whilst the *ortho* position takes less prominence. However 4-NPDA has an additional NH_2 group and therefore the electron donating contribution is the greatest (Table 3).

Several reports are available (Ref ES 1-3) on the catalytic reduction of NAs especially 2-NA and 4- NA however none is available for 3-NA. This is probably due to resistance of 3-NA against the action of catalyst because generally the 3-substituted position is more rigorous. However the nanomaterial was able to reduce all NAs easily thereby suggesting its stronger catalytic property. As a typical example, a plausible mechanism for the reduction of 4-NA to PPD (Fig. 13) is proposed. Herein the hydride ions derived from sodium borohydride initiates the reaction via $CuFe_2O_4$ NPs. The IL is strongly bonded among the NPs borohydride and BNONS, and this enhances the electron transitions: there is numerous cations and anions, so ionic moments occurs effectively. In this reaction initially due to some strong Van der Walls interaction, NA could be absorbed by BNONS and a high density of electrons stimulates more hydride ions for attacking nitro group for hydration. It is suggested that the formation of p-n junction among p-type $CuFe_2O_4$ NPs and thin layered n-type BNO semiconductors in the catalyst nanomaterial probably facilitates the reduction reaction by decreasing the hole and electron recombination rate. Furthermore, the hydride ion together with the electrons are easily released from BH_4^-. After the reduction reaction, desorption of PPD probably occurs rapidly hence allowing for the cycle to continue on the nanomaterial. In this mechanism, there is a sequential loss of water thereby promoting the reduction of the nitro

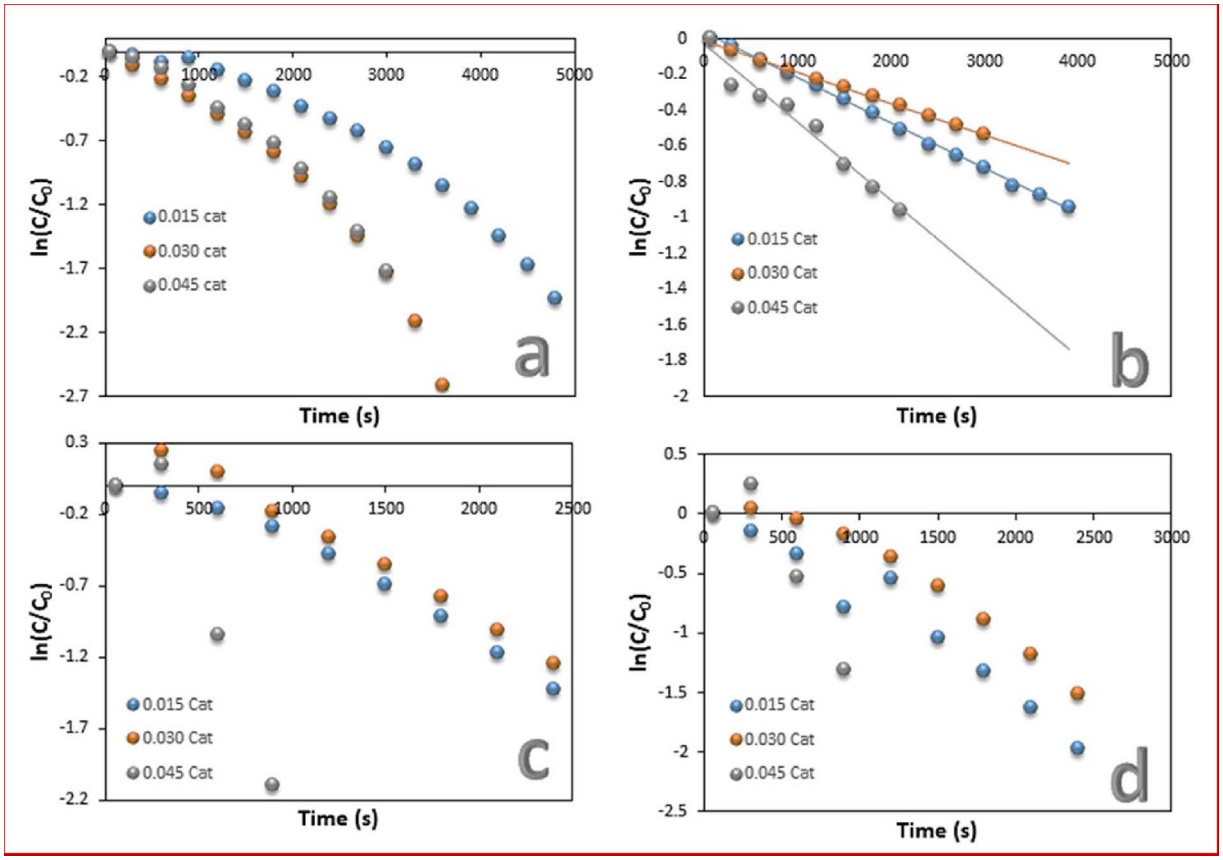

Fig. 16. Kinetic studies for reduction reaction of series of nitroanilines at various dosage of catalyst (TCPIL/$CuFe_2O_4$/BNO) such as 0.015 mL, 0.030 mL and 0.045 mL (2 mg/mL): a) 2-NA. b) 3-NA. c) 4-NA. d) 4-NPDA.

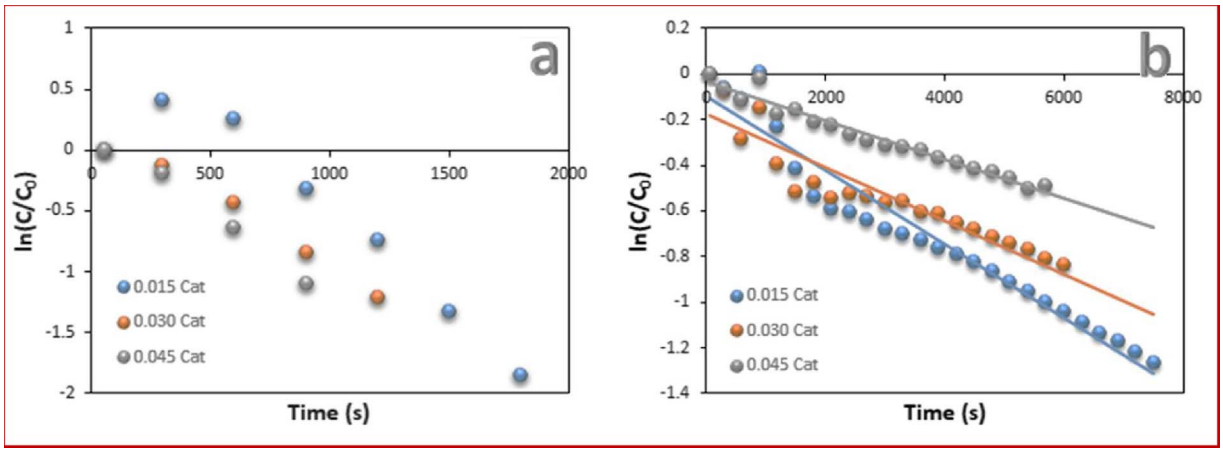

Fig. 17. Kinetic studies for reduction reaction of dyes at various dosage of catalyst (TCPIL/$CuFe_2O_4$/BNO) such as 0.015 mL, 0.030 mL and 0.045 mL (2 mg/mL): a) AR. b) MB.

Table 2
Comparison of rate constant and order of the reaction with reported catalyst.

S.NO	Catalyst	Reducing Agent	Catalyst quantity	Conversion time (in mint)	Order of the Reaction	Rate Constant (k)	Ref	Compound
1	AgNPs	$NaBH_4$	–	55	Pseudo first order	$0.1408 \times 10^{-3}\ s^{-1}$	[77]	2-NA
2	AgNPs/graphene oxide	$NaBH_4$	–	20	Pseudo first order	$0.4384 \times 10^{-3}\ s^{-1}$	[77]	2-NA
3	CuNi/Co_3O_4	$NaBH_4$	2 mg	30		$0.78 \times 10^{-3}\ min^{-1}$	[82]	2-NA
4	AgNPs/PDOP/AAOs	$NaBH_4$	–	20	Zero order	$3.4 \times 10^{-3}\ M$	[78]	2-NA
5	AgNPs	$NaBH_4$	–	20	Zero order	$2.683 \times 10^{-4}\ mim^{-1}$	[79]	2-NA
6	gold nanoparticles assisted by soapnut shells extract	$NaBH_4$	–	59	first order	$4.5 \times 10^{-2}\ k\ min^{-1}$	[80]	4-NA
7	CuNi/Co_3O_4	$NaBH_4$	2 mg	21	–	$1.71 \times 10^{-3}\ min^{-1}$	[82]	4-NA
8	AgNPs/T indica seed coat extract	$NaBH_4$	–	10	–	$6.22 \times 10^{-3}\ s^{-1}$	[81]	4-NA
9	CuNi/Co_3O_4	$NaBH_4$	2 mg	30	–	$1.26 \times 10^{-3}\ min^{-1}$	[82]	3-NA
10	$Ag_{50}Ni_{50}$/RGO nanocomposites	$NaBH_4$	–	0.2	–	$1.79 \times 10^{-4}\ s^{-1}$	[83]	3-NA
11	12.5Cu @ SBA-15	$NaBH_4$	–	8	Pseudo first order	$0.56\ min^{-1}$	[84]	MB
12	gold nanoparticles capped by salmalia malabarica gum	$NaBH_4$	–	9	Pseudo first order	$0.241\ min^{-1}$	[85]	MB
13	TCPIL/$CuFe_2O_4$/BNO	$NaBH_4$	0.015 ml (2 mg/ml)	80	Zero order	$1.93 \times 10^{-4}\ M\ s^{-1}$	This work	2-NA
14	TCPIL/$CuFe_2O_4$/BNO	$NaBH_4$	0.015 ml (2 mg/ml)	65	Pseudofirst order	$2.52 \times 10^{-4}\ s^{-1}$	This work	3-NA
15	TCPIL/$CuFe_2O_4$/BNO	$NaBH_4$	0.015 ml (2 mg/ml)	40	Zero order	$3.43 \times 10^{-4}\ M\ s^{-1}$	This work	4-NA
16	TCPIL/$CuFe_2O_4$/BNO	$NaBH_4$	0.015 ml (2 mg/ml)	40	Zero order	$3.6 \times 10^{-4}\ M\ s^{-1}$	This work	4-Nitro-2-Phenylenediamine
17	TCPIL/$CuFe_2O_4$/BNO	$NaBH_4$	0.015 ml (2 mg/ml)	120	Pseudo first order	$1.44 \times 10^{-4}\ s^{-1}$	This work	MB
18	TCPIL/$CuFe_2O_4$/BNO	$NaBH_4$	0.015 ml (2 mg/ml)	50	Zero order	$7.15 \times 10^{-4}\ M\ s^{-1}$	This work	Allura red

Table 3
Kinetic studies of rate constant, order of the reaction, ratio constant and activation energy.

S.No	Compound	Quantity of Catalyst (mg)	Order of the Reaction	Rate Constant	Ratio Constant (s^{-1} g)	Activation Energy (10^{-4} KJmol^{-1})
1	2-NA	0.3	Zero-Order	$1.93 \times 10^{-4}\ M\ s^{-1}$	0.6433	2.94
2	3-NA	0.3	Pseudofirst-Order	$2.52 \times 10^{-4}\ s^{-1}$	0.8400	1.31
3	4-NA	0.3	Zero-Order	$3.43 \times 10^{-4}\ M\ s^{-1}$	1.1433	7.74
4	4-Nitro-2-phenylenediamine	0.3	Zero-Order	$3.6 \times 10^{-4}\ M\ s^{-1}$	1.2000	1.14
5	Allura red	0.3	Zero-Order	$7.15 \times 10^{-4}\ M\ s^{-1}$	2.3833	5.96
6	Methylene blue	0.3	Pseudofirst-Order	$1.62 \times 10^{-4}\ s^{-1}$	0.5400	2.58

group. Furthermore, the nanomaterial did not show any loss in its catalytic activity even after being re-used for seven times, revealing its good reusability. It is expected that the greater catalytic performance of the TCPIL/$CuFe_2O_4$/BNONS nanomaterial can be elucidated as follows: (a) BNONS exhibit excellent physicochemical properties as that of its structural analogue, graphene and the multi heterocyclic structure of phosphonate IL enable NA to absorb via ionic interactions, resulting in a high concentration of NA near the $CuFe_2O_4$ bimetallic NPs on the surface of the BNONS (b) The small size of NPs and uniform distribution of ILs on the surface of BNONS led to an efficient catalytic reaction.

The difference of morphologies between NP and IL may be related to the oxidation-reduction potential and dosage of the copper and iron metal ions. The nanomaterial acted as a medium to relay the electrons from the donor $NaBH_4$ to the acceptor NA and dye molecule thereby facilitating the reduction reaction. Due to their greater surface area, high electron density and charge dispersion, the hydride ion, after

electron transfer to the material, approaches NAs to reduce it to PDs [89–91]. Two main parameters are important for catalytic activity of material, viz., the surface area available for electron transfer and the catalyst active sites on the surface for the electron transfer thereby removing the kinetic barrier [92].

4. Conclusions

In conclusion, a novel tri-cationic phosphonate IL, with different heterocyclic cations, was successfully synthesized and characterized. Furthermore, a partially oxidized BNONS and $CuFe_2O_4$NP were prepared and subsequently used to prepare a novel nanomaterial TCPIL/$CuFe_2O_4$/BNONS which was characterized by techniques such as FTIR, XRD, SEM, EDS, TEM, HRTEM, STEM, ED, XPS, AFM and DSC-TGA. This nanomaterial was effectively used as a heterogeneous catalyst for the efficient reduction of series of NAs to corresponding PDs, as well as for AR and MB. From kinetic studies, the rate constant, order of the reaction, constant ratio and activation energy was computed. Furthermore kinetic studies at various temperatures showed that an increase in temperature speeded the reaction whilst by increasing the amount of catalyst the reaction also occurred faster. The recovery and reusability (see Figure ES-10) of the nanomaterial is simple and performs well in aqueous solution, without heating or reducing agent and without the use of any special equipment. Moreover, it is possible to make different nanomaterials by combining different d-block metals such Zn, Pd, Pt and Mn with BNONSs for potential applications in biomedical, sensors and catalytic fields.

Acknowledgements

Mr. Vasanthakumar Arumugam is grateful to the National Research Foundation of the Innovation Doctoral Scholarship (Grant no: 101117 & 109839) for financial support and Durban University of Technology for providing a good environment and laboratory facilities for this work. Special thanks to Dr. T Singh, Department of Chemistry, Durban University of Technology for assisting with the kinetic studies aspects.

Note: This work is pending a patent.

Appendix A. Supplementary data

Supplementary data associated with this article can be found, in the online version, at http://dx.doi.org/10.1016/j.apcatb.2017.08.059.

References

[1] J.P. Hallett, T. Welton, Chem. Rev. 111 (2011) 3508–3576.
[2] T. Welton, Chem. Rev. 99 (1999) 2071–2083.
[3] M. Armand, F. Endres, D.R. MacFarlane, H. Ohno, B. Scrosati, Nat. Mater. 8 (2009) 621–629.
[4] B.H. Xu, J.Q. Wang, J. Sun, Y. Huang, J.P. Zhang, X.P. Zhang, S.J. Zhang, Green Chem. 17 (2015) 108–122.
[5] G. Fiorani, W. Guo, A.W. Kleij, Green Chem. 17 (2015) 1375–1389.
[6] W.E.S. Hart, J.B. Harper, L. Aldous, Green Chem. 17 (2015) 214–218.
[7] M. Taha, A.M.R. lmeida, F.A.E. Silva, P. Domingues, S.P.M. Ventura, J.A.P. Coutinho, M.G. Freire, J. Chem. Eur. 21 (2015) 4781–4788.
[8] J.W. Comerford, I.D.V. Ingram, M. North, X. Wu, Green Chem. 17 (2015) 1966.
[9] A. Taheri, B. Lai, C. Cheng, Y. Gu, Green Chem. 17 (2015) 812.
[10] S. Zhang, K. Dokko, M. Watanabe, Chem. Sci. 6 (2015) 3684.
[11] G. Godeau, L. Navailles, F. Nallet, X. Lin, T.J. McIntosh, M.W. Grinstaff, Macromolecules 45 (2012) 2509–2513.
[12] M. Wathier, M.W. Grinstaff, Macromolecules 43 (2010) 9529–9533.
[13] M. Wathier, M.W. Grinstaff, J. Am. Chem. Soc. 130 (2008) 9648–9649.
[14] G. Kamath, G.A. Baker, RSC Adv. 3 (2013) 8197–8202.
[15] J. Luo, N. Zhang, R. Liu, X. Liu, RSC Adv. 4 (2014) 64816–64824.
[16] Y. Mo, Y. Wan, A. Chau, F. Huang, Sci. Rep. 4 (2014) 1–8.
[17] A. Marimuthu, J. Zhang, S. Linic, Science 339 (2013) 1590–1593.
[18] J. Wang, K. Wang, F.B. Wang, X.H. Xia, Nat. Commun. 5 (2014) 1–9.
[19] A.M. Hengne, C.V. Rode, Green. Chem. 14 (2012) 1064–1072.
[20] A. Fornara, P. Johansson, K. Petersson, S. Gustafsson, J. Qin, E. Olsson, D. Ilver, A. Krozer, M. Muhameed, C. Johansson, Nano Lett. 8 (2008) 3423–3428.
[21] R.S. Singh, R.Y. Tay, W.L. Chow, S.H. Tsang, G. Mallick, E.H.T. Teo, Appl. Phys. Lett. 104 (2014) 163101.
[22] L.H. Li, J. Cervenka, K. Watanabe, T. Taniguchi, Y. Chen, ACS Nano 8 (2014) 1457–1462.
[23] A. Pakdel, C. Zhi, Y. Bando, D. Golberg, Mater. Today 15 (2012) 256–265.
[24] W. Lei, D. Portehault, D. Liu, S. Qin, Y. Chen, Nat. Commun. 4 (2013) 1–7.
[25] I. Jo, M.T. Pettes, J. Kim, K. Watanabe, T. Taniguchi, Z. Yao, L. Shi, Nano. Lett. 13 (2013) 550–554.
[26] G.H. Yang, J.J. Shi, S. Wang, W.W. Xiong, L.P. Jiang, C. Burda, J.J. Zhu, Chem. Commun. 49 (2013) 10757–10759.
[27] X. Chen, W. Zang, K. Vimalanathan, K.S. Iyer, C.L. Raston, Chem. Commun. 49 (2013) 1160–1162.
[28] C. Huang, C. Chen, X. Ye, W. Ye, J. Hu, C. Xu, X. Qiu, J. Mater Chem A 1 (2013) 12192–12197.
[29] X. Wang, G. Meng, C. Zhu, Z. Huang, Y. Qian, K. Sun, X. Zhu, Adv. Funct. Mater 23 (2013) 5771–5777.
[30] C. Huang, W. Ye, Q. Liu, X. Qiu, ACS Appl. Mat. Interfaces 6 (2014) 14469–14476.
[31] Q. Fu, Y. Meng, Z. Fang, Q. Hu, L. Xu, W. Gao, X. Huang, Q. Xue, Y.P. Sun, F. Lu, ACS Appl. Mater. Interfaces 9 (2017) 2469–2476.
[32] Y. Guo, W. Guo, Phys. Chem. Chem. Phys. 17 (2015) 16428–16433.
[33] J. Wu, L. Yin, ACS Appl. Mater. Interfaces 3 (2011) 4354–4362.
[34] H. Shen, C. Duan, J. Guo, N. Zhao, J. Xu, J. Mater Chem A 3 (2015) 16663–16669.
[35] Y. Lin, C.E. Bunker, K.A.S. Fernando, J.W. Connell, ACS Appl. Mater. Interfaces 4 (2012) 1110–1117.
[36] S. Dutta, C. Ray, S. Sarkar, M. Pradhan, Y. Negishi, T. Pal, ACS Appl. Mater. Interfaces 5 (2013) 8724–8732.
[37] L. Pan, Y.T. Liu, X.M. Xie, X.D. Zhu, J. Chem Asian 9 (2014) 1519–1524.
[38] X. Huang, B. Zheng, Z. Liu, C. Tan, J. Liu, B. Chen, H. Li, J. Chen, X. Zhang, Z. Fan, W. Zhang, Z. Guo, F. Huo, Y. Yang, L. Xie, W. Huang, H. Zhang, ACS Nano 8 (2014) 8695–8701.
[39] M. Srivastava, A.K. Das, P. Khanra, M.E. Uddin, N.H. Kim, J.H. Lee, J. Mater Chem A 1 (2013) 9792–9801.
[40] W. Wang, J. Gu, W. Hua, X. Jia, K. Xi, Chem. Commun. 50 (2014) 8889–8891.
[41] M. Ayan-Varela, M.J. Fernandez-Merino, J.I. Paredes, S. Villar-Rodil, C. Fernandez-Sanchez, L. Guardia, A. Martınez-Alonso, J.M.D. Tascon, J. Mater Chem A 2 (2014) 7295–7305.
[42] J.J. Lv, A.J. Wang, X. Ma, R.Y. Xiang, J.R. Chen, J.J. Feng, J. Mater Chem A 3 (2015) 290–296.
[43] Y. Yan, B. Xia, Z. Xu, X. Wang, ACS Catal. 4 (2014) 1693–1705.
[44] G.H. Gao, A. Mathkar, E.P. Martins, D.S. Galvao, D.Y. Gao, P.A.D. Autreto, C.J. Sun, L.T. Cai, P.M. Ajayan, J. Mater Chem A 2 (2014) 3148–3154.
[45] W. Shao, X. Liu, H. Min, G. Dong, Q. Feng, S. Zuo, ACS Appl. Mater. Interfaces 7 (2015) 6966–6973.
[46] C. Zhi, N. Hanagata, Y. Bando, D. Golberg, J. Chem Asian 6 (2011) 2530–2535.
[47] R.J. Smith, P.J. King, M. Lotya, C. Wirtz, U. Khan, S. De, A. O'Neill, G.S. Duesberg, J.C. Grunlan, G. Moriarty, J. Chen, J. Wang, A.I. Minett, V. Nicolosi, J.N. Coleman, Adv. Mater. 23 (2011) 3944–3948.
[48] J.L. Li, K.N. Kudin, M.J. McAllister, R.K. Prud'hommed, A.A. Aksay, R. Car, Phys. Rev. Lett. 96 (2006) 176101.
[49] A. Ying, Z. Li, J. Yang, S. Liu, S. Xu, H. Yan, C. Wu, J. Org. Chem. 79 (2014) 6510–6516.
[50] R. Hudson, Y. Feng, R.S. Varma, A. Moores, Green Chem. 16 (2014) 4493–4505.
[51] A. Schejn, T. Mazet, V. Falk, L. Balan, L. Aranda, G. Medjahdi, R. Schneider, Dalton Trans. 44 (2015) 10136–10140.
[52] S. Kotake, T. Hasegawa, K. Kamiya, Y. Suzuki, T. Masui, Y. Kangawa, Appl. Surf. Sci. 216 (2003) 72–77.
[53] S. Palaniappan, B. Boddula, B. Ravi, J. Appl Polym S.C.I. 130 (2013) 2995–3000.
[54] C.Y. Zhi, Y. Bando, C.C. Tang, D. Golberg, Appl. Phys. Lett. 86 (2005) 213110.
[55] J. Yu, Z. Zheng, H.C. Ong, K.Y. Wong, S. Matsumoto, W.M. Lau, J. Phys Chem B 110 (2006) 21073–21076.
[56] A.L.M. Reddy, A.E. Tanur, G.C. Walker, Int. J. Hydrogen Energy. 35 (2010) 4138–4143.
[57] F. Guo, Y.H. Ni, Y. Ma, N.N. Xiang, C. Liu, New J. Chem. 38 (2014) 5324–5330.
[58] Z.H. Farooqi, K. Naseem, R. Begum, A. Ijaz, J. Inorg. Organomet. Polym. Mater. 25 (2015) 1554–1568.
[59] K. Li, Z. Zheng, X. Huang, G. Zhao, J. Feng, J. Zhang, J. Hazard. Mater. 166 (2009) 213–220.
[60] Z. Dong, X. Le, X. Li, W. Zhang, C. Dong, J. Ma, Appl. Catal. B 158-159 (2014) 129–135.
[61] S. Gazi, R. Ananthakrishnan, Appl. Catal. B 105 (2011) 317–325.
[62] L. Li, Y. Feng, Y. Liu, B. Wei, J. Guo, W. Jiao, Z. Zhang, Q. Zhang, Appl. Surf. Sci. 363 (2016) 627–635.
[63] S.M. El-Sheikh, A.A. Ismail, J.F. Al-Sharab, New J. Chem. 37 (2013) 2399–2407.
[64] N.M. Patil, T. Sasaki, B.M. Bhanage, ACS Sustainable Chem. Eng. 4 (2) (2016) 429–436.
[65] R.N. Muthu, S. Rajashabala, R. Kannan, Renew. Energy. 85 (2016) 387–394.
[66] V. Linss, S. Rodilb, P. Reinkec, M. Garnierd, P. Oelhafend, U. Kreissige, F. Richtera, Thin Solid Films. 467 (2004) 76–87.
[67] M.A. Mannan, M. Nagano, T. Kida, N. Hirao, Y. Baba, J. Phys. Chem. Solids. 7 (2009) 20–25.
[68] S.Y. Kim, J. Park, H.C. Choi, J.P. Ahn, J.Q. Hou, H.S. Kang, J. Am. Chem. Soc. 129 (2007) 1705–1716.
[69] F.L. Huang, C.B. Cao, X. Xiang, R.T. Lv, H.S. Zhu, Mater 13 (2004) 1757–1760.
[70] J. Gao, P.K. Chow, A.V. Thomas, T.M. Lu, T. Borca-Tasciuc, N. Koratkar, Appl. Phys. Lett. 105 (2014) 123108.
[71] Y. Lin, J.W. Connell, Nanoscale 4 (2012) 6908–6939.

[72] M.A.A. Ahmed, S.R. Torati, C. Kim, Nanoscale 7 (2015) 12192–12204.
[73] K. Bahar, B. Maryam, N. Mahmoud, L Achillea millefolium, Journal of Colloid and Interface Science 493 (2017) 85–93.
[74] T. Zeng, H. Niu, Y. Ma, W. Li, Y. Cai, Appl Catal. B: Environ. 134–135 (2013) 26–33.
[75] H. Gu, J. Wang, Y. Ji, Z. Wang, W. Chen, G. Xue, J. Mater. Chem. A 1 (2013) 12471–12477.
[76] W. Hu, B. Liu, Q. Wang, Y. Liu, Y. Liu, P. Jing, S. Yu, L. Liu, J. Zhang, Chem. Commun. 49 (2013) 7596–7598.
[77] Y. Zhang, X. Yuan, Y. Wang, Y. Chen, J. Mater. Chem. 22 (2012) 7245–7251.
[78] B. Celen, D. Ekiz, E. Piskin, G. Demirel, J. Mol. Catal. A: Chem. 350 (2011) 97–102.
[79] T.V. Thu, P.J. Ko, N.H.H. Phuc, A. Sandhu, J. Nanopart. Res. 15 (2013) 1975.
[80] V. Reddy, R.S. Torati, S. Oh, C. Kim, Industrial & Engineering Chemistry Research 52 (2) (2013) 556–564.
[81] T.N.J.I. Edison, M.G. Sethuraman, Y.R. Lee, Research on Chemical Intermediates 42 (2) (2016) 713–724.
[82] P. Deka, R. Choudhury, R.C. Deka, P. Bharali, R.S.C Advances 6 (75) (2016) 71517–71528.
[83] R. Dhanda, M. Kidwai, J. Mat Chem A. 3 (38) (2015) 19563–19574.
[84] B.K. Ghosh, S. Hazra, B. Naik, N.N. Ghosh, Powder Technology 269 (2015) 371–378.
[85] B.R. Ganapuram, M. Alle, R. Dadigala, A. Dasari, V. Maragoni, V. Guttena, International Nano Letters 5 (4) (2015) 215–222.
[86] M. Jakob, H. Levanon, NanoLett. 3 (2003) 353–358.
[87] D. Huang, X. Bai, L. Zheng, J. Phys Chem C. 115 (2011) 14641–14647.
[88] Q. Zhou, G. Qian, Y. Li, G. Zhao, Y. Chao, J. Zheng, Thin Solid Films. 516 (2008) 953–956.
[89] M. Kumar, S. Deka, ACS Appl. Mater. Interfaces. 6 (2014) 16071–16081.
[90] X. Du, J. He, J. Zhu, L. Sun, S. An, Applied Surface Science. 258 (2012) 2717–2723.
[91] B. Naik, S. Hazra, V.S. Prasad, N.N. Ghosh, Catal. Commun. 12 (2011) 1104–1108.
[92] S. Kundu, M. Jayachandran, RSC Adv. 3 (2013) 16486–16498.

Nano-material as an excellent catalyst for reducing a series of nitroaniline and dyes: triphosphonated ionic liquid- $CuFe_2O_4$-modified boron nitride

Vasanthakumar Arumugam[a], Pavithra Sriram[b], Ta-Jen Yen[b], Gyanasivan Govindsamy Redhi[a], Robert Moonsamy Gengan[a*]

[a]*Department of Chemistry, Faculty of Applied Science, Durban University of Technology, Durban. South Africa*

[b]*Department of Materials Science and Engineering, National Tsing Hua University, Hsinchu 30013, Taiwan, R.O.C*

Corresponding Author: R. M. Gengan

Tel.: +27 031 373 2903

E-mail: genganrm@dut.ac.za

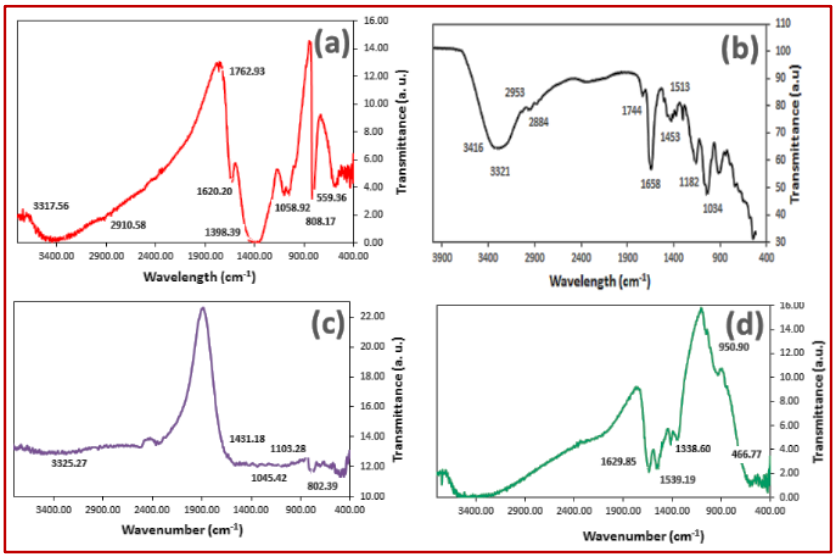

Fig. ES-1: FTIR spectra of PTCIL/$CuFe_2O_4$/BNONS nanomaterial (a), $CuFe_2O_4$ nanoparticles (b) partially oxidized h-BNONS (c).

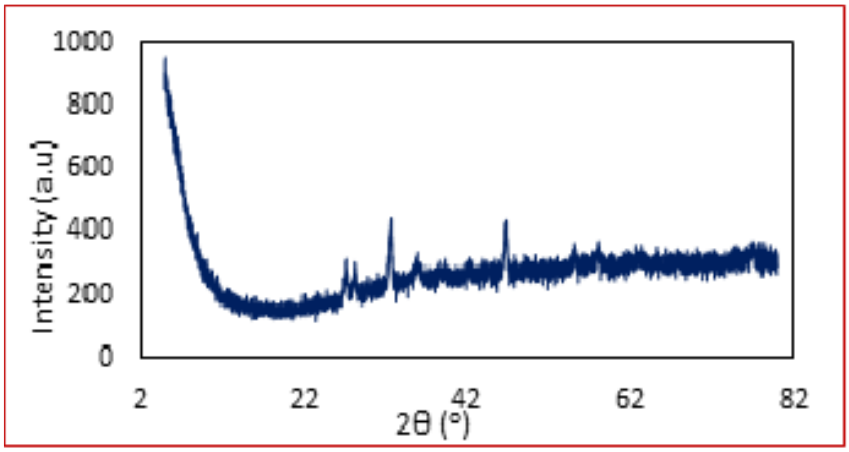

Fig. ES-2: Shows the XRD spectrum of PTCIL/$CuFe_2O_4$/BNONS nanomaterial.

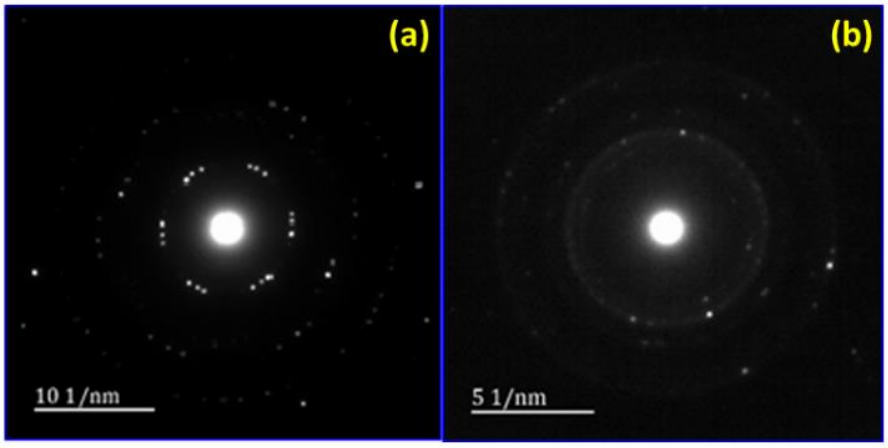

Fig. ES-3: The lattice spacing distance determined for PTCIL/$CuFe_2O_4$/BNONS nanomaterial (a) and Cu nanoparticles (b).

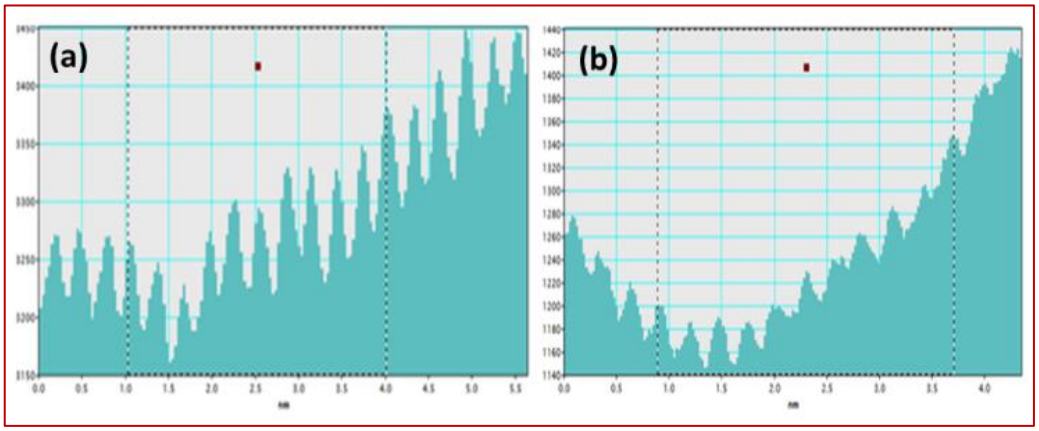

Fig. ES-4: Electron diffraction images for the PTCIL/$CuFe_2O_4$/BNONS nanomaterial (a) and Cu ferrite nanoparticle (b).

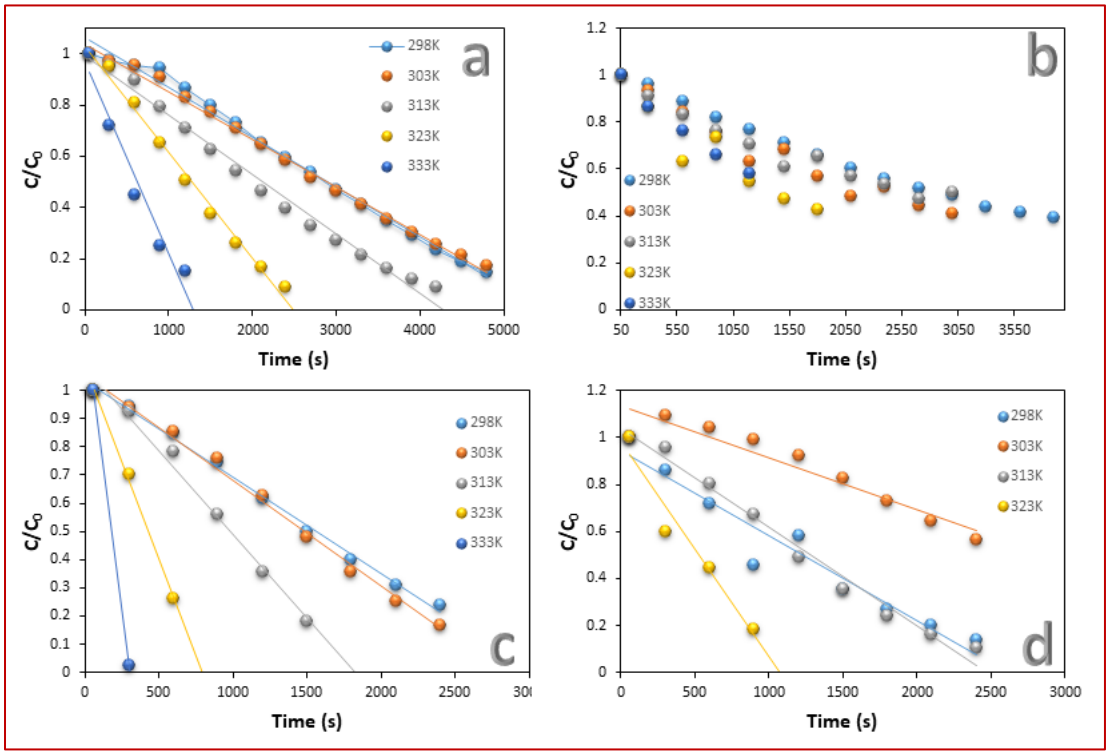

Fig ES- 5.: Kinetics studies of reduction reactions at various temperatures, the graph C/C_0 verse time a) 2-NA, b) 3-NA, c) 4-NA, d) 4-NPDA

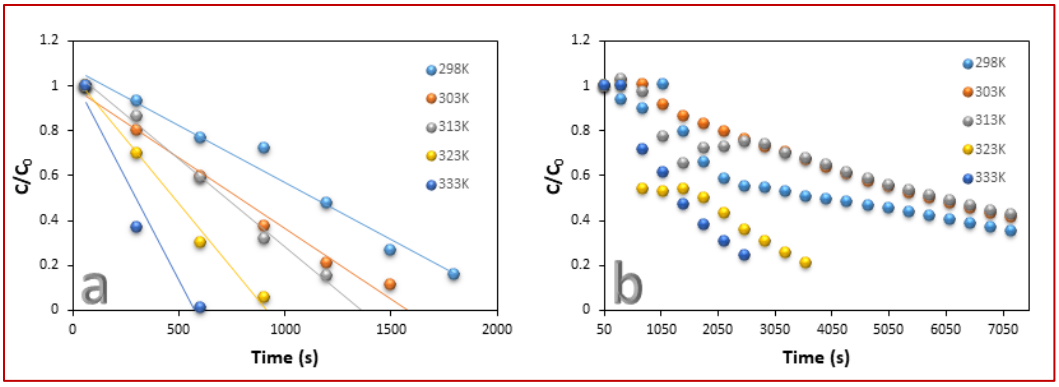

Fig ES- 6.: Kinetics studies of reduction reactions at various temperatures, the graph C/C_0 verse time a) Allura red, b) Methylene blue

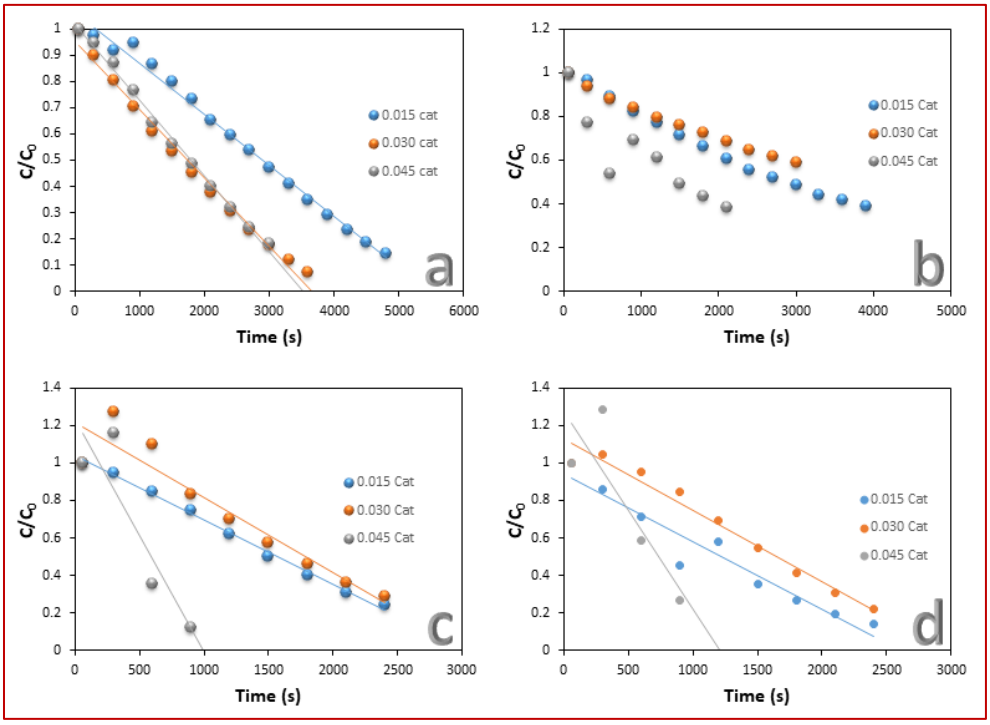

Fig ES- 7.: Kinetics studies of reduction reactions at various dosage of catalyst, the graph C/C_0 verse time a) 2-NA, b) 3-NA, c) 4-NA, d) 4-NPDA

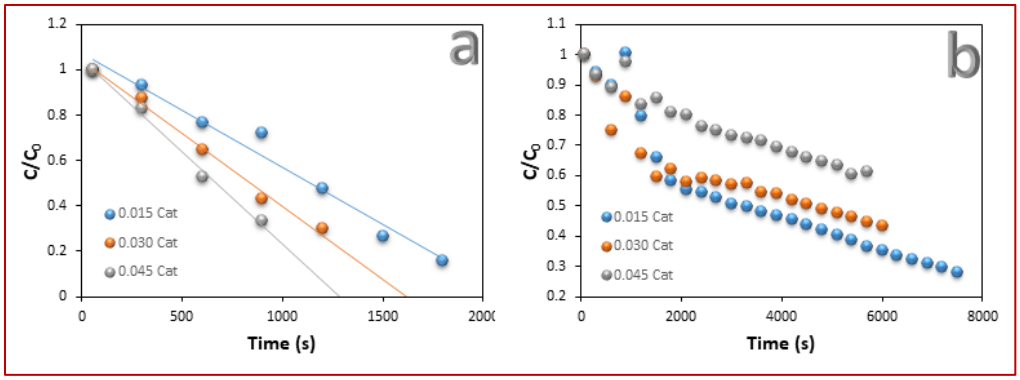

Fig ES- 8.: Kinetics studies of reduction reactions at various dosage of catalyst, the graph C/C_0 verse time a) Allura red,

1

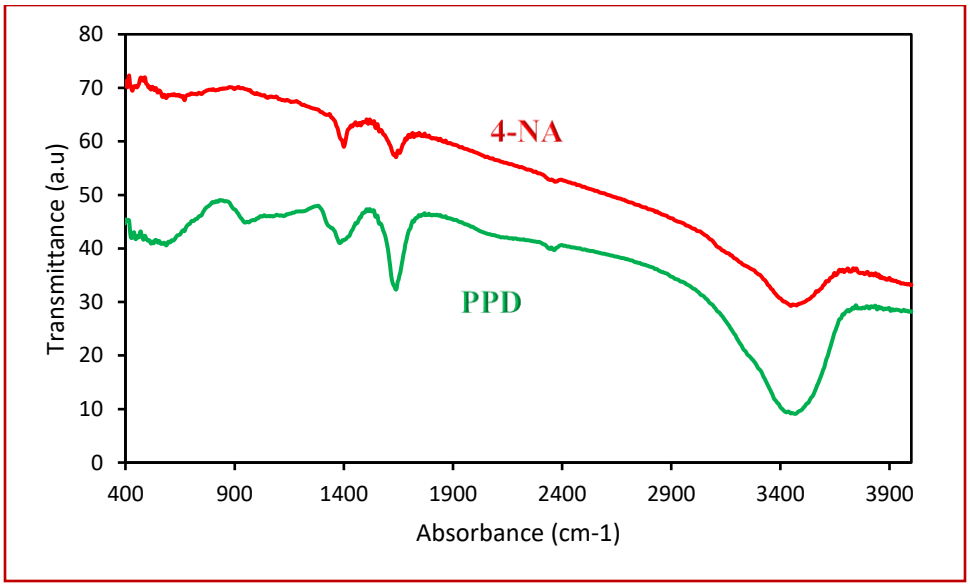

Fig. ES-9: FTIR spectrum for the 4-nitroaniline and reduction of (a-h) 1.0 mm 4-nitro aniline by the PTCIL/$CuFe_2O_4$/BNONS nanomaterial.

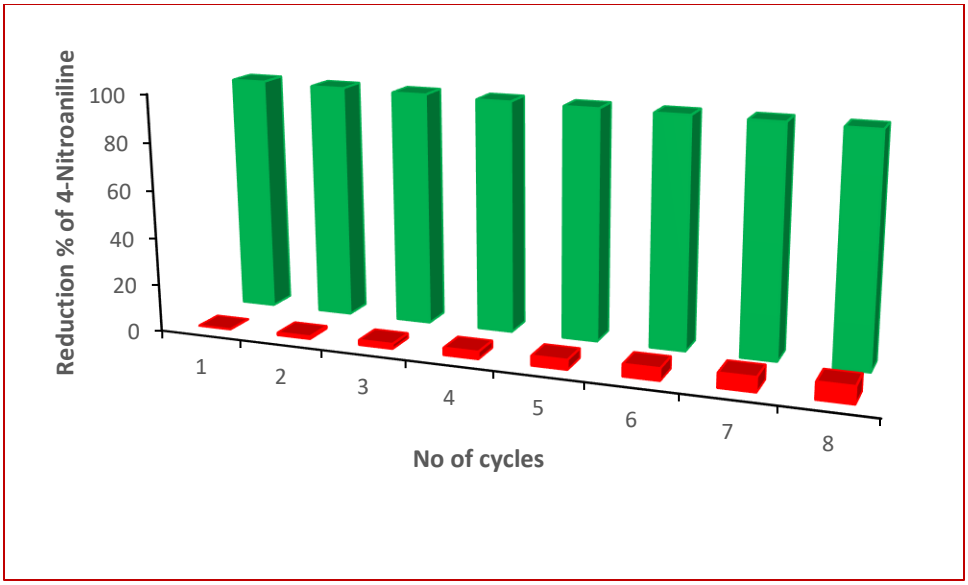

Fig. ES-10: Recycle and reusability graph for the reduction of (a-h) 1.0 mm 4-nitro aniline by the PTCIL/$CuFe_2O_4$/BNONS nanomaterial.

Table. ES-1 Catalytic performance of different boron nitride based catalysis

Catalyst	Time in (h)	Conversion	Reference
BNNS/Ag	0.10	95	1
Pd/BNNS	1.00	100	2
Ag/BCN	0.06	96	3
PTCIL/$CuFe_2O_4$/BNONS	0.14	100	Current work

Table ES-2: Rate constant of reduction reactions at various temperatures.

Compounds	*Rate Constant*				
	298 K	*303 K*	*313 K*	*323 K*	*333 K*
2-NA	1.93E-04	1.87E-04	2.32E-04	4.15E-04	7.49E-04
3-NA	2.52E-04	3.03E-04	2.46E-04	4.78E-04	4.70E-04
4-NA	3.43E-04	3.77E-04	5.94E-04	1.37E-03	4.06E-03
4-NPDA	3.60E-04	2.37E-04	4.19E-04	-	-
AR	7.15E-04	6.27E-04	7.80E-04	1.15E-03	1.81E-03
MB	1.44E-04	1.30E-04	1.11E-04	4.06E-04	6.04E-04

Table ES-3: Activation of reduction reactions at several temperatures.

Compounds	*Activation Energy*				
	298K	*303K*	*313K*	*323K*	*333K*
2-NA	3.70E-03	3.58E-03	4.45E-03	7.94E-03	1.43E-02
3-NA	4.83E-03	5.80E-03	4.72E-03	9.16E-03	9.00E-03
4-NA	6.57E-03	7.21E-03	1.14E-02	2.63E-02	7.77E-02
4-NPDA	6.90E-03	4.55E-03	8.03E-03	-	-
AR	1.37E-02	1.20E-02	1.49E-02	2.19E-02	3.46E-02
MB	2.75E-03	2.49E-03	2.12E-03	7.78E-03	1.16E-02

Table ES-4: Catalytic dosage at various quantity in reduction reactions

Compounds	*Rate Constant*			*Activation Energy*		
	0.015 cat	*0.030 cat*	*0.045*	*0.015 cat*	*0.030 cat*	*0.045 cat*
2-NA	1.93E-04	2.60E-04	2.89E-04	3.70E-03	4.98E-03	5.53E-03
3-NA	2.52E-04	1.35E-04	2.48E-04	4.83E-03	2.59E-03	4.76E-03
4-NA	3.43E-04	3.87E-04	1.24E-03	6.57E-03	7.41E-03	2.38E-02
4-NPDA	3.60E-04	3.79E-04	1.10E-03	6.90E-03	7.26E-03	2.11E-02
AR	5.06E-04	6.43E-04	8.15E-04	9.69E-03	1.23E-02	1.56E-02
MB	1.44E-04	1.16E-04	8.49E-05	2.75E-03	2.23E-03	1.63E-03

References:

1, Shen, H.; Duan, C.; Guo, J. Zhao, N.; Xu, J. Facile in situ synthesis of silver nanoparticles on boron nitride nanosheets with enhanced catalytic performance. *J. Mater. Chem. A*, **2015**, 3, 16663.

2, Sun, W.; Meng, Y.; Fu, Q.; Wang, F.; Wang, G.; Gao, W.; Huang, X-C.; Lu. F. High-Yield Production of Boron Nitride Nanosheet and Its Uses as a Catalyst Support for Hydrogenation of Nitroaromatics. *ACS Appl. Mater. Interfaces,* Just Accepted Manuscript • DOI: 10.1021/acsami.6b01008. **2016**,

3, Qiu, X.; Liu, Q.; Song, M.; Huang, C. Hydrogenation of nitroarenes into aromatic amines over Ag@BCN colloidal catalysts. *Journal of Colloid and Interface Science*, **2016**, 477, 131-137.

12.2 Critical review for 5th Publication

Nano-material as an excellent catalyst for reducing a series of nitroanilines and dyes: triphosphonated ionic liquid- $CuFe_2O_4$-modified boron nitride.

This research article describes the synthesis of a novel 4th generation multi-ionic IL-bonded copper ferrite magnetic nanoparticles decorated, partially oxidized h-boron nitride nanomaterial, its characterization and use as effective catalyst for the reduction of a series of nitroanilines. This class of 4th generation IL, which was synthesized for the first time, certainly provides hope for researchers wishing to synthesize different ILs in future. Initially, the synthetic part of this work was long, since three unique first step ILs were needed for synthesis of the novel 4th generation tri-cationic phosphonate IL (TCPIL). First of all synthesis of the three different ILs namely as $[DABCO\text{-}PDOL]^+[Cl]^-$, $[APIC\text{-}PDOL]^+[Cl]^-$ and $[PYR\text{-}PDOL]^+[Cl]^-$ was undertaken and therefore characterized with FTIR, ^1H NMR, ^{13}C NMR and elemental analyses. Another important aspect was the synthesis of novel TCPILs, which contains DABCO, 2-amino picoline, and 2-oxopyrrolidinium cations coordinated with aminotris (methylene phosphonic acid) (ATMP) based anions. The above synthesized ILs were joined together with the help of ATMP-like triphosphonates replacing the three chloride anions from those ILs. The synthesized novel TCPIL $\{[DABCO, PYR, APY\text{-}PDO]^+[ATMP]^-\}$ was characterized using FTIR, ^1H NMR, ^{13}C NMR and ^{31}P NMR techniques to confirm the chemical structure of the IL.

Graphene-like layered h-boron nitride (h-BN) nanosheet material was modified using some oxidizing chemicals in different ratios to get h-boron nitride modified partially oxidized h-BN. This is first time that this material has been reported for making a nanocomposite. These types of h-BN surface modified partially oxidized materials have more hetero atoms such as B, N and O and therefore they could help to create better bonds with other materials. The method of preparation of this material was developed from the method which is used to synthesize graphene oxide from graphite. The reason is that both are from a similar class of structures however h-BN is more stable than graphene, therefore the method was modified. The oxidation processes create a new interaction among the oxygen and B-N bonds and also reduces the electron cloud around the B-N atoms. The FTIR, XRD and Raman spectroscopy techniques were used to identify the modified h-boron nitride oxide material. These spectra showed new peaks compared to normal h-BN spectra. Furthermore, the texture and physical nature of the modified h-boron nitride partially oxidized material was different from the normal h-BN. The morphological changes were occurred

in the BNONS, for example, the nano layers or sheets were perpendicularly arranged. Additionally, these arrangements gave a specific space for the nanoparticles, so that, this will be helpful for their stability of the material and IL also support for thermostability, due to increasing in surface area of the catalytic activity further increases.

The heterocyclic compounds, organic moieties and substituted functional group of propanediol could help the IL to enhance its efficacy and interaction or bonding with BNONS and magnetic nanoparticles. Consequently, the cations and anions in the IL were catalytically active in nature. Generally, iron oxide magnetic nanoparticles alone has a good catalytic activity but the influence of the copper metal, further enriches its efficacy, Finally, $CuFe_2O_4$ NPs display significant catalytic activity. The synthesized IL was perfectly coated with $CuFe_2O_4$ NPs, and therefore copper and iron atoms interacted strongly with the phosphonate groups due to their metallic charges, ionic interaction and the extraordinary chelating power of the phosphonate groups in the IL. The resulting intermediated composition of the IL with bimetallic nanoparticles was further reacted with partially oxidized h-boron nitride modified material to fulfil the nanomaterial. This nanomaterial has good physical and chemical properties and of course outstanding catalytic efficiency as well. Characterization of the nanomaterial established which functional groups are present, element identification, chemical composition and morphological information.

The more active organic compounds such as DABCO, N-methyl-2-oxopyrrolidine and 2-amino picoline were used as cations with triphosphonate as an anion in this composition with the IL. Hence as expected, hypothetically it is more catalytically efficient. Finally, the three active environmental friendly materials were used to synthesize the novel nanomaterial. The inorganic $CuFe_2O_4$, TCPIL containing organic functional group compounds and surface functionalized BNONS modified materials were synthesized to produce this amazing nanocomposite material.

Characterization is very important since it can be explain the actual nature of the material, physical characterization, surface morphology and activity of the material, and will decide the application of this nanomaterial. FTIR identifies the functional groups which are present in the nanomaterial and furthermore it confirms the presence of the IL in the synthesized nanomaterial. EDS is one of the important techniques used to identify the elements and chemical composition of the nanomaterial and additionally confirms the presence of IL in this nanomaterial. The morphological information was obtained by SEM, TEM, and HRTEM techniques. This information provides

details about how the nanoparticles arrange or spread over the BNONS and the nanosheets of BNONS positions and their arrangements in the nanomaterial. In STEM, identification of the Cu and Fe metallic elements in the nanomaterial via bright and dark field investigated images was revealed. XPS is one of the most important techniques used to examine the bonding, for instance C-C, C-N, and C-P like that which is present in the nanocomposite. XRD clearly shows the crystalline natures and oxides of iron of the nanomaterial. In general, the h-BN nanomaterials have thin sheets with less than 8-10 layers and the lateral size of the nanosheets range from 1.5 to 2 μm. The AFM images of PTCIL/$CuFe_2O_4$/BNONS were obtained with different height profiles (50 nm and 500 nm). The height profile of the nanosheets revealed that they have multilayered nanosheets and their thickness was approximately ~2.5 nm. It was reported that there were no wrinkles on the surfaces of the CVD-grown BNONS even after transferring to the substrate.

The catalytic activity of the nanocomposite (PTCIL/$CuFe_2O_4$/BNONS) was determined by the reduction of a series of nitroanilines such as 2-NA, 3-NA, 4-NA and 4-nitro-2-diamino benzene to corresponding amine derivatives with $NaBH_4$ in aqueous solution at room temperature. The concentration of electrons in the nanomaterial was high and it contains IL, so it could provide support for the movement of the electrons in the nanomaterial. The $NaBH_4$ alone only slightly reduces 4-NA probably only reduced by a negligible percentage of 3 to 5 % even after one day. The electron transfer was prohibited from donor $NaBH_4$ to acceptor NA by some kinetic barrier. The catalytic activity of the prepared TCPIL/$CuFe_2O_4$/BNONS nanomaterial was evaluated for the reduction of 4-NA to 1,4-diamino benzene in the presence of $NaBH_4$. The typical absorption peaks of 2-NA to 1,2-diamino benzene at around 410 nm and 240 nm, 3-NA to 1,3-diamino benzene at around 360 nm as well as 300 nm, 4-NA and 1,4-diamino benzene at 380 nm and 240 nm and 2-nitro-3, 4-diamino benzene to 2, 3, 4-triaminobenzene were monitored. The absorption of methylene blue at 300 nm, 600 nm as well as 680 nm and allura red at 500 nm were monitored: as observed, the absorbance decreased with time corresponding to a recent report (Shown in **Paper V**). For example, the FTIR spectrum of 4-NA and 1,4-diamino benzene further confirms the reduction of 4-NA through the peaks at 1400 cm^{-1} and 1674 cm^{-1}.

Chemical kinetics for reduction reaction of series of nitroanilines and dyes:

The progress of the reduction reaction was indicated by the gradual decrease in the intensity in the UV-visible spectrum of each substrate. It is suggested that due to the lower band gap of $CuFe_2O_4$ NPs, the catalyst provides relatively better reduction ability. Therefore, the IL most probably acts as a medium for electron movement whereas BNONS and $CuFe_2O_4$ can accept as well as transfer the electrons from $NaBH_4$ to the substrate investigated at room temperature. It was observed that the reduction of 2-NA, 3-NA, 4-NA, 4-NPDA, AR and MB, in the presence of the catalyst, was completed within 80, 60, 30, 50, 40 and 120 minutes, respectively. Furthermore, by increasing the temperature of the reaction, it was observed that time decreased which indicated that the reaction occurred faster. The kinetics of the reaction was determined by varying the temperature of the reactions from 25 to 60 ^oC and concentration of the catalyst from 0.015 to 0.045 ml (0.2 mg/ml). The concentration of 2-NA, 3-NA, 4-NA, 4-NPDA, AR and MB used was 0.05 M, 0.05 M, 0.05 M, 0.05 M, 0.02 M and 0.02 M, respectively, whilst aqueous $NaBH_4$ was maintained at 0.5 M. The concentration of $NaBH_4$ was significantly higher than the concentration of NAs and dyes and it was maintained constant throughout the series of reaction. The value C/C_0, measured in terms of the relative intensity of UV-visible absorbance at the specific wavelength of the substrate was obtained. The linear correlation $\ln(C/C_0)$ or C/C_0 verses reaction time, as shown in **Paper V** demonstrates the reaction to be zero or pseudo first-order with respect to series of NAs and dyes concentration. The kinetic equation for the catalytic reduction is given by $\ln(C/C_0) = -kt$. The rate constant and activation energy of the reduction reaction at several temperatures as well as different concentrations of catalyst dose was computed and presented in **Paper V**.

The proposed mechanism for this reduction reaction was discussed in this article. Here the nanomaterial acts as an electronic medium for this reaction mixture and the hydrated ions from $NaBH_4$ acquired more energy via electrons from this nanomaterial. Moreover, the heterogeneous catalyst loses only a negligible amount of catalytic activity, even after being re-used 7 times, and thus it has been established that it is easy to recover and shows good reusability.

TCPIL/$CuFe_2O_4$/BNONS nanomaterial has extraordinary catalytic activity, and this has been expected due to the following reasons:

(a) The chemical composition of the nanomaterial was made by the effective materials such as BNONS, TCPIL, and $CuFe_2O_4$ nanoparticles.

(b) The significant physicochemical properties of BNONS and TCPIL.

(c) The TCPIL which is used for making of the nanomaterial has some unique properties like the formation of crabbing or chelation of metallic elements, resulting in greater stability and activity.

(d) The TCPIL in the nanomaterial easily absorbed the NA from the reaction mixture, and therefore the reaction was quick and effective.

(e) BNONS tightly held the TCPIL-bonded nanoparticles, therefore it did not lose its activity easily.

(f) The small sized of the nanoparticles spread uniformly on the surface of the BNONS, so these nanoparticles have a greater surface area compared to the normal one.

The morphological variations among the materials like nanoparticles, TCPIL and BNONS might be related to the oxidation-reduction potential with copper and iron metal ions that were used in different doses. Due to their greater surface area, high electron density and charge dispersion, the hydride ions, after electron transfer to the composite, approached NA to reduce it to corresponding amine compounds. The fast electron transfer via surface area of the catalyst and more active sites on the surface of the catalyst, combine two important qualities enabling the nanocomposite to act as an efficient catalyst. The mass ratio of chemical composition for the nanocomposite was 2:1:1 with respect to $CuFe_2O_4$, TCPIL and BNONS, respectively. However, this mean ratio may change depending on the reaction condition. Most important of this study is a simple, reliable, economically viable, eco-friendly and highly efficient approach was developed to synthesize a PTCIL/$CuFe_2O_4$/BNONS nanomaterial which displayed outstanding catalytic efficacy in a short reaction time.

13 Chapter 9

13.1 6th Publication

Efficient Catalytic Activity of Ionic Liquid-Supported $NiFe_2O_4$ Magnetic Nanoparticle Doped Titanium Dioxide Nano-Composite

Vasanthakumar Arumugam, Gyanasivan G. Redhi, and Robert M. Gengan

***Abstract*—In this work the author disclose an effective and environment-friendly approach to the preparation of an ionic liquid supported, magnetic nanoparticle doped titanium oxide nanocomposite. The novel ionic liquid N-(2′, 3′-epoxypropyl)-N-methyl-2- pyrrolidonium salicylate was first synthesized and characterized by ^{1}H-NMR, ^{13}C-NMR, elemental Analysis and FTIR. It was subsequently used for the preparation of a composite material by traditional protocols. This ionic liquid is able to connect the $NiFe_2O_4$ magnetic nanoparticles with titanium dioxide via strong ionic liquid interactions. The composite was characterized by FT-IR, Scanning Electron Microscopy (SEM), Energy Dispersive X-Ray (EDS) analysis, Transmission Electron Microscopy (TEM), High-Resolution Transmission Electron Microscopy (TEM) and Diffraction studies (DF). The catalytic activities of these composites were assessed by the reduction of nitro aniline with the aid of UV spectroscopy. Furthermore, the composite material was easily recovered and re-used with negligible loss of its catalytical activity.**

***Index Terms*—Pyrrolidone, $NiFe_2O_4$, salicylate, epoxypropyl, nanocomposite, nitroaniline, ionic liquid.**

I. Introduction

In the last decade, many researchers have focused on nanoscale metal oxide particles and found fascinating properties for novel applications [1], [2]. Many industries such as cosmetic, pharmaceutical, textile, food-processing and printing are using dyes and pigments in their products [3], however some environmental-friendly microorganisms are affected by highly toxic dyes due to those industries discarding them illegally [3]. Generally metal nanoparticles have some extraordinary physical and chemical properties such as large specific surface area, high number of active sites, high physical, chemical and thermal stabilities, strong electron transfer abilities and high activity and efficiency; these are the properties which are extensively exploited in the degradation of dyes [4], [5].

Most of the nanoscience scientists are doing their research with TiO_2 due to its interesting applications in numerous fields of materials engineering, dye-sensitized cells, paint industry, sensors and chemical engineering [6], [7]. The high number of applications of TiO_2 is because of their strongly influenced physiochemical properties such as phase structure, surface area and crystallite size [8], [9]. Titanium dioxide is a successful material which can be applied for the functionalization of magnetic nanoparticle and coating material [10]-[13]. In recent years, researchers have developed and improved heterogeneous catalyst systems which have solid phase supported nanoparticles such as titanium dioxide (NPS), gum and Fe_3O_4 [6], [14], [15].

Ionic liquid coated titanium dioxide composites have more applications due to their enhanced chemical properties and physical nature of the material. In general important properties of the room temperature ionic liquids such as low surface tension and vapor pressure enables it to act as a stabilizer to produce lower particle growth [16]-[18], and reduce the formed nanoparticle surface area [19]. In particular, the 1-pentyl-3-methylimidazolium bromide coated titanium dioxide ([PMIM]Br@TiO_2) dispersed in an organic solvent surrounded by a porous membrane and supported by capillary force and sinification [20].

Applications of magnetic nanoparticles include bioimaging [21] and easily separable and recyclable of heterogeneous nanoparticle catalysts [22]. Polystyrene -magnetite mesoporous titanium dioxide nanocomposite ($PS/Fe_3O_4/mTiO_2$) was synthesized by a facile method and these have potential application in the management of pollutants in water such as cyanobacteria [23]. The degradation of methylene blue under ultraviolet light irradiation was investigated with Fe_3O_4-TiO_2 nanocomposite and Abbasil. At.al. confirmed the photocatalytic activity of magnetite-titanium dioxide nanocomposite [24]. $NiFe_2O_4$/PAMA/Ag–TiO_2 nanocomposite was synthesized inexpensively and eco-friendly by facile reproducible citrate-gel methodology, these composites has been used as recyclable antibacterial material. [25].

The sono-catalytic activity and good magnetism of nanocomposite gama-Fe_2O_3 and TiO_2 NTs/c-Fe_2O_3 have been synthesized by a facile polyol method and exploited the principle of the isoelectric point method [26]. The phases of the titanium analogue such as anatase/rutile and silicon dioxide combined to form the nanocomposite with cobalt iron magnetite ($CoFe_2O_4$) nanoparticle, which has highly photocatalytic activity for oxidation of methylene blue under UV light. [27] Photo degradation of phenol under UV irradiation was investigated by using photo-catalytically active iron oxide (Fe_3O_4) nanoparticle functionalized TiO_2.

The present work related to synthesis of the novel N-(2´, 3´-epoxypropyl)-N-methyl-2- pyrrolidonium salicylate and its use to make the nanocomposite have been shown excellent

Manuscript received March 11, 2016; revised August 12, 2016. This work was supported in National Research Foundation (NRF) under South Africa for the Innovation Doctoral Grant (Grant UID: 101117).

A. Vasanthakumar, G. G. Redhi, and R. M. Gengan are with Chemistry, Department, Durban University of Technology, Durban, South Africa (e-mail: akumar.vasanth@gmail.com, redhigg@dut.ac.za, genganrm@dut.ac.za).

catalytic activity which was verified by the reduction of 2-nitroaniline to 2-aminoaniline, monitored using UV-vis spectroscopy.

II. Materials and Methods

A. Materials

N-methyl-2-pyrrolidone, epichlorohydrin, sodium salicylate, 2-nitroaniline, nickel sulphate, ferrous sulphate, ferric chloride, liquid ammonia, titanium dioxide acetonitrile, methanol, acetone, and hexane were purchased from Fluka with purity of ≥ 99%. Ultrapure deionized water was used in these experiments. The water content was found using a Metrohm Karl Fishcher coulometer to be 0.05% in $[EPPYRO]^+[SAL]^-$.

B. Synthesis of [EPPY]+[Cl]-

A 50 mL three-necked round bottom flask with a thermometer inlet over cold water flowing condenser was used. Nitrogen gas was flushed into the round bottom flask and addition of 0.1 mol of freshly distilled N-methyl-2-pyrrolidone mixed with 10 mL of acetonitrile, followed by 0.11 mol of epichlorohydrin. The mixture was brought to a moderate reflux (90-100)^{o}C, then heated under reflux for 48 hours with constant stirring and then cooled to room temperature. The volatile materials were removed under reduced pressure to give a yellow coloured ionic liquid, N-(2′, 3′-epoxypropyl)-N-methyl-2-pyrrolidonium chloride $[EPPY]^+[Cl]^-$ [28] see the scheme: 1. It was characterized by the following technique: NMR (1H and13C), elemental analysis and FTIR. Analytical data of the synthesized ionic liquid was checked by HPLC and found to be 98.1%. FTIR (ν=cm^{-1}): 3442, 2995, 1621, 1501, 1403, 1332, 1256, 1113, 967, 856, 756, 679, 561, 479. $[EPPY]^+[Cl]^-$ 1H NMR (400 MHz, DMSO): δ 3.48 - 3.51 (m, 1H), 3.30 - 3.32 (t, 2H), 2.76 - 3.29 (s, 1H), 2.61 - 2.62 (s, 3H). 2.26-2.30 (d, 1H) 1.96 - 1.98 (t, 2H) 1.90 - 1.94 (m, 2H) 13C NMR (100 MHz, DMSO): δ 175.03, 51.22, 49.38, 45.72, 45.00, 30.62, 29.50, and 17.59. Elemental Analysis (in %): Theoretical calculation for: $C_8H_{14}NO_2$: C, 50.14; H, 7.36; N, 7.31. The values found (in %): C, 50.45; H, 7.10; N, 7.17.

Scheme: 1

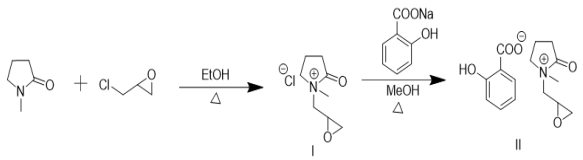

C. Synthesis of $[EPPY]^+[SAL]^-$

In a 50 mL round-bottomed flask, the desired quantity of sodium salicylate (0.112 mol) was dissolved in methanol to make a clear solution. Then the above synthesized intermediate ionic liquid $[EPPY]^+[Cl]^-$ was added to exchange salicylate anion. The product was purified by a solvent wash with acetone, followed by petroleum ether and hexane to remove unwanted starting materials and sodium chloride then distilled again at 80^{o}C for 10 hrs to get pure moisture-free ILs see the scheme: 1. The $[EPPY]^+[SAL]^-$ was characterized by the following methods: NMR (^{1}H and ^{13}C), elemental analysis and FTIR. Analytical data of the synthesized ionic liquid was checked by HPLC and found to be 98.9%. The structure of $[EPPY]^+[SAL]^-$ is as shown in FTIR (ν=cm^{-1}): 3442, 2995, 1621, 1501, 1403, 1332, 1256, 1113, 967, 856, 756, 679, 561, 479.$[EPPY]^+[SAL]^-$ 1H NMR (400 MHz, DMSO): δ1.9 - 2.0(M, 2H), 2.15 - 2.3(t, 2H), 2.7 - 2.8(s, 3H), 3.3 - 3.4(m, 3H), 3.5 -3.65(d, 2H), 3.66 - 3.90(m, 1), 4.0 - 4.2(m, 1), 6.75 - 6.85(t, 1H), 6.86 - 7.00(m, 1H), 7.10 - 7.30(t, 1H), 7.40 - 7.60(m, 1H), 7.65 - 7.95(d-d, 1H). 13C NMR (100 MHz, DMSO): δ18, 30, 33, 51, 65, 72, 75, 115, 120, 122, 132, 134, 138, 163 and 178. Elemental Analysis: Theoretical calculation for: C15H21NO4: C, 64.50; H, 7.58; N, 5.01; O, 22.91. The values found: C, 64.95; H, 7.10; N, 5.28; O, 23.36.

D. Preparation of $IL/Fe_3O_4/TiO_2$ Nanocomposite

The nickel ferrite magnetite nanoparticle was prepared according to the previous method [29], [30]. Briefly, 1.0 gram of nickel ferrite magnetic nanoparticle $NiFe_2O_4$ and N-(2 ´, 3 ´ -epoxypropyl)-N-methyl-2- pyrrolidonium salicylate ionic liquid (IL) were taken separately. The ionic liquid was dissolved in ultra-pure deionized water to which the above-weighed nickel ferrite magnetic nanoparticle was added slowly at constant stirring for 24 hrs at room temperature; it was then dried at 80^{o}C for 12 hrs to produce a dry brown powder then without purification of the material further it was dispersed in 20 mL of ultra-pure water and sonicated. Separately 2.0 gram of TiO_2 was dispersed in 20 mL water and sonicated for 15 minutes and this solution was add to above magnetic nanoparticle dispersion at constant stirring. The reaction mixture was transferred to round bottomed flask and placed in a temperature controlled oil bath with a magnetic stirrer. The temperature of the reaction was maintained at 140^{o}C for 16 hrs. The final product was dried under vacuum for 10 hrs to produce light brown coloured nanocomposite. It was purified by washing with ultrapure water and dispersed in ethanol. The composite was then characterized by FTIR, SEM, EDS and TEM.

III. Investigation of Catalytic Activity of Nanocomposite

The investigation of the catalytic activity of ionic liquid nickel-iron magnetite titanium dioxide nanocomposite for the reduction of 2-nitroaniline was carried out in room temperature monitoring under UV spectroscopy. In a general procedure, 2-nitroaniline (0.5 mL of 0.5 mM) was mixed with 0.5 mL of freshly prepared aqueous $NaBH_4$ solution (0.4M) and 1.95 mL of deionized water to form a deep yellow solution. Then, 0.05 mL of $IL/NiFe_2O_4/TiO_2$ nanocomposite dispersion (0.2 mg/mL) was added into the quartz cuvette. The above-mixed solution was detected by using UV-Vis spectrophotometer every ten minutes to monitor the variation of 2-nitroaniline concentration. After the solution became colorless, the $IL/NiFe_2O_4/TiO_2$ hybrid was separated from the reaction mixture under a magnetic field and it was then used for another cycle of 4-Nitroaniline (4-NA) reduction. The samples were filtered, centrifuged and their concentration was determined by UV–visible spectrometry.

IV. Result and Discussion

The novel synthesized nanocomposite was investigated by FT-IR spectroscopy to identify the valuable information on the shift in the stretching frequencies. The FT-IR spectra of TiO_2 and IL/$NiFe_2O_4$/TiO_2 nanocomposite are shown in Fig. 1 and 2. The peak at 3294 cm^{-1} corresponds to the OH stretching vibration of the IL. A band with medium intensity at 1252 cm^{-1} with two shoulders 1103 at and 1300 cm^{-1} corresponds to the stretching vibrations of C-O-C group and ring vibrational modes in the composition of cyclic structures was observed.

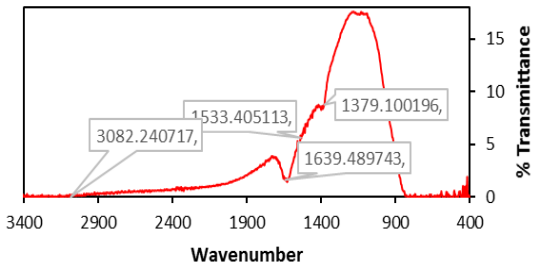

Fig. 1. FT-IR spectrum for TiO_2.

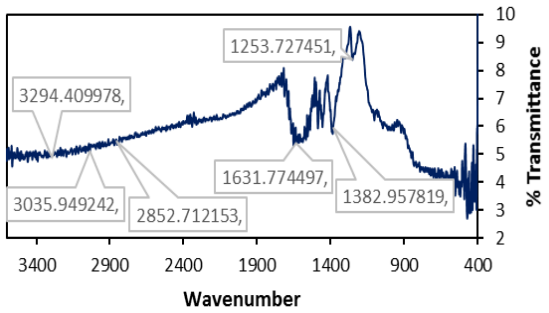

Fig. 2. FT-IR spectrum for $NiFe_2O_4$/IL/TiO_2 nanocomposite.

A broad band with low intensity arises at 1644 cm^{-1} indicates the carbonyl group nearby the amine group. The C-H aromatic stretching and bending vibrations of the IL is observed at 2997 cm^{-1} and 2344 cm^{-1}. The peak at 2850 cm^{-1} shows aliphatic C-H stretching and bending vibrations of IL. The OH stretching of the TiO_2 gives a peak at 3396 cm^{-1}. The peaks at 624 cm^{-1} and 471 cm^{-1} are attributed to Ti-O stretching mode [31], [32]; the main absorption bands at 578 cm^{-1} and 453 cm^{-1} belong to the metal–oxygen stretching vibrations of $NiFe_2O_4$ nano structures [33]. The C-O stretching vibration of the carboxylic group gives a peak at 1676 cm^{-1}. The spectrum displays a band at 3420 cm^{-1}, corresponding to the stretching mode of OH group of adsorbed hydroxyl group. The strong absorption band at 442 and 580 cm^{-1} corresponding to the $NiFe_2O_4$-TiO_2 lattice and broad absorption band at 3392 cm^{-1} are allocated to adsorbed OH group on the surface of the nanocomposite. There are no other important peaks related our nanocomposite. The peak 441 cm^{-1} could be corresponding to Ti-O stretching in rutile phase [34].These observations confirm the incorporation of IL/$NiFe_2O_4$ nanoparticle into the TiO_2 matrix

The surface morphology of the samples was observed by SEM (Fig. 1); the highly agglomerated porous foam-like structure of $NiFe_2O_4$, TiO_2 and IL, which is characteristic of the synthesized composite is observed in contrast to the bare $NiFe_2O_4$. The nanoscale crystallites could be noticeably distinguished from the SEM image of TiO_2 and $NiFe_2O_4$/TiO_2 nanocomposites. The $NiFe_2O_4$ nanoparticles are bonded or capped with IL to form the intermediate composite and the intermediate composite mixture was combined with titanium dioxide matrix that's why it showed cluster like images. Also, the $NiFe_2O_4$ nanoparticles with the average particle size around 150 nm dispersed on synthesized nanocomposites is observable. The SEM picture also reveals that the doping of $NiFe_2O_4$ magnetite nanoparticles has increased the surface area of the catalyst surface.

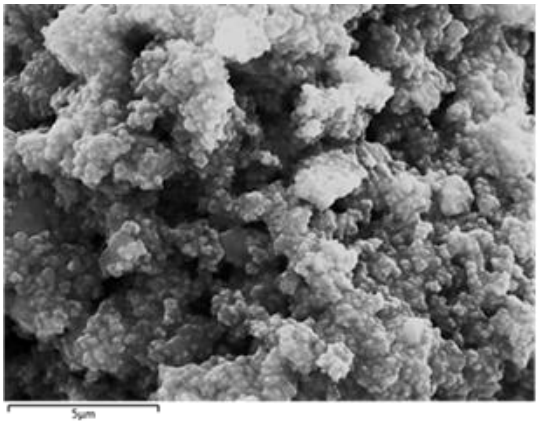

Fig. 3. SEM image of $NiFe_2O_4$/IL/TiO_2 nanocomposite.

The SEM image indicates (Fig. 3) that the spreading of $NiFe_2O_4$ on the surface of titanium dioxide is not uniform and the $NiFe_2O_4$/IL/TiO_2 catalyst contains irregularly shaped particles which may be due to the aggregation of ionic liquid and tiny crystals magnetic nanoparticles. The actual percentage of the elements in the composites was confirmed by energy dispersive spectroscopy [EDS] analysis. The identification of the elements from EDS spectra indicates the presence of Iron (4.46%), titanium (33.05%) oxygen (46.21%), carbon (14.76%) and nickel (1.51%) (Table I) which explains that the composite has been confirmed. Then EDS image (Fig. 4 and Table I) displays the percentage of all elements such as Ni, Fe, Ti, C, O except nitrogen due to the ionic liquids binding with the inner layer of titanium oxide and the percentage of the nitrogen is also low. The colouring map shows (Fig. 5) the presence of nitrogen but the EDS indicates zero percentage. The EDS only indicates the presence of ILs in composite via the presence of the C, O and N. The morphology of the resultant $NiFe_2O_4$/IL/TiO_2 nanocomposites was investigated.

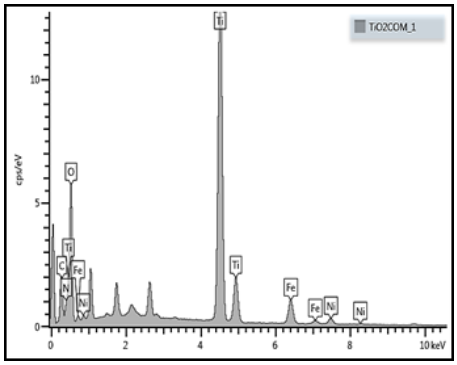

Fig. 4. EDS image of $NiFe_2O_4$/IL/TiO_2 nanocomposite.

TEM image of the resulting $NiFe_2O_4$/IL/TiO_2

nanocomposite clearly indicates that the surface was covered by IL, $NiFe_2O_4$ nanoparticle on titanium dioxide. Morphology of the synthesized nanocomposites was examined by TEM as shown in Fig. 6. The nickel-iron magnetic nanoparticles have been a cubic unit cell with both octahedral and tetrahedral.

TABLE I: EDS COMPOSITION FOR $NiFe_2O_4$/IL/TiO_2 NANOCOMPOSITE

TiO_2COM	Wt%	Wt% Sigma
C	14.76	0.33
N	0	0
O	46.21	0.39
Ti	33.05	0.26
Fe	4.46	0.09
Ni	1.51	0.08
Total	100	

Fig. 5. EDS colouring map for $NiFe_2O_4$/IL/TiO_2 nanocomposite.

Co-ordinated Fe^{3+} and Ni^{2+}. A typical high-resolution TEM image Fig. 7 display the lattice fringes with a spacing 0.51 nm; the average of these synthesized nanoparticles is about 30 nm. The diameter of the magnetite nanoparticle was increased when the temperature increased from 100 to 300°C. The above results clearly explain the growth of the $NiFe_2O_4$ catalyst during thermal treatment [35]. The formation of $NiFe_2O_4$/IL/TiO_2 nanocomposite was further analyzed by low and high magnification to identify the clear structure and crystallinity of nanoparticles.

TEM images of the nanocomposites also expose the nickel iron nanoparticle with ionic liquid was decorated in TiO_2. The HRTEM image shows (Fig. 7) the crystal lattice of the nickel-iron nanoparticles. Furthermore, to the characteristic diffraction peaks (Fig. 8) correspond to $NiFe_2O_4$ and TiO_2.

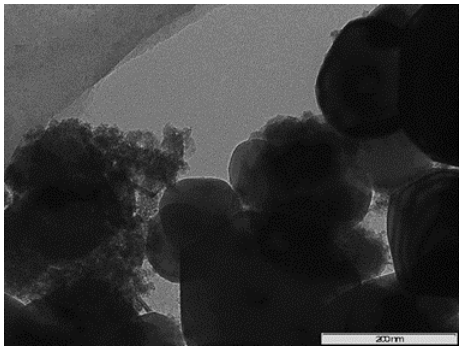

Fig. 6. TEM image of $NiFe_2O_4$/IL/TiO_2 nanocomposite.

The reduction and oxidation properties of TiO_2 nanocomposite are dependent on the negative conduction or positive valence band; more negative bands could be the reason for high reducing power, and high oxidation occurs due to the greater positive valence band in nature. Compatible band configuration and contact among $NiFe_2O_4$ and TiO_2 could extend the lifetime and stimulate spatial separation of generated charge carriers. Interestingly the catalytic performance of $NiFe_2O_4$/IL/TiO_2 nanocomposites might depend on the enhanced synergistic effect of the high reducing capability of TiO_2 and IL, exhaustive absorbance at the long wavelength light by $NiFe_2O_4$ particles, at preferred fractions of two kinds of IL and NPS materials. The appropriate amount of $NiFe_2O_4$ could act as a linker for an electron to increase the effectiveness of charge separation and inhibit the recombination of electrons and holes [36]. The catalytic activity of the Ni ferrite ionic liquid TiO_2 nanocomposite was investigated by monitoring the reduction of 2-nitroaniline in the presence of $NaBH_4$ in an aqueous solution, at room temperature. The synthesized composite is a good medium for electron transfer of BH_4 ions and the reaction was checked by recording of time-dependent UV-vis absorption spectra at 10 mints intervals. In Fig. 9, the absorption peak at 400 and 550 nm corresponding to 2-NA shows slow reduction and disappearance after 150 minutes, respectively.

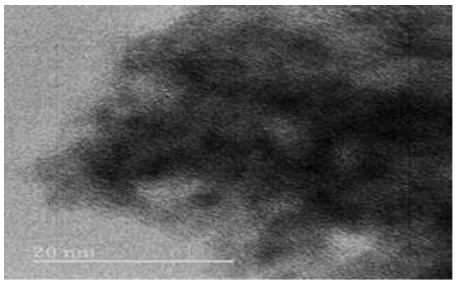

Fig. 7. HRTEM of $NiFe_2O_4$/IL/TiO_2 nanocomposite.

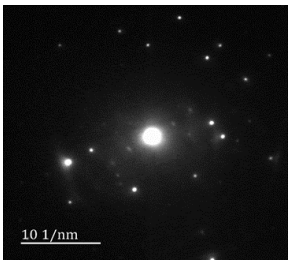

Fig. 8. Diffraction image of $NiFe_2O_4$/IL/TiO_2 nanocomposite.

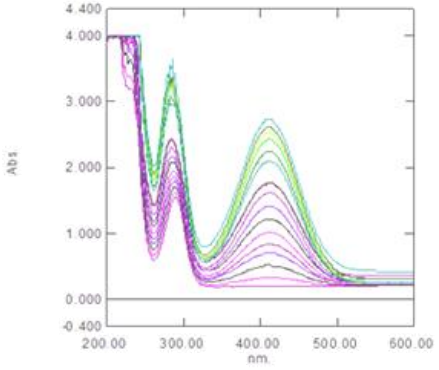

Fig. 9. UV spectrum for reduction of 2-nitroaniline.by $NiFe_2O_4$/IL/TiO_2 nanocomposite.

V. Conclusion

A nickel ferrite ionic liquid titanium dioxide ($NiFe_2O_4$/IL/TiO_2) nanocomposite was synthesized, characterized and applied to catalysis. The mass ratio of the nanocomposite is 2:1:1 of TiO_2, IL and $NiFe_2O_4$, due to the facilitation of interfacial charge transfer and inhibition of electron-hole recombination. The composite was successfully characterized by using SEM, EDS, TEM, HRTEM, DF and FT-IR techniques to identify the morphology, composition, crystallinity and important functional groups which are present in the composite. The advantage of this method is that it is an environmentally friendly safe protocol; less toxic, inexpensive and less harmful chemical are used; water is the solvent for the synthesis of nanocomposite under a green condition. In addition, it was easily recovered and re-used with negligible loss of catalytic activity. Moreover, the nanocomposite exhibited high catalytic activity for the reduction of 2-nitroaniline in water at room temperature.

Acknowledgment

Mr. Vasanthakumar Arumugam is grateful to the Durban University of Technology, the National Research Foundation (NRF) South Africa for the Innovation Doctoral Grant (Grant UID: 101117).

References

[1] B. Moghaddam, T. Nazari, J. Badraghi, and M. Kazemzad, "Synthesis of ZnO nanoparticles and electrodeposition of polypyrrole/ZnO nanocomposite film," *International Journal of Electrochemical Science*, vol. 4, pp. 247-257, 2009.

[2] M. R. Nabid, M. Golbabaee, A. B. Moghaddam, A. R. Mahdavian, and M. M. Amini, "Preparation of the -Al_2O_3/PANI nanocomposite via enzymatic polymerization," *Polymer Composites*, vol. 30, pp. 841-846, 2009.

[3] V. K. Vidhu and D. Philip, "Catalytic degradation of organic dyes using biosynthesized silver nanoparticles," *Micron*, vol. 56, pp. 54-62, 2014.

[4] N. Pradhan, A. Pal, and T. Pal, "Catalytic reduction of aromatic nitro compounds by coinage metal nanoparticles," *Langmuir*, vol. 17, vol. pp. 1800-1802, 2001.

[5] A. K. Sinha, M. Basu, S. Sarkar, M. Pradhan, and T. Pal, "Synthesis of gold nanochains via photoactivation technique and their catalytic applications," *Journal of Colloid and Interface Science*, vol. 398, pp. 13-21, 2013.

[6] M. Atarod, M. Nasrollahzadeh, and S. M. Sajadi, "Euphorbia heterophylla leaf extract mediated green synthesis of Ag/TiO_2 nanocomposite and investigation of its excellent catalytic activity for reduction of variety of dyes in water," *Journal of Colloid and Interface Science*, vol. 462, pp. 272-279, 2016.

[7] M. Nasrollahzadeh and S. M. Sajadi, "Synthesis and characterization of titanium dioxide nanoparticles using Euphorbia heteradena Jaub root extract and evaluation of their stability," *Ceramics International*, vol. 41, pp. 14435-14439, 2015.

[8] H. Liu, Y. Liang, H. Hu, and M. Wang, "Hydrothermal synthesis of mesostructured nano-crystalline TiO_2 in an ionic liquid–water mixture and its photocatalytic performance," *Solid State Sciences*, vol. 11, pp. 1655-1660, 2009.

[9] X. Y. Ma, Z. G. Chen, H. B. Jiang, J. Zou, and S. Z. Qiao, "Fabrication of uniform anatase TiO_2 particles exposed by {0 0 1} facets," *Chemical Communications*, vol. 46, pp. 6608-6610, 2010.

[10] S. Solinas, G. Piccaluga, M. P. Morales, and C. J. Serna, "Sol-gel formation of γ-Fe_2O_3/SiO_2 nanocomposites," *Acta Materialia*, vol. 49, pp. 2805-2811, 2001.

[11] S. C. Pang, S. Y. Kho, and S. F. Chin, "Fabrication of magnetite/silica/titania core-shell nanoparticles," *Journal of Nanomaterials*, 2012.

[12] Z. L. Shi, C. Du, and S. H. Yao, "Preparation and photocatalytic activity of cerium doped anatase titanium dioxide coated magnetite composite," *Journal of the Taiwan Institute of Chemical Engineers*, vol. 42, pp. 652-657, 2011.

[13] W. Fu, H. Yang, M. Li, M. Li, N. Yang, and G. Zou, "Anatase TiO_2 nanolayer coating on cobalt ferrite nanoparticles for magnetic photo catalyst," *Materials Letters*, vol. 59, pp. 3530-3534, 2005.

[14] M. Atarod, M. Nasrollahzadeh, and S. M. Sajadi, "Green synthesis of a Cu/reduced graphene oxide/Fe_3O_4 nanocomposite using Euphorbia wallichii leaf extract and its application as a recyclable and heterogeneous catalyst for the reduction of 4-nitrophenol and rhodamine B," *RSC Advances*, vol. 5, pp. 91532-91543, 2015.

[15] M. Nasrollahzadeh, "Green synthesis and catalytic properties of palladium nanoparticles for the direct reductive amination of aldehydes and hydrogenation of unsaturated ketones," *New Journal of Chemistry*, vol. 38, pp. 5544-5550, 2014.

[16] J. Lemus, J. Palomar, M. A. Gilarranz, and J. J. Rodriguez, "Characterization of supported ionic liquid phase materials prepared from different supports," *Adsorption*, vol. 17, pp. 561-571, 2011.

[17] C. Han, S. Ho, Y. Lin, Y. Lai, W. Liang, and Y. C. Yang, "Effect of stacking of water miscible ionic liquid template with different cation chain length and content on morphology of mesoporous TiO_2 prepared via sol–gel method and the applications," *Microporous and Mesoporous Materials*, vol. 131, pp. 217-223, 2010.

[18] L. W. L. Chang, B. Zhao, Z. Y. Gaosong, and S. W. Zheng, "Inorganic synthesis in ionic liquids," *Inorganic Chemistry*, vol. 47, pp. 1443-1452, 2008.

[19] I. Yavari, A. R. Mahjoub, E. Kowsari, and M. Movahedi, "Synthesis of ZnO nanostructures with controlled morphology and size in ionic liquids," *Journal of Nanoparticle Research*, vol. 11, pp. 861-868, 2009.

[20] E. Zarrin, N. Azizollah, S. Bahar, S. Bohlooli, and A. Banaei, "[PMIM]Br@TiO_2 nanocomposite reinforced hollow fiber solid/liquid phase micro-extraction: An effective extraction technique for measurement of benzodiazepines in hair, urine and wastewater samples combined with high-performance liquid chromatography," *Journal of Chromatography*, vol. B 980, pp. 55-64, 2015.

[21] A. Kale, S. Kale, P. Yadav, H. Gholap, R. Pasricha, J. P. Jog, B. Lefez, B. Hannoyer, P. Shastry, and S. Ogale, "Magnetite/CdTe magnetic-fluorescent composite nano-system for magnetic separation and bio-image," *Nanotechnology*, vol. 22, pp. 225101, 2011.

[22] D. Wang, L. Salmon, J. Ruiz, and D. Astruc, "A recyclable ruthenium (II) complex supported on magnetic nanoparticles: A region-selective catalyst for alkyne-azide cycloaddition," *Chemical communications*. vol. 49, pp. 6956-6958, 2013.

[23] F. Jing and S. Zhang, "Facile preparation of Fe_3O_4/mesoporous TiO_2 nanoparticles shell on polystyrene beads and its effective absorption of cyanobacteria in water," *Journal of Polymer Research*, vol. 22, pp. 182, 2015.

[24] A. Abbasil, D. Ghanbari, M. Salavati-Niasari, and M. Hamadanian, "Photo-degradation of methylene blue: photo-catalyst and magnetic investigation of Fe_2O_3-TiO_2 nanoparticles and nanocomposites," *The Journal of Materials Science: Materials in Electronics*, pp. 1-10, 2016.

[25] A. Allafchian, S. A. Hossein Jalali, H. Bahramian and H. Ahmadvand, "Preparation, characterization, and antibacterial activity of $NiFe_2O_4$/PAMA/Ag–TiO_2 nanocomposite," *Journal of Magnetism and Magnetic Materials*, vol. 404, pp. 14-20, 2016.

[26] Y. L. Pang, S. Lim, H. C. Ong and W. T. Chong, "Synthesis, characteristics and sono-catalytic activities of calcined c-Fe_2O_3 and TiO_2 nanotubes/c-Fe_2O_3 magnetic catalysts in the degradation of Orange G," *Ultrasonic Sono-chemistry*, vol. 29, pp. 317-327, 2016.

[27] Greene, R. Serrano-Garcia, J. Govan, and Y. K. Gun'ko, "Synthesis characterization and photocatalytic studies of cobalt ferrite-silica-titania nanocomposites," *Nanomaterials*, vol. 4, pp. 331-343, 2014.

[28] A. Vasanthakumar, I. Bahadur, G. G. Redhi, R. M. Gengan, and K. Anand, "Synthesis, characterization and thermophysical properties of ionic liquid N-methyl-N-(2 ´ ,3 ´ -epoxypropyl)-2-oxopyrrolidinium chloride and its binary mixtures with water or ethanol at different temperatures," *Journal of Molecular Liquids*. Vol. 219, pp. 685-693, 2016.

[29] A. A. Ensafi, B. Saeid, B. Rezaei, and A. R. Allafchian, "Differential pulse voltammetry determination of methyldopa using MWCNTs modified glassy carbon decorated with $NiFe_2O_4$ nanoparticles," *Ionics*, vol. 21, pp. 1435-1444, 2015.

[30] A. A. Ensafi, B. Arashpour, B. Rezaei, and A. R. Allafchian, "Voltammetric behavior of dopamine at a glassy carbon electrode modified with $NiFe_2O_4$ magnetic nanoparticles decorated with

multiwall carbon nanotubes," *Materials Science and Engineering*, vol. 39, pp. 78-85, 2014.
[31] M. Anastasios, V. Tiverios, T. Christos, T. Nadia, B. Detlef, and D. Ralf, "Hydroxyapatite/titanium dioxide nanocomposites for controlled photocatalytic NO oxidation," *Applied Catalysis B: Environmental*, vol. 106, pp. 398-404, 2011.
[32] M. Mohamed, M. Mater, and M. Al-Esaimi, "Characterization, adsorption and photocatalytic activity of vanadium-doped TiO_2 and sulfated TiO_2 (rutile) catalysts: Degradation of methylene blue dye" *Journal of Molecular Catalysis A: Chemical*, vol. 255, pp. 53-61, 2006.
[33] M. Kooti and A. N. Sedeh, "Synthesis and characterization of $NiFe_2O_4$ magnetic nanoparticles by combustion method," *Journal of Materials Science and Technology*, vol. 29, pp. 34-38, 2013.
[34] W. Lan, C. Yan, Y. S. Lin, Y. N. Wang, F. Z. Yi, and P. C. Peng, "High efficient photo-catalyst of spherical TiO_2 particles synthesized by a sol-gel method modified with glycol," *Colloids and Surfaces A: Physicochemical and Engineering Aspects*, vol. 461, pp. 195-201, 2014.
[35] N. Sobana, M. Muruganadham, and M. Swaminathan, "Nano-Ag particles doped TiO_2 for efficient photo-degradation of direct azo dyes," *Journal of Molecular Catalysis A: Chemical*, vol. 258, pp. 124-132, 2006.
[36] J. Bandara, U. Klehm, and J. Kiwi, "Raschig rings-Fe_2O_3 composite photo catalyst activate in the degradation of 4-chlorophenol and Orange II under daylight irradiation," *Applied Catalysis B: Environmental*, vol. 76, pp. 73-81, 2007.

Vasanthakumar Arumugam is doing PhD under Prof. G. G. Redhi and Prof. R. M. Gengan in the Department of Chemistry. Durban University of Technology. He was born on January 19, 1988 in Tindivanam, Tamil Nadu, India. He studied the bachelor of science (BSc) in Govt. Arts and Science College in Tiruvannamalai. He studied his master's degree (MSc) in Bharathiar University Coimbatore. After his master's he has started carrier as a researcher (R&D) in SDS Ramcides Crop Science Pvt Lt. His early years of research focused on Agrochemical especially specialty fertilizers, pesticides, herbicides and plant growth regulators.

His research interests broadly focus on ionic liquids with their characterization and applications. His work also includes the use of aqueous based reactions and the preparation of nanoparticles and nanocomposites materials for industrial applications. His interest in nano-chemistry includes the use of ionic liquids and nanoparticle combinations and ionic liquid capped nanoparticles and magnetic nanoparticles for industrial and environmental applications. His recent research focus is synthesis, characterization and application of novel ionic liquids.

G. G. Redhi holds a PhD in chemistry from the University of Kwa-Zulu Natal, South Africa. The focus of his research work is on the determination of liquid-liquid equilibrium data for the separation of aromatic from aliphatic components related to the petroleum industry, using conventional polar solvents as well ionic liquids. In addition activity coefficients as well excess properties of binary and ternary systems are measured using chromatography and densitometry respectively. These thermodynamic data are important in optimizing solvent extraction processes, as well as lead to a better understanding of the molecular interactions that occur between the components.

In addition Prof Redhi's research also involves the use of nanotechnology, ionic compounds and new materials in the development of robust and sensitive electrochemical sensors for various active ingredients in the pharmaceutical industry, using Voltammetric techniques.

Robert M Gengan is an Associate Professor in the Department of Chemistry. Durban University of Technology. He was born on June 27, 1958 in Durban and from humble back-ground, he studied diligently and earned a lecturing position at the ML Sultan Technikon in 1985. He holds BSc, BSc (Hons), MTech, H.E.D and PhD degrees from the University Natal. His early years of research focused on Mycotoxin studies but later he turned towards [illegible]emistry; his major contribution in this field was the introduction of Environmental Chemistry II as an offering for the Higher National Diploma in Chemistry. In 2003, he introduced Green Chemistry in the Organic Chemistry IV syllabus and this still remains an interesting study component, which are enjoyed by students. His keen interest in Green Chemistry was highlighted in a Research paper titled "A New philosophical Approach to teaching: Green chemistry is the way of life" which was presented at the ICESA Conference in 2013. His lectures in organic chemistry is interspersed with updated Green Chemistry knowledge which stimulates creativity amongst students.

Trained as a synthetic organic chemist, Professor Gengan's research interests broadly focus on green chemistry with specific emphasis on synthesis of organic molecules by green protocols such as microwave irradiation and photo energy. His work also includes the use of aqueous based reactions and the preparation of less toxic nano catalytsts for industrial applications. His interest in nano-chemistry includes the use of indigenous plants to reduce gold, silver and palladium to nanoparticles capped with biomolecules for application on human health and the environment. His research team also uses active pharmaceutical molecules which are then linked to gold nanoparticles as an application for drug delivery systems. His recent research focus is the synthesis of fluorescent dyes and organic photo cells for the capture of solar energy. Professor Gengan hopes to add value to the environment by using Green Chemistry Principles in a systematic and holistic approach for challenges of sustainability of natural resources, of improving the environment thereby enabling a better quality of life.

13.2 Critical review for 6th Publication

Efficient catalytic activity of ionic liquid-supported $NiFe_2O_4$ magnetic nanoparticle doped titanium dioxide nanocomposite.

In this study the synthesis and characterization of a catalytically active novel nanocomposite using N-2′,3′-epoxypropyl-N-methyl-2-oxopyrrolidinium salicylate, TiO_2 and $NiFe_2O_4$ bimetallic magnetic nanoparticles were reported. The new N-2′,3′-epoxypropyl-N-methyl-2-oxopyrrolidinium salicylate IL was synthesized and characterized by FTIR, ^{1}H NMR, ^{13}C NMR and elemental analysis to identify the structure of the IL. In addition, the synthesis of nickel ferrite ($NiFe_2O_4$) magnetic nanoparticles was undertaken by the traditional method. Finally, this IL and $NiFe_2O_4$ as well as TiO_2 was used to synthesize a unique environmental friendly catalytically active nanocomposite. The characterization was investigated using FTIR, SEM, EDS, TEM and ED techniques, to identify the functional groups, morphology, crystallinity and chemical compositions. In particular, this nanocomposite has been used as a catalyst for the reduction of 2-nitroaniline (2-NA) to 1,2-diamino benzene in aqueous solution at ambient temperature and this reaction was monitored by time dependent UV-visible spectroscopy. Since the used nanocomposite catalyst could be recovered easily and reused more than five time with negligible loss of activity, it is regarded as environmentally friendly.

The physical nature of the material was light brown, fine powdered and easily separated from the reaction mixture by an external magnet. The functional groups present in the nanocomposite were analysed and identified by FTIR spectroscopy. Furthermore, EDS also confirms the elements which are present in the nanocomposite, this information further confirmed the presence of IL in the nanocomposite. SEM and TEM images indicate the nature of the surface for the nanocomposite where the nanoparticles were speared over the titanium dioxide. Here titanium dioxide acts as a basal material for the nanocomposite, when it supports the nanoparticles. Electronic diffraction studies help to elucidate the electronic concentrations in the nanocomposite. Ultimately these characterizations disclose the whole physical nature of the nanocomposite.

This nanocomposite has an effective catalyst due to the chemical composition, and it does contain the unique IL, $NiFe_2O_4$ nanoparticles, and TiO_2. These are all somewhat catalytically active in nature when used individually, but in this case, all are clustered together to improve the efficacy tremendously. The IL could help to create bonds between nanoparticles and TiO_2. The

nanoparticles were also coated with the IL, and therefore they became more stable and reactive compared with normal nanoparticles. The catalytic activity of the nanocomposite was investigated by the reduction of 2-NA to 1,2-diamino benzene. The negative conduction and positive valence band of the TiO_2 determines the catalytic reduction or oxidation behaviour of TiO_2. Generally, high reducing power which occurs due to the negative band, could be the reason, whilst the oxidation reaction occurs because of the positive valence band in nature. The $NiFe_2O_4$ NPs and TiO_2 are responsible for increasing the stability and stimulate the charge carriers in the nanocomposite. The enhanced synergistic effect of the TiO_2 and IL could possibly be the reason for the effectiveness of the catalytic performance of the $NiFe_2O_4$/IL/TiO_2 nanocomposite. A suitable quantity of the $NiFe_2O_4$ NPs does act as a link for the moment of the electrons via increase of an activity and following the principle of the charge separation and electron holes recombination. Overall the synthesized nanocomposite was a good medium for the transfer of electrons from BH_4 to reaction mixtures. The above reduction reaction was monitored by time-dependent UV-visible spectroscopy, and spectra of the reaction mixture were run every 5 minutes. Moreover, this reaction was effectively done in an aqueous solution at room temperature with $NaBH_4$. The initial absorbance at 400 nm and 550 nm is due to the presence of the nitro groups, but after completion of the reaction, the absorbance started decreasing after 150 minutes in the same regions and the colour of the solutions turned from yellow to colourless. After completion of the reaction, the catalyst was recovered using external magnets and reused with negligible loss of its activity. The mass ratio of the chemical compositions in the nanocomposite was 2:1:1 for TiO_2, $[Eppyr]^+[SAL]^-$ IL and $NiFe_2O_4$ NP respectively, due to the recombination of the electron-hole and charge transfer of interfacial facilitation. Important advantages of this study are an environmental friendly, economically viable, safe protocol, low toxicity and relatively harmless chemicals were used to make this nanomaterial. In addition the reaction occurs in aqueous solution at room temperature and is easy to handle under green experimental conditions. Moreover, the heterogeneous catalyst loses only a negligible amount of catalytic activity, even after being re-used 5 times, and thus it has been established that it was easy to recover and shows good reusability (see Fig. 8). In future, this nanocomposite may also be used in some other applications for instance in sensors and as a catalyst for some other reactions.

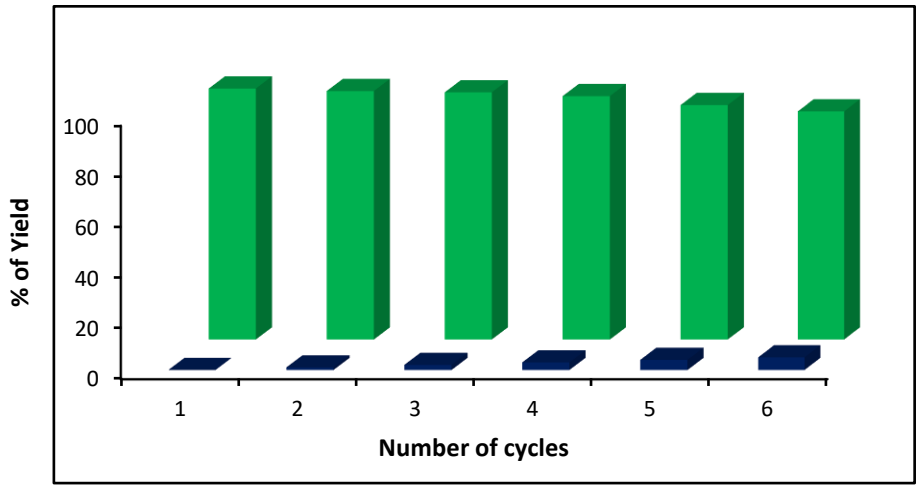

Figure 8: Recyclability and yield of the $NiFe_2O_4$ bonded TiO_2 nanocomposite

14 Interrelationship of the publications in this dissertation

The title of this dissertation is "Synthesis, characterization and applications of novel ionic liquids". This study is more related to and appropriate for this title of this dissertation. The title of the thesis mentioned that the synthesis and characterization of novel ILs and hence in this study, six novel ILs were synthesized and characterized successfully. Moreover, the binary mixtures of ILs with either molecular solvents or carboxylic acids, were investigated regarding their thermophysical properties such as density(ρ), speed of sound(u), viscosity(η), and refractive index(n). Furthermore, these thermophysical properties data were used to calculate the thermodynamic properties of excess molar volume(V_m^E), isentropic compressibility(k_s), deviations in isentropic compressibility(Δk_s) and intermolecular free length(L_f). Particularly, the information from the thermophysical and thermodynamic properties data explained the interactions, H-bonding, ion-dipole interactions and ionic interactions between the molecules of IL and solvents. In addition, these derived thermodynamic properties were correlated with the Redlich Kister polynomial equation. In the application part of this dissertation, the synthesized ILs were used to produce novel efficient nanomaterials. These nanomaterials were characterized using advanced microscopic and surface analysing techniques such as FTIR, XRD, SEM, EDS, TEM, HRTEM, STM, ED, XPS, TGA-DSC and AFM to determine their physical properties. In addition, this nanomaterial acts as an effective catalyst for the reduction reaction of a series of NAs and dyes. Furthermore, the kinetics studies of these reduction reaction were investigated to find the rate constant, order of the reaction and activation energy of the reduction reaction.

15 Conclusion

The N-2′,3′-epoxypropyl substituted N-methyl-2-oxopyrrolidinium cation with different anions such as acetate, chloride and salicylate based novel ILs were successfully synthesized and characterized. The thermophysical properties for these ILs and their binary mixtures with either water, ethanol, methanol, ethanoic acid or propanoic acid were investigated. The important thermophysical properties of ρ, η, u and n for binary mixtures of ILs were measured experimentally for the mole fraction ranges of 0.1 to 1.0 at various temperatures from 288.12 to 313.12 K at 5 K intervals, under atmospheric pressure. Additionally, the thermodynamic properties V_m^E, k_s, Δk_s and L_f were calculated. These thermodynamic values produced more information about the interactions amongst the molecules present in the liquid mixtures such as, hydrogen bonds and ionic interactions. Correlation for the calculated thermodynamic properties such as V_m^E, Δk_s and L_f values was done using the Redlich-Kister polynomial equation.

Novel propanediol substituted N-methyl-2-oxopyrrolidinium, 2-amino picoline, and DABCO ILs were effectively synthesized and characterized. Moreover, these ILs were used to synthesize a more effective novel 4th generation multi-ionic TCPIL and it was characterized successfully. Magnetic copper ferrite ($CuFe_2O_4$) and nickel ferrite ($NiFe_2O_4$) nanoparticles were synthesized and characterized. Novel h-boron nitride modified BNONS were prepared and characterized effectively. These three effective starting materials such as TCPIL, magnetic nanoparticle and boron nitride modified materials were used to synthesize the more efficient novel nanomaterial. Characterization of this nanomaterial (PTCIL/$CuFe_2O_4$/BNNS) using advanced techniques were used to analyse for functional groups, whilst surface analysing instruments such as FTIR, XRD, SEM, EDS, TEM, HRTEM, STEM, ED, XPS, and AFM. This nanomaterial has more effective catalytic activity, and this has been confirmed by using the reduction reaction of a series of NA to corresponding amine compounds in aqueous solution at room temperature, the reaction being monitored by time dependent UV-visible spectroscopy. The reaction was conducted in aqueous solution at room temperature and the nanocomposites were found to be easily recoverable and reusable for more than seven times. Finally, one more IL-bonded nanocomposite was synthesized using TiO_2, $NiFe_2O_4$ bimetallic magnetic nanoparticles and novel N-2′,3′-epoxypropyl-N-methyl-2-oxopyrrolidinium salicylate. The synthesized IL and the nanomaterial were characterized by various microscopic and surface analysing techniques. This nanocomposite was used for the reduction of 2-NA to 1,2-diamino benzene which was monitored by time-dependent UV-visible

spectroscopy. The reaction was conducted in aqueous solution at room temperature and these nanocomposites were found to be easily recoverable and reusable for more than five times.

16 Methodology

16.1 Materials

1-Methyl-2-pyrrolidinone (99.8 % purity), epichlorohydrin (99.0 % purity), acetonitrile (99.2 % purity), methanol, ethanol, acetone, sodium salicylate, ethanoic acid, propanoic acid, 2-nitroaniline (99.5 % purity), 3-nitroaniline (98.0 %), 4-nitroaniline (99.0 % purity), 4-nitro-2-phenylenediamine (95.0 %) nickel sulfate (99.8 % purity), titanium dioxide (99.8 % purity), sodium acetate (99.8 % purity), and hexane were purchased from Fluka with purity of ≥99 %. h-boron nitride (99.8 % purity), copper sulfate (99.5 % purity), ferric chloride (99.8 % purity), ferrous sulfate (99.9 % purity), liquid ammonia (30 % solution), amino trimethylene triphosphonic acid (ATMP) (98 % purity), 3-chloro-1,2-propanediol (99.8 % purity), 1,4-diazobicyclo[2.2.2]octane (99.2 % purity), 2-amino pyridine (APIC) (99.0 % purity), sodium nitrite (99.9 %), potassium permanganate (98.0 % purity), sulfuric acid (98 % purity) and hydrogen peroxide (30 % purity) were purchased from sigma Aldrich, South Africa.

16.2 Synthesis and characterization of N-(2′,3′-epoxypropyl)-N-methyl-2-oxopyrrolidinium chloride

Synthesis

The reaction system was set up as follows: The heating oil bath with an internal thermometer was mounted on a mechanical magnetic stirrer. A 500 mL three-necked round-bottomed flask with a thermometer inlet and cold water condenser was used (Fig. 9). The round bottom flask was flushed with nitrogen gas and thereafter 1 mol of freshly distilled N-methyl-2-oxopyrrolidine in 100 mL of acetonitrile and 1.1 mol of epichlorohydrin was added and then brought to a moderate reflux (90–100) °C internal temperature. The resulting solution was then heated under reflux for 48 hrs and thereafter cooled to room temperature. The volatile materials were removed in vacuum, to yield the yellow coloured IL, N-(2′,3′- epoxypropyl)-N-methyl-2-oxopyrrolidinium chloride. This product was purified by solvent washing with acetone and hexane, to remove the unwanted starting materials, and then further distilled again at 80 °C for 48 hrs to obtain moisture free IL. In 99.22 % yield was characterized by FTIR, ^{1}H NMR, ^{13}C NMR and elemental analysis. (Scheme: 1)

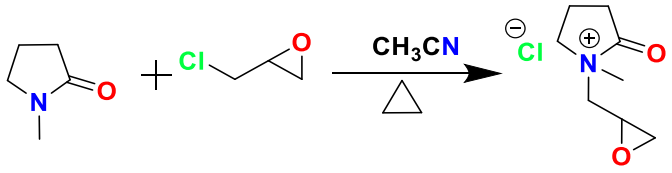

Scheme1:- Synthesis of N-(2′,3′-epoxypropyl)-N-methyl-2-oxopyrrolidinium chloride

Characterization

The $[Epmpyr]^+[Cl]^-$ was characterized by the following techniques: FTIR, ^1H NMR, ^{13}C NMR and elemental analysis. FTIR: (υ =cm^{-1}) 3442, 2995, 1621, 1501, 1403, 1332, 1256, 1113, 967, 856, 756, 679, 561, 479. ^1H NMR (400 MHz, $DMSOd_6$): δ 3.48-3.51 (m, 1H), 3.30-3.32 (t, 2H), 2.76-3.29 (s, 1H), 2.61-2.62 (s, 3H). 2.26- 2.30 (d, 2H) 1.96-1.98 (t, 2H) 1.90-1.94 (m, 2H) ^{13}C NMR (100 MHz, $DMSOd_6$): δ 175.03, 51.22, 49.38, 45.72, 45.00, 30.62, 29.50, and 17.59. Elemental Analysis: theoretical calculation for (in %): $C_8H_{14}NO_2$: C, 50.14; H, 7.36; N, 7.31; the values found (in %): C, 50.45; H, 7.10; N, 7.17.

16.3 Synthesis and characterization of N-(2′,3′-epoxypropyl)-N-methyl-2-oxopyrrolidinium salicylate

Synthesis

In a round bottom flask, sodium salicylate (179.2 g, 1.12 mol) is dissolved in methanol. Then, N-(2′,3′-epoxypropyl)-N-methyl-2-oxopyrrolidium chloride (200.90 g, 1.10 mmol) was added to exchange the salicylate anion. The reaction mixture in a round bottom flask were placed on a magnetic stirrer with an inner thermometer. The reaction temperature was kept at 80-90 ^oC for 10 hrs, with constant stirring. The product was partially purified by a solvent wash with acetone, petroleum ether, and hexane, sequentially, to remove unwanted starting materials and sodium chloride. The partially purified product was distilled at 80 ^oC for 48 hrs to produced moisture-free ILs. The product identity was established FTIR, ^1H NMR, ^{13}C NMR and elemental analysis and the yield of the product was 97.5 %. The scheme for synthesis of N-2′,3′-epoxypropyl-N-methyl-2-oxopyrrolidinium salicylate is given below: (Scheme: 2)

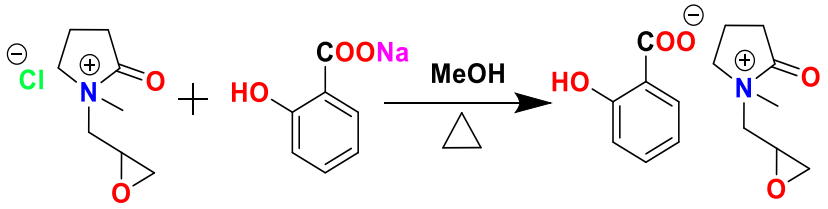

Scheme 2: synthesis of N-(2',3'-epoxypropyl)-N-methyl-2-oxopyrrolidinium salicylate

Characterization

The $[Epmpyr]^+[SAL]^-$ was characterized by the following techniques: ^1H NMR, ^{13}C NMR, elemental analysis and FTIR ($\upsilon=cm^{-1}$) 3442, 2995, 1621, 1501, 1403, 1332, 1256, 1113, 967, 856, 756, 679, 561, 479.$[Epmpyr]^+[SAL]^-$ ^1H NMR (400 MHz, $DMSOd_6$): δ 1.9 - 2.0(M, 2H), 2.15 - 2.3(t, 2H), 2.7-2.8(s, 3H), 3.3 - 3.4(m, 3H), 3.5 - 3.65(d, 2H), 3.66 - 3.90(m, 1), 4.0 - 4.2(m, 1), 6.75 - 6.85(t, 1H), 6.86 - 7.00(m, 1H), 7.10 - 7.30(t, 1H), 7.40 - 7.60(m, 1H), 7.65 - 7.95(d-d, 1H). ^{13}C NMR (100 MHz, $DMSOd_6$): δ 18, 30, 33, 51, 65, 72, 75, 115, 120, 122, 132, 134, 138, 163 and 178. Elemental Analysis (in %) Theoretical calculation for: $C_{15}H_{21}NO_4$: C, 64.50; H, 7.58; N, 5.01; O, 22.91; the values found (in %) are C, 64.95; H, 7.10; N, 5.28; O, 23.36.

16.4 Synthesis and characterization of N-2′,3′-epoxypropyl-N-methyl-2-oxopyrrolidinium acetate

Synthesis

In a round bottom flask, sodium acetate (91.87 g, 1.12 mol) is dissolved in methanol. Then, N-(2′,3′-epoxypropyl)-N-methyl-2-oxopyrrolidium chloride (200 g, 1.10 mmol) was added to exchange the acetate anion. The reaction mixture in a round bottom flask were placed on a magnetic stirrer with an inner thermometer. The reaction temperature was kept at 80-90 ^oC for 10 hrs, with constant stirring. The product was partially purified by a solvent wash with acetone, petroleum ether, and hexane, sequentially, to remove unwanted starting materials and sodium chloride. The partially purified product was distilled at 80 ^oC for 48 hrs to produced moisture-free ILs. The product identity was established FTIR, ^1H NMR, ^{13}C NMR and elemental analysis and

the yield of the product was 98.3 %. The scheme for synthesis of N-2′,3′-epoxypropyl-N-methyl-2-oxopyrrolidinium salicylate is given below (Scheme: 3).

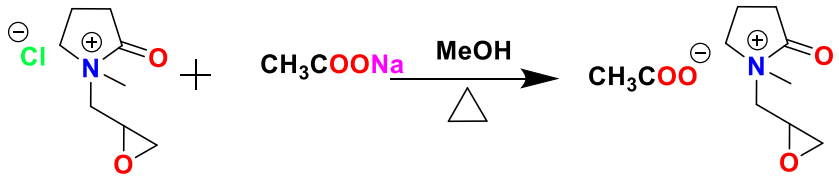

Scheme 3: Synthesis of N-2',3'-epoxypropyl-N-methyl-2-oxopyrrolidinium acetate

Characterization

The $[Epmpyr]^+[OAC]^-$ was characterized by the following techniques: ^1H NMR, ^{13}C NMR, elemental analysis and FTIR. The structure of $[Epmpyr]^+[OAC]^-$ is confirmed by the following techniques as shown in FTIR (ν=cm^{-1}): 3442, 2995, 1621, 1501, 1403, 1332, 1256, 1113, 967, 856, 756, 679, 561, 479.$[Epmpyr]^+[OAC]^-$ ^1H NMR (400 MHz, $DMSOd_6$): δ 1.1 – 1.2(t, 2H), 2.0 - 2.1(s, 3H), 2.1 - 2.2(q, 2H), 2.2-2.3(t, 2H), 2.3 - 2.4(t, 2H), 2.8(s, 3H), 3.4 - 3.5(t, 2H), and 5.3-5.6(s, 1H) ^{13}C NMR (100 MHz, $DMSOd_6$): δ 19, 26, 30, 33, 52, 55, 65, 75, 178 and 180. Elemental Analysis (in %) Theoretical calculation for: $C_{10}H_{17}NO_4$: C, 55.80; H, 7.96; N, 6.51; O, 22.91; the values found (in %) are C, 55.24; H, 7.86; N, 6.28.

16.5 Synthesis and characterization of N-2′,3′-dihydroxypropyl-N-methyl-2-oxopyrrolidinium chloride $[PYR\text{-}PDO]^+[Cl]^-$

Synthesis

Into a 100 mL three-necked round bottom flask, fitted with a thermometer and water condenser, was added 1-methyl-2-oxopyrrolidinine (4.45 g, 50 mmol) in ethanol (50 mL). Thereafter 3-chloro-1,2-propanediol (6.0819 g, 55 mmol) was added slowly in an ice box setup at a temperature of 8-10 ºC with constant stirring and thereafter the content was brought to a moderate reflux to 90-100 ºC on an oil bath, with constant stirring for 24 hrs. The flask was cooled and any volatile and unreacted materials were removed in *vacuo* to give a yellow coloured N-2′,3′ dihydroxy propyl-1-methyl -2-oxopyrrolidinium chloride $[PYR\text{-}PDO]^+[Cl]^-$ IL with 99.0 % of yield, reaction. (Scheme: 4).

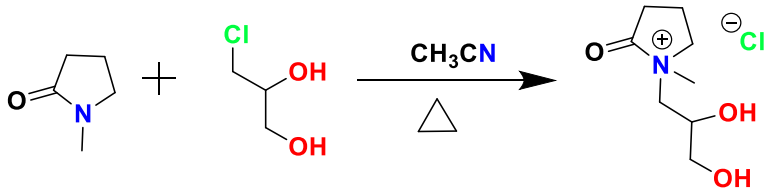

Scheme 4: Synthesis of N-2',3'-dihydroxypropyl-N-methyl-2-oxopyrrolidinium chloride [PYR-PDO]$^{+}$[Cl]$^{-}$

Characterization

It was characterized by the following techniques: FTIR, ^{1}H NMR, ^{13}C NMR and elemental analyses. [PYR-PDO]$^{+}$[Cl]$^{-}$. FTIR (υ=cm^{-1}): 3309, 2940, 2871, 1644, 1505, 1407, 1304, 1262 and 1036. ^{1}H NMR (400 MHz, $CDCl_3$): δ 4.3 (s, 2H), 3.8 (s, 1H), 3.7 (d, 2H), 3.4-3.6 (m, 2H), 3.3 (d, 2H), 2.7 (s, 3H), 2.2 (t, 2H), (1.9-2.0 (m, 2H). ^{13}C NMR (100 MHz, $CDCl_3$): δ 158, 135, 132, 130, 125, 88, 25, 15. The elemental composition (%) calculated for $C_8H_{16}ClNO_3$ is: C, 45.83; H, 7.69; N, 6.68, which are close to the values found: C, 45.56; H, 7.10; N, 6.29.

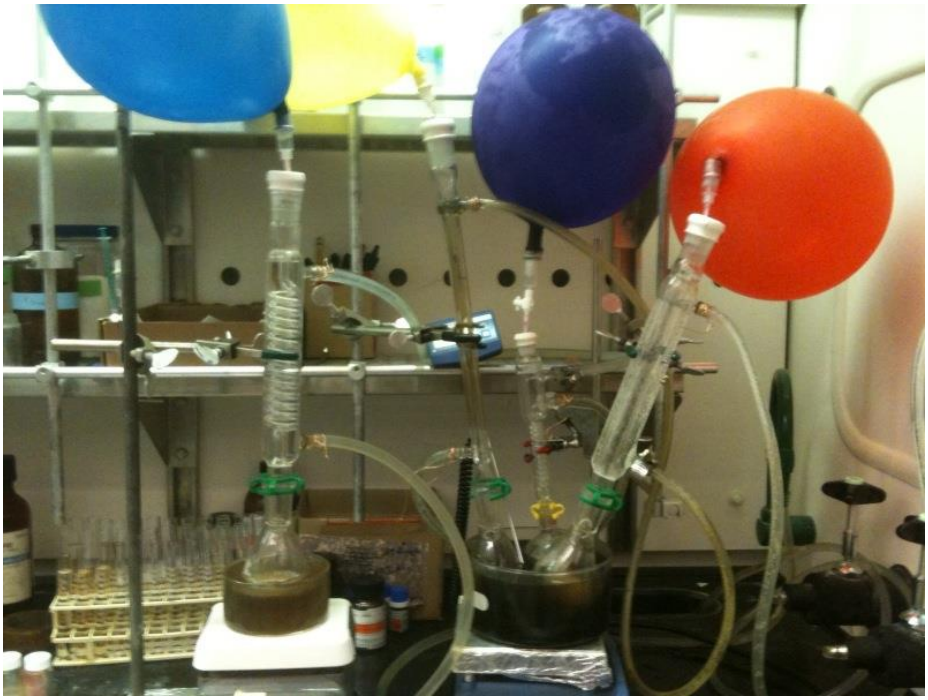

Figure 9: Reaction setup for synthesis of ionic liquids

16.6 Synthesis and characterization of N-2′,3′-dihydroxypropyl-2-Amino-4-methylpyridinium chloride $[APIC\text{-}PDO]^+[Cl]^-$

Synthesis

Into a 100 mL three-necked round bottom flask, fitted with a thermometer and water condenser, was added 2-amino-4-methyl-pyridine (APIC) (4.57 g, 50 mmol) in ethanol (50 mL). Thereafter 3-chloro-1,2-propanediol (6.0819 g, 55 mmol) was added slowly in an ice box setup at a temperature of 8-10 ^oC with constant stirring and the content was brought to a moderate reflux to 90-100 ^oC on an oil bath, with constant stirring for 24 hrs. The flask was cooled and any volatile and unreacted materials were removed *in vacuo* to give a yellow coloured N-2′,3′ dihydroxy propyl 2-amino pyridinium chloride $[APIC\text{-}PDO]^+[Cl]^-$ IL with 98.6% of yield shown in reaction Scheme 5.

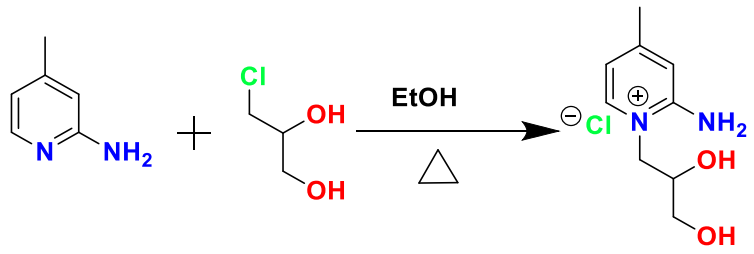

Scheme 5: Synthesis of N-2',3'-dihydroxypropyl-2-Amino-4-methylpyridinium chloride $[PYR\text{-}PDO]^+[Cl]^-$

Characterization

It was characterized by the following techniques: FTIR, ^1H NMR, ^{13}C NMR and elemental analyses. $[APIC\text{-}PDO]^+[Cl]^-$. FTIR ($\upsilon$=$cm^{-1}$): 3323, 3170, 2953, 2884, 1583, 1444, 1373, 1046 and 1034. ^1H NMR (400 MHz, CD_3ODd_4): δ 7.8 (d, 1H), 7.0 (s, 1H), 6.8 (d, 1H), 4.5-4.6 (d, 1H), 4.2-4.4 (d, 1H), 4.0-4.1 (d, 1H), 3.5-3.8 (m, 2H), 2.5-3.0 (s, 3H). ^{13}C NMR (100 MHz, CD_3ODd_4): δ 156, 142, 118, 115, 70, 65, 55, 22. The elemental composition (%) calculated for $C_9H_{15}ClN_2O_2$ is: C, 49.43; H, 6.91; N, 12.81, which are close to the values found: C, 49.56; H, 6.60; N, 12.59.

16.7 Synthesis and characterization of [DABCO, PYR, APIC-PDO]$^{+}$[ATMP]$^{-}$

Synthesis

Into a 100 mL three-necked round bottom flask, fitted with a thermometer and water condenser, was added sodium hydroxide (0.4 g, 20 mmol) in 50 mL of methanol. Thereafter amino tris (methyl phosphonic acid) (ATMP) (5.981 g, 20 mmol) was added dropwise, with constant stirring, on an ice bath. The reaction mixture was maintained at 8-10 ºC for 1h. Then 20 mmol of each of the ILs [DABCO-PDO]$^{+}$[Cl]$^{-}$, [PYR-PDO]$^{+}$[Cl]$^{-}$ and [DABCO-PDO]$^{+}$[Cl]$^{-}$ were added. The flask was transferred into an oil bath and the content was brought to reflux at 120 ºC for 24 hrs. The flask was cooled and any volatile and unreacted materials were removed *in vacuo* to give a yellow colored [DABCO, PYR, APY-PDO]$^{+}$[ATMP]$^{-}$ IL which was subsequently further purified by solvent washing and the yield was 97.3 % shown in reaction (Scheme 6).

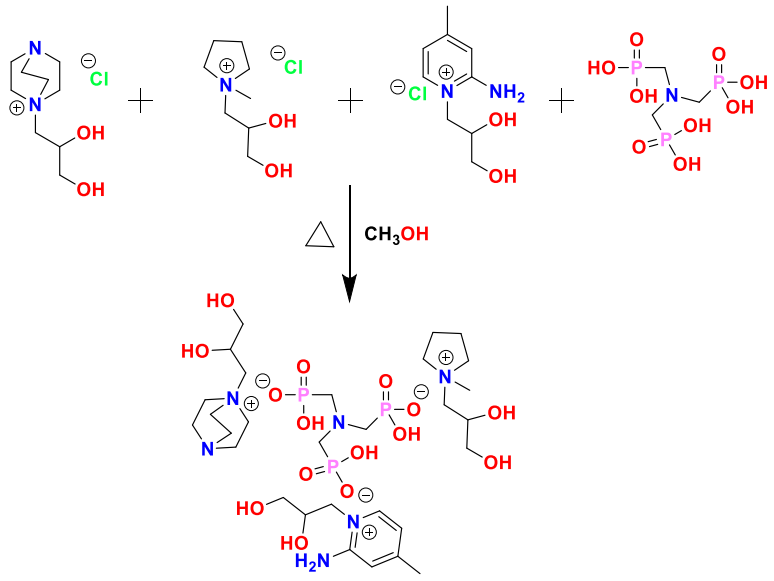

Scheme 6: Synthesis of [DABCO, PYR, APIC-PDO]$^{+}$[ATMP]$^{-}$

Characterization

It was characterized by the following techniques: FTIR, ^{1}H NMR, ^{13}C NMR, ^{31}P NMR and elemental analysis. [DABCO, PYR, APY PDO]$^{+}$[ATMP]$^{-}$. FTIR (υ = cm^{-1}): 3416, 3323, 2953, 2884, 1744, 1658, 1513, 1453, 1382, 1243, 1182, 1034, 915, 736, 654 and 569 (see Fig. 1b). ^{1}H NMR (400 MHz, D_2Od_2): δ 7.5 (d, 2H), 6.6-6.8 (m, 3H), 4.3-4.4 (s, 2H), 4.0-4.1 (s, 6H), 3.9-4.0 (t, 5H), 3.8-3.9 (m, 10H), 3.5-3.7 (m, 23H), 3.3-3.4 (t, 2H), 3.1-3.2 (s, 3H), 2.2-2.4 (m, 6H), 1.7-

2.1 (m, 2H). ^{13}C NMR (100 MHz, D_2Od_2): δ 180, 160, 155, 145, 135, 118, 72, 68, 67, 65, 64, 63, 62, 61, 58, 56, 55, 54, 53, 52, 50, 48, 46, 32, 30, 22, 18.

16.8 Moisture content

The percentage of the water content in synthesized ILs was determined using a Metrohm 702 SM Titrino Metter as below (Table. 6)

Table: 6 Moisture content in synthesized ILs

Synthesized ILs	Moisture content in %
$[EPMpyr]^+[Cl]^-$	0.060
$[EPMpyr]^+[SAL]^-$	0.050
$[EPMpyr]^+[OAC]^-$	0.065
$[DABCO\text{-}PDO]^+[Cl]^-$	0.055
$[PYR\text{-}PDO]^+[Cl]^-$	0.060
$[APIC\text{-}PDO]^+[Cl]^-$	0.070
$[DABCO\text{-}PYR\text{-}APY\text{-}PDO]^+[ATMP]^-$	0.075

17 Preparation of partially oxidized h-BN (BNONS)

The BNONS was prepared by modifying a chemical oxidation method. Briefly, h-BN powder (1 g, 40 mmol) was added to a solution of sodium nitrite (0.8 g) in concentrated sulfuric acid (50 mL) on an ice bath. Thereafter potassium permanganate (5.6 g) was added with vigorous stirring and maintained to 10 ^oC. The reaction vessel was removed from the ice bath, agitated for 3 hrs and heated at 40 ^oC. Then deionized water (100 mL) was subsequently added, the reaction vessel was transferred to an oil bath and heated at 120-130 ^oC for 45 minutes. The solution was diluted with 200 mL of deionized water followed by the addition of a 30 % solution of hydrogen peroxide (50 mL). The as-obtained partially oxidized BNONS powder (white colour) was repeatedly washed with deionized water and dilute HCl to remove sulfate ions. The final washings were tested with

$BaCl_2$ solution for sulfate. The as-purified partially oxidized BN (BNONS) powder was filtered and dried at 60 ^oC for 24 hrs.

18 Preparation of nanocomposite (TCPIL/$CuFe_2O_4$/BNONS)

The TCPIL/$CuFe_2O_4$/BNONS nanocomposite was synthesized by co-precipitation of the as-prepared TCPIL /$CuFe_2O_4$ nanoparticles in BNONS aqueous solution. In a typical synthesis, 1g of TCPIL {[(APIC-DABCO-PYR)-PDOL]$^+$[ATMP]$^-$} was dissolved in deionized water (20 mL). Then, $CuFe_2O_4$ (2 g) nanoparticles were added to the above solution and heated at 120 ^oC for 24 hrs with constant stirring. Thereafter sodium dodecyl lauryl sulfate (0.1 g) was added followed by addition of BNNONS solution and 30% ammonia solution (25 mL) with vigorous stirring to dissolve all materials. This solution was heated at 150 ^oC with constant stirring for 12 hrs. Then the pH of the solution was adjusted to 9-10 with dilute ammonia solution. The mixture was stirred for 1 h and cooled to reach ambient temperature. Finally, the mixture was centrifuged and filtered to obtain TCPIL /$CuFe_2O_4$/BNONS brown powder. The product was washed several times with deionized water and dried under vacuum at 70 ^oC. The final product was dispersed in ethanol (20 mL). The mass ratio of $CuFe_2O_4$, IL, and BNONS in the TCPIL /$CuFe_2O_4$/BNONS nanocomposite was calculated as 2:1:1.

19 Catalytic reduction of serious of nitro anilines and dyes

The catalytic activity of TCPIL/$CuFe_2O_4$/BNONS was investigated by the reduction of series of NAs (Scheme: 5) and dyes. Briefly, 2-NA (0.5 mL, 0.05 M), 3-NA (0.75 mL, 0.05 M), 4-NA (0.75, 0.01 M), 4-NPDA (0.75, 0.005 M) as well as MB (0.75, 0.01 M) and AR (0.50 mL, 0.05 M) solution was added separately into a quartz cuvette followed by $NaBH_4$ (0.75 mL, 0.5 M) and finally by deionized water (1.485 mL). However, a smaller quantity of 4-nitro-2-phenylene diamine derivative (0.75 mL, 0.1 mmol) was used due to its poor solubility. Finally, an aqueous solution of TCPIL/$CuFe_2O_4$/BNONS nano12 material (0.03 mL, 0.2 mg/mL) was added into the quartz cuvette and the reaction was monitored by UV-visible spectrophotometry. The UV-visible absorption spectra were recorded every three minutes. During the reduction of NAs and dyes, the solution changed to colourless thereby indicating a visual confirmation of the reduction process. After completion of the reaction, small aliquots of NH_4Cl solution was added to neutralize excess $NaBH_4$ solution and the catalyst was recovered by external magnets.

20 Preparation of IL/$NiFe_2O_4$/TiO_2 nanocomposite

The nickel ferrite magnetite nanoparticle was prepared according to the previous method. Briefly, 1.0 g of nickel ferrite magnetic nanoparticle $NiFe_2O_4$ and N-(2′,3′-epoxypropyl)-N-methyl-2-oxopyrrolidinium salicylate IL were taken separately. The IL was dissolved in ultra-pure deionized water to which the above weighed nickel ferrite magnetic nanoparticle was added slowly with constant stirring for 24 hrs at room temperature; it was then dried at 80 ^oC for 12 hrs to produce a dry brown powder then without purification of the material further it was dispersed in 20 mL of ultra-pure water and sonicated. Separately 2.0 gram of TiO_2 was dispersed in 20 mL water and sonicated for 15 minutes and this solution was added to above magnetic nanoparticle dispersion at constant stirring. The reaction mixture was transferred to round bottomed flask and placed in a temperature controlled oil bath with a magnetic stirrer. The temperature of the reaction was maintained at 140 ^oC for 16 hrs. The final product was dried under vacuum for 10 hrs to produce the light brown coloured nanocomposite. It was purified by washing with ultrapure water and dispersed in ethanol. The composite was then characterized by FTIR, SEM, EDS and TEM.

21 Investigation of catalytic activity of nanocomposite (IL/$NiFe_2O_4$/TiO_2)

The investigation of the catalytic activity of IL nickel-iron magnetite titanium dioxide nanocomposite for the reduction of 2-nitroaniline was carried out in room temperature monitoring under UV-visible spectroscopy. In a general procedure, 2-nitroaniline (0.5 mL of 0.5 mM) was mixed with 0.5 mL of freshly prepared aqueous $NaBH_4$ solution (0.4M) and 1.95 mL of deionized water to form a deep yellow solution. Then, 0.05 mL of IL/$NiFe_2O_4$/TiO_2 nanocomposite dispersion (0.2 mg/mL) was added into the quartz cuvette. The above mixed solution was measured using a UV-Visible spectrophotometer every five minutes to monitor the variation of 2-nitroaniline concentration by absorbance measurements at 400 and 550 nm. After the solution became colourless, the IL/$NiFe_2O_4$/TiO_2 hybrid was separated from the reaction mixture under a magnetic field and it was then used for another cycle of 2-nitroaniline (2-NA) reduction. The samples were filtered, centrifuged and their concentration was determined by UV-visible spectrometry.

22 Appendix

22.1 The Fourier Transform Infra-Red spectra (FTIR) for synthesized novel ILs

22.1.1 FTIR spectrum of $[Epmpyr]^+[Sal]^-$

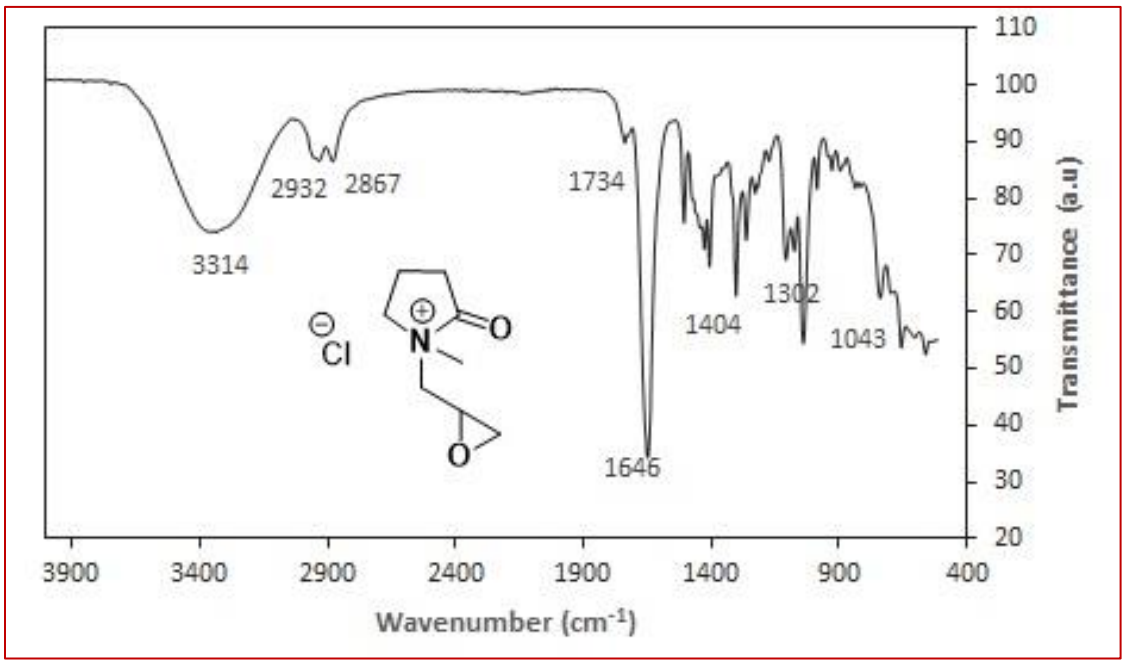

22.1.2 FTIR spectrum of $[Epmpyr]^+[Sal]^-$

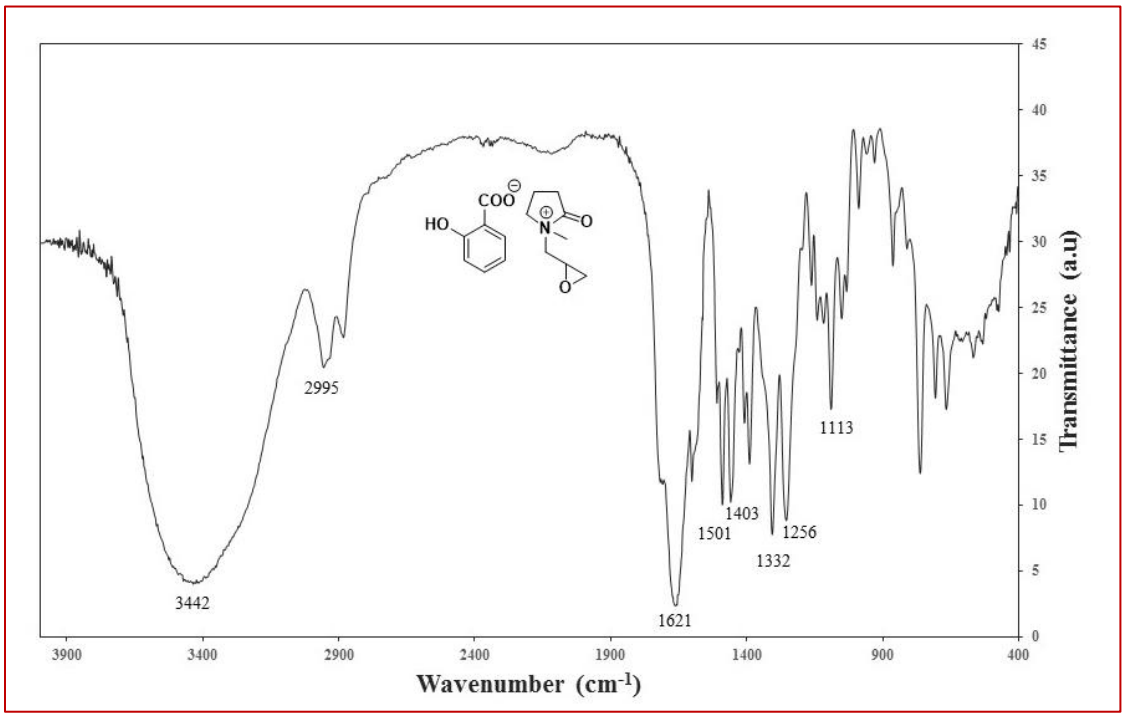

22.1.3 FTIR spectrum of $[Epmpyr]^{+}[OAC]^{-}$

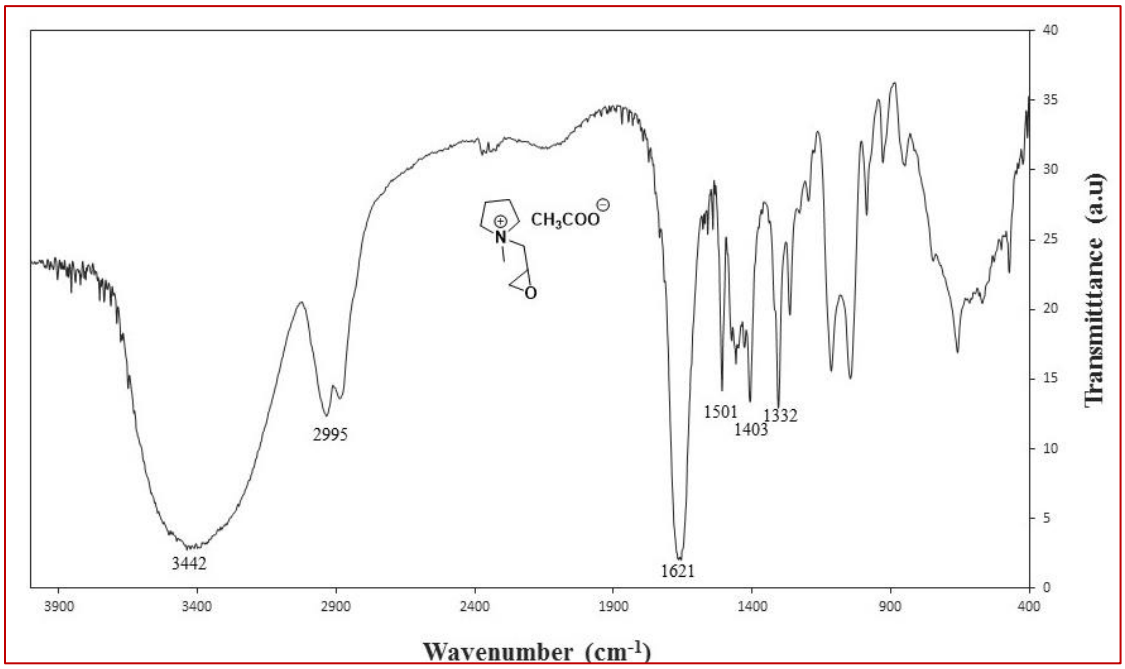

22.1.4 FTIR spectrum of $[MPyr\text{-}PDOL]^{+}[Cl]^{-}$

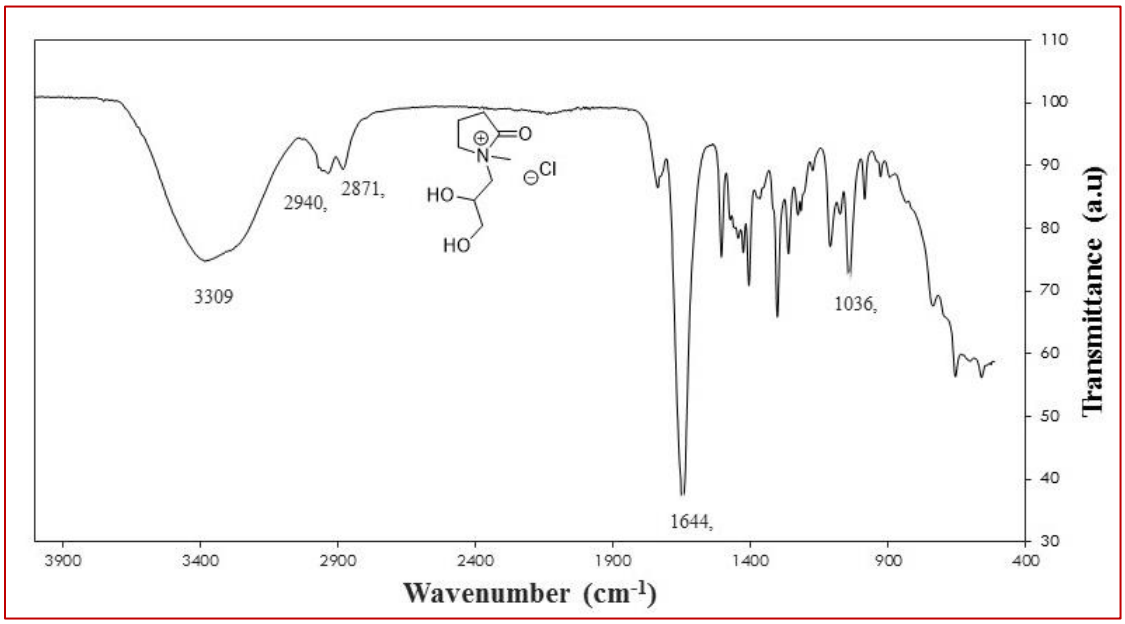

22.1.5 FTIR spectrum of $[APIC- PDOL]^{+}[Cl]^{-}$

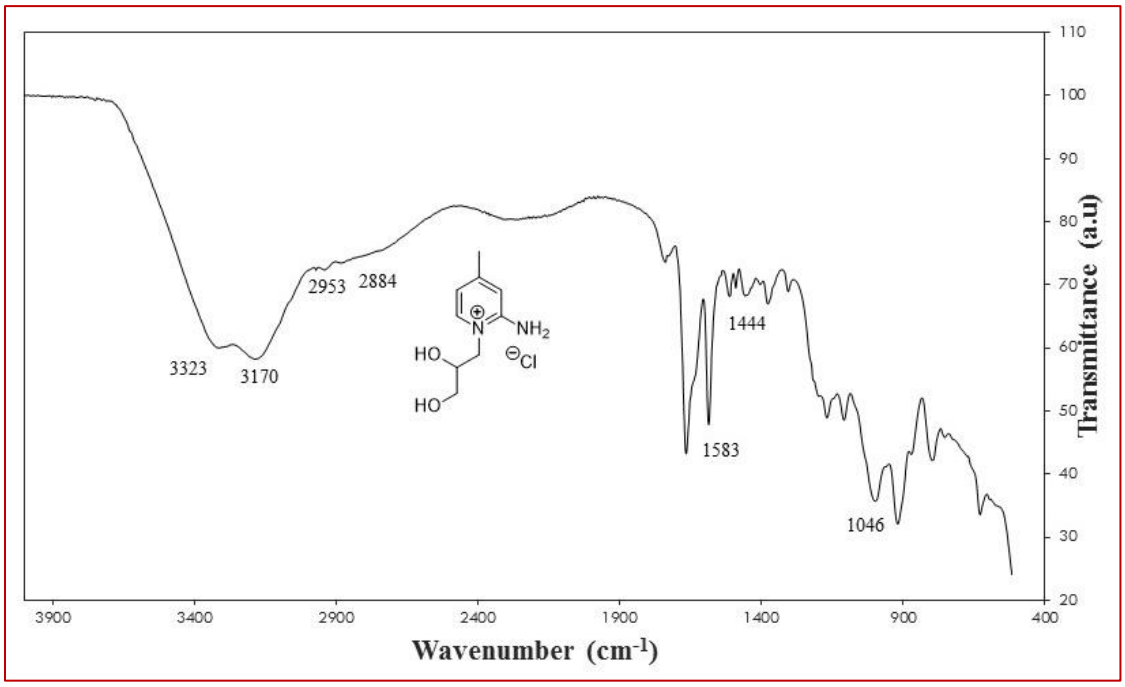

22.1.6 FTIR spectrum of $[DABCO, PYR, APIC-PDO]^{+}[ATMP]^{-}$

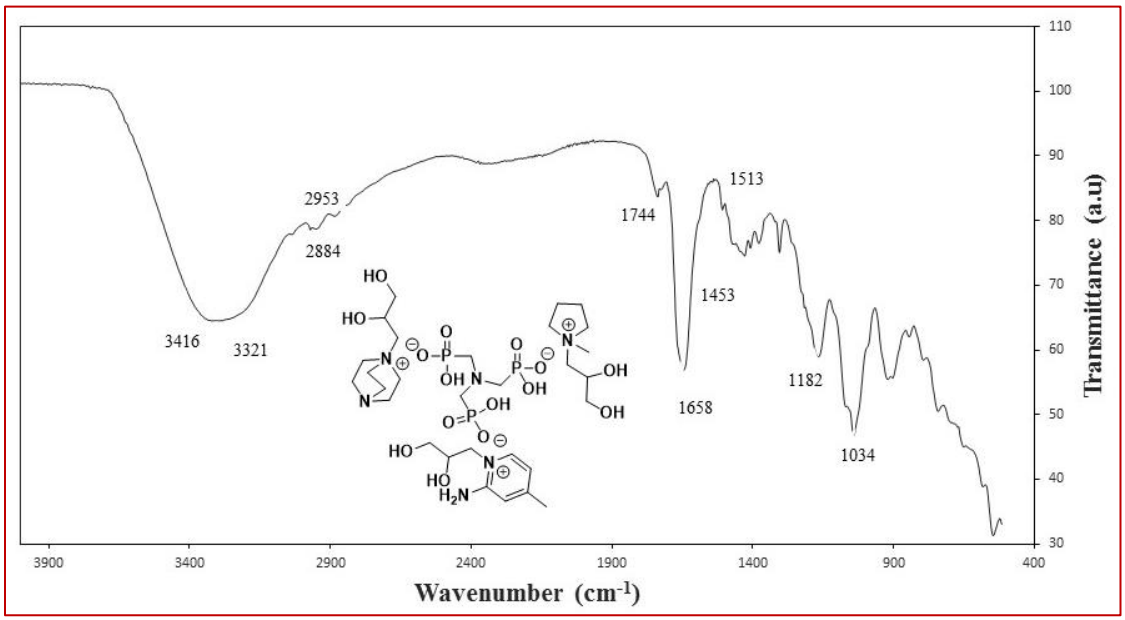

22.2 The Proton Nuclear Magnetic Resonance spectra (^{1}H NMR) of synthesized novel ILs

22.2.1 ^{1}H NMR spectrum of $[Epmpyr]^+[Cl]^-$

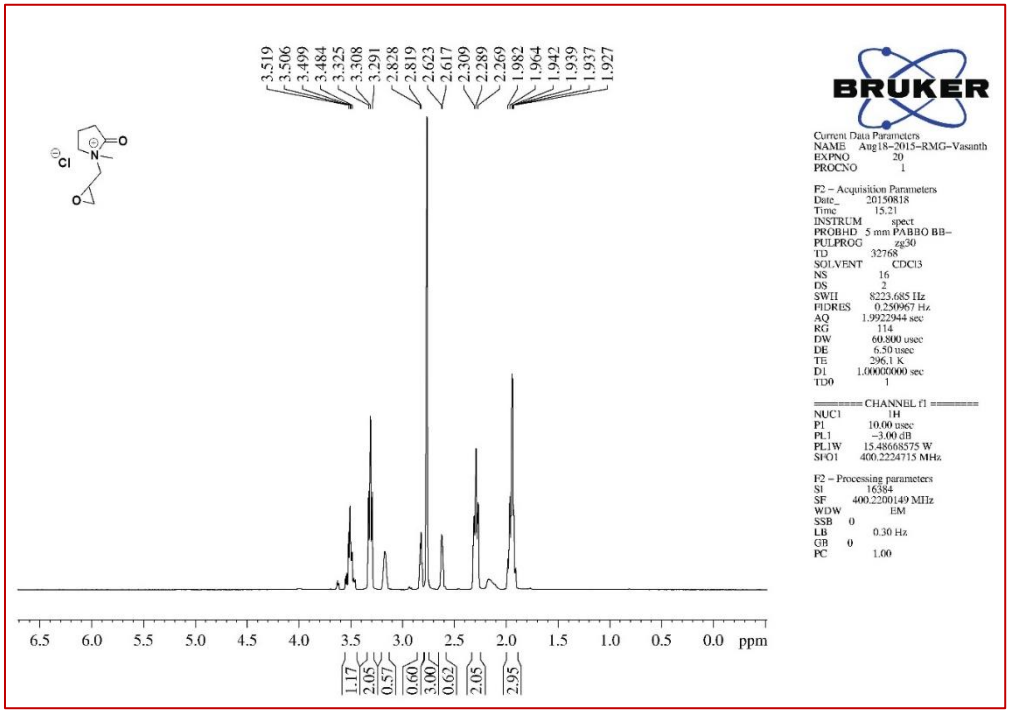

22.2.2 ^{1}H NMR spectrum of $[Epmpyr]^+[Sal]^-$

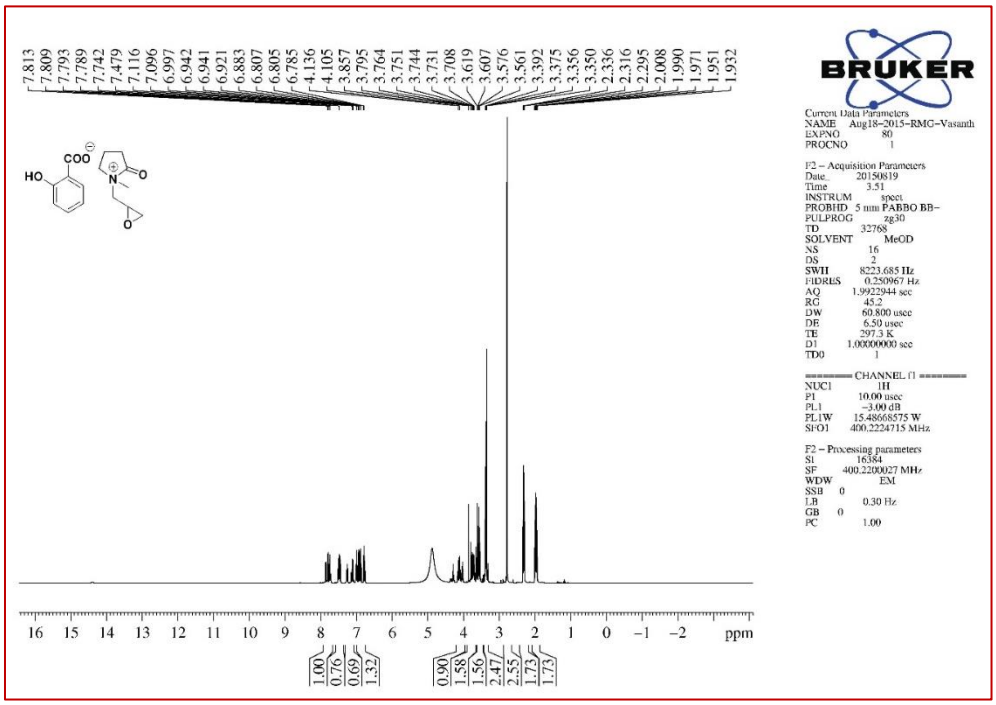

22.2.3 ^{1}H NMR spectrum of $[Epmpyr]^{+}[OAC]^{-}$

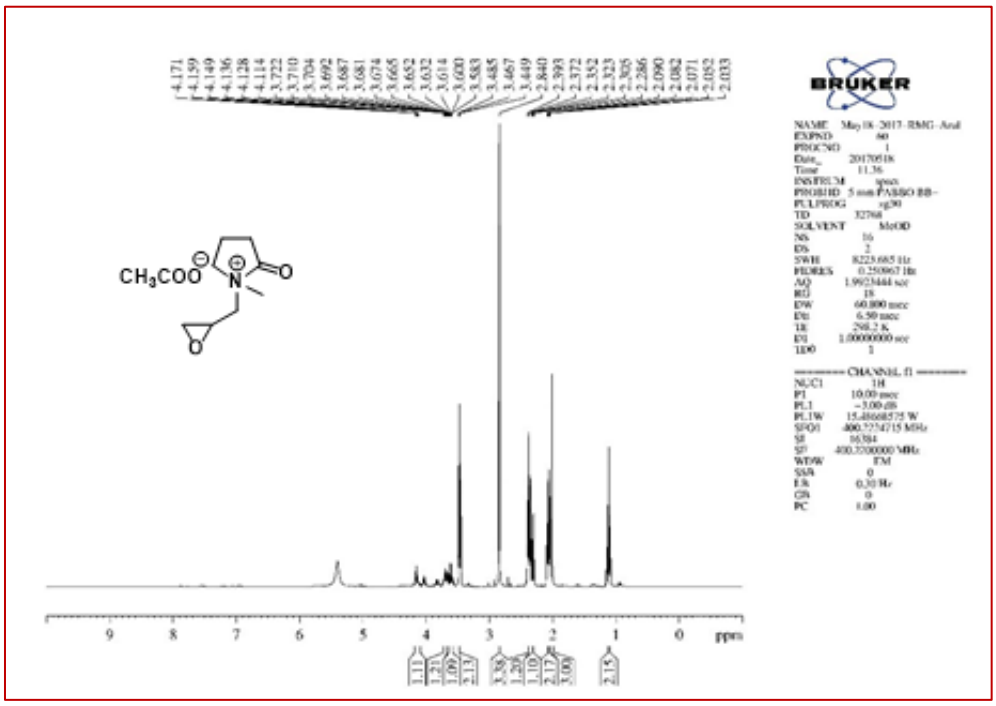

22.2.4 ^{1}H NMR spectrum of $[MPyr\text{-}PDOL]^{+}[Cl]^{-}$

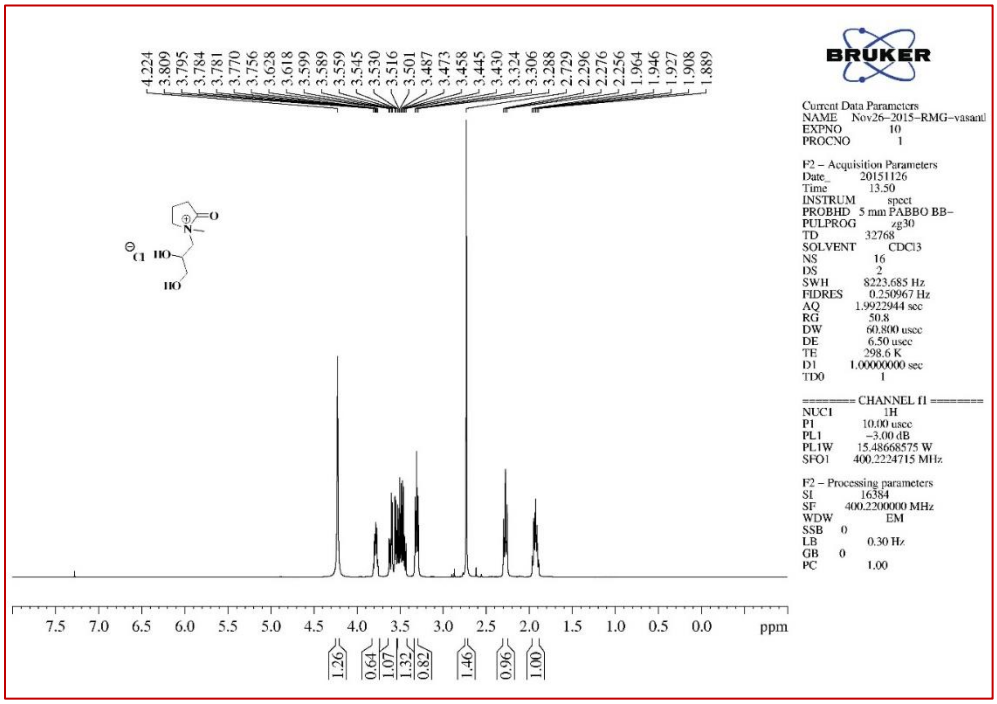

22.2.5 ^{1}H NMR spectrum of [APIC-PDOL]$^{+}$[Cl]$^{-}$

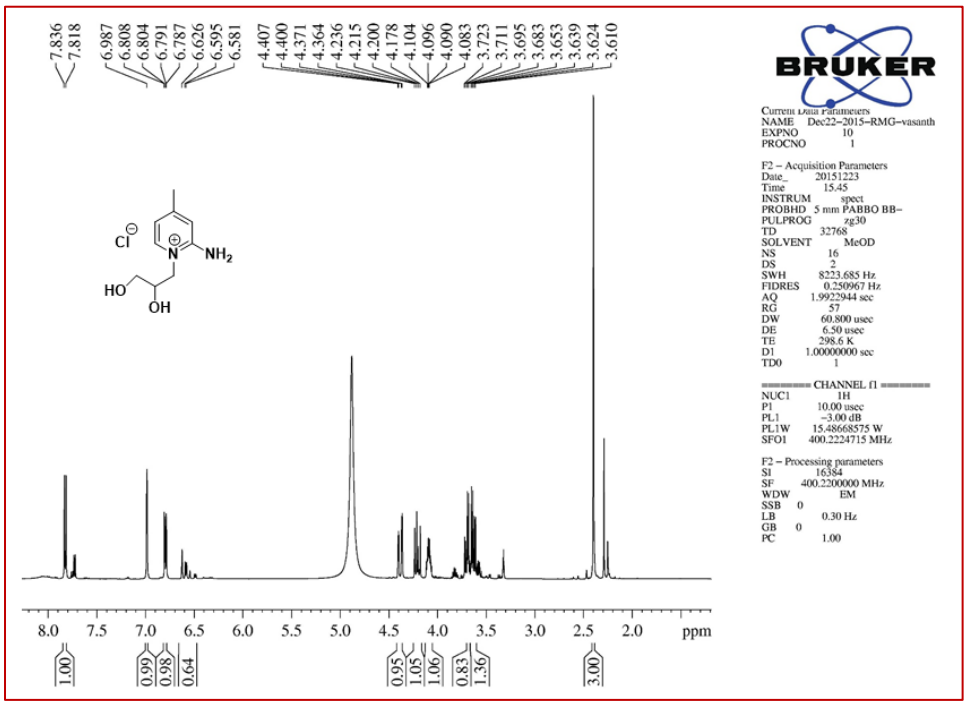

22.2.6 ^{1}H NMR spectrum of [DABCO, PYR, APIC-PDOL]$^{+}$[ATMP]$^{-}$

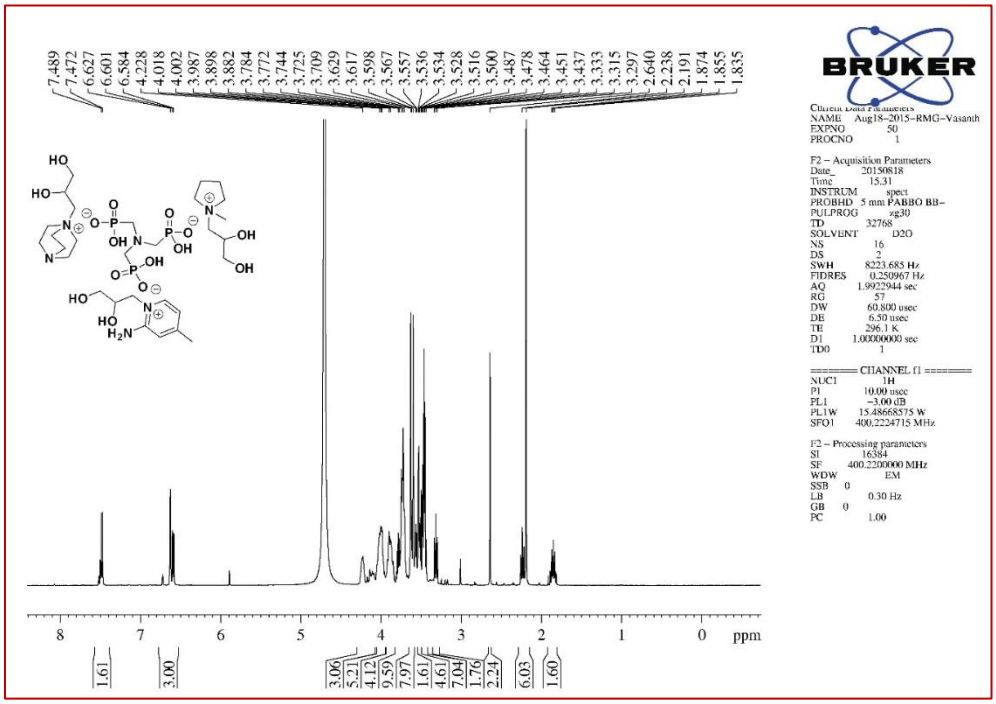

22.3 The Carbon Nuclear Magnetic Resonance spectra (^{13}C NMR) for synthesized novel ILs

22.3.1 ^{13}C NMR spectrum of $[Epmpyr]^+[Cl]^-$

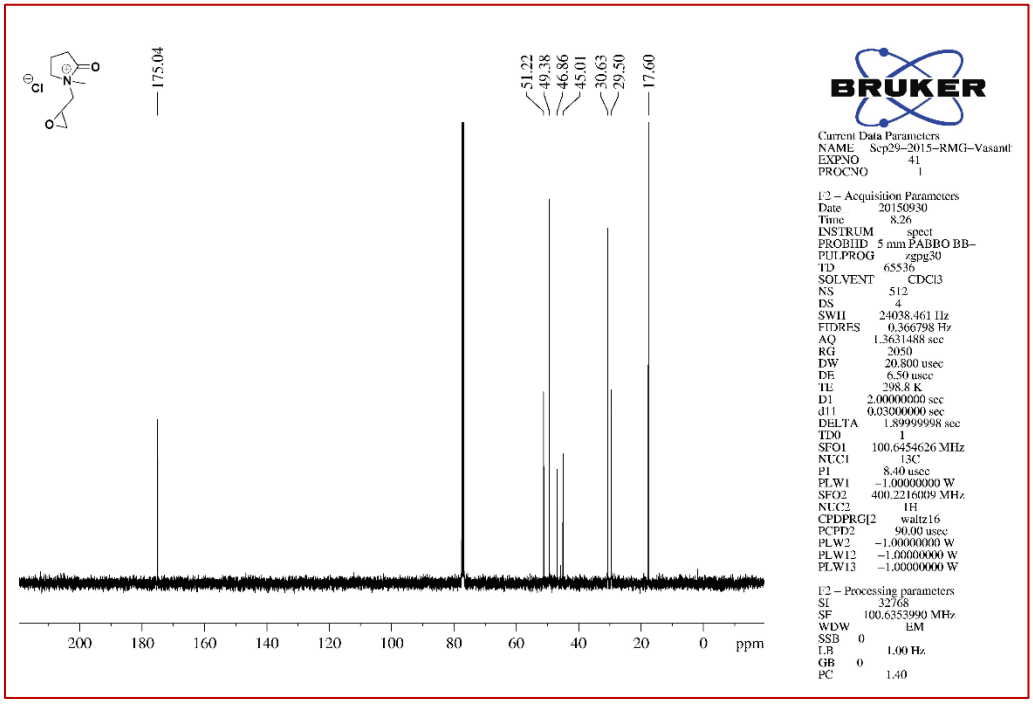

22.3.2 ^{13}C NMR spectrum of $[Epmpyr]^+[Sal]^-$

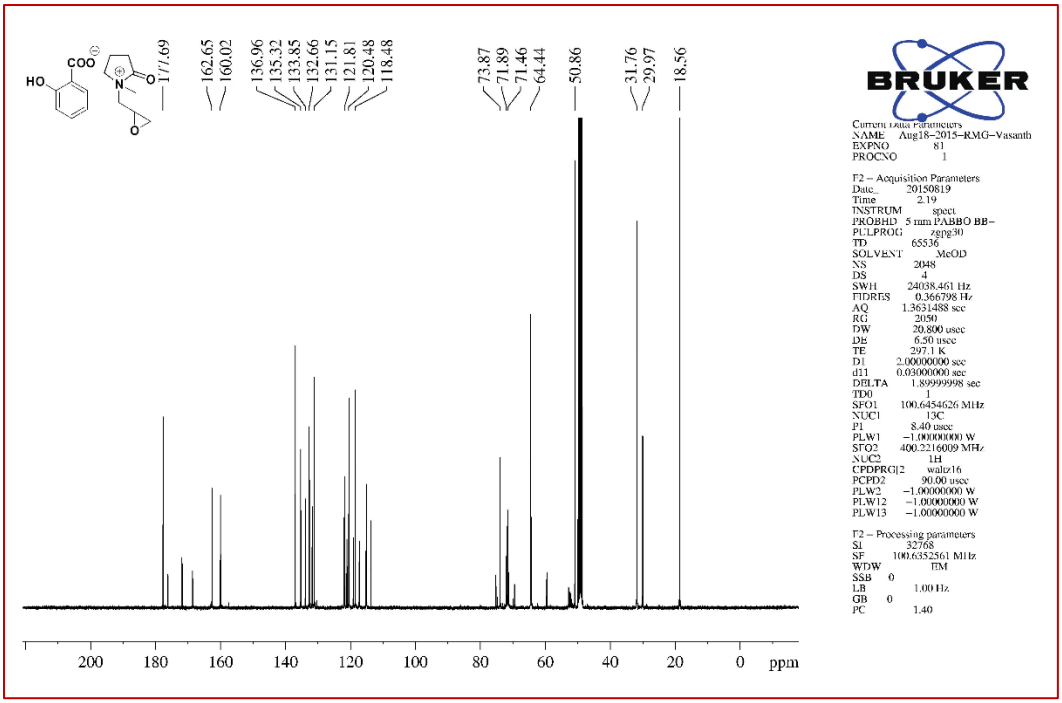

22.3.3 ^{13}C NMR spectrum of $[Epmpyr]^+[OAC]^-$

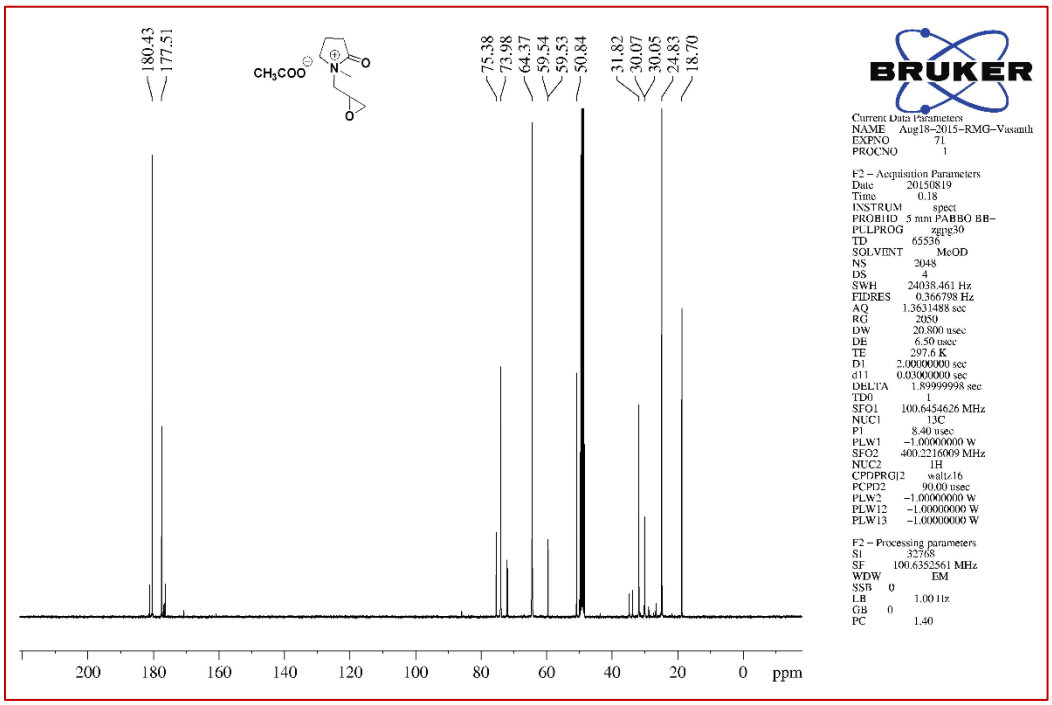

22.3.4 ^{13}C NMR spectrum of $[MPyr\text{-}PDOL]^+[Cl]^-$

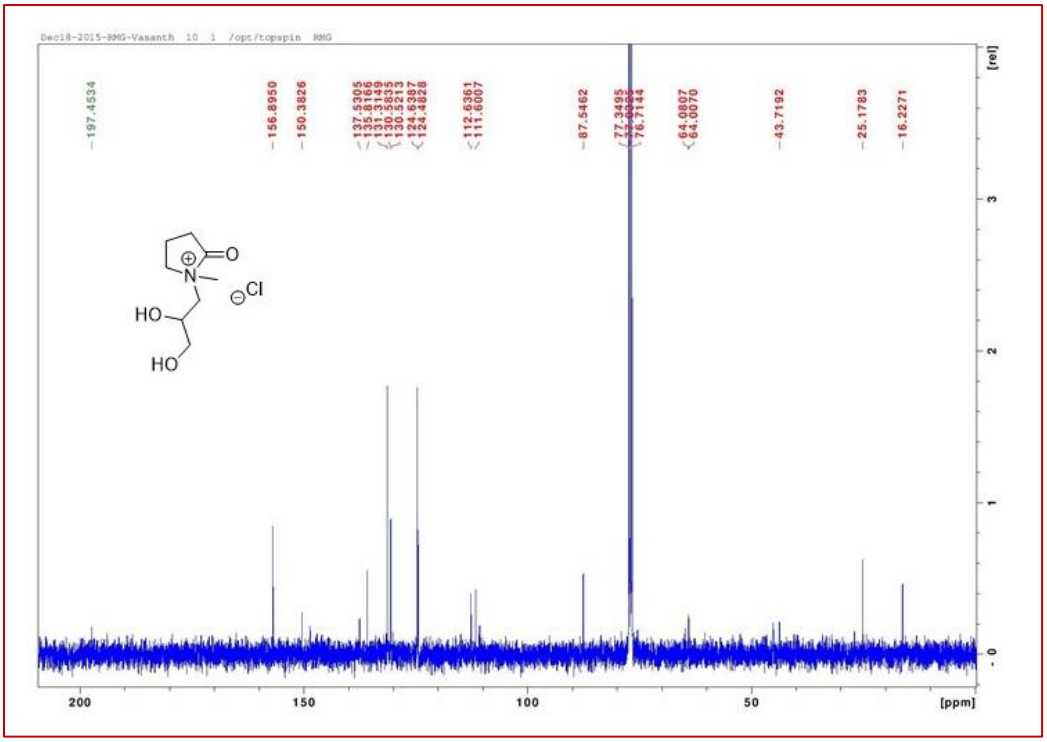

22.3.5 ^{13}C NMR spectrum of $[APIC\text{-}PDOL]^{+}[Cl]^{-}$

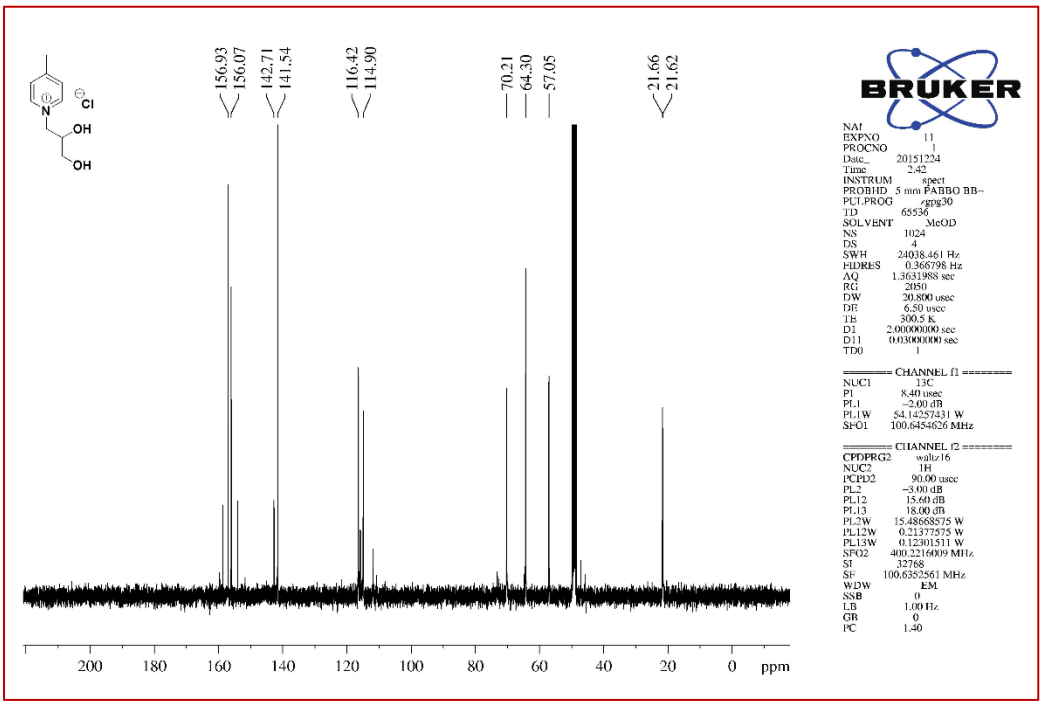

22.3.6 ^{13}C NMR spectrum of $[DABCO, PYR, APY\text{-}PDO]^{+}[ATMP]^{-}$

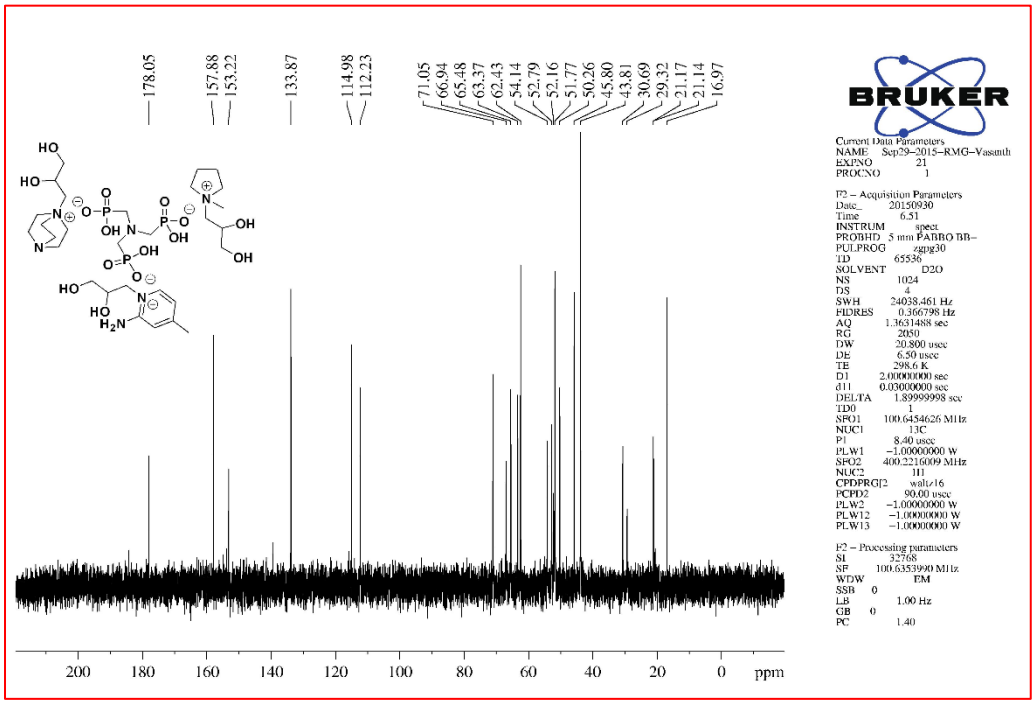

22.4 The Phosphorus Nuclear Magnetic Resonance spectra (^{31}P NMR) for synthesized novel ILs

22.4.1 ^{31}P NMR spectrum of $[DABCO, PYR, APY\text{-}PDO]^{+}[ATMP]^{-}$